

DYNAMICS OF FLUCTUATIONS IN DRIVEN DIFFUSIVE SYSTEMS: FINITE-SIZE EFFECTS

A thesis submitted to
Tata Institute of Fundamental Research, Mumbai, India
for the degree of
Doctor of Philosophy
in
Physics

By
Shamik Gupta



Department of Theoretical Physics
Tata Institute of Fundamental Research
Mumbai - 400 005, India

November 2008

Declaration

I state that the work, embodied in this thesis, forms my own contribution to the research work carried out under the guidance of Professor Mustansir Barma. I also collaborated with Professor Satya N. Majumdar from Laboratoire de Physique Théorique et Modèles Statistiques, Université Paris-Sud, Orsay, France and Professor Claude Godrèche from Service de Physique Théorique, CEA Saclay, France. This work has not been submitted for any other degree to this or any other University or body. Whenever references have been made to previous works of others, it has been clearly indicated.

(Shamik Gupta)

In my capacity as the supervisor of the candidate's thesis, I certify that the above statements are true to the best of my knowledge.

(Mustansir Barma)

Thou hast made me endless, such is thy pleasure.
This frail vessel thou emptiest again and again, and fillest it ever with fresh life.
This little flute of a reed thou hast carried over hills and dales,
and hast breathed through it melodies eternally new.
At the immortal touch of thy hands, my little heart loses its limits in
joy and gives birth to utterance ineffable.
Thy infinite gifts come to me only on these very small hands of mine.
Ages past, and still thou pourest, and still there is room to fill.

-Gitanjali

Rabindranath Tagore

আমারে তুমি অশেষ করেছ, এমনি লীলা তব-
ফুরায়ে ফেলে আবার ভরেছ, জীবন নব নব ॥
কত-যে গিরি কত-যে নদী -তীরে
বেড়ালে বহি ছোটো এ বাঁশিটরে,
কত-যে তান বাজালে ফিরে ফিরে
কাহারে তাহা কব ॥
তোমারি ওই অমৃতপরশে আমার হিয়াখানি
হারালো সীমা বিপুল হরষে, উথলি উঠে বাণী ॥
আমার শুধু একটি মুঠি ভরি
দিতেছ দান দিবস-বিভাবরী-
হল না সারা কত-না যুগ ধরি
কেবলই আমি লব ॥

—রবীন্দ্রনাথ ঠাকুর

To

Four People Ever Precious

*My Father,
My Mother,
Mustansir,
Anandamohan*

Acknowledgements

मैं अकेला ही चला था जानीब-ए-मंजिल मगर
लोग साथ आते गये और कारवाँ बनता गया ।

मजरूह सुलतानपुरी

This thesis could not have been possible without the active support of many people — relatives, friends, colleagues, acquaintances — whose sense of participation in the making of it has been beyond measure, and all of whom have been inspirations, direct or indirect. My grateful thanks to all of you. I spent some of the greatest moments of my life in the association of Mustansir. Interactions with him have enriched me as a physicist, and, more importantly, as a human being. It gave me immense pleasure in spending time with Mustansir's family. Both Rashida and Mustansir have been most caring and affectionate throughout and I could never thank them enough for their support. My parents stood by me through hard times, cared for me in moments of despair and more than merit the dedication made in this thesis. A special word of thanks goes to Rajeev Kapri for great help in preparation of this document.

Contents

Synopsis	v
Publications	xix
1 Introduction	1
1.1 Nonequilibrium <i>vis-à-vis</i> equilibrium stationary states	1
1.2 Driven diffusive systems	3
1.2.1 The asymmetric simple exclusion process	5
1.2.2 The zero-range process	5
1.2.3 The exclusion process with extended objects	6
1.3 Fluctuations in nonequilibrium stationary states: Universality classes	7
1.4 Finite-size effects in equilibrium stationary states	10
1.5 Finite-size effects in nonequilibrium stationary states: Our results, plan of the thesis	11
References	18
2 The Asymmetric Simple Exclusion Process (ASEP)	19
2.1 The ASEP on a ring	21
2.2 The stationary state measure	22
2.3 The equal-time density-density correlation	24
2.4 Motion of particles and density fluctuations in the stationary state	25
2.5 The unequal-time density-density correlation	27
2.6 Coarse-grained description of the ASEP	29
2.7 Mapping of the ASEP density profile to an interface	32
2.8 Scaling properties of the interface equation	34
2.9 Universality classes: The KPZ, the EW and the SDF	37
References	41
3 Tagged particle correlations in the ASEP	42
3.1 Tagged particle correlations: Definitions	43
3.1.1 Average over histories and initial conditions: $\sigma^2(L, t)$	44

3.1.2	Average over histories only: $s^2(L, t)$	45
3.2	Review of earlier work	46
3.2.1	$\sigma^2(L, t)$	46
3.2.2	$s^2(L, t)$	46
3.3	Infinite system	46
3.3.1	Representation of the tagged particle displacement in an infinite system	47
3.3.2	Tagged particle correlations: Physical arguments	48
3.4	Finite system	51
3.4.1	Summary of our results	51
3.4.2	Tagged particle correlations: Physical arguments	52
3.5	Center-of-mass motion	56
	References	58
4	Linear interface model: Analytical results	59
4.1	Interface mapping	60
4.2	Linear interface: Exact solution	62
4.2.1	$\sigma^2(L, t)$	63
4.2.2	$s^2(L, t)$	68
4.2.3	Center-of-mass motion	70
	References	72
5	Correspondence of the linear interface model to different interacting particle systems	73
5.1	Correspondence to the KLS model	73
5.1.1	The model	74
5.1.2	The variance of the displacement	75
5.2	Correspondence to the ARAP	77
	References	80
6	The Zero-Range Process (ZRP)	81
6.1	The model	82
6.2	Mapping to a generalized exclusion process	83
6.3	The stationary state measure	84
6.3.1	Stationary state measure within the grand canonical ensemble in the thermodynamic limit	85
6.3.2	Proof of stationarity	86
6.4	The condensation transition	87
6.5	The case $u(n) = 1 + \frac{b}{n}$ with $b > 2$	89
6.5.1	The critical density ρ_c and the phase diagram	89

6.5.2	Single site occupancy distribution within the canonical ensemble . . .	90
6.5.3	Particle current	93
6.5.4	Kinematic wave velocity	94
References		98
7	Current fluctuations in the ZRP	99
7.1	Integrated current fluctuations: Definitions	100
7.2	Coarse-grained description of the density profile for $\rho \leq \rho_c$	101
7.3	Behavior in different phases	103
7.3.1	Disordered phase	103
7.3.2	Critical point	105
7.3.3	Condensed phase	106
References		114
8	The Exclusion Process with Extended Objects	115
8.1	The model with periodic boundary conditions	117
8.2	The stationary state measure	118
8.3	The wheeling effect	120
8.4	The equal-time density-density correlation	122
8.5	The unequal-time density-density correlation	124
8.6	Concluding remarks	126
References		127
9	Summary and discussion	128
9.1	Generalization and future direction	132
References		136
A	A Primer on Kinematic Waves	137
References		140
B	Derivation of the equation of the interface corresponding to the tagged particle displacement	141
References		144
C	Evaluation of the integral $\int_{k=0}^{\infty} \frac{dk}{k^2} [1 - e^{-ck^2} \cos(k)]$	145
D	Proof of the Poisson distribution for the integrated current in the ZRP	146
References		150

E Survival time of the condensate in the ZRP	151
References	155

Synopsis

(A) Introduction

Nonequilibrium phenomena abound in nature. In a class of systems, a nonequilibrium stationary state is maintained by driving a macroscopic current of a conserved quantity through the system, e.g., an electrical resistor connected to a battery. For a system in thermal equilibrium at temperature T , the stationary state occurs with the Boltzmann-Gibbs measure: if \mathcal{H} is the system Hamiltonian, the probability distribution over the configuration space is proportional to $e^{-\mathcal{H}/T}$. Such a measure, however, does not hold for a system out of equilibrium in which case, the stationary state measure is to be obtained by solving the Master equation describing the time evolution of the configurations of the system. Such a task proves to be daunting for a general many-particle interacting system, thereby motivating study of simple models with nonequilibrium dynamics for which the stationary state can be obtained relatively simply, e.g., by exploiting symmetries such as translational invariance.

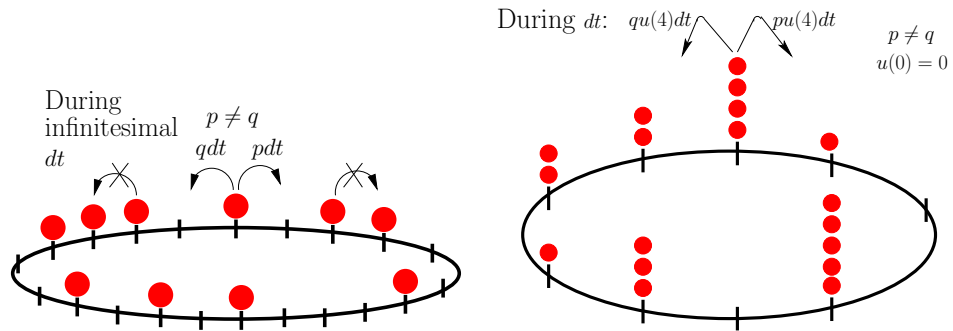


Figure 1: Definition of the ASEP and the ZRP on a one-dimensional ring. The probabilities for a particle from a site to go to its two nearest neighbor sites in a small time dt are also shown in the figure for the two processes. In the ASEP, the disallowed particle movements are marked by crosses. In the ZRP, $u(n)$ denotes the hop rate out of a site with occupancy n .

In recent years, simple models of interacting particles undergoing biased diffusion on a lattice have proved useful in studying current-carrying stationary states. In these models, configurations evolve through a local stochastic dynamics which allows particles to move

preferentially in one lattice direction. Models of this kind exemplify driven diffusive systems [1]. Some of these systems, without tuning of any external parameters, self organize into a stationary state in which certain observables develop power law correlations. This is in contrast to an equilibrium system for which, to observe power law correlations, external parameters like temperature and pressure are to be fine tuned to be at the critical point of a second-order phase transition.

In this thesis, we study two paradigmatic models with driven diffusive dynamics, namely, the asymmetric simple exclusion process (ASEP) [2, 3] and the zero-range process (ZRP) [4], both in one dimension; see Fig. 1 for a schematic view of the two processes. The ASEP involves particles exhibiting biased diffusion on a lattice. Hard core interaction between the particles implies that the lattice sites are either singly-occupied or empty. The ZRP, on the other hand, allows multiple occupancy of particles at sites. Particles hop from site to site with a rate which depends on the occupancy at the departure site. For certain classes of the hop rates, the ZRP shows a phase transition from a low-density disordered phase to a high-density condensed phase where a macroscopic number of particles condenses on to a single site. Both the ASEP and the ZRP model many physical systems. For example, the ASEP dynamics mimics the motion of molecular motors on a one-dimensional microtubule inside living cells, where the ASEP particles represent the motors and the underlying lattice the microtubule [3]. Besides, the ASEP serves as a prototypical nonequilibrium system [5]. The ZRP models, e.g., traffic flows, where the ZRP sites are identified with the cars moving on a single-lane road, while the occupancy of a site maps on to the headway in front of the corresponding car [4]. The condensation transition referred to earlier then manifests itself in the form of jamming in the traffic model.

A microscopic configuration in the stationary state, either equilibrium or nonequilibrium, is characterized by statistical fluctuations of macroscopic observables about their time-independent average values; these typical fluctuations are what have been dealt with in this thesis. In particular, we study the *dynamics of fluctuations in nonequilibrium stationary states* with a focus on *size effects* arising from the finiteness of the underlying lattice.

Finite-size effects could arise from the interaction of system constituents with the boundaries. Such effects can be eliminated by endowing the system with periodic boundary conditions; even then, size effects are observed, e.g., in equilibrium systems close to the critical point of a second-order phase transition. For an infinite system, such a transition is associated with an infinite correlation length and various response functions like the susceptibility, specific heat etc., developing power law singularities. In a finite system, however, these singularities are rounded off and one finds that the system size enters as a parameter into the scaling properties of the response functions [6]. Our studies on size effects in nonequilibrium current-carrying stationary states reveal that the behavior of fluctuations in time is marked by various time regimes, with the crossover times as well as certain correlation functions exhibiting finite-size scaling with the system size. We base our findings on extensive Monte

Carlo simulations, scaling arguments and analytic solutions under suitable approximations.

The principal results of this thesis are the following.

(a) For the one-dimensional ASEP on a periodic lattice of L sites, we study tagged particle correlations; in particular, we show that the variance of the displacement of a tagged particle in time monitors the dynamics of stationary state density fluctuations [7].

- Scaling collapse of simulation data and physical arguments reveal that the variance of the tagged particle displacement, when averaged over initial stationary ensemble and stochastic evolution, has two time scales, $T_1 \sim L$ and $T_2 \sim L^{3/2}$, the former being set by the return time of a kinematic wave of density fluctuations while T_2 is given by the time for this wave to decay. The variance is linear for both the regimes $t \ll T_1$ and $t \gg T_2$, with the proportionality constant for the latter regime scaling with the system size as $\frac{1}{\sqrt{L}}$. In the intermediate regime $T_1 \ll t \ll T_2$, the variance shows pronounced oscillations with period $\sim L$.
- The variance of the tagged particle displacement, starting from an arbitrary but fixed initial configuration, drawn from the stationary ensemble, and averaged over stochastic evolution captures the dissipation of the density fluctuations in time. Here, from scaling collapse of simulation data and supporting physical arguments, we conclude that the problem has only one time scale, $T^* \sim L^{3/2}$ such that the variance behaves as $t^{2/3}$ for $t \ll T^*$ while the behavior is linear for $t \gg T^*$.

(b) For the one-dimensional ZRP on a periodic lattice of L sites, we show that the dynamics of density fluctuations is effectively measured by the variance of the integrated particle current which shows striking differences in behavior in the disordered and the condensed phases [8].

- In the disordered phase, the variance shows damped oscillations in time due to the kinematic wave of density fluctuations; the behavior of the variance in time is similar to that of the tagged particle correlations in the ASEP, discussed above, and hence, is characterized by the two time scales, $T_1 \sim L$ and $T_2 \sim L^{3/2}$.
- In the condensed phase, however, the kinematic wave cannot pass through the condensate; thus, fluctuations do not circulate around. Numerical simulations and strong scaling arguments show that the fluctuation dynamics is governed by the condensate relocation from site to site. The variance of the integrated current has four distinct time regimes, corresponding to two time scales $T_s \sim L^b$ and $T_r \sim L^2$, where $b > 2$ is a parameter defining the hop rate in the ZRP. The time scale T_s measures the characteristic time for which the condensate stays on one site while T_r sets the scale over which the condensate relocates from one site to another.

Below, we give a detailed description of the problems studied and the results obtained.

(B) Results for the asymmetric simple exclusion process (ASEP)

We consider the ASEP on a one-dimensional periodic lattice of L sites. N indistinguishable hard core particles are distributed over the lattice sites with each site either singly-occupied or empty. The system evolves according to a stochastic dynamics: during an infinitesimal time interval dt , a particle attempts to hop to the site to its right with probability pdt , to the left neighboring site with probability qdt , and continues to occupy the original site with probability $1 - (p + q)dt$; see Fig. 1. The attempted hop is successful only if the sought site is empty before the hop. For the totally asymmetric simple exclusion process (TASEP), the motion of the particles is entirely in one direction, i.e., $p = 1, q = 0$ or, vice versa. Note that with $p = q$, each particle moves symmetrically to the left and to the right. The model then reduces to the symmetric Simple Exclusion Process (SEP), an equilibrium model of hard core particles diffusing on a lattice.

In the limit $t \rightarrow \infty$, a system with the ASEP dynamics settles into a nonequilibrium stationary state in which all configurations have the same weight [2]. In the stationary state, the ASEP supports a steady current of particles whose mean value is given by $J = (p - q)\rho(1 - \rho) + O(\frac{1}{L})$, where $\rho = \frac{N}{L}$ is the particle density. Correspondingly, the mean velocity of a particle in the stationary state, given by $v_P = \frac{J}{\rho}$, equals $v_P = (p - q)(1 - \rho) + O(\frac{1}{L})$. Besides particle motion, there is also a motion associated with the coarse-grained density fluctuations in the stationary state of the ASEP. It is well known from a hydrodynamic treatment of the density fluctuations that on a coarse-grained level, density fluctuations are transported as a kinematic wave with velocity $v_K = \frac{\partial J}{\partial \rho}$ [9]. For the ASEP, $v_K = (p - q)(1 - 2\rho) + O(\frac{1}{L})$. Thus, relative to the average drift of the particles, the density fluctuations ‘slide’ with velocity $v_K - v_P$. We refer to this relative motion as the sliding density fluctuations (SDF). Stochasticity and nonlinearity in the dynamics lead to dissipation of the density profile so that the wave of fluctuations ultimately dies down in time.

The ASEP density profile in the stationary state can be mapped to a growing interface in the Kardar-Parisi-Zhang (KPZ) universality class [10]. The mapping involves interpreting the presence of a particle at a site in the ASEP with an up slope at the same site in the equivalent interface, while a vacancy maps on to a down slope in the interface model [2, 11]. The flipping of a hill of the interface to a valley then corresponds to the motion of a particle in the ASEP. Through this mapping, the density fluctuations in the ASEP are mapped on to the height fluctuations of the interface. On a coarse-grained level, the interface evolution is governed by the KPZ time-evolution equation. From the scaling properties of the KPZ equation, it then follows that in the ASEP, in the scaling limit of large distances and long times, density fluctuations at a spatial point grow with time as $t^{1/3}$, with an autocorrelation time that scales with the system size as $L^{3/2}$ [10].

- In order to study the dynamics of stationary state density fluctuations, we monitor the variance $\sigma^2(L, t)$ of the displacement of a *tagged* particle around its average in time t , starting from the stationary ensemble of configurations. Some asymptotic results for

$\sigma^2(L, t)$ as a function of time were already known in the literature prior to our studies [12]. We provide a complete characterization of the behavior of $\sigma^2(L, t)$ in time. Our studies show that the behavior of $\sigma^2(L, t)$ as a function of time is governed by the motion of density fluctuations around the system as a dissipating kinematic wave and can be characterized by two time scales $T_1 \sim L$ and $T_2 \sim L^{3/2}$, as shown in Fig. 2. Thus, there are three distinct time regimes, namely, (i) $t \ll T_1$, (ii) $T_1 \ll t \ll T_2$, and (iii) $t \gg T_2$. The associated behavior of $\sigma^2(L, t)$ in each of the regimes is summarized below.

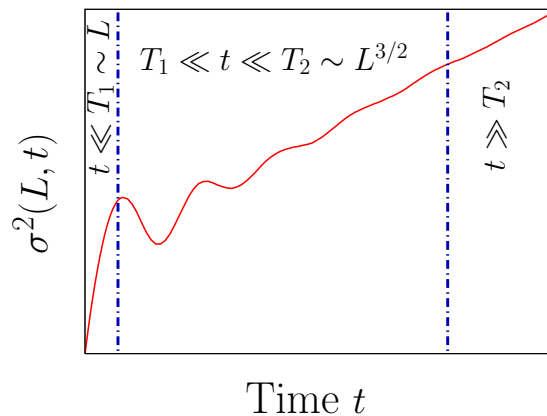


Figure 2: Schematic plot showing the behavior of the tagged particle correlations $\sigma^2(L, t)$ in the ASEP on a periodic lattice of finite size L .

(i) $t \ll T_1$. In this regime, the variance $\sigma^2(L, t) \sim D_0 t$, where $D_0 = (p - q)(1 - \rho)$. In the frame of the density fluctuations, the tagged particle with an average velocity $v_P - v_K$ traverses in time t a sequence of density fluctuations over a distance $(v_P - v_K)t$, with each fluctuation adding a random noise to its motion. The variance $\sigma^2(L, t)$ is thus proportional to t for large t , by virtue of the central limit theorem. The coefficient of proportionality D_0 can be derived using the above picture of drift of the tagged particles relative to the density fluctuations [13].

(ii) $T_1 \ll t \ll T_2$. Here, the quantity $\sigma^2(L, t)$ oscillates as a function of time. The amplitude of oscillations is proportional to the system size L while the time period of oscillations is $T = L/u$, where u is the average drift velocity of the particles relative to the kinematic velocity of the density fluctuations: $u = v_P - v_K$. The oscillations are due to the tagged particle returning to its initial environment at an interval of time equal to T . The lower envelope of the oscillations is determined by the dissipation of the initial density profile. Since density fluctuations in the ASEP grow with time as $t^{1/3}$, it then follows that the lower envelope behaves in time as $t^{2/3}$.

(iii) $t \gg T_2$. In this late time regime, the initial density profile has dissipated away completely [14]. Thus, the fluctuations $\sigma^2(L, t)$ are entirely due to the diffusive motion

of the center-of-mass: $\sigma^2(L, t) \sim D(L)t$ with $D(L) \sim \frac{1}{\sqrt{L}}$. The scaling of $D(L)$ with the system size L is obtained by matching the behavior of $\sigma^2(L, t)$ across T_2 .

The behavior of $\sigma^2(L, t)$ in time can be put into the following scaling form.

$$\sigma^2(L, t) \sim Lg\left(\frac{t}{L}, \frac{t}{L^{3/2}}\right), \quad (1)$$

where the scaling function $g(u, v)$ behaves in the following manner. $g(u, v) \sim v$ for $v \gg 1$, while, $g(u, v) \sim u$ for $u \ll 1$. For $u \gg 1, v \ll 1$, the scaling function behaves as $g(u, v) \sim v^{2/3}$.

- In measuring the fluctuations, if one does not start from the stationary ensemble, but instead from an arbitrary but *fixed* configuration drawn from the stationary ensemble, the corresponding variance $s^2(L, t)$ of the tagged particle displacement behaves very differently from $\sigma^2(L, t)$. Since, in measuring $s^2(L, t)$, one uses the same initial condition, the tagged particle moves through the same sequence of density fluctuations in every measurement. Nevertheless, the dissipation of the density profile is different for different histories, and $s^2(L, t)$ captures this.

The quantity $s^2(L, t)$ was first considered by van Beijeren who obtained its behavior for an infinite system: $s^2(t) \equiv \lim_{L \rightarrow \infty} s^2(L, t) \sim t^{2/3}$ [15]. For a finite system, we find that the time variation of $s^2(L, t)$ can be characterized by a single time scale $T^* \sim L^{3/2}$ (see Fig. 3(a)). Thus, there are two distinct time regimes in the behavior of $s^2(L, t)$, namely, $t \ll T^*$ and $t \gg T^*$; the associated behavior in each of these regimes is given below.

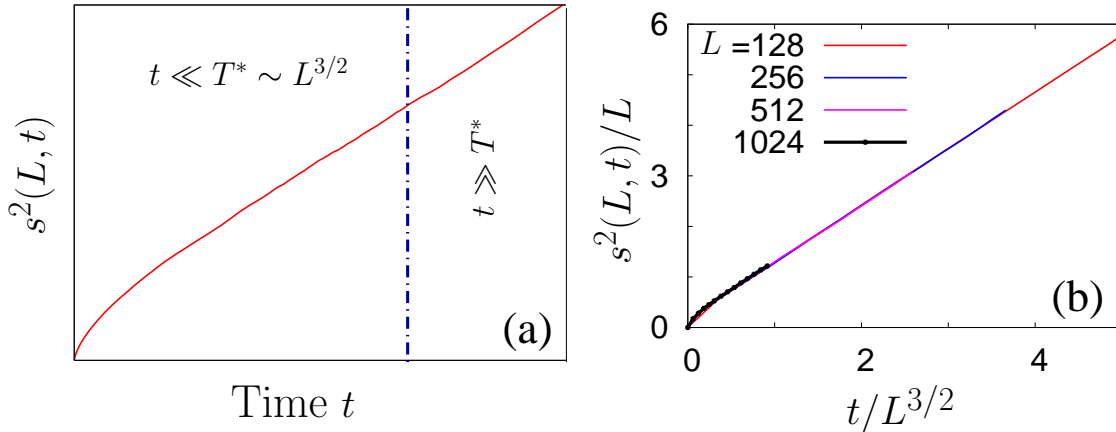


Figure 3: (a). Schematic plot showing the behavior of the tagged particle correlations $s^2(L, t)$ when starting from a fixed initial configuration, drawn from the stationary ensemble. (b) Scaling of $s^2(L, t)$ for different system sizes in accordance with Eq. 2. The data are obtained from Monte Carlo simulations. Here, the particle density $\rho = 0.25$, the parameter $p = 1$, while $q = 0$. The system sizes are marked in the figure.

(i) $t \ll T^*$. In this regime, $s^2(L, t) \sim t^{2/3}$. This follows from the fact that typical density fluctuations in the ASEP grow with time as $t^{1/3}$.

(ii) $t \gg T^*$. Here, $s^2(L, t) \sim D(L)t$ with $D(L) \sim \frac{1}{\sqrt{L}}$. This behavior is due to the diffusive motion of the center-of-mass of the system.

The behavior of $s^2(L, t)$ in time can be put into the following scaling form.

$$s^2(L, t) \sim Lf\left(\frac{t}{L^{3/2}}\right), \quad (2)$$

where the scaling function $f(u)$ behaves in the following manner. $f(u) \sim u^{2/3}$ for $u \ll 1$, while, $f(u) \sim u$ for $u \gg 1$. The validity of the scaling form in Eq. 2 is confirmed by the scaling plot of Fig. 3(b).

- The tagged particle correlations in the ASEP can be translated directly into the height fluctuations of a nonequilibrium growing interface in the KPZ universality class [10]. This is achieved by interpreting the particle label as horizontal coordinate for the interface, while the particle location maps on to the local height of the interface [16] (Note that this procedure of mapping is different from that discussed previously, where the ASEP density profile maps on to the interface profile in the KPZ class). The resultant time-evolution equation for the interface is the usual KPZ equation, augmented by a drift term which accounts for the SDF. For the symmetric Simple Exclusion Process, the corresponding time-evolution equation for the equilibrium interface is given by the Edwards-Wilkinson (EW) equation [17]. Our studies show that both the EW and the KPZ fixed points are unstable with respect to the SDF fixed point, a flow towards which is generated on adding a drift term to the EW and the KPZ time-evolution equations. This means that the least amount of drift in either the KPZ or the EW equations would make the large distance long time behavior of fluctuations for these equations be determined by the SDF fixed point.
- The KPZ equation with the drift term, written in terms of the height variables for the interface, is nonlinear and hence, cannot be solved exactly. Hence, we consider the equation in the linear approximation, by setting the nonlinear term to zero. Thus, we get the EW equation with the drift term, which we solve exactly for $\sigma^2(L, t)$ and $s^2(L, t)$. Our analytical solution captures not only the essential qualitative features seen in these two quantities for the ASEP, but also the scaling properties of the tagged particle correlations in the ASEP. Moreover, we show that the EW equation with the drift term is an exact coarse-grained description of two specific microscopic models of interacting particles, the asymmetric random average process [18] and the Katz-Lebowitz-Spohn model [19] at a specific value of the temperature. The former generalizes the ASEP to a continuum while the later adds an Ising interaction to the hard core exclusion between particles in the ASEP. Our analytic solution quantitatively describes the behavior of the tagged particle correlations for these two models.

(C) Results for the zero-range process (ZRP)

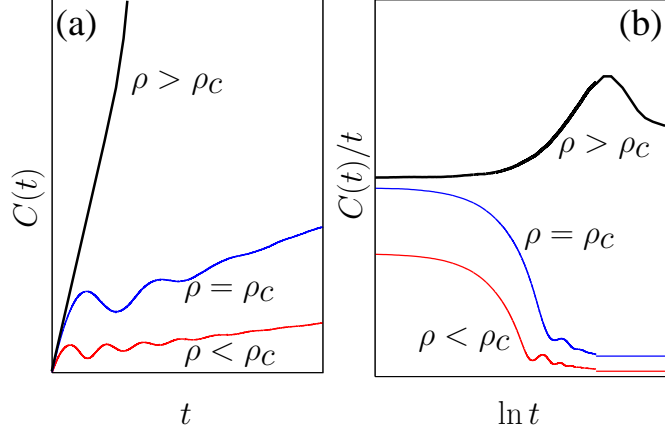


Figure 4: (a). Schematic plot of the integrated current fluctuations $C(t)$ across a bond in the stationary state of the ZRP as a function of time t in the disordered phase ($\rho < \rho_c$), at the critical point ($\rho = \rho_c$) and in the condensed phase ($\rho > \rho_c$). (b). Schematic plot of $C(t)/t$ as a function of t in all the phases.

The ZRP involves N particles of unit mass on a one-dimensional periodic lattice of L sites. Arbitrary occupancy of particles is allowed at any site. In an infinitesimal time dt , a particle hops out of a randomly selected site i with occupancy n_i and goes to the right neighboring site $i + 1$ with probability $pu(n_i)dt$, while it goes to the left neighboring site $i - 1$ with probability $qu(n_i)dt$, where $p + q = 1$; see Fig. 1. For totally asymmetric particle motion (i.e., $p = 1, q = 0$ or, vice versa), the ZRP can be mapped to a generalization of the totally asymmetric simple exclusion process (TASEP) by interpreting the ZRP sites as particles in the TASEP, while the particles at a ZRP site become holes preceding the corresponding TASEP particle [4]. The hop rate $u(n)$ for a TASEP particle, now a function of the headway to the next particle, induces a long-ranged particle hopping.

At long times, a system with the ZRP dynamics reaches a nonequilibrium stationary state which has a factorized form in that the probability of any configuration is given by a product of factors, one for each site of the system; the factor is uniquely determined by the hop rate $u(n)$. We consider the hop rate $u(n) = 1 + b/n$ with $b > 2$ for which the system undergoes a nonequilibrium phase transition [4]. As the particle density ρ crosses the critical value $\rho_c = 1/(b - 2)$ [20], a low-density disordered phase with mass of $O(1)$ at each site evolves to a high-density condensed phase where a macroscopic collection of particles of average mass $(\rho - \rho_c)L$ condenses onto a randomly selected site, while the remaining sites have the average mass ρ_c .

To address the dynamics of density fluctuations in the ZRP, we examine the variance $C(t)$ of the integrated particle current across any bond in the stationary state. We find

that $C(t)$ shows strong differences in behavior in the disordered and the condensed phases, reflecting very different underlying physical processes in the two phases (Fig. 4). The main results for the dynamics in various phases are summarized below.

- *Disordered phase:* The behavior of $C(t)$ in this phase is identical to that of the tagged particle correlation in the ordinary ASEP, discussed in Section (B). There are two time scales $T_1 \sim L$, set by the circulation time of a kinematic wave of density fluctuations, and $T_2 \sim L^{3/2}$, given by the time taken by this wave to decay. Also, $C(t)$ obeys the scaling form of Eq. 1.
 - (i) $t \ll T_1$. Here, $C(t)$ grows linearly in time. This follows from the result that in this time regime, the integrated current across any bond is Poisson-distributed. We prove this result [21] by noting that the population at a ZRP site undergoes a time-reversible birth-death process, and invoking Burke's theorem from queuing theory [22].
 - (ii) $T_1 \ll t \ll T_2$. In this regime, $C(t)$ oscillates as a function of time due to density fluctuations moving around the system as a dissipating kinematic wave. A measure of the growth of dissipation in time is given by the lower envelope of the oscillations, which behaves as $t^{2/3}$.
 - (iii) $t \gg T_2$. Here, the variance grows diffusively: $C(t) \sim D(L)t$, where $D(L) \sim \frac{1}{\sqrt{L}}$, as for the ordinary ASEP, discussed in Section (B).
- *Critical point:* At the critical density ρ_c , the variance behaves differently when $2 < b \leq 3$ and when $b > 3$. For $2 < b \leq 3$, the kinematic wave speed can be computed to be zero [20]. Thus, there is no moving kinematic wave. Hence, the integrated current is Poisson-distributed, implying that the variance $C(t)$ continues to grow linearly in time. For $b > 3$, however, the kinematic wave speed is non-zero and the variance $C(t)$ oscillates in time as for $\rho < \rho_c$, with return time T_1 and decay time T_2 of the kinematic wave.
- *Condensed phase:* For $\rho > \rho_c$, a finite fraction of the total mass (the condensate) resides on one site for the characteristic survival time $T_s \sim (\rho - \rho_c)^{b+1} L^b$ [23]. It then relocates to another site over the relocation time scale $T_r \sim (\rho - \rho_c)^2 L^2$, as discussed below. The behavior of $C(t)$ in this phase is best depicted by plotting $C(t)/t$ as a function of time; as shown schematically in Fig. 5(a), the behavior is characterized by the two time scales T_s and T_r , with four distinct time regimes detailed below.
 - (i) $t \ll T_s$. Here, $C(t)/t$ equals 1, with a mild upward deviation for longer times.
 - (ii) $t \sim T_s$. In this regime, $C(t)/t$ rises rapidly in time. The collapse of the rise times in the scaling plot of Fig. 5(b) confirms the existence of the time scale T_s .
 - (iii) $t \gtrsim T_s + T_r$. Here, $C(t)/t$ falls slowly in time.
 - (iv) $t \gg T_s + T_r$. Here, $C(t)/t$ begins to approach a size-dependent constant: $C(t) \sim [L^{-\theta}(\rho - \rho_c)^{-(b+1)} + 1]t$, with $\theta = b - 1$ for $b > 3$. For b between 2 and 3, we find that

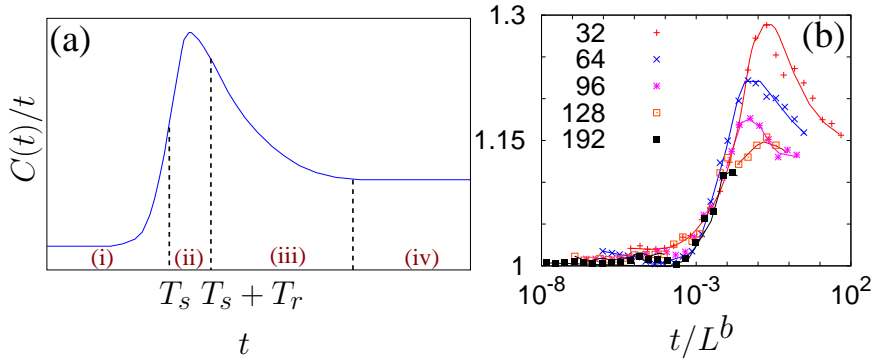


Figure 5: (Color online) (a) $C(t)/t$ as a function of t in the condensed phase, shown schematically with various regimes (see text). (b) Scaling of the rise time T_s with t/L^b for $b = 3$. The particle density $\rho = 4$, the parameters $p = 1, q = 0$. The data points, obtained from MC simulations, are connected by smooth curves.

$$\theta = (b^2 - b - 2)/(b - 1).$$

Features (ii), (iii) and (iv) result from enhanced fluctuations due to the relocation of the condensate which proceeds through the following dynamics. The largest mass in the stationary state fluctuates in time about the average value $M_0 = (\rho - \rho_c)L$. These fluctuations may build up in time, and over the time scale T_s , the largest mass is depleted to $\sim M_0/2$, while a mass $\sim M_0/2$ also builds up at another site. Subsequent to this, two sites with mass $\sim M_0/2$ exchange particles between themselves resulting in relatively rapid (of the order of 1 Monte Carlo time step) alternating relocations of the largest mass from one site to the other. The difference of masses on these two sites performs an unbiased random walk in time until fluctuations populate one of the sites to $\sim M_0$ at the expense of the other, which happens over the time scale $T_r \sim (\rho - \rho_c)^2 L^2$.

The survival probability distribution $P_s(\tau)$ of the largest mass, obtained by computing the distribution of the time interval τ between successive relocations in Monte Carlo simulations, is shown in Fig. 6(a). $P_s(\tau)$ has two parts (i) a power law part $\sim \tau^{-3/2}$ and (ii) another part, which corresponds to the hump in Fig. 6(a), and has the scaling form $(\rho - \rho_c)^{-(b+2)} L^{-(b+1)} f(\tau/T_s)$ (confirmed by the scaling of the hump with different system sizes as shown in Fig. 6(b)). The power law part holds for times when the two sites with mass $\sim M_0/2$ compete to hold the largest mass. The random walk argument of the preceding paragraph predicts a $\tau^{-3/2}$ decay, since $P_s(\tau)$ then stands for the probability for the random walker to cross the origin for the first time. The second part in $P_s(\tau)$ arises from the relatively long time for which the condensate is stationary on one site.

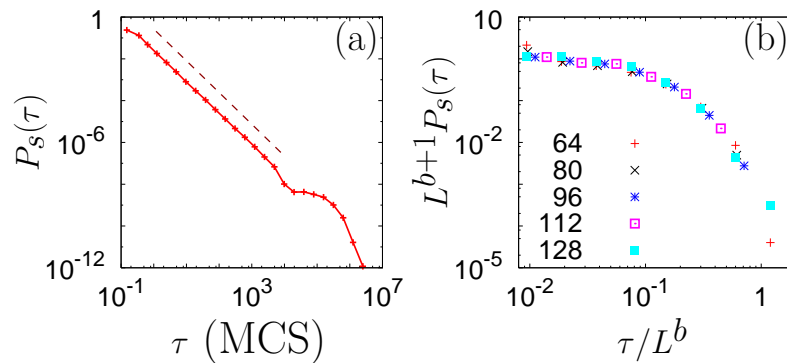


Figure 6: (a). Survival probability distribution $P_s(\tau)$ of the largest mass in the condensed phase of the ZRP. The time interval τ between successive relocations of the largest mass is measured in Monte Carlo Steps (MCS). The system size $L = 128$, and the parameter $b = 3$, the particle density $\rho = 4$, the parameters $p = 1, q = 0$. The dashed line is a guide to the eye for the part of $P_s(\tau)$ behaving as $\tau^{-3/2}$. (b). Scaling of the hump in $P_s(\tau)$ with system size L . The data are obtained from Monte Carlo simulations for the same set of parameter values as in (a).

(D) Conclusions

In this thesis, we considered the effect of finite size on the dynamics of fluctuations in nonequilibrium current-carrying stationary states, pursued within the ambit of two paradigmatic models, the asymmetric simple exclusion process (ASEP) and the zero-range process (ZRP). We showed how size effects result in interesting dynamical properties like oscillations in tagged particle correlations, modified dynamical properties across a nonequilibrium phase transition. We characterized all the relevant time scales in the dynamics of fluctuations for both the ASEP and the ZRP, and understood the resulting dynamical properties in terms of the underlying physical processes.

Bibliography

- [1] B. Schmittmann and R. K. P. Zia, in *Phase Transitions and Critical Phenomena*, edited by C. Domb and J. L. Lebowitz (Academic, London, 1995), Vol. 17.
- [2] T. M. Liggett, *Interacting Particle Systems* (Springer-Verlag, New York, 1985).
- [3] R. A. Blythe and M. R. Evans, *J. Phys. A* **40**, R333 (2007).
- [4] M. R. Evans and T. Hanney, *J. Phys. A* **38**, R195 (2005).
- [5] O. Golinelli and K. Mallick, *J. Phys. A* **39**, 12679 (2006).
- [6] M. E. Fisher, in *Critical Phenomena, Proc. 51st Enrico Fermi Summer School*, edited by M. S. Green (Academic Press, New York, 1972).
- [7] S. Gupta, S. N. Majumdar, C. Godrèche, and M. Barma, *Phys. Rev. E* **76**, 021112 (2007).
- [8] S. Gupta, M. Barma, and S. N. Majumdar, *Phys. Rev. E Rapid Comm.* **76**, 060101 (2007).
- [9] M. J. Lighthill and G. B. Whitham, *Proc. R. Soc. London A* **229**, 281 (1955).
- [10] M. Kardar, G. Parisi, and Y. C. Zhang, *Phys. Rev. Lett.* **56**, 889 (1986).
- [11] M. Plischke, Z. Racz, and D. Liu, *Phys. Rev. B* **35**, 3485 (1987).
- [12] A. De Masi and P. A. Ferrari, *J. Stat. Phys.* **38**, 603 (1985); R. Kutner and H. van Beijeren, *ibid.* **39**, 317 (1985); B. Derrida, M. R. Evans, and D. Mukamel, *J. Phys. A* **26**, 4911 (1993); B. Derrida and K. Mallick, *ibid.* **30**, 1031 (1997).
- [13] M. Barma, *J. Phys. A* **25**, L693 (1992).
- [14] D. Dhar, *Phase Transitions* **9**, 51 (1987); L. -H. Gwa and H. Spohn, *Phys. Rev. A* **46**, 844 (1992).
- [15] H. van Beijeren, *J. Stat. Phys.* **63**, 47 (1991).
- [16] S. N. Majumdar and M. Barma, *Phys. Rev. B* **44**, 5306 (1991).

-
- [17] J. M. Hammersley, in *Proceedings of the fifth Berkeley Symposium on Mathematical Statistics and Probability*, edited by L. M. Le Cam and J. Neyman (University of California Press, Berkeley, 1967); S. F. Edwards and D. R. Wilkinson, Proc. R. Soc. London, Ser A **381**, 17 (1982).
- [18] J. Krug and J. Garcia, J. Stat. Phys. **99**, 31 (2000); R. Rajesh and S. N. Majumdar, *ibid.* **99**, 943 (2000).
- [19] S. Katz, J. L. Lebowitz, and H. Spohn, Phys. Rev. B **28**, 1655 (1983); J. Stat. Phys. **34**, 497 (1984).
- [20] S. Großkinsky, G. Schütz, and H. Spohn, J. Stat. Phys. **113**, 389 (2003); C. Godrèche, J. Phys. A **36**, 6313 (2003).
- [21] We are grateful to J. Lebowitz and E. Speer for pointing out the applicability of the Burke's theorem to the ZRP.
- [22] P. J. Burke, Oper. Res. **4**, 699 (1956); E. Reich, Ann. Math. Stat. **28**, 768 (1957).
- [23] C. Godrèche and J. M. Luck, J. Phys. A **38**, 7215 (2005).

Publications

- *Tagged particle correlations in the asymmetric simple exclusion process: Finite-size effects,*
S. Gupta, S. N. Majumdar, C. Godrèche, and M. Barma, Phys. Rev. E **76**, 021112 (2007).
- *Finite-size effects on the dynamics of the zero-range process,*
S. Gupta, M. Barma, and S. N. Majumdar, Phys. Rev. E Rapid Comm. **76**, 060101 (2007).

Chapter 1

Introduction

“Begin at the beginning,” the King said, very gravely, “and go on till you come to the end: then stop.”

Lewis Carroll

In this thesis, we are concerned with how the dynamics of fluctuations in driven diffusive systems gets affected by the finiteness of the system size. Driven diffusive systems encompass a large number of examples in which the constituent particles of the system, in addition to a diffusive motion, have a systematic drift due to an external field. In the limit of long times, these systems settle into a nonequilibrium stationary state. This chapter begins with viewing nonequilibrium *vis-à-vis* equilibrium stationary states. This is followed in Section 1.2 by a discussion on driven diffusive systems, in particular, the two paradigmatic examples in this class, the asymmetric simple exclusion process (ASEP) and the zero-range process (ZRP). In the absence of a general framework to analyze nonequilibrium fluctuations, our studies of size effects are done within the ambit of the ASEP and the ZRP. We also discuss an exclusion process with extended objects, where our studies reveal that size effects, arising from the finite extent of the system constituents, affect the spatial correlation functions in an interesting way. This is followed by a summary, in Section 1.3, of the universality classes associated with fluctuations in nonequilibrium stationary states. Next, in Section 1.4, we discuss finite-size effects in equilibrium stationary states. In the concluding section, we provide a brief summary of our main results on size effects in nonequilibrium stationary states, besides giving the overall plan of the thesis.

1.1 Nonequilibrium *vis-à-vis* equilibrium stationary states

In daily life, we come across a wide variety of systems which evolve under the influence of an external field. Some commonplace examples are conductors in an electric field, fluids under a pressure gradient, heat conductors subject to a temperature gradient, and many others. These systems are typically not kept in isolation, but, rather, in constant interaction with the environment. Instead of modeling the environment and its explicit interaction with the

system, a simplified approach often adopted is to replace the effect of the environment by some stochasticity in the evolution of the system. The underlying principle behind such an approach is the assumption that the environment represents the ‘fast’ degrees of freedom which equilibrate on a much shorter time scale compared to the ones governing the evolution of the system, which, therefore, only serve to drive noise into the system. The dynamics of the system being stochastic, it calls for a statistical description, wherein the system, at every instant during its evolution, is characterized by the probability distribution over the space of its microscopic configurations [1].

In some of the example systems, cited above, the probability measure over configurations converges, at long times, to a well-defined distribution, constant in time; then the system is said to have attained a stationary state. In such a state, due to the external field, a nonvanishing macroscopic current of a conserved quantity like particle density, etc., flows through the system, making the stationary state a generic nonequilibrium one. By contrast, an equilibrium stationary state does not support any macroscopic current through the system. To exemplify this point, consider a system in contact with two heat baths placed at the opposite ends of the system. If the temperatures of the two baths are equal, the system eventually relaxes to an equilibrium stationary state in which the average temperature of the system equals that of the baths, and there is no net flow of energy from one bath to the other through the system. On the other hand, a slight difference in the temperature of the two baths sets up a steady energy flux through the system at long times, and the system is said to have settled into a nonequilibrium stationary state.

The presence of a macroscopic current in a nonequilibrium stationary state is manifested by having a net nonzero probability current between some or all microscopic configurations. In models of nonequilibrium systems, e.g., in those involving aggregation and fragmentation of masses, relevant to explaining formation of colloidal suspensions and gels [2], there is no macroscopic mass current, but the dynamics generates a net nonzero probability current between configurations in the stationary state. For an equilibrium stationary state, there is no net probability current between any pair of configurations [3]. The latter fact, encoded in the condition of detailed balance, is often identified with the statement that the dynamics, governing the evolution of an equilibrium system, necessarily obeys time-reversal invariance, which, however, is broken in a nonequilibrium stationary state [3]. By time-reversal invariance, what is meant is that the probability of occurrence of a certain sequence of configurations during the evolution of the system in a given time is exactly equal to the probability of occurrence of the time-reversed sequence; this statement is proved easily on invoking the condition of detailed balance [3]. To summarize, a net nonzero probability current in the configuration space is what distinguishes a nonequilibrium stationary state from an equilibrium one.

Traditionally, an equilibrium system is defined by the energy function $E(C)$ specified for every microscopic configuration C . An equilibrium stationary state is well described by the Gibbs-Boltzmann formalism of statistical mechanics. Thus, the stationary state

weight of any configuration C is proportional to $e^{-E(C)/T}$, where T is the temperature at which the system is in equilibrium. For an equilibrium system, the dynamics of transition from configuration to configuration is constructed on an *ad hoc* basis, being guided by the principle that the dynamics should lead to an equilibrium stationary state at long times, and hence, must satisfy the condition of detailed balance described above [4].

A nonequilibrium system, on the other hand, is defined by specifying the dynamical rules following which the system evolves from one configuration to another. A nonequilibrium stationary state is not described by the Gibbs-Boltzmann measure. In a Master equation approach, one defines a vector space whose basis vectors are the possible configurations of the system. Then, one defines \mathcal{P} to represent the column vector of the probabilities of all the configurations of the system. The time evolution of \mathcal{P} is governed by the Master equation, given by

$$\frac{\partial \mathcal{P}}{\partial t} = \mathcal{W}\mathcal{P}, \quad (1.1)$$

where \mathcal{W} is the transition matrix whose elements are given by the rates of transitions between the configurations of the system [3]. In the stationary state, the probabilities of occurrence of configurations become time-independent; thus, the stationary state is obtained as the solution of the above equation with the left hand side set to zero.

An important feature of a large class of nonequilibrium systems is that they involve an assembly of many constituents which interact with one another, leading to many-body collective effects, and thus, to a whole range of complex and interesting phenomena. In some examples like traffic flows, earthquakes, stock markets, etc., interesting collective effects (e.g., spontaneous formation of jam in traffic flows) emerge out of local interactions of the entities constituting the system. In examples, such as sandpile models and river networks, the system self-organizes itself into a critical state with self-similar structures and complex scaling behavior. For a generic system in this class, in view of the many-body character, it proves formidable to obtain even the stationary state distribution by solving the Master equation, Eq. 1.1. This problem is circumvented partially by construction of specific model systems, for which the stationary state can be obtained rather simply, e.g., by exploiting various symmetries following from the conservation laws obeyed by the system during its dynamical evolution. These models should be simple enough to allow an exact and thorough mathematical analysis, yet exhibit interesting phenomenology to be of physical relevance. Two such models much studied in recent times are the asymmetric simple exclusion process and the zero-range process, both belonging to the general class of driven diffusive systems which we now discuss.

1.2 Driven diffusive systems

The term driven diffusive system applies to a wide variety of systems involving many interacting particles, where each particle has a diffusive motion in addition to an overall systematic drift [5]. The diffusive motion results from conservation of particles in the bulk,

tending to equalize local variation in density, while the systematic drift is a result of an external field acting on the system which tends to drive the particles preferentially in one direction, thereby setting up a net current through the system. The local particle current contains a diffusive component, a systematic part due to the external field, and a noise reflective of the underlying stochastic dynamics. Thus, in this class of systems, the attribute ‘driven’ refers to bulk drive and not specifically to the drive at the boundaries, which may independently be set up. For sufficiently small boundary drive, and with no bulk drive, the system may be considered to have been perturbed slightly away from equilibrium; this is sensible, since, locally, the net current is very small, and hence, the system is close to thermodynamic equilibrium. However, such a scheme would not work in the presence of a bulk drive because, even locally, there is a significant current of particles through the system.

A major development in the study of driven diffusive systems happened with the work of Katz, Lebowitz and Spohn [6]; see also [5]. Motivated partly by the physics of fast ionic conductors [7], and mainly by an interest in nonequilibrium stationary states, they modified the equilibrium dynamics of the well-known Ising model through introduction of an external bias. A lattice model of the ionic conductor is related to the Ising model on identifying the presence of an ion on a lattice site with an up-spin, while a down-spin may be taken to represent the absence of the ion on the site. For the model that Katz, Lebowitz and Spohn developed, called the KLS model, they started with the Ising model with nearest-neighbor ferromagnetic interaction between spins, and which, at a given temperature, evolves under the exchange of nearest-neighbor pairs of opposite spins. Then they introduced an external field which causes preferential exchange of one type of spin pairs to the other, i.e., an up spin would preferentially exchange with a next neighbor down spin in the direction of the field than in the opposite direction. In the absence of the field, the system eventually relaxes to an equilibrium stationary state, while the presence of the external field drives it into a nonequilibrium stationary state. On a two-dimensional lattice, even in the presence of a field, the system displays the same qualitative features as seen in its absence, i.e., a second-order phase transition from a high-temperature disordered phase across a critical temperature to a low-temperature phase-separated phase. However, unlike the equilibrium case, the spatio-temporal correlations of fluctuations in various quantities display power-law behaviors at all finite temperatures above the critical temperature. This came as a great surprise in the backdrop of our acquired wisdom of equilibrium systems where such power-law behaviors are usually observed when the system is fine-tuned to be precisely at the critical point. Arguments have been adduced to show that such power laws in the behavior of fluctuations are generic to nonequilibrium systems under suitable conditions, i.e., in Ref. [8], the authors, by studying noisy, nonequilibrium Langevin models, concluded that systems with conserving deterministic dynamics and noise that violates the conservation law always have spatial and temporal correlations decaying as power laws under generic conditions. On the other hand, for systems with both conserving deterministic dynamics

and conserving noise, the requirement to see power-law behavior in correlations is spatial anisotropy in the system.

In the next two subsections, we discuss respectively two paradigmatic examples of driven diffusive systems, the asymmetric simple exclusion process and the homogeneous zero-range process. We also discuss the exclusion process with extended objects.

1.2.1 The asymmetric simple exclusion process

The asymmetric simple exclusion process (ASEP) in one dimension involves biased diffusion of hard core particles on a lattice [9, 10]. The process evolves by a stochastic Markovian dynamics. The bias simulates the effect of an external field. The ASEP is the infinite temperature limit of the KLS model, discussed above. The ASEP serves as a prototypical example of driven diffusive systems, and is one of the very few examples for which the stationary state distribution of configurations is known exactly. Over the years, the ASEP has played a fundamental role in unveiling many surprising features of nonequilibrium stationary states, e.g., boundary-induced phase transition in one dimension [11]. Many exact results have been obtained for the ASEP, using two complementary approaches, the Matrix Product technique and the Bethe Ansatz. In the Matrix Product technique, the stationary state weight of configurations is obtained as the matrix element of a product of a set of noncommuting matrices (for a review, see [12, 13]); this technique has proved to be extremely useful in computation of various stationary state properties of the ASEP like the equal-time correlation functions, current fluctuations [14] and large deviation functionals [15]. Recently, such large deviation functionals have been argued to provide a possible way of extending the notion of free energy to nonequilibrium systems [16]. In the Bethe Ansatz technique, the Markov matrix encoding the stochastic dynamics of the ASEP is written in terms of the Pauli matrices; this way, the ASEP becomes equivalent to a non-Hermitian spin chain of the XXZ type. The Bethe Ansatz is then employed to derive spectral information about the evolution operator, such as the spectral gap [17, 18, 19, 20, 21].

On the application side, the ASEP models diverse physical situations: transport of macromolecules through thin vessels [22], traffic flow [23], surface growth [24, 25], and molecular motors [26].

1.2.2 The zero-range process

The homogeneous zero-range process (ZRP) involves biased hopping of particles between nearest neighbor sites of a periodic lattice with a rate which is a function solely of the occupancy at the departure site. Here, the hop rate function is the same for all sites. The process was introduced by Spitzer as an example of interacting Markov processes [9]. The stationary state measure of the process is known exactly in any dimension, for any choice of the hop rates, and even in the presence of quenched disorder, thereby offering an opportunity for analyzing many stationary state properties of the ZRP. For certain classes

of the hop rates, the ZRP, as a function of the particle density, undergoes a continuous phase transition from a low-density disordered phase with uniform average density to a condensed phase at high density, where a finite fraction of particles accumulates on a single site. In view of the condensation phenomena, the ZRP or modifications thereof has been applied to model many physical situations, e.g., wealth condensation in macroeconomics [27], jamming in traffic [28, 29], gelation in networks [30, 31], and many others. Besides, it has recently been invoked to provide a criterion for phase separation in one-dimensional driven diffusive systems [32].

1.2.3 The exclusion process with extended objects

The exclusion process with extended objects is a generalization of the ASEP to the case where particles in the ASEP are replaced by objects of finite extent, moving along a lattice in accordance with a stochastic hopping dynamics. The original concept was due to MacDonald *et al.* [33, 34], who were trying to model protein synthesis inside living cells. The synthesis proceeds with the ribosomes moving from codon to codon along the messenger RNA (m-RNA), reading off genetic information, and thereby, generating the protein step-wise. In the exclusion process with extended objects, the moving ribosomes are modelled by the extended objects, while the lattice sites represent the codons. The finite extent of the objects is to account for the blocking of several codons by a single ribosome. Steric hindrance, excluding overlap of ribosomes, necessitates the exclusion constraint, whereby a single lattice site can be occupied by at most one extended object at a time. Ribosomes, attaching to the m-RNA to initiate the protein synthesis, and detaching at the point of termination are modelled with open boundaries, whereby the extended objects enter and exit the lattice at the boundaries. Macdonald *et al.* treated the model at the mean-field level in deriving the stationary state density profile [33, 34]. More recently, several authors have studied the process, analyzing the time-dependent conditional probabilities of finding the extended objects on specific sites at a given time, starting with a given initial distribution of them on lattice sites [35], the dynamical exponent [36], the phase diagram of the open system [37, 38, 39, 40], the hydrodynamic limit governing the evolution of density [41], and the effects of defect locations [42]. In this thesis work, we will consider the exclusion process with extended objects on a one-dimensional lattice with periodic boundary conditions. We will show, using a mapping to an equivalent ASEP [43], that many stationary state properties of the model like the two-point correlation functions can be computed in closed form; these functions show characteristic oscillations arising from the finite extent of the extended objects.

1.3 Fluctuations in nonequilibrium stationary states: Universality classes

Fluctuations in an equilibrium stationary state play an important role in determining the bulk properties of the system, particularly close to the critical point of a second-order phase transition. Such a point is associated with a diverging correlation length, which determines the typical scale over which fluctuations in the order parameter characterizing the transition are correlated [44]. The fact that fluctuations get correlated over infinite distances (for a system in the thermodynamic limit) has consequences on several thermodynamic response functions like the specific heat, the susceptibility, etc., showing a power-law divergence near the critical point. Quite remarkably, the exponents characterizing such divergences are the same for transitions in a large number of apparently disparate systems, e.g., the order-disorder critical point in uniaxial magnets, the liquid-gas critical point in a mixture of the two, transition in alloys from a phase, rich in one species to one rich in the other, etc. This universality of critical exponents has been clarified by the renormalization group (RG) theory which predicts that the thermodynamic properties near a critical point depend on a small number of factors like the dimensionality of the system and the symmetries in its Hamiltonian, and are insensitive to the underlying microscopic properties of the system [45]. The key idea behind the RG theory is the observation of a diverging correlation length near a critical point. Subsequently, the RG techniques were applied to understand universality in nonequilibrium situations, which revealed a much more complicated structure of universality classes than is present in equilibrium [46].

Two complementary approaches have been adopted in understanding universality in nonequilibrium stationary states, one based on the analysis of stochastic partial differential equations (generalized Langevin equations) governing the time development of appropriate coarse-grained variables, while the other employs numerical studies of lattice models whose microscopic rules of evolution are constructed to mimic the real systems. In the case of driven diffusive systems, the appropriate variable is the coarse-grained particle density $\rho(\mathbf{r}, t)$, whose evolution is governed by the continuity equation: $\partial_t \rho + \nabla \cdot \vec{J} = 0$. The particle current \vec{J} , coarse-grained over mesoscopic scales, contains a diffusive part, \vec{J}_{diff} , a systematic part, \vec{J}_{sys} and a noisy part $\eta(\mathbf{r}, t)$, where the noise is usually chosen to be of zero-mean, $\overline{\eta(\mathbf{r}, t)} = 0$, and of short-ranged correlation in space and time: $\overline{\eta(\mathbf{r}, t)\eta(\mathbf{r}', t')} = A\delta^d(\mathbf{r} - \mathbf{r}')\delta(t - t')$ in d spatial dimensions. Here, the overline denotes averaging with respect to the stationary distribution of configurations. In one spatial dimension, the time development of the density fluctuations, $\delta\rho(x, t) = \rho(x, t) - \rho$, about the mean density $\rho = \overline{\rho(x, t)}$ is then governed by the following equation.

$$\frac{\partial(\delta\rho)}{\partial t} = -\frac{\partial}{\partial x} \left[-\Gamma \frac{\partial(\delta\rho)}{\partial x} + J_0 + v_K \delta\rho + \frac{\lambda}{2} (\delta\rho)^2 + \dots + \eta(x, t) \right], \quad (1.2)$$

where we assumed phenomenological forms for the diffusive and the systematic parts of

the current: $J_{\text{diff}} = -\Gamma \frac{\partial(\delta\rho)}{\partial x}$, and $J_{\text{sys}} = J_0 + v_K \delta\rho + \frac{\lambda}{2}(\delta\rho)^2 + \dots$. Here, v_K is the kinematic wave velocity of density fluctuations. In writing the systematic part, one usually stops at the second-order term in $\delta\rho$, since the higher-order terms are less relevant in the sense of the renormalization group, in determining the large-distance, long-time behavior of fluctuations. The irrelevance of higher-order terms can be seen most simply by mapping the density fluctuations $\delta\rho$ to the height fluctuations of a growing interface; see Eq. 1.3 below. Equation 1.2 then describes the time evolution of a growing interface, see Eq. 1.4 below. As we discuss below, the interface exhibits scaling properties in the sense that on scaling the space, the height variable scales by a certain power of the scaling parameter, while the time variable scales by a different power of the scaling parameter. On counting the power of the scaling parameter for each term in the time-evolution equation, Eq. 1.4, it directly follows that the higher-order terms in the systematic part of the current are less relevant.

The drift term, $v_K \delta\rho$, can be eliminated from Eq. 1.2 by the help of a Galilean transformation, $x \rightarrow x' = x - v_K t$, which involves going to a co-moving frame of velocity v_K . The resulting equation is known as the noisy Burgers equation [47, 48]. Its deterministic version (without the noise term η) was employed earlier in studying shocks in fluids [49].

The density fluctuations $\delta\rho$ can be related to the height fluctuations of a growing interface through identifying the local height gradient with the density fluctuation as

$$\frac{\partial h}{\partial x} = -\delta\rho, \quad (1.3)$$

where $h(x, t)$ is the height of the interface at spatial location x at time t [50]. In that case, Eq. 1.2 describes the evolution of the interface in time.

$$\frac{\partial h}{\partial t} = J_0 + \Gamma \frac{\partial^2 h}{\partial x^2} - v_K \frac{\partial h}{\partial x} + \frac{\lambda}{2} \left(\frac{\partial h}{\partial x} \right)^2 + \eta(x, t). \quad (1.4)$$

The constant, J_0 , on the right can be eliminated by doing a boost transformation, $h \rightarrow h' = h + J_0 t$. After doing the Galilean transformation, $x \rightarrow x' = x - v_K t$, the above equation describes the time evolution of an interface in the Kardar-Parisi-Zhang (KPZ) universality class [51].

$$\frac{\partial h}{\partial t} = \Gamma \frac{\partial^2 h}{\partial x^2} + \frac{\lambda}{2} \left(\frac{\partial h}{\partial x} \right)^2 + \eta(x, t). \quad (1.5)$$

Here, the first term on the right acts like a surface tension, tending to reduce the curvature of the interface, while the second term, accounting for the lateral growth of the interface, plays the most dominant role in determining the morphology and the large-scale dynamics of the interface [52].

In the limit of large distances and long times, the correlation function characterizing the

height fluctuations of the interface assumes a scaling form. Thus, one has

$$S(x, t) = \overline{\left\langle \left[h(x, t) - h(0, 0) - \overline{h(x, t) - h(0, 0)} \right]^2 \right\rangle} \sim t^{2\beta} Y\left(\frac{x}{t^{1/z}}\right), \quad (1.6)$$

in the asymptotic limit $x, t \rightarrow \infty$, with $x/t^{1/z} = \text{constant}$. In Eq. 1.6, the overline denotes averaging with respect to the stationary distribution of configurations, while the angular brackets represent averaging over stochastic evolution of configurations. Here, β is the growth exponent, while z is the dynamical exponent. These exponents as well as the scaling function Y are the same for all systems belonging to the same universality class. The scaling function $Y(s)$ has the property that $Y(s) \rightarrow \text{constant}$ as $s \rightarrow 0$, implying that the height autocorrelation $S(0, t)$ behaves as $S(0, t) \sim t^{2\beta}$. Further, as $s \rightarrow \infty$, the function $Y(s) \rightarrow s^{2\alpha}$. Here, α is the critical exponent related to z and β through $z = \alpha/\beta$ [52]. It determines the roughness of the interface through $S(x, 0) \sim x^{2\alpha}$. We conclude from the above discussion that on scaling the spatial variable x by the scaling parameter b as $x \rightarrow x' = bx$, the time variable scales as $t \rightarrow t' = b^z t$, while the height of the interface scales as $h \rightarrow h' = b^\alpha h$.

In the case that the nonlinear term λ is zero and all the higher order nonlinearities are absent, Eq. 1.2 represents an equilibrium lattice gas of hard core particles. In the language of the interface, Eq. 1.5 with $\lambda = 0$ describes the fluctuations of an equilibrium interface about its mean position and is known as the Edwards-Wilkinson (EW) equation [53]. This being a linear equation, its complete solution is possible and one obtains $\beta = 1/4, z = 2$ [53, 52].

The nonlinear term breaks the time reversal symmetry present in the equilibrium system, and consequently, changes the dynamical behavior of fluctuations. Scaling analysis with respect to the linear equation shows that the nonlinear term is relevant in spatial dimensions less than two. In one dimension, one has, for the KPZ class, $\beta = 1/3, z = 3/2$, calculated using mode coupling schemes [48], Bethe Ansatz [17, 18] and renormalization group techniques [47, 51]. The determination of the exponents could be possible because of a certain identity ($\alpha + z = 2$) that followed from the Galilean invariance of the Burgers equation [54, 52].

A goal of the present work is to show that the drift term, $v_K \delta \rho$, which, in the interface language, reads $-v_K \frac{\partial h}{\partial x}$, provides a relevant perturbation for both the EW and the KPZ fixed points, making them unstable, and generating a flow from them towards a third fixed point, which we refer to as the fixed point due to the sliding density fluctuations (SDF). In other words, presence of a least amount of drift in either the EW equation or the KPZ equation would make the large-distance long-time behavior of fluctuations for these equations be governed by the SDF fixed point. However, such an effect is observed in the limit of an infinite system. For a finite system, in addition, there are other interesting effects seen in the behavior of fluctuations, the elucidation of which is the main goal of this research work. Before summarizing our main results on finite-size effects in nonequilibrium

stationary states, it may be worthwhile to first take stock of our knowledge of finite-size effects in equilibrium stationary states.

1.4 Finite-size effects in equilibrium stationary states

Finite-size effects in equilibrium systems often arise from the interaction of system constituents with the boundaries. Such effects can be eliminated by defining the system with periodic boundary conditions; even then, finite-size effects are seen most prominently close to the critical point of a second-order phase transition. This is because only in the thermodynamic limit does the correlation length for fluctuations in the order parameter characterizing the transition diverge. For a system of finite extent, the correlation length in a particular spatial direction has an upper bound, set by the characteristic linear dimension of the system in that direction. Size effects are mirrored in the behavior of response functions like the specific heat, susceptibility, etc., which, instead of diverging at the critical point, have peaks with a finite height, which grows with the size of the system, i.e., the sharp limiting transition of the thermodynamic system is rounded off by size effects [44]. Moreover, the occurrence of the peak is at a point which is only close to the true or limiting critical value of the parameter for which the transition is observed, i.e., temperature in the case of magnetic systems. Such size effects, instead of proving a nuisance, turn out to be rather precious in the investigation of critical phenomena, thanks to the finite size scaling Ansatz [44]. This Ansatz is based on the assumption that close to the critical point, finite size behavior of thermodynamic quantities is exclusively governed by the ratio L/ξ_∞ , where L is the linear dimension of the system, while ξ_∞ is the correlation length of the infinite system. When this ratio is large, the system has basically reached its thermodynamic limit, while, when it is small, it is in the scaling regime. Specifically, let us discuss the situation for a magnetic system close to the critical temperature T_c . Consider any intensive quantity, O , (energy density, magnetization density, magnetic susceptibility, etc.) which behaves in the thermodynamic limit as

$$\langle O \rangle_\infty(t) \propto |t|^{-x_O}, \text{ as } t \rightarrow 0. \quad (1.7)$$

Here, t is the reduced temperature: $t \equiv \frac{T-T_c}{T_c}$. The subscript ∞ on the left emphasizes the large volume limit. For a finite size of characteristic length L , the scaling Ansatz states that Eq. 1.7 is modified to

$$\langle O \rangle_L = L^{x_O/\nu} g_O(L/\xi_\infty), \quad (1.8)$$

where the scaling function g_O is an analytic function of its argument, close to zero. Moreover, it is the same for all systems belonging to the same universality class, although it is dependent on the boundary conditions imposed on the system. In Eq. 1.8, ν is the critical exponent characterizing the divergence of the correlation length close to the critical point: $\xi_\infty \propto |t|^{-\nu}$. The scaling function has the limiting behavior that $g(u) \sim u^{-x_O/\nu}$ as $u \rightarrow \infty$ so

that when $L \gg \xi_\infty$, and the system has reached its thermodynamic limit, one recovers the behavior for an infinite system, Eq. 1.7. To summarize, for a finite system, the system size enters as a parameter into the scaling properties of thermodynamic quantities. Let us end this section by noting that finite-size rounding is also observed for a first-order transition [55].

1.5 Finite-size effects in nonequilibrium stationary states: Our results, plan of the thesis

In this thesis work, we have studied size effects on the dynamics of fluctuations in the nonequilibrium stationary states of driven diffusive systems. We have performed the study within the ambit of two paradigmatic models, the asymmetric simple exclusion process (ASEP) and the zero-range process (ZRP). Thus, this thesis has two broad divisions, one devoted to the ASEP (Chapters 2 - 5), while the other is devoted to the ZRP (Chapters 6 - 7). We considered the ASEP and the ZRP on a one-dimensional periodic lattice with a finite number of sites. The specific issue that we address for each of the two models is what are the size-dependent time scales that govern the behavior of fluctuations in the stationary state. Although some studies have been pursued in the past to characterize the behavior of fluctuations in time, they typically dealt with a thermodynamic system, and hence, failed to capture the entire domain over which fluctuations exhibit interesting and varied behavior in time. Our analysis of stationary state fluctuations in the ASEP [56] and the ZRP [57], provides, to our knowledge, the first systematic and exhaustive study of size effects on the dynamics of fluctuations in nonequilibrium stationary states. For both the processes, we determined all the time scales in the behavior of fluctuations and provided a simple physical basis for the underlying processes. Our studies are based on extensive Monte Carlo simulations, scaling analysis, physical arguments, and analytic solutions under suitable approximations.

We begin in Chapter 2 with an introduction to the one-dimensional ASEP on a periodic lattice. We discuss its stationary state weight of configurations [10], the equal-time density-density correlation function, and point out that in the stationary state, the coarse-grained density fluctuations move relative to the drift of the particles with the characteristic kinematic velocity [58], a phenomenon we refer to as sliding density fluctuations (SDF). Next, we discuss the behavior of unequal-time density-density correlation function in the limit of large distances and long times. In the following section, we show that density fluctuations in the ASEP can be mapped to those of a nonequilibrium interface in the KPZ universality class [50] (also, [10]), much along the same lines as in Section 1.3. The resultant time-evolution equation for the interface is the KPZ equation, augmented by a drift term accounting for the SDF. If the bias on particle motion in the ASEP is turned off, the particles move symmetrically, and the ASEP reduces to the symmetric simple exclusion process (SEP) [10]. For the SEP, the corresponding interface is an equilibrium one, governed by

the EW time-evolution equation. The chapter ends with a brief discussion on the scaling properties of the EW and the KPZ equations, and the proposition, which we prove in later chapters, that the EW and the KPZ fixed points become unstable in the presence of the SDF, which provides a relevant perturbation for both these fixed points and govern the interface fluctuations in the large-distance long-time limit.

In Chapter 3, we give a precise definition of the quantity of interest to us in studying finite-size effects in the ASEP, namely, the tagged particle correlations. In this, we measure the variance in the displacement of a tagged particle in the ASEP about its average displacement where the average could be over (i) both initial stationary ensemble and stochastic evolution, or, (ii) only stochastic evolution [59]. The resulting variances for the two cases have been studied previously in certain limits, and especially, in an infinite system, which we briefly review here [60, 61, 59]. Next, we propose a schematic representation for the tagged particle displacement in an infinite system on the basis of scaling arguments. We show that the representation correctly predicts the earlier studied behavior for the variances. Moreover, we adduce cogent physical arguments in support of the proposed representation and the observed behavior of the variances. The main result of this chapter is a complete characterization of the variances for a finite system, where we point out all the size-dependent time scales and the associated behavior. The variance, averaged over both initial stationary ensemble and stochastic evolution, captures motion of density fluctuations as a dissipating kinematic wave, and consequently, shows pronounced oscillations in time with a size-dependent time period. Its behavior in time is characterized by two size-dependent time scales, set by the circulation time and the decay time of the kinematic wave of density fluctuations, respectively. On the other hand, the variance, which involves averaging over stochastic evolution only, captures the dissipation of the kinematic wave, and has a single size-dependent time scale, given by the decay time of such a wave. The occurrence of the time scales are supported by scaling analysis of data obtained from extensive Monte Carlo simulations. Moreover, we give arguments in the form of a simple physical picture for the dynamics underlying each of the time scales. There is also a section in this chapter devoted to the motion of the center-of-mass of the system, which, as we show in the same chapter, dictates the long-time behavior of the tagged particle correlations.

Next, we move on to relate the tagged particle correlations to the height fluctuations of a nonequilibrium interface in the KPZ class in Chapter 4. This is achieved through a novel mapping, explained in this chapter, which uses the tagging process of particles in a direct and essential way in the translation [62]. The time-evolution equation of the interface, which we derive in Appendix B, is found to be the KPZ equation with a drift term proportional to the SDF, but the essential difference from the mapping discussed in Chapter 2 is that now the function measuring the height fluctuations of the interface, when interpreted in the language of the ASEP, is just the variance of the tagged particle displacement, introduced in Chapter 3. In an attempt to develop an analytic understanding of the occurrence of the size-dependent time scales in the tagged particle correlations, we solve for them exactly in the

case when the KPZ equation with the drift term reduces to the EW equation with the drift term, i.e., when the nonlinear term in the KPZ equation is zero. We call the corresponding interface the linear interface. The exact solution for the variance of the tagged particle displacement, obtained for the EW equation with the drift term, correctly predicts the size dependence of the time scales for the corresponding quantities in the ASEP, as we show in this chapter.

Chapter 5 is devoted to showing that the EW equation with the drift term, describing a linear interface, not just provides a linear approximation to the KPZ equation, but actually arises in the coarse-grained description of two specific models of interacting particles in the class of driven diffusive systems. These are the KLS model, mentioned above, considered at a particular value of the temperature, and the asymmetric random average process (ARAP) [63]. The ARAP is a generalization of the ASEP to a continuum, i.e., in the ARAP, particles, instead of hopping on a lattice, move on a continuous line. With Chapter 5, we end our discussion of the results for the ASEP.

In Chapter 6, we come to the second model system studied in this thesis, namely, the zero-range process (ZRP). In this chapter, we provide a self-contained review of the homogeneous ZRP on a one-dimensional periodic lattice [9] (see [64] for a recent review). This process can be mapped to a generalization of the totally asymmetric simple exclusion process; we summarize this mapping in this chapter. Next, we obtain the stationary state measure of the process, and discuss in detail the condensation transition (see Section 1.2.2 above), deriving conditions on the hop rate that induces such a transition. For one class of hop rate that induces condensation, we summarize the already known results on the single site occupancy distribution within the canonical ensemble in the disordered phase, at the critical point, and also, in the condensed phase, pointing out the typical occupancy that characterizes each phase. It is interesting to look at finite-size effects on the behavior of current for the ZRP; we study this numerically within the canonical ensemble. The chapter ends with a section on the kinematic wave that transports density fluctuations. We outline the basic steps in deriving the kinematic velocity at a particular density. It turns that in a certain parameter regime, the kinematic velocity at the critical point precisely evaluates to zero; we discuss this issue in this last section.

In Chapter 7, we report our results on size effects on the dynamics of fluctuations in the ZRP, for a particular choice of the hop rate that induces a condensation transition from a low-density disordered phase to a high-density condensed phase. We start by defining the quantity of interest, namely, the variance of the integrated current across a bond in the ZRP. As we report in this chapter, the variance shows striking differences in behavior as the system goes over from the disordered to the condensed phase. In the disordered phase, and also at the critical point, the variance behaves similarly to the tagged particle correlations in the ASEP, summarized in Chapter 3. Thus, the variance exhibits damped oscillations in time due to the kinematic wave of density fluctuations, and has two size-dependent time scales, set by the circulation time and the decay time of the kinematic wave, respectively. On

the contrary, in the condensed phase, numerical simulations and strong scaling arguments lend strong evidences in support of the fact that the fluctuation dynamics is governed by the condensate relocation from site to site; here, the variance has four distinct size-dependent time regimes, the two relevant time scales being the survival time and the relocation time of the condensate. This chapter contains a detailed explanation of the behavior of the variance in various phases, including the size-dependent time scales relevant to each of the phases, and an elaboration of the underlying physical processes. We also discuss in detail the dynamics through which the condensate relocates from one site to another. This is done by studying the survival probability distribution of the largest mass in the system. The distribution is seen to have two parts, one representing the relatively long time for which the condensate stays on one site, while the other, a power-law part, valid for small time intervals, accounts for the shorter time scale over which reorganization of mass in the bulk leads to a relocation of the condensate. At the end of this chapter, we introduce a simple relocation model to compute the long-time behavior of the variance in the condensed phase. With this chapter, we end our discussion on the ZRP.

In Chapter 8, we consider the exclusion process with extended objects, i.e., k -mers that occupy k adjacent sites on a lattice, with $k > 1$. These k -mers undergo stochastic hopping in the presence of an external drive. Specifically, a k -mer advances either forward or backward by one lattice site with unequal probabilities, if, correspondingly, there is a vacant site in front or behind the k -mer. In this chapter, we consider the model in one dimension with periodic boundary conditions. We show that many stationary state properties of the k -mer system, e.g., the correlation functions for site occupancies can be derived rather simply by mapping every configuration in the k -mer problem to an equivalent and unique configuration in an ASEP on a smaller lattice [43]. We show that these correlation functions show distinctive size effects like characteristic oscillations, etc., arising from the finite size of the extended objects, and have scaling forms in the proper continuum limit of the model.

Chapter 9 contains a summary of our main results; we also discuss possible generalizations of our results and some open issues.

References

- [1] R. Stinchcombe, *Adv. Phys.* **50**, 431 (2001).
- [2] S. N. Majumdar, S. Krishnamurthy, and M. Barma, *Phys. Rev. Lett.* **81**, 3691 (1998).
- [3] N. G. van Kampen, *Stochastic Processes in Physics and Chemistry* (North Holland, Amsterdam, 1992).
- [4] R. J. Glauber, *J. Math. Phys.* **4**, 294 (1963).
- [5] B. Schmittmann and R. K. P. Zia, in *Phase Transitions and Critical Phenomena*, edited by C. Domb and J. L. Lebowitz (Academic, London, 1995), Vol. 17.
- [6] S. Katz, J. L. Lebowitz, and H. Spohn, *Phys. Rev. B* **28**, 1655 (1983); *J. Stat. Phys.* **34**, 497 (1984).
- [7] W. Dietrich, P. Fulde, and I. Peschel, *Adv. Phys.* **29**, 257 (1980); and references therein.
- [8] G. Grinstein, D. -H. Lee, and S. Sachdev, *Phys. Rev. Lett.* **64**, 1927 (1990).
- [9] F. Spitzer, *Adv. Math.* **5**, 246 (1970).
- [10] T. M. Liggett, *Interacting Particle Systems* (Springer-Verlag, New York, 1985).
- [11] J. Krug, *Phys. Rev. Lett.* **67**, 1882 (1991).
- [12] B. Derrida, *Phys. Rep.* **301**, 65 (1998).
- [13] G. M. Schütz, in *Phase Transitions and Critical Phenomena*, edited by C. Domb and J. L. Lebowitz (Academic Press, San Diego, 2001), Vol. 19.
- [14] B. Derrida and K. Mallick, *J. Phys. A* **30**, 1031 (1997).
- [15] B. Derrida, J. L. Lebowitz, and E. Speer, *J. Stat. Phys.* **110**, 775 (2003).
- [16] B. Derrida, *Pramana*, **64**, 695 (2005).
- [17] D. Dhar, *Phase Transitions* **9**, 51 (1987).
- [18] L. -H. Gwa and H. Spohn, *Phys. Rev. A* **46**, 844 (1992).

- [19] D. Mallick, Phys. Rev. E **52**, 3512 (1995).
- [20] O. Golinelli and K. Mallick, J. Phys. A **37**, 3321 (2004).
- [21] O. Golinelli and K. Mallick, J. Phys. A **38**, 1419 (2005).
- [22] D. G. Levitt, Phys. Rev. A **8**, 3050 (1973).
- [23] *Traffic and Granular Flow '97*, edited by M. Schreckenberg and D. Wolf (Springer, New York, 1998); for a recent review, see D. Chowdhury, L. Santen, and A. Schadschneider, Phys. Rep. **329**, 199 (2000)
- [24] T. Halpin-Healy and Y-C Zhang, Phys. Rep. **254**, 215 (1995).
- [25] J. Krug, Adv. Phys. **46**, 139 (1997).
- [26] S. Klumpp and R. Lipowsky, J. Stat. Phys. **113**, 233 (2003).
- [27] Z. Burda, D. Johnston, J. Jurkiewicz, M. Kaminski, M. A. Novak, G. Papp, and I. Zahed, Phys. Rev. E **65**, 026102 (2002).
- [28] M. R. Evans, Europhys. Lett. **36**, 13 (1996).
- [29] D. Chowdhury, L. Santen, and A. Schadschneider, Phys. Rep. **329**, 199 (2000).
- [30] P. L. Krapivsky, S. Redner, and F. Leyvraz, Phys. Rev. Lett. **85**, 4629 (2000).
- [31] G. Bianconi and A-L Barabási, Phys. Rev. Lett **86**, 5632 (2001).
- [32] Y. Kafri, E. Levine, D. Mukmael, G. M. Schütz, and J. Török, Phys. Rev. Lett. **89**, 035702 (2002).
- [33] C. T. MacDonald, J. H. Gibbs, and A. C. Pipkin, Biopolymers **6**, 1 (1968).
- [34] C. T. MacDonald and J. H. Gibbs, Biopolymers **7**, 707 (1969).
- [35] T. Sasamoto and M. Wadati, J. Phys. A **31**, 6057 (1998).
- [36] F. Alacaraz and R. Z. Bariev, Phys. Rev. E **60**, 79 (1999).
- [37] G. Lakatos and T. Chou, J. Phys. A **36**, 2027 (2003).
- [38] L. B. Shaw, R. K. P. Zia, and K. H. Lee, Phys. Rev. E **68**, 021910 (2003).
- [39] L. B. Shaw, A. B. Kolomeisky, and K. H. Lee, J. Phys. A **37**, 2105 (2004).
- [40] L. B. Shaw, J. P. Sethna, and K. H. Lee, Phys. Rev. E **70**, 021901 (2004).
- [41] G. Schönherr and G. M. Schütz, J. Phys. A **37**, 8215 (2004).
- [42] J. J. Dong, B. Schmittmann, and R. K. P. Zia, Phys. Rev. E **76**, 051113 (2007).

- [43] M. Barma, M. D. Grynberg, and R. B. Stinchcombe, *J. Phys.: Condens. Matter* **19**, 065112 (2007).
- [44] M. E. Fisher, in *Critical Phenomena, Proceedings of the 51st 'Enrico Fermi' Summer School, Varenna, Italy*, edited by M. S. Green (Academic, New York, 1971). Also, see any standard textbook on critical phenomena, e.g., D. J. Amit and V. Martin-Mayor, *Field Theory, the Renormalization Group, and Critical Phenomena*, (World Scientific, 2005).
- [45] K. G. Wilson and J. Kogut, *Phys. Rep.* **12**, 75 (1974).
- [46] P. C. Hohenberg and B. I. Halperin, *Rev. Mod. Phys.* **49**, 435 (1977).
- [47] D. Forster, D. R. Nelson, and M. J. Stephen, *Phys. Rev. A* **16**, 732 (1977).
- [48] H. van Beijeren, R. Kutner, and H. Spohn, *Phys. Rev. Lett.* **54**, 2026 (1985).
- [49] J. M. Burgers, in *The Nonlinear Diffusion Equation*, (Reidel, Dordrecht, 1974).
- [50] M. Plischke, Z. Racz, and D. Liu, *Phys. Rev. B* **35**, 3485 (1987). See also, [10].
- [51] M. Kardar, G. Parisi, and Y. C. Zhang, *Phys. Rev. Lett.* **56**, 889 (1986).
- [52] A. -L. Barabasi and H. E. Stanley, *Fractal Concepts in Surface Growth* (Cambridge University Press, Cambridge, 1995).
- [53] S. F. Edwards and D. R. Wilkinson, *Proc. R. Soc. London, Ser A* **381**, 17 (1982).
- [54] E. Medina, T. Hwa, M. Kardar, and Y. C. Zhang, *Phys. Rev. A* **39**, 3053 (1989).
- [55] V. Privman and M. E. Fisher, *J. Stat. Phys.* **33**, 385 (1983).
- [56] S. Gupta S. N. Majumdar, C. Godrèche, and M. Barma, *Phys. Rev. E* **76**, 021112 (2007).
- [57] S. Gupta, M. Barma, and S. N. Majumdar, *Phys. Rev. E Rapid Comm.* **76**, 060101 (2007).
- [58] M. J. Lighthill and G. B. Whitham, *Proc. R. Soc. London A* **229**, 281 (1955).
- [59] H. van Beijeren, *J. Stat. Phys.* **63**, 47 (1991).
- [60] A. De Masi and P. A. Ferrari, *J. Stat. Phys.* **38**, 603 (1985); R. Kutner and H. van Beijeren, *ibid.* **39**, 317 (1985).
- [61] B. Derrida, M. R. Evans, and D. Mukamel, *J. Phys. A* **26**, 4911 (1993); B. Derrida and K. Mallick, *ibid.* **30**, 1031 (1997).
- [62] S. N. Majumdar and M. Barma, *Phys. Rev. B* **44**, 5306 (1991).

- [63] J. Krug and J. Garcia, *J. Stat. Phys.* **99**, 31 (2000); R. Rajesh and S. N. Majumdar, *ibid.* **99**, 943 (2000).
- [64] M. R. Evans and T. Hanney, *J. Phys. A* **38**, R195 (2005).

Chapter 2

The Asymmetric Simple Exclusion Process (ASEP)

“Would you tell me, please, which way I ought to go from here?” “That depends a good deal on where you want to get to,” said the Cat. “I don’t much care where—” said Alice. “Then it doesn’t matter which way you go,” said the Cat.

Lewis Carroll

The asymmetric simple exclusion process (ASEP) serves as a prototype model for studying nonequilibrium phenomena in the context of lattice gases [1]. On a one-dimensional lattice, the process involves hard core particles occupying lattice sites, and attempting to jump preferentially to nearest neighbor sites; the jumps are stochastic, and are completed only if the target site is unoccupied. In the lattice with open boundaries, particles get injected into the system at the left boundary site, move through the bulk, and finally, are drained at the right boundary site. Figure 2.1 shows a schematic view of the process with open boundaries.

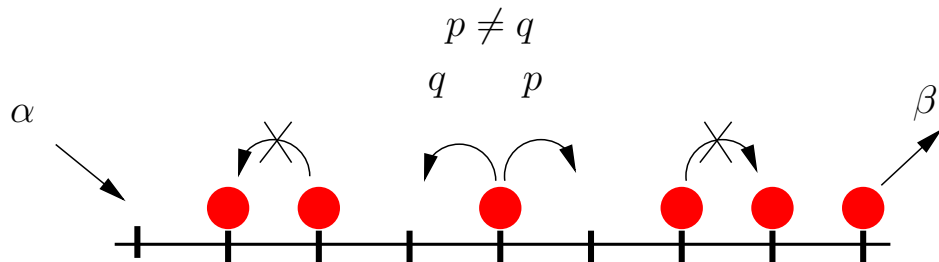


Figure 2.1: The asymmetric simple exclusion process in one dimension with open boundaries. Here, α is the injection rate at the left boundary, while β is the rate at which particles are drained at the right boundary. An allowed transition is also shown in the figure; transitions which are disallowed due to the hard core constraint are marked by crosses.

The ASEP provides a simple example of a system of interacting particles belonging to the general class of driven diffusive systems which at long times settle into a current-

carrying nonequilibrium stationary state [2]. The process was initially studied as a purely mathematical model to analyze interaction of Markov processes [3, 1]. The connection becomes evident on recognizing the ASEP as a collection of particles, each executing a biased random walk (a Markov process), and interacting through hard core exclusion.

In recent years, the ASEP has been applied to study diverse physical situations: hopping conductivity in solid electrolytes [4], transport of macromolecules through thin vessels [5], reptation of polymer in a gel [6], as a discrete version of the noisy Burgers equation to study microscopic structure of shocks in fluids [7], traffic flow [8], surface growth [9, 10], sequence alignment [11] and molecular motors [12]. On the theoretical side, the model provides the minimal setting to study systems out of equilibrium, and therefore, enjoys an iconic status much like that of the Ising model in equilibrium statistical mechanics. The ASEP, or modifications thereof, has served to exemplify many features of current-carrying stationary states which are forbidden by the general principles of equilibrium statistical mechanics, e.g., occurrence of boundary-induced phase transitions and spontaneous symmetry breaking in one dimension with short-ranged interactions [13, 14, 15]. For example, in the model with open boundaries, the competition of the boundary dynamics of injection and drainage with the transport in the bulk limits the current through the system. This leads to a rich phase diagram with first and second-order phase transitions upon varying the two boundary rates [13, 16, 17, 18, 19, 20]. The phase diagram is shown in Fig. 2.2.

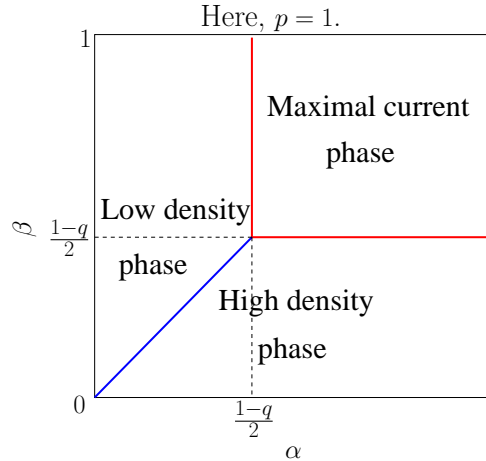


Figure 2.2: The phase diagram of the ASEP with open boundaries for the parameter values $p = 1$ and for arbitrary q (cf. Fig. 2.1). The red lines represent the second-order transition lines, while the blue line represents first order coexistence. In the high density phase, the bulk current is determined by the drainage rate β , while, in the low density phase, the injection rate α determines the bulk current. In the maximal current phase, the maximum possible bulk current flows through the system, independent of the boundary rates.

In this thesis, we are concerned with the ASEP on a one-dimensional periodic lattice. This chapter begins with a precise definition of the model in Section 2.1, followed in Section 2.2 by a discussion of its rather simple stationary state measure which allows all possible

configurations with equal weights. Next, in Section 2.3, we discuss the equal-time density-density correlation in the ASEP, both on a lattice and also in the continuum limit. In Section 2.4, we discuss different stationary state motions in the system attributed to individual particles and density fluctuations. In Section 2.5, we discuss the unequal-time density-density correlation in the ASEP. In the following section, we discuss a coarse-grained description of the ASEP density profile in the stationary state and derive its time-evolution equation. In Section 2.7, we discuss a mapping of the ASEP density profile to a growing interface in the Kardar-Parisi-Zhang (KPZ) universality class. Section 2.8 contains a discussion of the scaling properties of a general interface equation, a special case of which is the KPZ equation. We conclude this chapter with a discussion on the different universality classes in the behavior of height fluctuations of an interface.

2.1 The ASEP on a ring

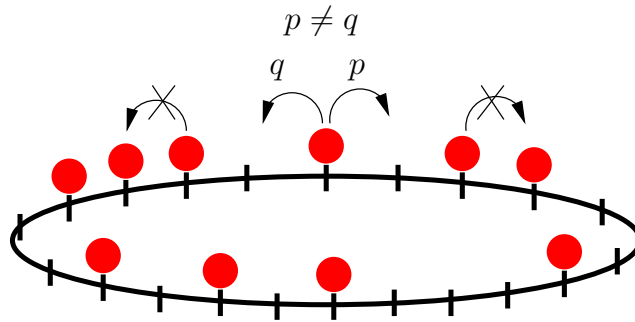


Figure 2.3: The asymmetric simple exclusion process on a one-dimensional ring. An allowed transition is shown in the figure; transitions that disobey the hard core constraint are disallowed and are marked by crosses.

We consider the ASEP on a periodic lattice of L sites. N indistinguishable hard core particles are distributed over the lattice sites with each site either singly-occupied or empty. The lattice spacing a is finite and may be taken to equal the linear extent of each particle. The total length of the lattice is La . In the following, we always measure distances in units of a , unless stated otherwise. The particle density $\rho = \frac{N}{L}$ is held constant when the limit $L \rightarrow \infty, N \rightarrow \infty$ is taken. The system evolves according to a stochastic dynamics: a site is chosen at random; if the site is occupied, the particle there attempts to hop to the site to its right with probability p , to the left neighboring site with probability q , and continues to occupy the original site with probability $1 - (p + q)$ (see Fig. 2.3). The attempted hop is successful only if the sought site is empty before the hop. Each of L attempted hops defines an elementary time step of the dynamics, which, together, constitute one time step. Clearly, the total number of particles is conserved under the dynamics. For the totally asymmetric simple exclusion process (TASEP), the motion of the particles is entirely in one

direction, i.e., $p = 1$ and $q = 0$ or, vice-versa. Note that with $p = q$, each particle moves symmetrically to the left and to the right. The model then reduces to the symmetric simple exclusion process (SEP), an equilibrium model of hard core particles diffusing on a lattice.

2.2 The stationary state measure

From the definition of the model, it is evident that the ASEP dynamics is ergodic, i.e., every configuration with the same number of particles can be reached from every other by following the dynamical rules of evolution. In the limit of long times, the system settles into a nonequilibrium stationary state. Ergodicity ensures uniqueness of the stationary state. On a lattice of L sites with N particles, the total number of possible configurations is given by the number of ways in which N out of L sites may be chosen to be occupied and thus, equals $\binom{L}{N} = \frac{L!}{N!(L-N)!}$. For this system, the stationary state is one in which all configurations \mathbf{C} have the same weight $p(\mathbf{C}) = \frac{N!(L-N)!}{L!}$ [1]. We prove this result below by invoking the condition of pairwise balance on the probability fluxes between configurations in the stationary state.

We begin by recapitulating the concept of a stationary state for a stochastic Markovian system defined by the transition rates $W(\mathbf{C} \rightarrow \mathbf{C}')$, which give the probability per unit time to go from any configuration \mathbf{C} to any configuration \mathbf{C}' . In the ASEP, the W 's are identified with the rates p and q , e.g., if the transition $\mathbf{C} \rightarrow \mathbf{C}'$ involves hopping of a particle from a site to its right neighbor, $W(\mathbf{C} \rightarrow \mathbf{C}') = p$. Now, the probability $\mathcal{P}(\mathbf{C}, t)$ for the system to be in configuration \mathbf{C} at time t evolves following the Master equation [21], namely,

$$\frac{\partial \mathcal{P}(\mathbf{C}, t)}{\partial t} = \sum_{\mathbf{C}'} W(\mathbf{C}' \rightarrow \mathbf{C}) \mathcal{P}(\mathbf{C}', t) - \sum_{\mathbf{C}'} W(\mathbf{C} \rightarrow \mathbf{C}') \mathcal{P}(\mathbf{C}, t). \quad (2.1)$$

The stationary state of the dynamics is given by the set of time independent probabilities $\{p(\mathbf{C})\}$ that satisfies the above equation. Thus, the stationary state is one in which the total incoming flux into any configuration \mathbf{C} [the first sum in Eq. 2.1] equals the total flux out of \mathbf{C} [the second sum in Eq. 2.1]. A sufficient condition for the existence of the stationary state is provided by the condition of pairwise balance, which states that for every configuration \mathbf{C}' contributing to the outflux of probability from any arbitrary configuration \mathbf{C} is associated a configuration \mathbf{C}'' whose influx contribution to \mathbf{C} precisely cancels that outflux [22]. In symbols, the pairwise balance condition is represented as

$$W(\mathbf{C} \rightarrow \mathbf{C}') p(\mathbf{C}) = W(\mathbf{C}'' \rightarrow \mathbf{C}) p(\mathbf{C}''). \quad (2.2)$$

That Eq. 2.2 is a sufficient condition that ensures stationarity can be checked by its direct substitution into Eq. 2.1 when the right hand side evaluates to zero as it should in the stationary state. Note that the pairwise balance condition generalizes the condition of detailed balance for equilibrium stationary states to nonequilibrium ones. The condition of

detailed balance ensures no net probability flux between any pair of configurations in the stationary state [21]. In Fig. 2.4, we show schematically the two conditions.

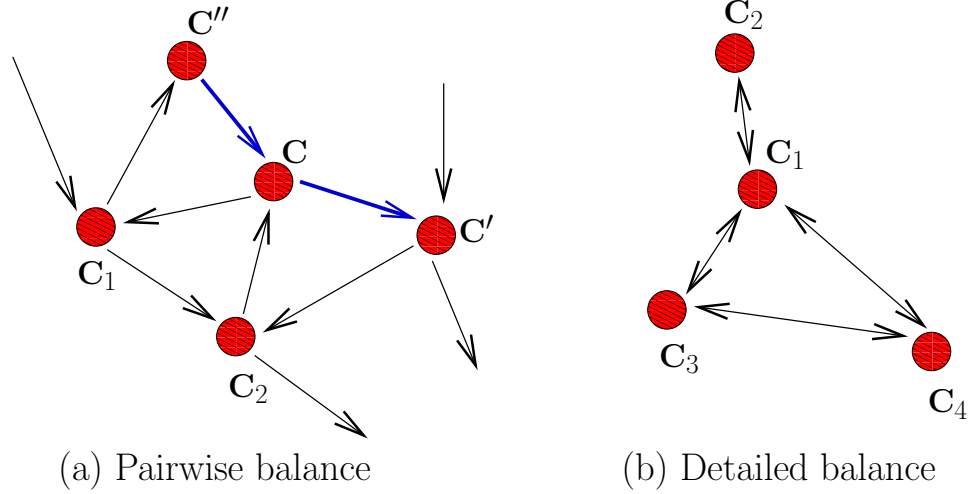


Figure 2.4: Condition of (a) pairwise balance and (b) detailed balance. Filled circles represent configurations of the system in the configuration space and the arrows denote the allowed transitions between configurations. In (a), fluxes into and out of a given configuration (C) are balanced for pairs of transitions, $C'' \rightarrow C$ and $C \rightarrow C'$. In (b), mutual forward and backward fluxes between two configurations balance. The detailed balance condition holds for equilibrium stationary states and the condition of pairwise balance generalizes it to nonequilibrium stationary states.

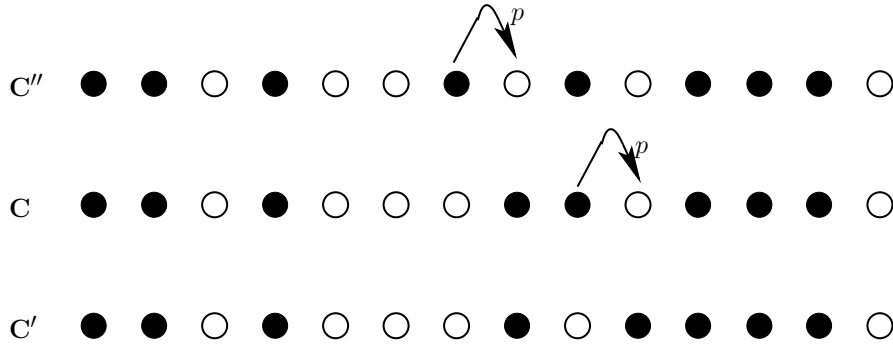


Figure 2.5: Pairwise balance between configurations in the stationary state of the ASEP on a ring. Here, filled circles denote particles while open ones stand for vacancies.

For the ASEP, we make the Ansatz that the stationary state allows every possible configuration to occur with the same weight, and show that this Ansatz satisfies the pairwise balance condition, Eq. 2.2. To see this, first note that any configuration C is composed of alternating segments of particles and holes. In one elementary time step, C may evolve to any other configuration C' in two ways,

- (i) by moving the rightmost particle in one of the particle segments in C one step to

the right with rate p (so that $W(\mathbf{C} \rightarrow \mathbf{C}') = p$), or,

(ii) by moving the leftmost particle in one of the particle segments in \mathbf{C} one step to the left with rate q (so that $W(\mathbf{C} \rightarrow \mathbf{C}') = q$).

In case (i), the configuration \mathbf{C}'' is easily constructed by moving the leftmost particle in the same particle segment in \mathbf{C} one step to the left so that in the next elementary time step, the same particle hops into its position in \mathbf{C} with rate p and the pairwise balance condition is satisfied. This case is illustrated for a particular particle segment in \mathbf{C} in Fig. 2.5.

In case (ii), the configuration \mathbf{C}'' is constructed by moving the rightmost particle in the same particle segment in \mathbf{C} one step to the right so that in the next elementary time step, the same particle hops into its position in \mathbf{C} with rate q and the pairwise balance condition is satisfied.

Thus, the Ansatz that all configurations occur with equal probabilities does indeed satisfy the condition of pairwise balance and hence, represents a stationary state of the ASEP dynamics. That such a measure is indeed the stationary state of the ASEP dynamics follows from the uniqueness of the stationary state.

2.3 The equal-time density-density correlation

Let $n_i = 0, 1$ with $i = 1, 2, \dots, L$ denote the occupancy of the i -th site. In the thermodynamic limit $N \rightarrow \infty, L \rightarrow \infty, \frac{N}{L} = \rho = \text{finite}$, the average density $\overline{n_i} = \rho$. Here, as in the rest of this chapter, the overbar is used to denote an average over the stationary ensemble of configurations, i.e., with respect to the stationary measure $p(\mathbf{C}) = \frac{N!(L-N)!}{L!}$. The equal-time (unsubtracted) density-density correlation function $C(r)$ is defined as

$$C(r = |i - j|) \equiv \overline{n_i n_j} \text{ for } i \neq j. \quad (2.3)$$

Since, in the stationary state, all configurations have the same weight, the function $C(r)$ is simply given by the ratio of the number of ways in which $N - 2$ particles may be distributed over $L - 2$ sites to the total number of configurations, and hence, equals $\frac{\binom{L-2}{N-2}}{\binom{L}{N}} = \frac{N(N-1)}{L(L-1)}$; in the thermodynamic limit, the right hand side equals ρ^2 with corrections of $O(\frac{1}{L})$. Thus, in the thermodynamic limit, we get

$$C(r) \approx \rho^2, \quad (2.4)$$

i.e., to leading order in the system size, the two-point density-density correlation function factorizes into the product of probabilities that each of the two sites is occupied, independently of the other. In view of all configurations being equally likely in the stationary state, this factorization property remains true for all higher-order correlations. It thus follows that in the thermodynamic limit, to leading order in L , a site in the ASEP is occupied with probability ρ and left vacant with probability $1 - \rho$, independently of any other site. Thus, the stationary state has a product measure form.

It is interesting to consider the equal-time density-density correlation in the limit in which the ASEP lattice is replaced by a continuum. This limit is achieved by letting the lattice spacing, a , to go to zero in such a way that the total length of the lattice, namely, La , remains finite. In this limit, each ASEP particle reduces to a point particle of infinitesimal size ($a \rightarrow 0$), distributed over a continuous line of finite length La ; the particle density is given by $\rho_0 = N/La = \rho/a$. In order to keep ρ_0 finite while taking the limit $a \rightarrow 0$, it is thus required that we also take the ASEP particle density ρ to go to zero. In the continuum limit, we no longer measure distances in units of a ; instead, we consider their actual values. We ask: What is the probability for the gap between two successive point particles to lie within the interval $(R, R+dR)$? This probability is given by $C(R)dR$, where the probability density $C(R)$ is the density-density correlation function in the continuum. To compute the function $C(R)$, we break up the continuous line of length R into a lattice of m sites and lattice spacing equal to a , such that $ma = R$. We first take a to be finite, compute the joint probability that each of the m sites is empty so that the next particle is at least R distance away, and finally, take the limit $a \rightarrow 0, m \rightarrow \infty$, keeping the product $R = ma$ finite. For finite a , the joint probability for each of the m sites to be empty is $(1 - \rho)^m$. Thus, $C(R)$ is given by

$$\begin{aligned} C(R) &\propto \lim_{a \rightarrow 0, m \rightarrow \infty, R=ma=\text{Finite}} (1 - \rho)^m. \\ &= \lim_{a \rightarrow 0, m \rightarrow \infty, R=ma=\text{Finite}} (1 - \rho_0 a)^{R/a}. \end{aligned} \quad (2.5)$$

Using the known result, $\lim_{a \rightarrow 0} (1 - ax)^{1/a} = e^{-x}$, we get

$$C(R) \propto \exp(-\rho_0 R). \quad (2.6)$$

On normalizing $C(R)$ such that $\int_0^\infty dR C(R) = 1$, we finally get

$$C(R) = \rho_0 \exp(-\rho_0 R). \quad (2.7)$$

Thus, in the continuum limit of the ASEP, the equal-time density-density correlation decays as an exponential.

2.4 Motion of particles and density fluctuations in the stationary state

In the stationary state, the ASEP supports a steady current of particles, which, between sites i and $i + 1$, is given by

$$J_{i,i+1} = pn_i(1 - n_{i+1}) - qn_{i+1}(1 - n_i). \quad (2.8)$$

Here, the first term on the right corresponds to a particle hop from site i to right neighbor site $i + 1$, while the second term represents a hop in the reverse direction from $i + 1$ to i . The mean current $J = \overline{J_{i,i+1}}$ is the same across every pair of neighboring sites in the stationary state. For a system of L sites, the mean current J is given by

$$J = (p - q)\rho(1 - \rho) + O\left(\frac{1}{L}\right), \quad (2.9)$$

in view of the product measure for the stationary state. Correspondingly, the mean velocity of a particle in the stationary state, given by $v_P = \frac{J}{\rho}$, equals

$$v_P = (p - q)(1 - \rho) + O\left(\frac{1}{L}\right). \quad (2.10)$$

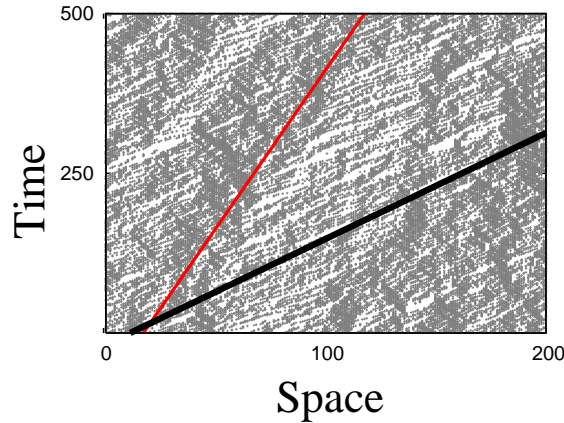


Figure 2.6: Time evolution for a stationary TASEP configuration on a ring. Here, the system size $L = 200$, the density $\rho = 0.4$. Black spots denote particles, while white ones stand for vacancies. Following a black spot in time, we get the trajectory of a particle; the thick black line stands for the mean trajectory. The inverse of the slope of the thick black line is the velocity of a particle $v_P \approx (p - q)(1 - \rho) = 0.6$. On a coarse-grained level, one can see black and white stripes inclined at a certain angle to the time axis; these represent trajectories of density fluctuations, the thin red line being the mean trajectory with the inverse of its slope equaling the velocity of the density fluctuations $v_K \approx (p - q)(1 - 2\rho) = 0.2$.

Besides particle motion, there is also a motion associated with the coarse-grained density fluctuations in the stationary state of the ASEP. The density fluctuations are transported as a kinematic wave with velocity $v_K = \frac{\partial J}{\partial \rho}$ (see Appendix A). Thus, relative to the average drift of the particles, the density fluctuations ‘slide’ with velocity $v_K - v_P$. We refer to this relative motion as the sliding density fluctuations (SDF). Stochasticity and nonlinearity in the dynamics lead to dissipation of the density profile so that the wave of fluctuations ultimately dies down in time. Utilizing the expression for the mean current J given in Eq.

2.9, the kinematic wave velocity¹ is given by

$$v_K = (p - q)(1 - 2\rho) + O\left(\frac{1}{L}\right). \quad (2.11)$$

Figure 2.6 shows the time evolution of a stationary ASEP configuration. One clearly sees that the space-time trajectory of a particle is distinctly different from that for a coarse-grained density fluctuation.

2.5 The unequal-time density-density correlation

The unequal-time density-density correlation function $C(r, t)$ is defined as

$$C(r = |i - j|, t) \equiv \overline{\langle n_i(0)n_j(t) \rangle} - \rho^2, \quad (2.12)$$

where $n_i(0)$ is the occupancy of the i -th site at time 0, while $n_j(t)$ is the occupancy of the j -th site at time t . Here, ρ is the ASEP particle density, the overbar represents averaging over the initial stationary distribution of the ASEP configurations, while the angular brackets denote averaging over the stochastic evolution of the configurations in time. One can rewrite Eq. 2.12 as

$$C(r = |i - j|, t) = \overline{[n_i(0) - \rho][n_j(t) - \rho]}. \quad (2.13)$$

Thus, the function $C(r, t)$ correlates the fluctuation in the density at the i -th site, given by $[n_i(0) - \rho]$, with the fluctuation in the density at the j -th site, given by $[n_j(t) - \rho]$. As discussed in Section 2.4, the density fluctuations are transported through the system with the kinematic velocity v_K .

In the long-time scaling regime, the function $C(r, t)$ is of the form [23]

$$C(r, t) \propto t^{-2/3} f(u), \quad u = \frac{1}{2}(Jt^2)^{-1/3}(r - v_K t), \quad (2.14)$$

where $f(u)$ represents the scaling function. In Eq. 2.14, J is the mean current in the stationary state, given by Eq. 2.9, while v_K is the kinematic wave velocity, given by Eq. 2.11. We can rewrite Eq. 2.14 in the scaling form as

$$C(r, t) \sim t^{-2/3} f\left(\frac{r - v_K t}{t^{2/3}}\right). \quad (2.15)$$

In the limit of large u , the function $f(u)$ is known to behave asymptotically as $f(u) \sim \exp(-\mu|u|^3)$ with the constant $\mu \approx -0.295$ [23]. Thus, at long times, the function $C(r, t)$ decays as an exponential in time.

An exception to the exponential decay of $C(r, t)$ is when the co-moving condition $r =$

¹This velocity also appears as the imaginary part of the low-lying eigenvalues of the Markov matrix governing the time evolution of the ASEP in the totally asymmetric case $q = 0$; see D. Kim, Phys. Rev. E **52**, 3512 (1995); O. Golinelli and K. Mallick, J. Phys. A **38**, 1419 (2005).

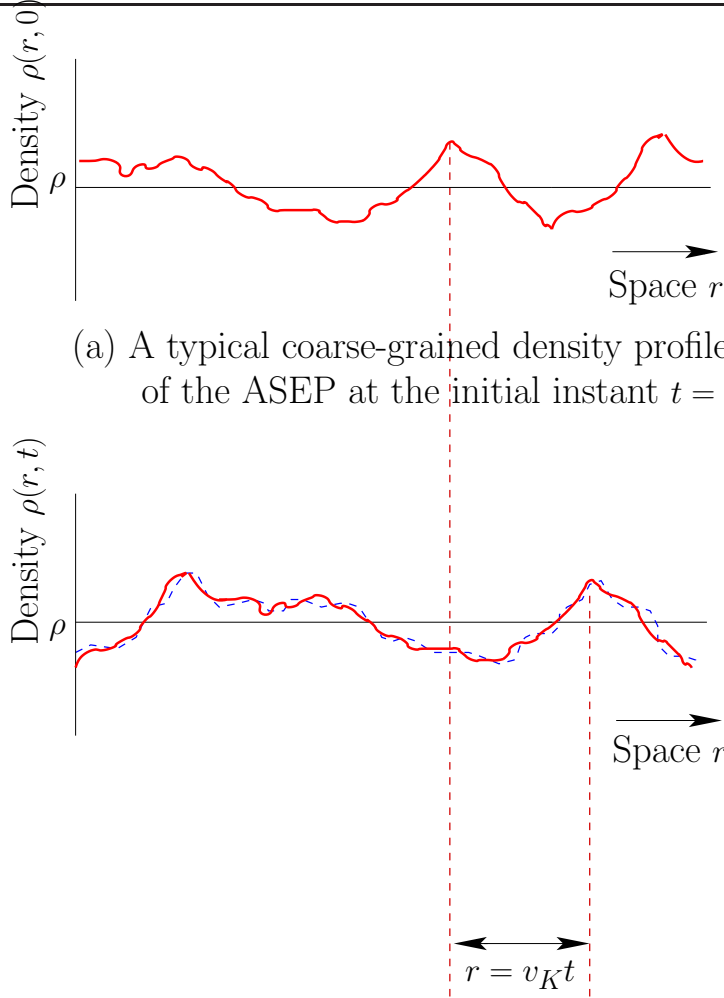


Figure 2.7: The figure shows a typical coarse-grained density profile of the ASEP at time $t = 0$, and the same one, shifted in space due to the kinematic wave of density fluctuations. The dotted blue line in (b) represents the slight distortion in the density profile in time due to the stochasticity of the ASEP dynamics. When the co-moving condition $r = v_K t$ is satisfied, the function $C(r, t)$, defined in Eq. 2.12, monitors the time development of the fluctuations at the same point on the density profile, during its motion as a kinematic wave.

$v_K t$ is satisfied. In this case, the function $C(r, t)$ measures the correlations in the density fluctuation at a spatial point at a given time with the same fluctuation, transported by the kinematic wave so as to occur at the spatial point $r = v_K t$ at time t . In other words, the function $C(r, t)$ monitors the time development of the fluctuations at the same point on the density profile, during its motion as a kinematic wave; this is shown schematically in Fig. 2.7. When the co-moving condition is satisfied, the function $C(r, t)$ decays as a power law as $C(r, t) \propto t^{-2/3}$.

A special case of the co-moving condition is when one looks at the density autocorrelation, given by $C(0, t)$. Here, the co-moving condition implies that $v_K = 0$, which, in turn,

implies from Eq. 2.11 that the ASEP particle density is $\rho = 1/2$. At this density, the autocorrelation $C(0, t)$ behaves as a power-law in time as $t^{-2/3}$. At all other densities, the autocorrelation decays as an exponential in time.

All the above behaviors of the function $C(r, t)$ can be explained from the scaling properties of the interface-equivalent of the ASEP. As we explain below in Section 2.7, the ASEP density profile may be mapped to an interface, which is defined on a one-dimensional substrate, and which is growing in time. The scaling properties of the interface imply that on rescaling the spatial variable for the substrate, the height variable of the interface also scales by a certain power of the scaling parameter, while the time variable scales by a different power of the scaling parameter. We will explain in Section 2.8 how these scaling considerations may be invoked to explain the behavior of the function $C(r, t)$, discussed above.

2.6 Coarse-grained description of the ASEP

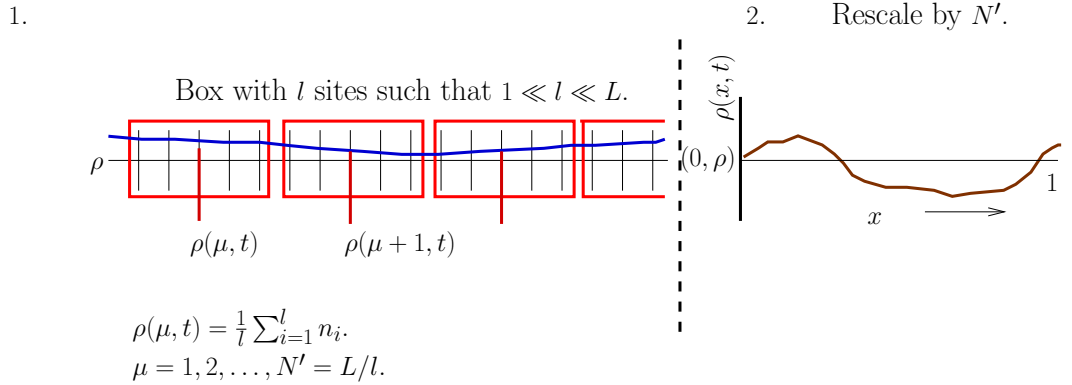


Figure 2.8: Steps involved in obtaining the coarse-grained description of the ASEP

We consider the ASEP on a one-dimensional ring in the thermodynamic limit with finite particle density ρ . An ASEP configuration in the stationary state represents fluctuations in site occupancies n_i about the mean occupancy ρ . The occupancies change in time due to the ASEP dynamics, and it is interesting to ask about how does the density profile, defined by the set $\{n_j, j = 1, 2, \dots, L\}$, considered on a coarse-grained level, evolve in time. Below, we give a simple derivation of the time evolution for the coarse-grained density profile; for a more rigorous derivation, see [24].

In obtaining the resultant time-evolution equation, the various steps involved are summarized below, with the first two steps shown schematically in Fig. 2.8.

1. The first step is to consider the lattice to be broken up into ‘mesoscopic’ regions of l sites with $1 \ll l \ll L$ (see Fig. 2.8). Thus, each mesoscopic region contains many sites, enough in number that one can be oblivious of the variation in the particle density over the lattice sites within the region, and replace it by a flat profile given by the ‘mean’

density $\rho(\mu, t)$ (where the mean is over the sites in the mesoscopic region). Here, the index μ ($= 1, 2, \dots, L/l$) may arbitrarily be taken to represent the central site in each mesoscopic region, and runs over the total number of mesoscopic regions in the system, given by $N' = L/l$. Variation in $\rho(\mu, t)$ over space occurs as one passes from one mesoscopic region to the next, i.e., as one passes from μ to $\mu + 1$ for $1 \leq \mu < L/l - 1$. Since $\rho(\mu, t)$ represents an average occupancy over many sites, several particle motions are required out of these sites to cause an appreciable change in $\rho(\mu, t)$ in time. Thus, time t here is a ‘macroscopic’ variable in the sense that it is much longer than the elementary time scale over which a single particle jumps in the ASEP. Because the ASEP dynamics conserves particle number locally, the time variation of $\rho(\mu, t)$ (for $\mu = 1, 2, \dots, N' = L/l$) follows the equation of continuity, and hence, reads

$$\frac{\partial \rho(\mu, t)}{\partial t} = [J_{\mu-1, \mu}(t) - J_{\mu, \mu+1}(t)], \quad (2.16)$$

where $J_{\mu-1, \mu}(t)$ represents the particle current at time instant t between the mesoscopic regions with their central sites at $\mu - 1$ and μ , respectively. Since we have periodic boundary conditions on the ASEP lattice, it follows that $J_{N', N'+1} = J_{N', 1}$ and $J_{0, 1} = J_{N', 1}$. The term within the square brackets on the right represents the net particle influx into the site μ in unit time. Next, one assumes that the various contributions to the current $J_{\mu-1, \mu}(t)$ just add up to give

$$J_{\mu-1, \mu}(t) = \Gamma [\rho(\mu - 1, t) - \rho(\mu, t)] + (p - q)\rho(\mu - 1, t)(1 - \rho(\mu - 1, t)) + \eta(\mu - 1, t). \quad (2.17)$$

Here, the first term on the right represents the diffusive contribution to the current resulting from the difference in the particle densities at the two locations ($\mu - 1$) and μ , with Γ representing the diffusion constant. The second term represents the current flowing into the region μ due to the ASEP dynamics of particles within the mesoscopic region $\mu - 1$. To understand why the second term has the form indicated, recall that the mean ASEP current within a region with a flat density profile ρ equals $(p - q)\rho(1 - \rho)$. Now, within the coarse-grained description, the density profile within a mesoscopic region has been taken to be essentially flat, justifying the form of the second term on the right of Eq. 2.17. That the density profile within a mesoscopic region is not flat adds a noise to the current, and is represented by the third term on the right of Eq. 2.17; $\eta(\mu - 1, t)$ is a random variable taking values depending on the particular ASEP configuration under consideration. Its average over the stationary ensemble of the ASEP configurations is zero: $\overline{\eta(\mu, t)} = 0$. Also, the noise $\eta(\mu, t)$ is taken to be uncorrelated in space and time: $\overline{\eta(\mu, t)\eta(\nu, t')} = 2A\delta_{\mu, \nu}\delta(t - t')$, where the constant A represents the strength of the noise. This is based on the assumption that (i) between points μ and ν , the microscopic density profile n_i changes sufficiently random number of times, and (ii) between times t and t' , the microscopic profile at a point undergoes large number of random changes in time.

Combining Eq. 2.16 and Eq. 2.17, we finally have

$$\begin{aligned} \frac{\partial \rho(\mu, t)}{\partial t} &= \Gamma [\rho(\mu - 1, t) - \rho(\mu, t)] - \Gamma [\rho(\mu, t) - \rho(\mu + 1, t)] \\ &+ (p - q) [\rho(\mu - 1, t)(1 - \rho(\mu - 1, t)) - \rho(\mu, t)(1 - \rho(\mu, t))] \\ &+ \eta(\mu - 1, t) - \eta(\mu, t). \end{aligned} \quad (2.18)$$

2. Now that one has a system of sites $\{\mu = 1, 2, \dots, N' = L/l\}$ with associated densities given by the set $\{\rho(\mu, t)\}$, one defines a new set of variables $\{x_\mu\}$, with $x_\mu = \mu/N'$, and then take the limit $N' \rightarrow \infty$ so that the set $\{\rho(x_\mu, t)\}$ maps onto a density profile $\rho(x, t)$ defined over the continuous spatial variable $x \in [0, 1]$ (see Fig. 2.8). In this limit, Eq. 2.18 turns into the following equation.

$$\frac{\partial \rho(x, t)}{\partial t} = \Gamma \frac{\partial^2 \rho(x, t)}{\partial x^2} - (p - q)(1 - 2\rho(x, t)) \frac{\partial \rho(x, t)}{\partial x} - \frac{\partial \eta(x, t)}{\partial x}. \quad (2.19)$$

3. Since we are interested in finding the time evolution of the density fluctuations, $\delta\rho(x, t) \equiv \rho(x, t) - \rho$, about the global mean ρ , we expand both sides of Eq. 2.19 about ρ ; we finally get

$$\frac{\partial \delta\rho(x, t)}{\partial t} = \Gamma \frac{\partial^2 \delta\rho(x, t)}{\partial x^2} - (p - q)(1 - 2\rho) \frac{\partial \delta\rho(x, t)}{\partial x} + (p - q) \frac{\partial (\delta\rho)^2}{\partial x} - \frac{\partial \eta(x, t)}{\partial x}. \quad (2.20)$$

Note from Eq. 2.11 that in the thermodynamic limit, the kinematic wave velocity is given by $v_K = (p - q)(1 - 2\rho)$. Also, in this limit, from the expression of the current, Eq. 2.9, it follows that $\frac{\partial^2 J}{\partial \rho^2} = (p - q)$. We have, finally, for the time evolution of the coarse-grained density profile,

$$\frac{\partial \delta\rho(x, t)}{\partial t} = \Gamma \frac{\partial^2 \delta\rho(x, t)}{\partial x^2} - v_K \frac{\partial \delta\rho(x, t)}{\partial x} + \frac{\lambda}{2} \frac{\partial (\delta\rho)^2}{\partial x} - \frac{\partial \eta(x, t)}{\partial x}, \quad (2.21)$$

where the noise $\eta(x, t)$ satisfies: $\overline{\eta(x, t)} = 0$, $\overline{\eta(x, t)\eta(x', t')} = 2A\delta(x - x')\delta(t - t')$. Also, $v_K = \frac{\partial J}{\partial \rho} = (p - q)(1 - 2\rho)$, while $\lambda = 2\frac{\partial^2 J}{\partial \rho^2} = 2(p - q)$. The drift term, $-v_K \frac{\partial \delta\rho(x, t)}{\partial x}$, in Eq. 2.21 can be removed by a Galilean transformation, $x \rightarrow x' = x - v_K t$, which leaves us with what is known (for $\lambda = 1$) as the stochastic Burgers equation [25]. This equation was employed to study, e.g., randomly stirred fluids [26] and fluctuations in the exclusion process [27].

Note that Eq. 2.21 does not represent the ‘actual’ coarse-grained description of the ASEP, in the sense that various unproven assumptions have gone into deriving it, e.g., the validity of the additivity of various contributions to the current as done in Eq. 2.17. Yet, the expectation is that the scaling properties of the correlation functions for the actual coarse-grained ASEP density profile and that for Eq. 2.21 are governed by the same renormalization group fixed point, and hence, are described by the same critical exponents and scaling functions. Such an expectation stems from the observation that Eq. 2.21 contains all the

conservation laws, and hence, all the resulting symmetries inherent in the ASEP dynamics, e.g., mass conservation.

2.7 Mapping of the ASEP density profile to an interface

Equation 2.21, describing the time evolution of the coarse-grained ASEP density profile, also describes the time evolution of a growing interface in the Kardar-Parisi-Zhang (KPZ) universality class [28]. To see this connection, one introduces the height function $h(x, t)$ through the time-integrated particle current,

$$h(x, t) = \int_0^t ds j(x, s), \quad (2.22)$$

where $j(x, t)dxdt$ gives the net number of particles flowing out of the length between x and $x + dx$ of the system, between times t and $t + dt$, and is defined such that $\frac{\partial j(x, t)}{\partial x} dx$ is nothing but the continuum limit of the coarse-grained current differences, $J_{\mu, \mu+1}(t) - J_{\mu-1, \mu}(t)$ (see Eq. 2.16). Now, since $\frac{\partial \rho(x, t)}{\partial t} = -\frac{\partial j}{\partial x}$ (Eq. 2.16), and also, $\rho(x, t) = \rho + \delta\rho(x, t)$, we get

$$\frac{\partial h(x, t)}{\partial x} = -[\delta\rho(x, t) - \delta\rho(x, 0)]. \quad (2.23)$$

If we now supplement the last equation with the initial condition, $\delta\rho(x, 0) = 0$, we get

$$\frac{\partial h(x, t)}{\partial x} = -\delta\rho(x, t). \quad (2.24)$$

Equation 2.24 defines the mapping of the coarse-grained ASEP density profile to an interface, both defined on the continuum. Note that the left hand side, $\frac{\partial h(x, t)}{\partial x}$, gives the local slope of the interface. On the discrete level of a lattice, since the local slope, $h_{i+1}(t) - h_i(t)$ can take only two values, ± 1 , the above mapping on the discrete level has to be modified to read

$$h_{i+1}(t) - h_i(t) = -\text{Sign}[\delta n_i(t)] = -\text{Sign}[n_i(t) - \rho]. \quad (2.25)$$

Since the site occupancy variable $n_i(t)$ can be either 0 or 1, while the particle density $\rho \in [0, 1]$, the above relation maps the presence of a particle in the ASEP with a downward slope of the interface, while the absence of a particle represents an upward slope of the interface, as shown in Fig. 2.9 [1, 29].

Some comments are in order regarding the mapping, Eq. 2.24. Since we are dealing with a periodic system, $\delta\rho(x, t)$, and hence, the local slope, $\frac{\partial h(x, t)}{\partial x}$, must match at the boundaries. Moreover, since the ASEP dynamics conserves total number of particles, we have $\int_0^1 dx \delta\rho(x, t) = 0$, which is true for all times. It follows from Eq. 2.24 that the height of the interface must also match at the boundaries.

Substituting Eq. 2.24 into Eq. 2.21, integrating both sides with respect to x , one gets

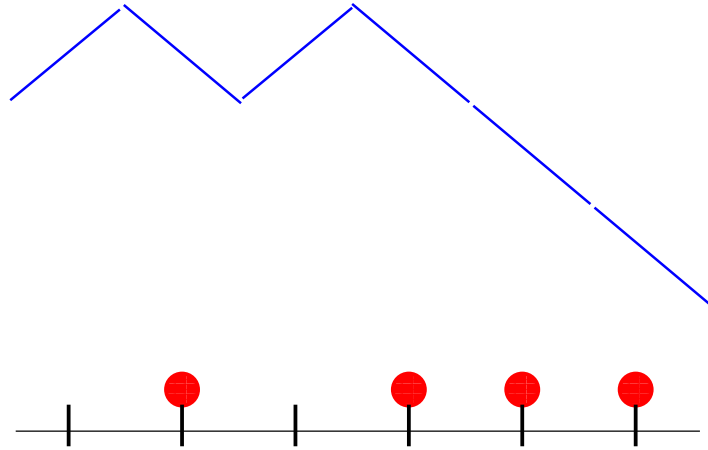


Figure 2.9: Mapping the ASEP density profile to an equivalent interface.

the equation of motion of the interface as

$$\frac{\partial h(x, t)}{\partial t} = \Gamma \frac{\partial^2 h}{\partial x^2} - v_K \frac{\partial h}{\partial x} + \frac{\lambda}{2} \left(\frac{\partial h}{\partial x} \right)^2 + \eta(x, t), \quad (2.26)$$

where $v_K = (p - q)(1 - 2\rho)$, $\lambda = 2(p - q)$. In obtaining the above equation, the constant of integration (call it C) has been set equal to zero, since, even if it were nonzero, it can be easily eliminated from the above equation by redefining the height variable as $h \rightarrow h' = h + Ct$. The sign of the noise term has been changed from negative in Eq. 2.21 to positive in Eq. 2.26, since the noise is represented by a random variable which is as probable to be positive as to be negative (so that $\overline{\eta(x, t)} = 0$), and hence, the sign of the noise term really does not matter. Recall from the last section that $\langle \eta(x, t) \eta(x', t') \rangle = 2A \delta(x - x') \delta(t - t')$. The drift term, $-v_K \frac{\partial h}{\partial x}$, in Eq. 2.26 can be eliminated by a Galilean transformation, as already explained in the last section. As a result of all these transformations, Eq. 2.26 now describes the time-evolution of a KPZ interface in one spatial dimension [28], which is thus given by

$$\frac{\partial h(x, t)}{\partial t} = \Gamma \frac{\partial^2 h}{\partial x^2} + \frac{\lambda}{2} \left(\frac{\partial h}{\partial x} \right)^2 + \eta(x, t). \quad (2.27)$$

It can be shown that the probability distribution of interface configurations in the stationary state for the KPZ interface is given by [30]

$$P[\{h(x, t)\}] \propto \exp \left[-\frac{\Gamma}{2A} \int dx (\partial_x h)^2 \right]. \quad (2.28)$$

Equation 2.28 implies that the local slopes, $\partial_x h$, follow a Gaussian distribution, i.e., they are random and uncorrelated. Summing up local random slopes gives us the KPZ interface which is nothing but a Brownian motion.

The KPZ equation, Eq. 2.27, does not have the $h \rightarrow -h$ symmetry; this is reflective of

the fact that this equation describes an interface which is growing in time. The net velocity $v_{\text{interface}}$ of the KPZ interface is given by $\int_0^1 dx \overline{\frac{\partial h(x,t)}{\partial t}}$, where the overbar denotes averaging with respect to the stationary interface distribution, Eq. 2.28. It follows from Eq. 2.27 that $v_{\text{interface}}$ is given by

$$v_{\text{interface}} = \frac{\lambda}{2} \int_0^1 dx \overline{\left(\frac{\partial h}{\partial x}\right)^2} = (p - q) \int_0^1 dx \overline{\left(\frac{\partial h}{\partial x}\right)^2}, \quad (2.29)$$

since (i) $\overline{\eta(x,t)} = 0$, and (ii) $\int_0^1 dx \frac{\partial^2 h}{\partial x^2}$ is zero due to the boundary condition on the interface.

For the symmetric exclusion process (SEP), one has $p = q$ so that $v_{\text{interface}} = 0$. Thus, the corresponding interface does not move bodily; it, rather, fluctuates about a stationary profile and hence, represents a system in equilibrium. The time evolution of the interface is governed by the Edwards-Wilkinson (EW) equation in one spatial dimension [31], which is obtained by setting $p = q$ in Eq. 2.26, implying $v_K = 0$, $\lambda = 0$, so that

$$\frac{\partial h(x,t)}{\partial t} = \Gamma \frac{\partial^2 h}{\partial x^2} + \eta(x,t). \quad (2.30)$$

For the EW equation also, the probability distribution of interface configurations in the stationary state is given by Eq. 2.28 [30]. Note however the fact that the same probability distribution describes the stationary interface for the EW and the KPZ equations is true only in one spatial dimension; although a generalization of Eq. 2.28 remains to be true for the EW in all higher dimensions, it does not hold for the KPZ equation in two and higher spatial dimensions.

Equation 2.26 and Eq. 2.30 are special cases of the general form, given by

$$\frac{\partial h(x,t)}{\partial t} = \Gamma \frac{\partial^2 h}{\partial x^2} + \sum_{m=0}^{\infty} \lambda_m \left(\frac{\partial h}{\partial x}\right)^m + \eta(x,t), \quad (2.31)$$

where, e.g., $\lambda_1 = -v_K$, $\lambda_2 = \lambda/2$, etc. The different coefficients λ_m in Eq. 2.31 determine the scaling properties of the height fluctuations, as discussed below. λ_0 can be eliminated by redefining the height variable $h \rightarrow h' = h + \lambda_0 t$. The first-order gradient term, $\lambda_1 \frac{\partial h}{\partial x}$, can be eliminated from Eq. 2.31 by Galilean shift $x \rightarrow x' = x + \lambda_1 t$.

2.8 Scaling properties of the interface equation

The stationary state height fluctuations are measured by

$$S(x,t) = \left\langle \left[\overline{h(x+x',t) - h(x',0)} - \overline{\overline{h(x+x',t) - h(x',0)}} \right]^2 \right\rangle, \quad (2.32)$$

where, as discussed earlier in this chapter, the overbar represents averaging over the initial stationary distribution of the interface configurations (for example, Eq. 2.28 for the KPZ and EW in one dimension), while the angular brackets denote averaging over the stochastic

evolution of the interface in time.

If λ_1 in Eq. 2.31 is nonzero, the autocorrelation function $S(0, t)$ of the interface grows as $S(0, t) \sim t$ for large t [32, 33, 34]. This can be explained in terms of sliding density fluctuations (SDF) with respect to the particle motion, as will be discussed in Chapter 3 and Chapter 4. If $\lambda_0 = \lambda_1 = 0$ in Eq. 2.31, the function $S(x, t)$ assumes the scaling form

$$S(x, t) \sim t^{2\beta} Y\left(\frac{x}{t^{1/z}}\right), \quad (2.33)$$

in the asymptotic limit $x, t \rightarrow \infty$, with $x/t^{1/z} = \text{constant}$. Here, β is the growth exponent, while z is the dynamical exponent. These exponents as well as the scaling function Y are the same for all systems belonging to the same universality class. The scaling function $Y(s)$ has the property that $Y(s) \rightarrow \text{constant}$ as $s \rightarrow 0$, implying that the height autocorrelation $S(0, t)$ behaves as $S(0, t) \sim t^{2\beta}$. Further, as $s \rightarrow \infty$, the function $Y(s) \rightarrow s^{2\alpha}$. Here, α is the critical exponent related to z and β through $z = \alpha/\beta$ [30]. It determines the roughness of the interface through $S(x, 0) \sim x^{2\alpha}$.

For a finite system, the height autocorrelation has the scaling form

$$S(0, t) \sim t^{2\beta} f\left(\frac{t}{L^z}\right), \quad (2.34)$$

where the scaling function $f(s)$ has the property that $f(s) \rightarrow \text{constant}$ for $s \ll 1$, while $f(s) \rightarrow 0$ for $s \gg 1$. Thus, typical height fluctuations at a point on the interface grow with time as t^β with an autocorrelation time $\sim L^z$. Similarly, the correlation function $S(x, 0)$ has the following form for a finite system.

$$S(x, 0) \sim x^{2\alpha} g\left(\frac{x}{L}\right), \quad (2.35)$$

where the scaling function $g(s) \rightarrow \text{constant}$ for $s \ll 1$, while $g(s) \rightarrow 0$ for $s \gg 1$.

We conclude from the above discussions that on scaling the spatial variable x by the scaling parameter b as $x \rightarrow x' = bx$, the time variable scales as $t \rightarrow t' = b^z t$, while the height of the interface scales as $h \rightarrow h' = b^\alpha h$.

Now, we derive the scaling properties of the unequal-time density-density correlation function $C(x, t)$ of the ASEP (defined in Eq. 2.12) from the scaling properties of the interface-equivalent of the ASEP, described above. Since the density fluctuations in the ASEP are related to the local slopes of the interface through Eq. 2.24, we first look at how the local slopes of the interface at two spatial points are correlated in time. Thus, we study the function $C_{\text{interface}}(x, t)$, defined as

$$C_{\text{interface}}(x, t) \equiv \left\langle \overline{\frac{\partial h(x', 0)}{\partial x} \frac{\partial h(x + x', t)}{\partial x}} \right\rangle, \quad (2.36)$$

where the overbar represents averaging over the initial stationary distribution of the interface configurations (for example, Eq. 2.28 for the KPZ and EW in one dimension), while

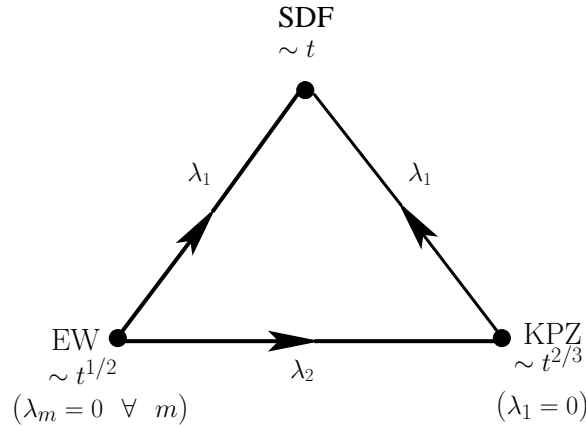


Figure 2.10: Schematic representation of relative stabilities of various fixed points, showing the associated behavior of the autocorrelation function $S(0, t)$, defined in the text. The figure is adapted from Ref. [32].

the angular brackets denote averaging over the stochastic evolution of the interface in time.

Under the scaling transformations, $x \rightarrow x' = bx$, $t \rightarrow t' = b^z t$, and $h \rightarrow h' = b^\alpha h$ for arbitrary scaling parameter b , Eq. 2.36 scales as

$$C_{\text{interface}}(x, t) = b^{2\alpha} C(bx, b^z t). \quad (2.37)$$

Since the scaling parameter b is arbitrary, we choose it such that $b^z t = 1$. As a result, we get, from Eq. 2.37,

$$C_{\text{interface}}(x, t) \sim t^{-2\alpha/z} f\left(\frac{x}{t^{1/z}}\right). \quad (2.38)$$

The scaling function $f(u)$ has the property that $f(u) \rightarrow \text{constant}$ for $u \ll 1$, while, for $u \gg 1$, the function $f(u) \rightarrow 0$. These properties emerge from the following requirements.

(1) For the scaling behavior of the equal-time correlation of the local slopes of the interface at two points far apart, one needs to consider $C(x, t)$ in the limit $t \rightarrow 0$. The corresponding function $C(x, 0)$ must evaluate to zero in the limit of large x . This follows from the fact that the probability distribution of the interface configurations in the stationary state is Gaussian, so that the local slopes of the interface at equal times are uncorrelated over long distances, see Eq. 2.28. In the limit $t \rightarrow 0$, with x fixed at a large value, so that $u = x/t^{1/z} \gg 1$, the scaling function $f(u)$ has to go to zero to ensure the above mentioned behavior of the function $C(x, 0)$.

(2) To find the scaling behavior of the autocorrelation of the local slope of the interface at a given point in space, one needs to consider the function $C(x, t)$ in the limit $x \rightarrow 0$, with t fixed and large. The fact that the scaling function $f(u)$ with $u = x/t^{1/z}$ goes to a constant for $u \ll 1$ ensures that the autocorrelation of the local slope dies down algebraically in time. This is in accordance with the Gaussian distribution for the interface configurations, which precludes any correlation between local slopes at long times.

The scaling properties of the unequal-time density-density correlation of the ASEP, given by $C(x, t)$, will be the same as that of the function $C_{\text{interface}}(x - v_K t, t)$. This is because the time-evolution equation of the interface-equivalent of the ASEP, given by Eq. 2.26, is brought to the KPZ form, Eq. 2.27, through the Galilean transformation $x \rightarrow x' = x - v_K t$. We get

$$C(x, t) \sim t^{-2\alpha/z} f\left(\frac{x - v_K t}{t^{1/z}}\right). \quad (2.39)$$

Since, as we discuss in the next section, $z = 3/2$ and $\alpha = 1/2$ for the KPZ class, we recover the scaling form of $C(x, t)$ given in Eq. 2.15. Moreover, when the co-moving condition $x = v_K t$ is satisfied, using the properties of the scaling function $f(u)$ discussed above, one concludes that $C(x, t) \sim t^{-2/3}$ for large t , in accordance with the discussions in Section 2.5.

2.9 Universality classes: The KPZ, the EW and the SDF

From a perturbative renormalization group (RG) analysis of Eq. 2.31, it is known that there are two distinct fixed points in the parameter space. These two fixed points define two universality classes. The first class is the one in which all $\lambda_m = 0$. In this case, Eq. 2.31 reduces to the EW equation, Eq. 2.30. The resulting linear growth problem was also studied by Hammersley in a different context, namely, in addressing the question of whether the Euclidean space in certain dimension can suffer random distortion (an example of distortion of a two-dimensional Euclidean space could be crumpling of paper) [35]. The values of the critical exponents for the EW class are [31]

$$\beta = 1/4, \quad z = 2 \quad (\text{EW in 1 dimension}). \quad (2.40)$$

The EW fixed point also controls the behavior in systems where only odd-order terms λ_m with $m \geq 3$ are present. The lowest-order nonlinearity is provided by the cubic term. Under a scaling transformation $x \rightarrow x' = bx, t \rightarrow t' = b^z t, h \rightarrow h' = b^\alpha h$, we see that the cubic nonlinear term is marginal around the EW fixed point. Calculations based on mode coupling theory [36] and renormalization group [37, 38] show that it is actually marginally irrelevant, leading to multiplicative logarithmic corrections to the power law in the height autocorrelation: $S(0, t) \sim t^{1/2} (\ln t)^{1/4}$, a behavior that has been verified by numerical simulation study [37, 38, 39].

Even-order coefficients lead to a breaking of $h \rightarrow -h$ symmetry of Eq. 2.31, causing a change in the universality class. The second-order perturbation λ_2 is a relevant perturbation for the EW fixed point that drives the system away from the EW to a new KPZ fixed point. The KPZ fixed point is characterized by the exponent values [28]

$$\beta = 1/3, \quad z = 3/2 \quad (\text{KPZ in 1 dimension}). \quad (2.41)$$

If $\lambda_1 \neq 0$, under the scaling transformation $x \rightarrow x' = bx, t \rightarrow t' = b^z t, h \rightarrow h' = b^\alpha h$,

both the EW and KPZ fixed points are unstable, and a flow towards a third fixed point (SDF) is generated (Fig. 2.10), as we will show in the next two chapters. Specifically, in the next chapter, we discuss in detail our results on size effects on fluctuations in the ASEP, as captured by the tagged particle correlations measuring the variance of the displacement of a tagged ASEP particle about its average displacement.

References

- [1] T. M. Liggett, *Interacting Particle Systems* (Springer-Verlag, New York, 1985).
- [2] B. Schmittmann and R. K. P. Zia, in *Phase Transitions and Critical Phenomena*, edited by C. Domb and J. L. Lebowitz (Academic, London, 1995), Vol. 17.
- [3] F. Spitzer, *Adv. Math.* **5**, 246 (1970).
- [4] P. M. Richards, *Phys. Rev. B* **16**, 1393 (1977).
- [5] D. G. Levitt, *Phys. Rev. A* **8**, 3050 (1973).
- [6] B. Widom, J. L. Viovy, and A. D. Defontaine, *J. Physique I* **1**, 1759 (1991).
- [7] B. Derrida, S. A. Janowsky, J. L. Lebowitz, and E. R. Speer, *Europhys. Lett.* **22**, 651 (1993).
- [8] *Traffic and Granular Flow '97*, edited by M. Schreckenberg and D. Wolf (Springer, New York, 1998); for a recent review, see D. Chowdhury, L. Santen, and A. Schadschneider, *Phys. Rep.* **329**, 199 (2000)
- [9] T. Halpin-Healy and Y-C Zhang, *Phys. Rep.* **254**, 215 (1995).
- [10] J. Krug, *Adv. Phys.* **46**, 139 (1997).
- [11] R. Bundschuh, *Phys. Rev. E* **65**, 031911 (2002).
- [12] S. Klumpp and R. Lipowsky, *J. Stat. Phys.* **113**, 233 (2003).
- [13] J. Krug, *Phys. Rev. Lett.* **67**, 1882 (1991).
- [14] M. R. Evans, D. P. Foster, C. Godrèche, and D. Mukamel, *Phys. Rev. Lett.* **74**, 208 (1995); *J. Stat. Phys.* **80**, 69 (1995).
- [15] C. Godrèche, J. M. Luck, M. R. Evans, D. Mukamel, S. Sandow, and E. R. Speer, *J. Phys. A* **28**, 6039 (1995).
- [16] B. Derrida, E. Domany, and D. Mukamel, *J. Stat. Phys.* **69**, 667 (1992).
- [17] B. Derrida, M. R. Evans, V. Hakim, and V. Pasquier, *J. Phys. A* **26**, 1493 (1993).

- [18] G. M. Schütz and E. Domany, *J. Stat. Phys.* **72**, 277 (1993).
- [19] B. Derrida, *Phys. Rep.* **301**, 65 (1998).
- [20] G. M. Schütz in *Phase Transitions and Critical Phenomena*, edited by C. Domb and J. L. Lebowitz (Academic, London, 2001), Vol. 19.
- [21] N. G. van Kampen, in *Stochastic Processes in Physics and Chemistry* (North Holland, Amsterdam, 1992).
- [22] G. M. Schütz, R. Ramaswamy, and M. Barma, *J. Phys. A* **29**, 837 (1996).
- [23] M. Prähofer and H. Spohn in *In and Out of Equilibrium (Progress in Probability Vol. 51)*, edited by V. Sidoravicius (Boston, MA: Birkhauser), pp 185-204: also, eprint:arXiv:cond-mat/010200.
- [24] J. L. Lebowitz, E. Presutti, and H. Spohn, *J. Stat. Phys.* **51**, 841 (1988).
- [25] J. M. Burgers, in *The Nonlinear Diffusion Equation*, (Reidel, Dordrecht, 1974).
- [26] D. Forster, D. R. Nelson, and M. J. Stephen, *Phys. Rev. A* **16**, 732 (1977).
- [27] H. van Beijeren, R. Kutner, and H. Spohn, *Phys. Rev. Lett.* **54**, 2026 (1985).
- [28] M. Kardar, G. Parisi, and Y. C. Zhang, *Phys. Rev. Lett.* **56**, 889 (1986).
- [29] M. Plischke, Z. Racz, and D. Liu, *Phys. Rev. B* **35**, 3485 (1987).
- [30] A. -L. Barabasi and H. E. Stanley, *Fractal Concepts in Surface Growth* (Cambridge University Press, Cambridge, 1995).
- [31] S. F. Edwards and D. R. Wilkinson, *Proc. R. Soc. London, Ser A* **381**, 17 (1982).
- [32] S. N. Majumdar and M. Barma, *Phys. Rev. B* **44**, 5306 (1991).
- [33] S. N. Majumdar and M. Barma, *Physica A* **177**, 366 (1991).
- [34] M. Barma, *J. Phys. A* **25**, L693 (1992).
- [35] J. M. Hammersley, in *Proceedings of the fifth Berkeley Symposium on Mathematical Statistics and Probability*, edited by L. M. Le Cam and J. Neyman (University of California Press, Berkeley, 1967).
- [36] B. Derrida, J. L. Lebowitz, E. R. Speer, and H. Spohn, *Phys. Rev. Lett.* **67**, 165 (1991); *J. Phys. A* **24**, 4805 (1991).
- [37] M. Paczuski, M. Barma, S. N. Majumdar, and T. Hwa, *Phys. Rev. Lett.* **69**, 2735 (1992).
- [38] P. M. Binder, M. Paczuski and M. Barma, *Phys. Rev. E* **49**, 1174 (1994).

-
- [39] B. Subramanian, G. T. Barkema, J. L. Lebowitz and E. Speer, *J. Phys. A* **29**, 7475 (1996).

Chapter 3

Tagged particle correlations in the ASEP

“When you are describing a shape, sound or tint;
Don’t state the matter plainly,
But put it in a hint;
And learn to look at all things,
With a sort of mental squint.”

Lewis Carroll

In this chapter, we come to our main research topic, namely, studying how does the dynamics of stationary state density fluctuations in the asymmetric simple exclusion process (ASEP) get affected by the finite size of the lattice underlying the process. We address this issue by examining how the tagged particle correlations in the ASEP behave as a function of time. Specifically, we study the variance of the displacement of a tagged particle around its average displacement, where the averaging is over (i) the initial stationary ensemble of ASEP configurations, and (ii) subsequent stochastic evolution of the configurations in time. As we will show in this chapter, the variance captures the motion of density fluctuations around the system as a kinematic wave and consequently, shows pronounced oscillations in time with a well-defined size-dependent time period. The behavior of the variance in time can be characterized by two size-dependent time scales, set by the circulation time and the decay time of the kinematic wave, respectively. While monitoring the variance of the tagged particle displacement, if one does not average over the initial stationary ensemble, and instead, chooses to start from an arbitrary but fixed configuration, drawn from the stationary ensemble, the corresponding variance, which involves averaging over only stochastic evolution, does not oscillate in time; as we show and discuss in this chapter, this quantity effectively captures the growth of the dissipation of the kinematic wave in time.

The layout of this chapter is as follows. We start in Section 3.1 by defining the quantity of interest to us, namely, the tagged particle correlations involving the variance of the tagged

particle displacement. As discussed in the preceding paragraph, the variance may involve averaging over both the initial stationary ensemble and stochastic evolution, or, just the latter. Some results on tagged particle correlations in certain limits were already known in the literature prior to our work; we review this body of work in Section 3.2. Our purpose is to obtain the complete behavior of the tagged particle correlations for a finite system. There are two broad sections in this chapter, one (Section 3.3) dealing with the ASEP on an infinite lattice, while the other, Section 3.4, deals with the finite lattice. In Section 3.3.1, on the basis of the discussions on the motion of particle and coarse-grained density fluctuations in Chapter 2, supplemented by the scaling properties of the Kardar-Parisi-Zhang (KPZ) equation describing the time evolution of the density fluctuations, we propose a schematic representation for the tagged particle displacement in an infinite system. We show how the representation correctly predicts the limiting behavior of the tagged particle correlations, summarized in Section 3.2. Next, in Section 3.3.2, we provide cogent physical arguments in support of the observed behavior of the tagged particle correlations in an infinite system. In Section 3.4.1, we provide a summary of our results characterizing the complete behavior of the tagged particle correlations in a finite system, pointing out all the size-dependent time scales. This is followed in Section 3.4.2 by physical arguments in favor of the observed time scales in the tagged particle correlations. In the last section, Section 3.5, we discuss the motion of the center-of-mass in the ASEP.

3.1 Tagged particle correlations: Definitions

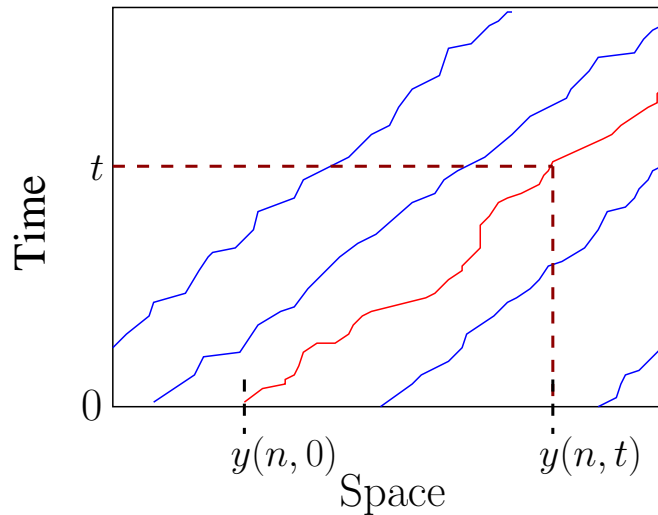


Figure 3.1: Defining the tagged particle displacement $y(n, t)$. The red and the blue lines represent the space-time trajectories of ASEP particles.

We consider N particles executing the ASEP dynamics on a one-dimensional periodic lattice of L sites. At the initial instant $t = 0$, we start with a configuration of particles on

the lattice; we choose this configuration randomly from the stationary ensemble of ASEP configurations. Since the stationary state allows all configurations with N particles to occur with equal probability, every configuration generated that has N particles distributed on L sites is a stationary configuration (see Chapter 2, Section 2.2). Next, we ‘tag’ the particles and label them by the integer $n = 1, 2, \dots, N$. Because of the hard core constraint, the particles do not overtake each other; thus, the ordering of particles, done at the initial instant, is preserved as the configuration evolves in time, following the ASEP dynamics. Let $y(n, t)$ denote the location of the n -th tagged particle at time instant t , as shown in Fig. 3.1. Then, $y(n, t) - y(n, 0)$ measures the displacement of the n -th tagged particle in time t , where our convention is that when the particle has made one complete trip round the ring, the displacement would just be added up, instead of being considered modulo L . In order to find the average displacement of the n -th particle in time t , one has to average over (i) the initial stationary configuration, and (ii) the subsequent stochastic evolution of the configuration in time t . In other words, one randomly draws an initial configuration from the stationary ensemble, lets the configuration evolve in time for a total time t and measures the displacement of the n -th tagged particle at the end of the time t . This process is repeated by randomly choosing the initial configuration over and over again from the stationary ensemble, letting the configuration evolve in time, and finally, making the measurement of the displacement. But, as we discuss below, one may choose to average over only stochastic evolution by starting over and over again from an arbitrary but fixed initial configuration, drawn from the stationary ensemble.

3.1.1 Average over histories and initial conditions: $\sigma^2(L, t)$

Here we start with the stationary ensemble of the ASEP configurations at $t = 0$ and monitor the motion of a tagged particle. Let $\Delta_n(t)$ denote the deviation in the displacement of the n -th tagged particle from its average value in time t , the averaging being with respect to both the initial stationary ensemble at $t = 0$ and stochasticity in the evolution of configurations. In symbols,

$$\Delta_n(t) \equiv y(n, t) - y(n, 0) - \overline{\langle [y(n, t) - y(n, 0)] \rangle} \quad \text{[Ensemble of Initial Conditions]}. \quad (3.1)$$

The angular brackets denote averaging over the stochasticity in the evolution of configurations, while the overbar is used to denote averaging with respect to the initial stationary ensemble at $t = 0$. In the function $\Delta_n(t)$, the quantity $\overline{\langle [y(n, t) - y(n, 0)] \rangle}$ gives the average displacement of the n -th tagged particle in time t in the stationary state, and hence is equal to $v_P t$, where $v_P = (p - q)(1 - \rho) + O(\frac{1}{L})$ (Eq. 2.10). The variance of the displacement, measuring the stationary state fluctuations in $\Delta_n(t)$, is given by

$$\sigma^2(L, t) \equiv \overline{\langle \Delta_n^2(t) \rangle}. \quad (3.2)$$

Since the system is translationally invariant, the above quantity is the same for all particles, and hence we may perform an additional averaging of $\sigma^2(L, t)$ over the particles, without changing the answer.

In this thesis work, we study how the finiteness of the system size L affects the behavior of $\sigma^2(L, t)$ in time, in Section 3.4.1.

3.1.2 Average over histories only: $s^2(L, t)$

Beginning with an arbitrary but *fixed* configuration, chosen from the stationary ensemble and following its evolution in time, it is interesting to monitor the fluctuations in the displacement of a tagged particle, and study how finite size effects come into play here. These fluctuations were first studied by van Beijeren for an infinite system in [1]. In this case, one averages only over the stochasticity in the evolution of the configuration. We define $d_n(t)$ to be the deviation in the displacement of the n -th tagged particle from its mean value in time t , starting from an arbitrary but fixed configuration, drawn from the stationary ensemble at $t = 0$. Explicitly,

$$d_n(t) \equiv y(n, t) - y(n, 0) - \langle [y(n, t) - y(n, 0)] \rangle$$

[Fixed Initial Condition]. (3.3)

The corresponding variance is given by

$$s^2(L, t) \equiv \langle d_n^2(t) \rangle. \tag{3.4}$$

The system being translationally invariant, the above quantity is also averaged over the particles. Moreover, as will see in this chapter, the behavior of $s^2(L, t)$ does not depend on the initial configuration and so, $s^2(L, t)$ may be additionally averaged over different initial configurations.

We note that the behavior of both $\sigma^2(L, t)$ and $s^2(L, t)$ can be extracted from two different limiting values of a single function that measures the fluctuation in the displacement of a tagged particle in the stationary state. At time $t = 0$, we start with an arbitrary but fixed configuration \mathbf{C}_0 , drawn from the stationary ensemble of configurations. After \mathbf{C}_0 has evolved in time for an interval t_0 , we start measuring the variance $C_L(t_0, t_0 + t)$ of the displacement of a tagged particle around its average:

$$C_L(t_0, t_0 + t) \equiv \langle [y(n, t_0 + t) - y(n, t_0) - \langle [y(n, t_0 + t) - y(n, t_0)] \rangle]^2 \rangle, \tag{3.5}$$

where the angular brackets denote averaging with respect to stochastic evolution.

(1) On taking the limit $t_0 \rightarrow 0$, when the averaging is only with respect to stochastic evolution, we get the function $s^2(L, t)$.

(2) On the other hand, since the system is ergodic, in the limit $t_0 \rightarrow \infty$, the initial configuration \mathbf{C}_0 evolves into an ensemble of stationary configurations. Thus, the function

$\lim_{t_0 \rightarrow \infty} C_L(t_0, t_0 + t)$ measures fluctuations in the stationary state where the averaging is with respect to both the initial stationary ensemble and stochastic evolution. Hence, this quantity is identical to $\sigma^2(L, t)$.

3.2 Review of earlier work

3.2.1 $\sigma^2(L, t)$

In studying the quantity $\sigma^2(L, t)$, two different limits have been considered earlier.

(a) On taking the limit $L \rightarrow \infty$ first, followed by the limit $t \rightarrow \infty$, the fluctuations are diffusive, growing linearly in time: $\sigma^2(t) \equiv \lim_{L \rightarrow \infty} \sigma^2(L, t) \sim D_0 t$. Here, D_0 is a known function of the particle density and the external bias and is given by $D_0 = (p - q)(1 - \rho)$ [2].

(b) In the opposite limit with $t \rightarrow \infty$ before $L \rightarrow \infty$, $\sigma^2(L, t)$ again behaves diffusively, i.e., $\sigma^2(L, t) \sim D(L)t$, but now the diffusion constant $D(L)$ depends on the system size L and scales as $D(L) \sim \frac{1}{\sqrt{L}}$ for large L [3].

3.2.2 $s^2(L, t)$

In studying the quantity $s^2(L, t)$, only one limit has been considered earlier, namely, the limit $L \rightarrow \infty$ first, followed by $t \rightarrow \infty$; in this limit, one has $s^2(t) \equiv \lim_{L \rightarrow \infty} s^2(L, t) \sim t^{2/3}$, independent of the initial configuration [1].

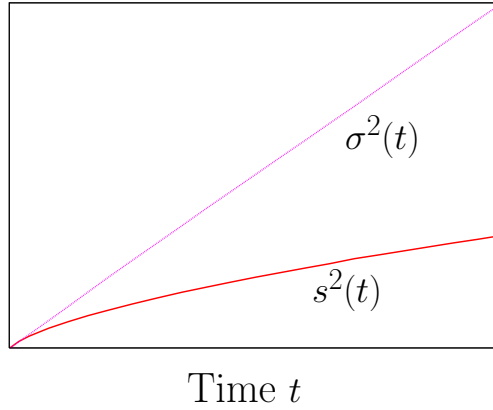


Figure 3.2: Behavior of the tagged particle correlations $\sigma^2(t)$ and $s^2(t)$ for an infinite system.

3.3 Infinite system

As discussed in the preceding section, for an infinite system one has $\sigma^2(t) \equiv \lim_{L \rightarrow \infty} \sigma^2(L, t) \sim D_0 t$, while one has $s^2(t) \equiv \lim_{L \rightarrow \infty} s^2(L, t) \sim t^{2/3}$. The behavior of the quantities $\sigma^2(t)$ and $s^2(t)$ are shown schematically in Fig. 3.2.

3.3.1 Representation of the tagged particle displacement in an infinite system

On the basis of the discussion in Chapter 2, Section 2.4, we conclude that in the stationary state, the displacement of the n -th tagged particle, $y(n, t) - y(n, 0)$, has contributions from three distinct physical sources, namely, systematic drift, sliding density fluctuations, and their dissipation. Correspondingly we write

$$y(n, t) - y(n, 0) \approx v_P t + t^\alpha G_n(t) + t^\beta \chi_n(t), \quad (3.6)$$

where $\alpha = \alpha_{KPZ} = 1/2$ is the roughness exponent while $\beta = \beta_{KPZ} = 1/3$ is the growth exponent of the interface equivalent to the ASEP. The representation, Eq. 3.6, is based on the following arguments. First, the coarse-grained density fluctuations for the ASEP are described by the KPZ interface whose fluctuation profile moves with the velocity $v_K - v_P$, relative to the particle (Section 2.7). As a result, in time t , the particle senses the fluctuations over a spatial stretch of length $(v_K - v_P)t$. From the scaling analysis of the interface summarized in Section 2.8, the typical fluctuation over this distance scales as $[(v_K - v_P)t]^\alpha \sim t^\alpha$ (Eq. 2.35). This fact is encoded in the second term in Eq. 3.6 where $G_n(t)$ is a random variable which depends only on the initial configuration, drawn from the stationary ensemble, but is independent of the stochastic noise in the evolution of configurations. The fluctuations arising from the dissipation typically grow with time as t^β (Eq. 2.34) and are represented by the last term in Eq. 3.6. Here $\chi_n(t)$ is a random variable that depends only on the noisy history in the evolution of configurations, but is independent of the initial configuration.

We show below how the form, Eq. 3.6, accounts for the observed behavior of correlation functions for an infinite system, summarized in Section 3.2.

- On averaging with respect to both the initial stationary ensemble and stochastic evolution, we get

$$\overline{\langle y(n, t) - y(n, 0) \rangle} \approx v_P t + t^\alpha \overline{G_n} + t^\beta \langle \chi_n \rangle, \quad (3.7)$$

where, as previously, the angular brackets denote averaging with respect to the stochastic evolution, while the overbar is used to denote averaging with respect to the initial stationary ensemble.

It follows that for the variable defined in Eq. 3.1,

$$\Delta_n(t) \approx t^\alpha (G_n - \overline{G_n}) + t^\beta (\chi_n - \langle \chi_n \rangle). \quad (3.8)$$

With $\alpha = 1/2$ and $\beta = 1/3$ for the ASEP (which is in the KPZ universality class), the first term on the right hand side dominates for large t . We recover the result for $\sigma^2(L, t) = \overline{\langle \Delta_n^2(t) \rangle}$ for an infinite system [2] (described in Section 3.2.1(a)), given by

$$\sigma^2(t) = \lim_{L \rightarrow \infty} \sigma^2(L, t) \stackrel{t \rightarrow \infty}{\sim} \overline{t(G_n - \overline{G_n})^2} \sim t. \quad (3.9)$$

- For fixed initial condition, averaging over noise history, we get

$$\langle y(n, t) - y(n, 0) \rangle \approx v_P t + t^\alpha G_n + t^\beta \langle \chi_n \rangle. \quad (3.10)$$

Thus, for the displacement variable defined in Eq. 3.3, we have

$$d_n(t) \approx t^\beta [\chi_n - \langle \chi_n \rangle]. \quad (3.11)$$

The fluctuations in $d_n(t)$ are measured by $s^2(L, t)$ according to the definition, Eq. 3.4. Thus, one has

$$s^2(t) = \lim_{L \rightarrow \infty} s^2(L, t) \stackrel{t \rightarrow \infty}{\sim} t^{2\beta} \langle (\chi_n - \langle \chi_n \rangle)^2 \rangle \sim t^{2\beta}. \quad (3.12)$$

With $\beta = 1/3$, we get the result $s^2(t) \sim t^{2/3}$ [1] for the growth of the variance of the displacement of a tagged particle in an infinite system, starting from an arbitrary fixed initial configuration drawn from the stationary ensemble, as discussed in Section 3.2.2.

3.3.2 Tagged particle correlations: Physical arguments

$\sigma^2(t)$

As the averaging in Eq. 3.2 is with respect to both the initial stationary ensemble and stochastic noise in the evolution of configurations, the average drift in time t is $v_P t$, and fluctuations in the tagged particle displacement are defined with respect to this. In the rest frame of the density fluctuations, the tagged particle has an average velocity $u = v_P - v_K$. In time t , it traverses a sequence of density fluctuations over a distance $(v_P - v_K)t$, with each fluctuation adding a stochastic noise to the motion of the tagged particle. The noise is uncorrelated since the stationary state configurations have a product measure. The variance $\sigma^2(t)$ is thus proportional to t for large t , by virtue of the central limit theorem. The coefficient of proportionality D_0 is known to be $v_P = (p - q)(1 - \rho)$ [2]. This expression for D_0 can be easily derived using the above picture of drift of the tagged particles relative to the density fluctuations [4].

$s^2(t)$

For $s^2(t)$, the fluctuations are measured by starting from a single fixed configuration, drawn from the ensemble of stationary states. Thus, in every measurement, the particle passes through the *same* sequence of density fluctuations. However, dissipation of the density profile is different from history to history.

Define the deviation in the displacement of a tagged particle from $v_P t$ by

$$D_n(t) = y(n, t) - y(n, 0) - v_P t. \quad (3.13)$$

The dissipation in the density profile being different for different histories shows up in $D_n(t)$, as depicted by the gray trajectories in Fig. 3.3. Notice that the mean over histories, $\langle D_n(t) \rangle$, is nonvanishing, as depicted by the black curve in Fig. 3.3. Also, the mean, $\langle D_n(t) \rangle$, depends on the initial configuration, drawn from the stationary ensemble.

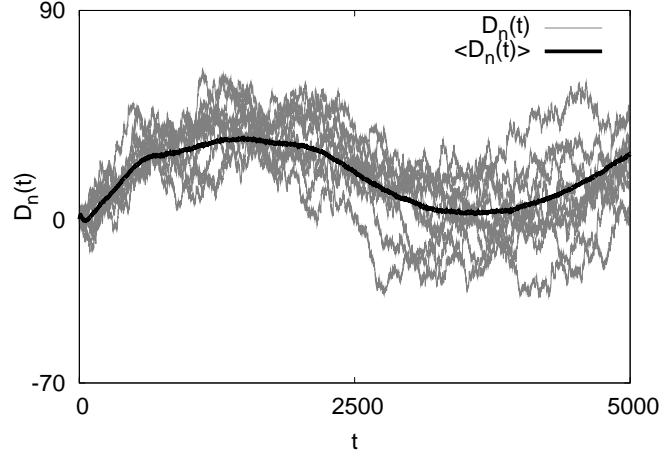


Figure 3.3: The gray curves show the distance covered, $D_n(t)$, in time t about the mean $v_P t$ by the n -th tagged particle for 10 Monte Carlo runs for a single fixed initial configuration, drawn from the stationary ensemble of the TASEP. The black curve shows the mean displacement, $\langle D_n(t) \rangle$, obtained by averaging over 500 histories. Here, $L = 10,000$, the particle density $\rho = 0.25$.

Since the variance $s^2(t)$ of the fluctuation in Eq. 3.4 is measured with respect to $v_P t + \langle D_n(t) \rangle$, it is able to sense the dissipation of the density profile in time, without the effects of sliding density fluctuations (represented by the term $t^\alpha G_n(t)$ in Eq. 3.6, see Eq. 3.14 below). Moreover, although $\langle D_n(t) \rangle$ depends on the initial configuration, since $s^2(t)$ measures fluctuations about $v_P t + \langle D_n(t) \rangle$, it does not depend on the initial configuration. From Eq. 3.6, with $\alpha = 1/2$ and $\beta = 1/3$, we get $D_n(t) = t^{1/2} G_n(t) + t^{1/3} \chi_n(t)$; on averaging over stochastic evolution, we get

$$\langle D_n(t) \rangle = t^{1/2} G_n(t) + t^{1/3} \langle \chi_n(t) \rangle. \quad (3.14)$$

The first term in Eq. 3.14 dominates, and thus at large t , $\langle D_n(t) \rangle$ is primarily determined by the pattern of spatial density fluctuations in the initial configuration. Ignoring the dissipative component (the second term in Eq. 3.14), we expect $\langle D_n(t) \rangle$ to be given by $D_n^*(t) \approx (p - q) \int_0^t dt' \{ (1 - \rho(x)) - (1 - \rho) \}$ (see Fig. 3.4). Making a change of variable from t to x , and noting that the Jacobian of transformation from t to x is $1/(v_P - v_K)$, we get

$$D_n^*(t) \approx \frac{(p - q)}{v_P - v_K} \int_{y(n,0)}^{y(n,0) + (v_P - v_K)t} dx \{ (1 - \rho(x)) - (1 - \rho) \}. \quad (3.15)$$

The upper limit of the integral incorporates the relative distance moved by the particle,

$(v_P - v_K)t$, neglecting fluctuations of $O(t^{1/2})$ coming from the second term in Eq. 3.6.

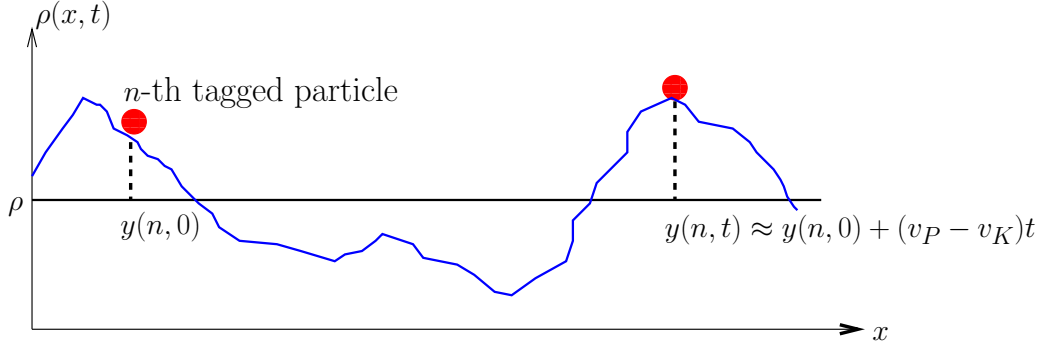


Figure 3.4: Integrating the spatial density fluctuations in the initial configuration to obtain $D_n^*(t)$, defined in the text.

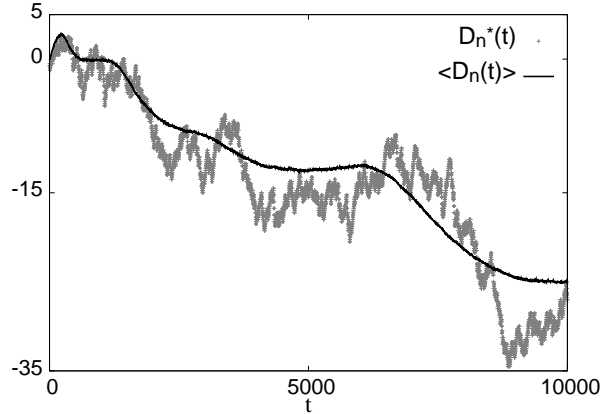


Figure 3.5: Comparison between $\langle D_n(t) \rangle$ and $D_n^*(t)$ for a fixed initial stationary configuration of the TASEP. $\langle D_n(t) \rangle$ was obtained from simulations, and involves averaging over 1000 histories. $D_n^*(t)$ was obtained by integrating the initial density profile according to Eq. 3.15 (see text). Here, $L = 10,000$, while the density $\rho = 0.25$.

In Fig. 3.5, we have compared $\langle D_n(t) \rangle$ with $D_n^*(t)$ for a randomly chosen initial configuration. $\langle D_n(t) \rangle$ was obtained from simulations, while $D_n^*(t)$ was obtained by integrating the initial density profile, following Eq. 3.15. We see that there is good agreement between the signals for $\langle D_n(t) \rangle$ and $D_n^*(t)$. Fluctuations over a distance δx dissipate in a time $t \sim (\delta x)^z$ with $z = 3/2$. Thus, with increasing t , spatial fluctuations in the initial profile are smeared out over larger distances, a fact which is borne out by Fig. 3.5. We have also measured the overlap function for the signs of the two signals, $\langle D_n(t) \rangle$ and $D_n^*(t)$, for 10 different randomly chosen initial configurations at stationarity, and found a mean value 0.8, which indicates a fairly good degree of correlation between the two signals.

3.4 Finite system

3.4.1 Summary of our results

$\sigma^2(L, t)$

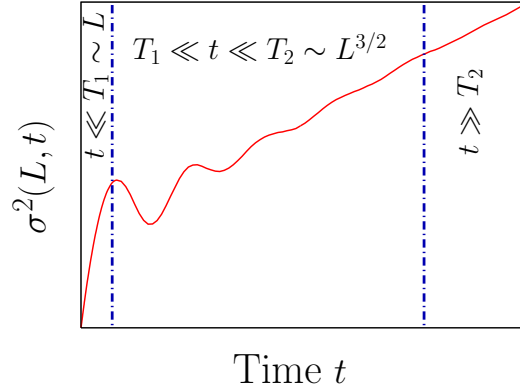


Figure 3.6: Behavior of the variance $\sigma^2(L, t)$ as a function of time for finite L ; the relevant time scales are also marked.

The behavior of $\sigma^2(L, t)$ as a function of time can be characterized by two time scales $T_1 \sim L$ and $T_2 \sim L^{3/2}$, as shown in Fig. 3.6.

(a) In the initial linear regime ($t \ll T_1$), the variance $\sigma^2(L, t) \sim D_0 t$, where $D_0 = (p - q)(1 - \rho)$ [5].

(b) In the oscillatory regime ($T_1 \ll t \ll T_2$), the quantity $\sigma^2(L, t)$ oscillates as a function of t . The amplitude of oscillations is proportional to the system size L , while the time period of oscillations is $T = L/u$, where $u = v_P - v_K$. Here, v_P is the mean velocity of the particles, while v_K is that of the coarse-grained stationary state density fluctuations.

(c) In the late time regime ($t \gg T_2$), the quantity $\sigma^2(L, t) \sim D(L)t$ with $D(L) \sim \frac{1}{\sqrt{L}}$.

The behavior of $\sigma^2(L, t)$ in time can be put into the following scaling form.

$$\sigma^2(L, t) \sim Lg\left(\frac{t}{L}, \frac{t}{L^{3/2}}\right), \quad (3.16)$$

where the scaling function $g(u, v)$ behaves in the following manner. $g(u, v) \sim v$ for $v \gg 1$, while, $g(u, v) \sim u$ for $u \ll 1$. For $u \gg 1, v \ll 1$, the scaling function behaves as $g(u, v) \sim v^{2/3}$.

Note that when the limit $L \rightarrow \infty$ is taken first, followed by the limit $t \rightarrow \infty$, the correlation $\sigma^2(L, t)$ is in the initial linear regime and behaves linearly in time with the coefficient $D_0 = (p - q)(1 - \rho)$. On the other hand, when the limit $t \rightarrow \infty$ is taken first, followed by the limit $L \rightarrow \infty$, the correlation $\sigma^2(L, t)$ is in the late time regime and behaves linearly in time with the coefficient $D(L) \sim \frac{1}{\sqrt{L}}$. These predictions are consistent with results known earlier, summarized in Section 3.2.

$s^2(L, t)$

The time variation of $s^2(L, t)$ is independent of the initial configuration and can be characterized by a single time scale $T^* \sim L^{3/2}$, as shown in Fig. 3.7.

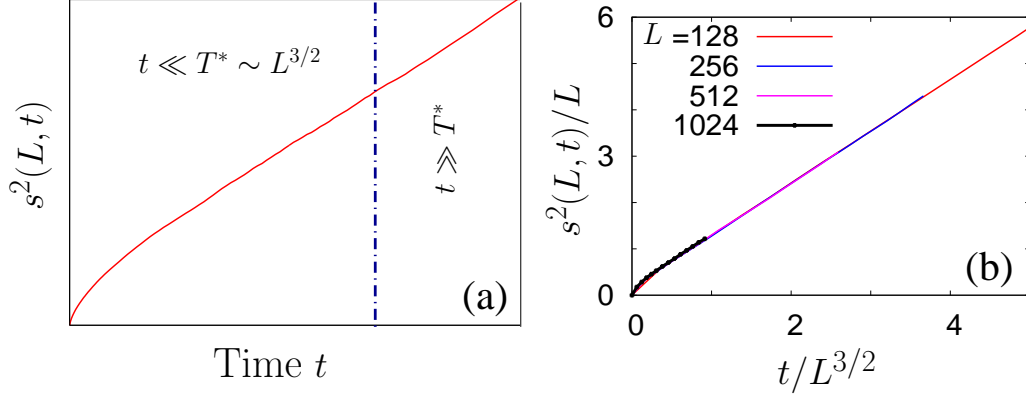


Figure 3.7: (a) Behavior of the variance $s^2(L, t)$ as a function of time for finite L ; the relevant time scales are also marked. (b) Scaling of $s^2(L, t)$ for different system sizes in accordance with Eq. 3.17. The data are obtained from Monte Carlo simulations of the TASEP. Here, the particle density $\rho = 0.25$. The system sizes are marked in the figure.

(a) $t \ll T^*$: In this regime, $s^2(L, t) \sim t^{2/3}$.

(b) $t \gg T^*$. Here, $s^2(L, t) \sim D(L)t$ with $D(L) \sim \frac{1}{\sqrt{L}}$.

The behavior of $s^2(L, t)$ in time can be put into the following scaling form.

$$s^2(L, t) \sim Lf\left(\frac{t}{L^{3/2}}\right), \quad (3.17)$$

where the scaling function $f(u)$ behaves in the following manner. $f(u) \sim u^{2/3}$ for $u \ll 1$, while, $f(u) \sim u$ for $u \gg 1$. The validity of the scaling form in Eq. 3.17 is confirmed by the scaling plot of Fig. 3.7(b).

Note that when the limit $L \rightarrow \infty$ is taken first, followed by the limit $t \rightarrow \infty$, the correlation $s^2(L, t)$ is in the regime $t \ll T^*$. The corresponding predicted behavior of $t^{2/3}$ growth in time is consistent with the result known earlier, summarized in Section 3.2.

The long-time behavior of both the functions $\sigma^2(L, t)$ and $s^2(L, t)$ is diffusive, with the same diffusion constant $D(L)$ which scales with the system size as $D(L) \sim \frac{1}{\sqrt{L}}$. This behavior is attributed to the motion of the center-of-mass.

The variation of $\sigma^2(L, t)$ and $s^2(L, t)$ with time for two different system sizes are shown in Fig. 3.8.

3.4.2 Tagged particle correlations: Physical arguments

We now turn to explaining the behavior of $\sigma^2(L, t)$ and $s^2(L, t)$ on a finite lattice.

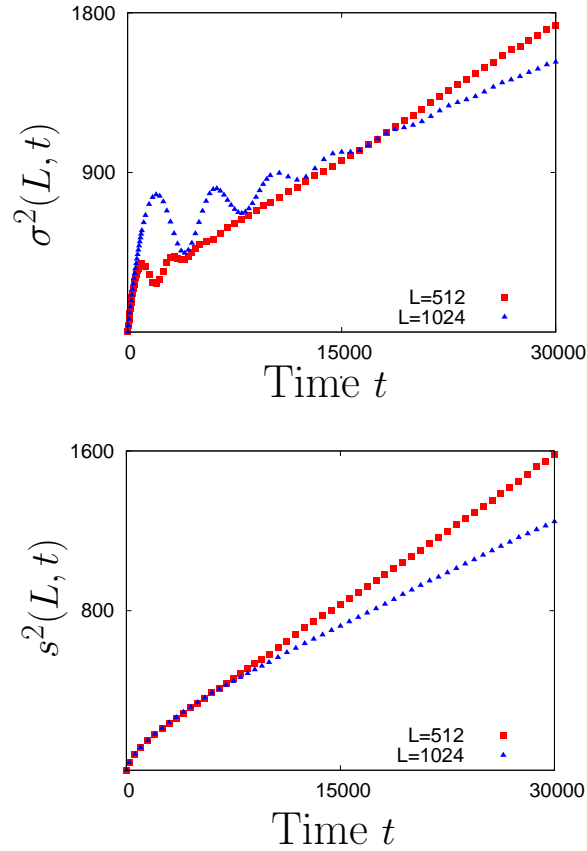


Figure 3.8: Monte Carlo simulation results for the time dependence of the variance of the displacement for the TASEP on a finite lattice for $\sigma^2(L, t)$ and $s^2(L, t)$. In both cases, the averaging is over 10^5 MC runs. Here, the density $\rho = 0.25$. The two system sizes are 512 and 1024.

$$\sigma^2(L, t)$$

In the rest frame of the density fluctuations, a tagged particle has velocity $u = v_P - v_K$ and would take time $T = L/u$ to return to its initial environment of density fluctuations. Thus the variance of the tagged particle displacement should increase from 0 at $t = 0$, reach a maximum at around $T/2$, and come down to almost zero at $t = T$. The difference from zero at $t = T$ is due to dissipation in the density profile arising from stochasticity in the dynamics. This scenario recurs at integral T 's; the time period of oscillations is $T = L/u = L/[(p - q)\rho]$

The oscillations do not continue forever because of the cumulative effect of dissipation. An estimate for the time taken to completely dissipate an initial pattern of density fluctuations is $T_2 \sim L^z$, where the dynamical exponent z is known to have the value $3/2$ [6]. For times $t \gg T_2$, when the initial density profile has completely dissipated away, the fluctuations are entirely due to the motion of the center-of-mass: $\sigma^2(L, t) \sim D(L)t$ with $D(L) \sim \frac{1}{\sqrt{L}}$. Now, we explain why, when $t \gg T_2$, the fluctuations are entirely due to the

diffusive motion of the center-of-mass. First, note that at time t , the number of independent density fluctuations in the system is $\sim L/\delta x$, where δx is the typical length over which density fluctuations (equivalently, height fluctuations, because of the mapping in Chapter 2, Section 2.7) are correlated in a given configuration. From the scaling properties of the time-evolution equation of the interface, it follows that δx increases with time as $\delta x \sim t^{1/z}$ with $z = 3/2$ (see Section 2.8). Now, when $t \gg T_2 \sim L^{3/2}$, the interface starts moving as a whole, i.e., this is the regime in which the center-of-mass starts to move, and exhibit an unbiased diffusive motion in time.

The lower envelope $\Lambda^2(L, t)$ of the oscillations in $\sigma^2(L, t)$ is determined by the dissipation of the stationary state density profile, and can be studied by the method of sliding tags [4, 7, 8, 9, 10, 11, 12, 13]. In order to monitor the dissipation of the moving density profile, we need to correlate, at different times, the location of two different particles. Since in the frame of the density fluctuations, particles move with velocity $u = v_P - v_K$, we need to examine the function

$$\Lambda^2(L, t) = \left\langle \left[\overline{y(n', t) - y(n, 0)} - \overline{\overline{[y(n', t) - y(n, 0)]}} \right]^2 \right\rangle, \quad (3.18)$$

where

$$n' = n - \rho ut. \quad (3.19)$$

The tag shift ρut accounts for the relative motion of the particles and the density profile, and ensures that the time evolution of the same density patch is being recorded at every instant. Equation 3.19, representing sliding of the tag, is tantamount to a Galilean shift that gets rid of the drift term, $u \frac{\partial h}{\partial x}$, in Eq. 2.26. In Fig. 3.9, we show how the method of sliding tags discussed above gives the lower envelope $\Lambda^2(L, t)$ of the oscillatory quantity $\sigma^2(L, t)$. This envelope grows with time as $t^{2/3}$ until times $T_2 \sim L^{3/2}$, beyond which $\Lambda^2(L, t) \sim D(L)t$ with $D(L) \sim \frac{1}{\sqrt{L}}$. Thus, beyond $T_2 \sim L^{3/2}$, there is no distinction between the temporal behavior of $\sigma^2(L, t)$ and $\Lambda^2(L, t)$. The scaling of $D(L)$ with the system size L is obtained by matching the behavior of $\Lambda^2(L, t)$ across T_2 .

$s^2(L, t)$

Since we always use the same initial condition in this case, the particle moves through the same sequence of density fluctuations in every measurement. Nevertheless, the dissipation of the density profile is different for different histories, and $s^2(L, t)$ captures this. Moreover, since $s^2(L, t)$ measures dissipation about the mean density profile (which depends on the initial configuration), it follows that $s^2(L, t)$ is independent of the initial configuration. Typical fluctuation grows with time as $t^{1/3}$, following Eq. 3.6, with $\beta = 1/3$. This leads to $s^2(L, t) \sim t^{2/3}$. This behavior continues until $t \gg T^* \sim L^{3/2}$ when the fluctuations are due to the diffusive motion of the center-of-mass, as explained in Section 3.4.2. This gives $s^2(L, t) \sim D(L)t$ with $D(L) \sim \frac{1}{\sqrt{L}}$. One obtains the scaling of $D(L)$ with the system size L

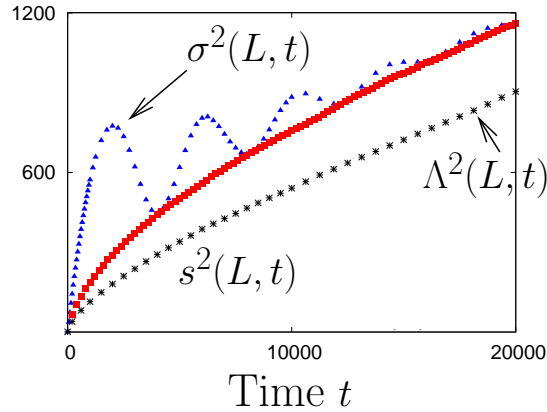


Figure 3.9: Monte Carlo simulation results for various tagged particle correlations. The topmost curve refers to the variance $\sigma^2(L, t)$ of the displacement when the averaging is over both the initial stationary ensemble and stochastic evolution. The middle curve is the sliding tag correlation function $\Lambda^2(L, t)$ defined in the text; it coincides with $\sigma^2(L, t)$ at the local minima of the latter. The lowermost curve shows the variance $s^2(L, t)$ when the averaging is only over stochastic evolution. Here, $\rho = 0.25$. The system size is 1024. The averaging is over 10^5 Monte Carlo runs.

by a simple match in the behavior of $s^2(L, t)$ across $T^* \sim L^{3/2}$.

From the discussions in Sections 3.4.1 and 3.4.2, it follows that both the quantities $\Lambda^2(L, t)$ and $s^2(L, t)$ have similar behavior in time. Thus, both behave as $t^{2/3}$ until time $T^* \sim L^{3/2}$. Beyond T^* , both the quantities behave linearly in time with the constant of proportionality scaling with the system size L as $\frac{1}{\sqrt{L}}$. However, the numerical value of the corresponding constant of proportionality in each of the two time regimes, $t \ll T^*$ and $t \gg T^*$, is larger in $\Lambda^2(L, t)$ than in $s^2(L, t)$. The constant of proportionality for both the quantities in the two time regimes may be computed for a linear interface model, which we introduce in Chapter 4. This model is in the EW universality class, and hence, the following quantities behave differently. (i) The time scale T^* scales with the system size as $T^* \sim L^2$, and not as $L^{3/2}$, as for the ASEP. (ii) For $t \ll T^*$, both the quantities $\Lambda^2(L, t)$ and $s^2(L, t)$ behave in time as \sqrt{t} , and not as $t^{2/3}$, as for the ASEP. (iii) For $t \gg T^*$, both the quantities $\Lambda^2(L, t)$ and $s^2(L, t)$ behave linearly in time, as for the ASEP. However, the corresponding constant of proportionality for both $\Lambda^2(L, t)$ and $s^2(L, t)$ scales as the inverse of the system size, and not as the inverse square root of the system size, as for the ASEP. The exact solution of the linear interface model will be detailed in Chapter 4. For the time being, we just note that the solution of the linear interface model also supports the fact that the numerical value of the corresponding constant of proportionality in each of the two time regimes, $t \ll T^*$ and $t \gg T^*$, is larger in $\Lambda^2(L, t)$ than in $s^2(L, t)$, as shown below.

- For $t \ll T^*$ ($\sim L^2$),

$$\Lambda^2(L, t) \approx \frac{2A}{\sqrt{\pi\Gamma}} \sqrt{t}, \quad (3.20)$$

$$s^2(L, t) \approx A \sqrt{\frac{2}{\pi\Gamma}} \sqrt{t}. \quad (3.21)$$

- For $t \gg T^*$,

$$\Lambda^2(L, t) \approx \frac{2A}{L} t + \frac{AL}{\pi^2\Gamma} \left(\frac{\pi^2}{6} \right), \quad (3.22)$$

$$s^2(L, t) \approx \frac{2A}{L} t + \frac{AL}{2\pi^2\Gamma} \left(\frac{\pi^2}{6} \right). \quad (3.23)$$

In the above equations, A and Γ are constants; their expressions are given in the paragraph following Eq. 4.2 in Chapter 4.

3.5 Center-of-mass motion

In this section, we examine the motion of the center-of-mass for the ASEP, defined as

$$Y_{CM}(t) = \frac{1}{N} \sum_{n=1}^N y(n, t). \quad (3.24)$$

Define, for fixed initial configuration, drawn from the stationary ensemble,

$$d_{CM}(t) = Y_{CM}(t) - Y_{CM}(0) - \langle Y_{CM}(t) - Y_{CM}(0) \rangle, \quad (3.25)$$

where, as usual, angular brackets denote averaging over noise in the evolution of configurations. On the basis of the representation in Eq. 3.6, we have

$$y(n, t) - y(n, 0) - \langle y(n, t) - y(n, 0) \rangle = t^\beta [\chi_n(t) - \langle \chi_n(t) \rangle]. \quad (3.26)$$

This gives

$$d_{CM}(t) = \frac{t^\beta}{N} \sum_{n=1}^N [\chi_n(t) - \langle \chi_n(t) \rangle]. \quad (3.27)$$

Hence,

$$\langle d_{CM}^2(t) \rangle = \frac{t^{2\beta}}{N^2} \sum_{n,m} [\langle \chi_n(t) \chi_m(t) \rangle - \langle \chi_n(t) \rangle \langle \chi_m(t) \rangle]. \quad (3.28)$$

The bracketed quantity on the right hand side, in the stationary state, becomes a function, $f(n - m, t)$, of the difference. Putting this in Eq. 3.28, we get

$$\langle d_{CM}^2(t) \rangle = \frac{t^{2\beta}}{N} \sum_{n-m} f(n - m, t). \quad (3.29)$$

The random variables $\chi_n(t)$ are correlated only up to $\xi(t) \sim t^{1/z}$; this follows from the scaling properties of the interface equation (equivalently, the coarse-grained density profile), summarized in Chapter 2, Section 2.8. We write

$$\sum_{n-m} f(n-m, t) = \rho \int_0^{\xi(t)} dx f(x, t) \sim \rho t^{1/z} \int_0^1 dy g(y). \quad (3.30)$$

In arriving at the second step in the above equation, we have made a transformation of the tag variable $(n-m)$ to the spatial variable x . Plugging Eq. 3.30 in Eq. 3.29, we get

$$\langle d_{CM}^2(t) \rangle \sim \frac{t^{2\beta+1/z}}{L}. \quad (3.31)$$

The above result is derived on the basis of the representation for the tagged particle displacement, Eq. 3.6, based on a scaling argument. Eq. 3.31 is expected to hold for an interface with nonequilibrium dynamics with critical exponents β and z for times $t \ll L^z$. For large times $t \gg L^z$, the fluctuations are expected to grow diffusively, as indicated by the linear behavior of the variances $\sigma^2(L, t)$ and $s^2(L, t)$. Thus, for $t \gg L^z$, we expect $\langle d_{CM}^2(t) \rangle \sim D(L)t$. Matching the behavior of $\langle d_{CM}^2(t) \rangle$ at the crossover time $t^* \sim L^z$, we get $D(L) \sim L^{(2\beta-1)z}$.

With $z = z_{KPZ} = 3/2$ and $\beta = \beta_{KPZ} = 1/3$ for the ASEP, we have

$$\langle d_{CM}^2(t) \rangle \sim \begin{cases} \frac{t^{4/3}}{L} & \text{if } t \ll L^{3/2}, \\ \frac{t}{\sqrt{L}} & \text{if } t \gg L^{3/2}. \end{cases} \quad (3.32)$$

The result $\langle d_{CM}^2(t) \rangle \sim \frac{t^{4/3}}{L}$ for $t \ll L^{3/2}$ for the ASEP has already been observed by van Beijeren *et al.* in [14].

For the EW class with $\beta = \beta_{EW} = 1/4, z = z_{EW} = 2$, we get $D(L) \sim \frac{1}{L}$. Thus, we expect, on the basis of our representation for the tagged particle displacement Eq. 3.6,

$$\langle d_{CM}^2(t) \rangle \sim \frac{t}{L}, \quad (3.33)$$

true for all times.

In order to gain an analytic understanding of the tagged particle correlations in the ASEP, in the next chapter, we relate the tagged particle correlations to the height fluctuations of a nonequilibrium interface in the Kardar-Parisi-Zhang (KPZ) universality class [15]. This is achieved by interpreting the particle label as horizontal coordinate for the interface, while the particle location maps onto the local height of the interface [7]; the mapping is discussed in detail in the next chapter. For the case when the nonlinear term in the KPZ equation is zero, we solve the equation exactly for the tagged particle correlations. We outline the exact solution in the next chapter, and also discuss how the exact solution correctly predicts the size dependence of the time scales T_1, T_2 and T^* , observed for the tagged particle correlations in the ASEP.

References

- [1] H. van Beijeren, J. Stat. Phys. **63**, 47 (1991).
- [2] A. De Masi and P. A. Ferrari, J. Stat. Phys. **38**, 603 (1985); R. Kutner and H. van Beijeren, J. Stat. Phys. **39**, 317 (1985).
- [3] B. Derrida, M. R. Evans, and D. Mukamel, J. Phys. A **26**, 4911 (1993); B. Derrida and K. Mallick, *ibid* **30**, 1031 (1997).
- [4] M. Barma, J. Phys. A **25**, L693 (1992).
- [5] In the absence of the external drive, it is known that $\sigma^2(L, t) \sim t^{1/2}$ [T. E. Harris, J. Appl. Probab. **2**, 323 (1965); R. Arratia, Ann. Probab. **11**, 362 (1983); see also T. M. Liggett, *Interacting Particle Systems* (Springer-Verlag, New York, 1985). In the ASEP, if the external drive is small, there is a size-independent short-time precursor to the initial linear regime where $\sigma^2(L, t) \sim t^{1/2}$.
- [6] D. Dhar, Phase Transitions **9**, 51 (1987); L. -H. Gwa and H. Spohn, Phys. Rev. A **46**, 844 (1992).
- [7] S. N. Majumdar and M. Barma, Phys. Rev. B **44**, 5306 (1991).
- [8] S. N. Majumdar and M. Barma, Physica A **177**, 366 (1991).
- [9] M. Paczuski, M. Barma, S. N. Majumdar, and T. Hwa, Phys. Rev. Lett. **69**, 2735 (1992).
- [10] P. M. Binder, M. Paczuski, and M. Barma, Phys. Rev. E **49**, 1174 (1994).
- [11] G. Tripathy and M. Barma, Phys. Rev. Lett. **78**, 3039 (1997).
- [12] D. Das, A. Basu, M. Barma, and S. Ramaswamy, Phys. Rev. E **64**, 021402 (2001).
- [13] A. A. Ferreira and F. C. Alcaraz, Phys. Rev. E **65**, 052102 (2002).
- [14] H. van Beijeren, R. Kutner, and H. Spohn, Phys. Rev. Lett. **54**, 2026 (1985).
- [15] M. Kardar, G. Parisi, and Y. C. Zhang, Phys. Rev. Lett. **56**, 889 (1986).

Chapter 4

Linear interface model: Analytical results

“The time has come,” the Walrus said,
“To talk of many things:
Of shoes—and ships—and sealing-wax—
Of cabbages—and kings—
And why the sea is boiling hot—
And whether pigs have wings.”

Lewis Carroll

The tagged particle correlations in the ASEP, discussed in the last chapter, can be translated directly into the height fluctuations of a nonequilibrium growing interface in the Kardar-Parisi-Zhang (KPZ) universality class. This is achieved through a mapping of the ASEP, configuration by configuration, to a nonequilibrium interface; specifically, one interprets the particle tag in the ASEP as horizontal coordinate for the interface, while the particle location maps onto the local height of the interface [1]. This procedure of mapping employs the tagging process of the particles in a direct and essential way in the translation, and is different from that discussed in Chapter 2, Section 2.7, where the ASEP density profile was mapped onto an interface profile in the KPZ class by interpreting presence of an ASEP particle as a downward slope of the interface, while a vacancy was mapped onto an upward slope of the interface. The mapping discussed in this chapter results in a time-evolution equation for the interface, which is the usual KPZ equation, augmented by a drift term which accounts for the sliding density fluctuations, i.e., the phenomena of coarse-grained density fluctuations sliding past the tagged particles (Chapter 2, Section 2.4). The KPZ equation is nonlinear and hence, cannot be solved exactly. By dropping the nonlinear term in the KPZ equation, we obtain a linear interface in the Edwards-Wilkinson (EW) universality class. The resultant time-evolution equation is the EW equation with a drift term, which we solve exactly for the height fluctuations (equivalently, the tagged particle correlations for the microscopic models which map onto the EW equation with the drift

term, see Chapter 5). As we discuss in this chapter, this exact solution helps us to predict the occurrence of the size-dependent time scales in the tagged particle correlations in the ASEP.

This chapter is organized as follows. In Section 4.1, we discuss the mapping of the ASEP configuration to that of an interface. This is followed by Section 4.2, where we obtain the exact solution for the tagged particle correlations, $\sigma^2(L, t)$ and $s^2(L, t)$, for the linear interface in the EW class, and also discuss the corresponding expected behavior for the ASEP.

4.1 Interface mapping

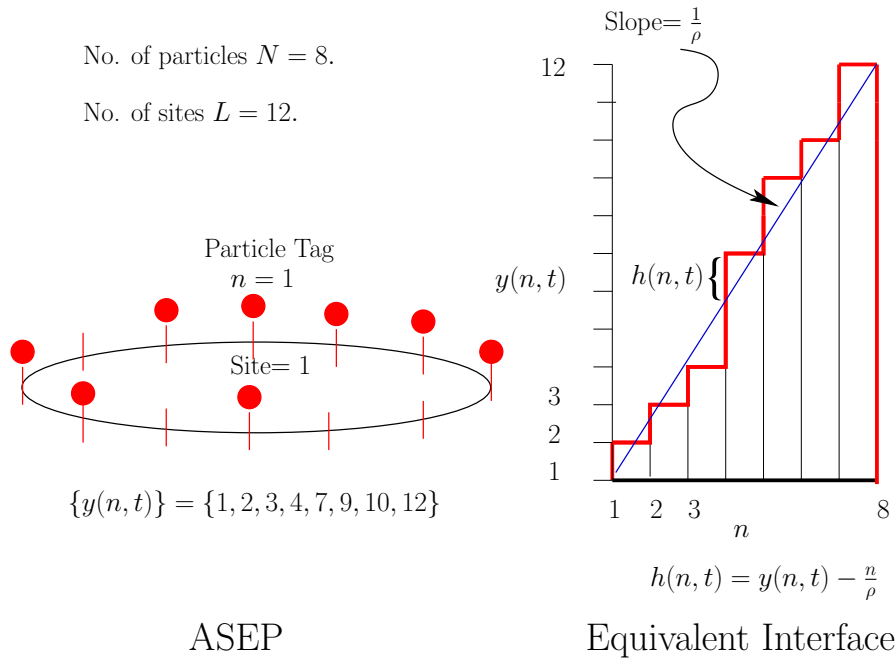


Figure 4.1: Mapping of the ASEP configuration to an interface.

We consider the ASEP comprising N particles on a one-dimensional periodic lattice of L sites. Let the particles be labeled $1, 2, \dots, N$ sequentially at the initial instant. Since the particle motion is in one dimension, and there is no overtaking, the ordering of particles will be preserved for all subsequent times. The corresponding interface is obtained by identifying the tag label n with the horizontal coordinate n for the interface, while the set $\{y(n, t)\}$, denoting the particle locations at time t , maps onto the set of local interface heights $\{h(n, t)\}$ as follows [1].

$$h(n, t) = y(n, t) - \frac{n}{\rho}. \quad (4.1)$$

Fig. 4.1 shows an example of the mapping. Since the inequality $y(n + 1, t) \geq y(n, t) + 1$

holds, it follows that the interface heights satisfy $h(n+1, t) \geq h(n, t) + 1 - \frac{1}{\rho}$. Periodic boundary condition implies $y(n \pm N) = y(n) \pm L$, and correspondingly, $h(n \pm N, t) = h(n, t)$.

The dynamics of the interface involves the following moves in one elementary time step: the move $h(n, t) \rightarrow h(n, t+1) = h(n, t) + 1$ occurs with probability p while the move $h(n, t) \rightarrow h(n, t+1) = h(n, t) - 1$ takes place with probability q . The interface height remains the same with probability $1 - (p+q)$. The attempt to increase, respectively decrease, succeeds only if $y(n+1, t) - y(n, t) > 1$, respectively $y(n, t) - y(n-1, t) > 1$.

ASEP	Lattice Interface Model
Particle Label n	Spatial coordinate n
Displacement $y(n, t)$	Height $h(n, t) + \frac{n}{\rho}$
Mean Velocity v_P	Mean growth rate $\frac{\partial \langle h \rangle}{\partial t}$

Table 4.1: Mapping ASEP to the interface.

Following the above prescription, the ASEP with N particles and L sites maps onto a lattice model of the interface of length N . In order to get the continuum equation for the interface, we (i) coarse-grain the particle labels so that the discrete tag label n becomes the continuous tag variable x , and (ii) divide x by the particle density ρ to make x into a spatial variable running between 0 and L . The equation of motion of the interface, to lowest order of nonlinearity, is given by

$$\frac{\partial h(x, t)}{\partial t} = v_P + \Gamma \frac{\partial^2 h}{\partial x^2} + u \frac{\partial h}{\partial x} + \frac{\lambda}{2} \left(\frac{\partial h}{\partial x} \right)^2 + \eta(x, t), \quad (4.2)$$

where $v_P = (p - q)(1 - \rho)$, $\Gamma = \frac{1}{2}$, $u = \rho(p - q)$, $\lambda = -2\rho(p - q)$. Here, $\eta(x, t)$ represents a Gaussian noise with $\langle \eta(x, t) \rangle = 0$, $\langle \eta(x, t) \eta(x', t') \rangle = 2A \delta(x - x') \delta(t - t')$, where $A = \frac{1}{2} \left(\frac{1 - \rho}{\rho} \right)$. The boundary condition $h(n \pm N, t) = h(n, t)$ on the height variable for the discrete interface now reads $h(x \pm L, t) = h(x, t)$ in the continuum. The derivation of Eq. 4.2 is relegated to the Appendix B. The constant term v_P and the drift term $u \frac{\partial h}{\partial x}$ in Eq. 4.2 can be eliminated by a boost ($h \rightarrow h' = h + v_P t$) and a Galilean shift ($x \rightarrow x' = x - ut$), respectively. In that case, Eq. 4.2 describes the time evolution of a KPZ interface [2]. Note that Eq. 4.2 is not an exact description of the time evolution for the ASEP density profile. It is rather a coarse-grained description of the ASEP. In the same spirit as in the coarse-grained description of the ASEP in Chapter 2, Section 2.7, one expects that the scaling properties of the correlation functions for both the ASEP and its interface-equivalent are governed by the same KPZ fixed point, and hence, are described by the same critical exponents and scaling functions.

For the symmetric exclusion process (SEP), the corresponding interface is an equilibrium one that does not move bodily. Rather, it fluctuates about a stationary profile, and its time evolution is governed by the Edwards-Wilkinson (EW) equation [3], obtained by setting

$p = q$, implying $v_P = 0, u = 0, \lambda = 0$, so that

$$\frac{\partial h(x, t)}{\partial t} = \Gamma \frac{\partial^2 h}{\partial x^2} + \eta(x, t). \quad (4.3)$$

4.2 Linear interface: Exact solution

The existence of size-dependent time scales in $\sigma^2(L, t)$ and $s^2(L, t)$ for the ASEP, discussed in Chapter 3, can be explained qualitatively by exactly solving the continuum equation, Eq. 4.2, for the case $\lambda = 0$. This is possible as, in this limit, Eq. 4.2 is linear, and hence, solvable. We refer to the corresponding interface as a linear interface. The relevant time-evolution equation is

$$\frac{\partial h(x, t)}{\partial t} = v_P + \Gamma \frac{\partial^2 h}{\partial x^2} + u \frac{\partial h}{\partial x} + \eta(x, t). \quad (4.4)$$

In this section, we outline the exact computation of the two quantities $\sigma^2(L, t)$ and $s^2(L, t)$ for the linear interface. Note that, through the mapping outlined in Table 4.1, the function $\sigma^2(L, t)$ measures the autocorrelation of the interface (compare with the definition of the autocorrelation function in Chapter 2, Section 2.8). We will see that the drift term, $u \frac{\partial h}{\partial x}$ in Eq. 4.4, that makes it different from the usual EW equation, plays a crucial role in determining the temporal behavior of these functions.

Our aim is to compute $\sigma^2(L, t)$ and $s^2(L, t)$ for the linear interface. For this, we look at the function $C_L(t_0, t_0 + t)$, defined in Eq. 3.5, which, utilizing the mapping outlined in Table 4.1 with n replaced by the continuous variable x , reads

$$C_L(t_0, t_0 + t) = \langle [h(x, t_0 + t) - h(x, t_0) - \langle [h(x, t_0 + t) - h(x, t_0)] \rangle]^2 \rangle. \quad (4.5)$$

As discussed in Chapter 3, Section 3.1, $\sigma^2(L, t)$ can be obtained from the limiting behavior of the function $C_L(t_0, t_0 + t)$ in the limit $t_0 \rightarrow \infty$. On the other hand, one recovers $s^2(L, t)$ from the limiting behavior of the function $C_L(t_0, t_0 + t)$ in the limit $t_0 \rightarrow 0$.

To compute $C_L(t_0, t_0 + t)$, we need to solve Eq. 4.4 for $h(x, t)$. Before doing so, we note that the constant term on the right of Eq. 4.4 can be gotten rid of by going to a co-moving frame moving with velocity v_P . This is equivalent to making the transformation $h \rightarrow h + v_P t$. The resultant equation is the usual time-evolution equation for the EW interface, Eq. 4.3, with an additional drift term, $u \frac{\partial h}{\partial x}$, and can be solved by going to Fourier space. To this end, utilizing the boundary condition $h(x \pm L, t) = h(x, t)$ on the height variable, we write $h(x, t)$ in terms of its Fourier modes $\tilde{h}(m, t)$. We have

$$h(x, t) = \sum_{m=-\infty}^{\infty} \tilde{h}(m, t) e^{\frac{i2\pi m}{L}(x+ut)}. \quad (4.6)$$

Thus, $\tilde{h}(m, t) = \frac{1}{L} \int_0^L dx h(x, t) e^{-\frac{i2\pi m}{L}(x+ut)}$. Equation 4.4 now reads

$$\frac{\partial \tilde{h}(m, t)}{\partial t} = -\Gamma \frac{4\pi^2 m^2}{L^2} \tilde{h}(m, t) + \tilde{\eta}(m, t), \quad (4.7)$$

where $\tilde{\eta}(m, t) = \frac{1}{L} \int_0^L dx \eta(x, t) e^{-\frac{i2\pi m}{L}(x+ut)}$. Utilizing $\langle \eta(x, t) \eta(x', t') \rangle = 2A \delta(x-x') \delta(t-t')$, we have, for the Fourier modes,

$$\langle \tilde{\eta}(m, t) \tilde{\eta}(m', t') \rangle = \frac{2A}{L} \Delta_{m, -m'} \delta(t - t'), \quad (4.8)$$

where $\Delta_{m, n}$ is the Kronecker delta.

Equation 4.7 can be solved for $\tilde{h}(m, t)$ to get

$$\tilde{h}(m, t) = \tilde{h}(m, 0) e^{-\Gamma \frac{4\pi^2 m^2}{L^2} t} + e^{-\Gamma \frac{4\pi^2 m^2}{L^2} t} \int_0^t dt' \tilde{\eta}(m, t') e^{\Gamma \frac{4\pi^2 m^2}{L^2} t'}. \quad (4.9)$$

The condition $\langle \eta(x, t) \rangle = 0$ gives, for its Fourier modes, $\langle \tilde{\eta}(m, t) \rangle = 0 \forall m$. Using this in Eq. 4.9, we get $\langle \tilde{h}(m, t) \rangle = \langle \tilde{h}(m, 0) \rangle e^{-\Gamma \frac{4\pi^2 m^2}{L^2} t}$.

From Eq. 4.9, with the help of Eq. 4.8, we get

$$\begin{aligned} \langle \tilde{h}(m, t) \tilde{h}(m', t') \rangle &= \langle \tilde{h}(m, 0) \tilde{h}(m', 0) \rangle e^{-\Gamma \frac{4\pi^2}{L^2} (m^2 t + m'^2 t')} \\ &+ \frac{AL}{4\pi^2 \Gamma} \frac{\Delta_{m, -m'}}{m^2} \left[e^{-\Gamma \frac{4\pi^2 m^2}{L^2} |t-t'|} - e^{-\Gamma \frac{4\pi^2 m^2}{L^2} (t+t')} \right]. \end{aligned} \quad (4.10)$$

4.2.1 $\sigma^2(L, t)$

The quantity $\sigma^2(L, t)$ measures the variance of the displacement of the tagged particle, while averaging over both the initial stationary ensemble of ASEP configurations and their stochastic evolutions in time, see Chapter 3, Eq. 3.2. As discussed following Eq. 3.5, this quantity may be obtained from the quantity $C_L(t_0, t_0 + t)$, in the limit in which $t_0 \rightarrow \infty$. Hence, we will compute

$$\begin{aligned} \sigma^2(L, t) &= \lim_{t_0 \rightarrow \infty} C_L(t_0, t_0 + t) \\ &= \lim_{t_0 \rightarrow \infty} \langle [h(x, t_0 + t) - h(x, t_0) - \langle [h(x, t_0 + t) - h(x, t_0)] \rangle]^2 \rangle. \end{aligned} \quad (4.11)$$

In the limit $t_0 \rightarrow \infty$, the quantity $\langle h(x, t_0 + t) - h(x, t_0) \rangle$ goes to zero. Thus, the function $\sigma^2(L, t)$ reduces to $\sigma^2(L, t) = \lim_{t_0 \rightarrow \infty} \langle [h(x, t_0 + t) - h(x, t_0)]^2 \rangle$.

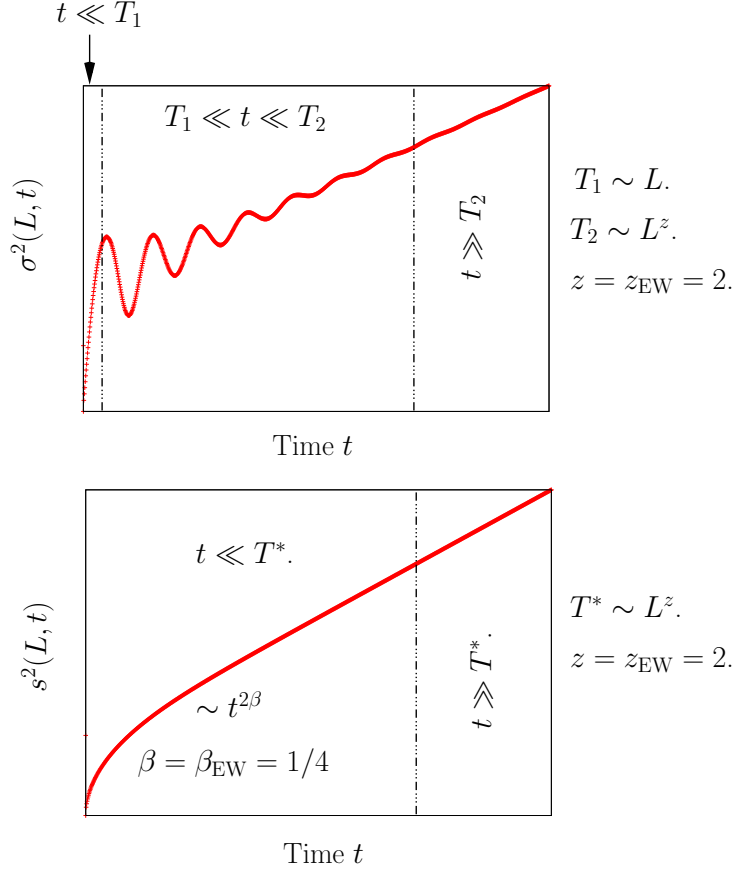


Figure 4.2: Exact solution within the linear interface model for $\sigma^2(L, t)$ (Eq. 4.14) and $s^2(L, t)$ (Eq. 4.32).

Utilizing Eq. 4.10, we get

$$\begin{aligned}
\langle h(x, t)h(x, t') \rangle &= \langle \tilde{h}^2(0, 0) \rangle + \frac{2A}{L} \min(t, t') \\
&+ \frac{AL}{4\pi^2\Gamma} \sum_{m=-\infty, m \neq 0}^{\infty} \frac{1}{m^2} \left[e^{-\Gamma \frac{4\pi^2 m^2}{L^2} |t-t'|} - e^{-\Gamma \frac{4\pi^2 m^2}{L^2} (t+t')} \right] \\
&\times e^{\frac{i2\pi m u}{L} (t-t')}.
\end{aligned} \tag{4.12}$$

In the last equation, the contribution from the initial condition, $\langle \tilde{h}(m, 0)\tilde{h}(m', 0) \rangle \times e^{-\Gamma \frac{4\pi^2 m^2}{L^2} (m^2 t + m'^2 t')}$ for $m, m' \neq 0$ has been dropped, since, eventually when we set $t = t_0$ and $t' = t_0 + t$ and let $t_0 \rightarrow \infty$, this exponential term goes to 0. By combining the m and

– m terms in the summation in Eq. 4.12, we get

$$\begin{aligned} \langle h(x, t)h(x, t') \rangle &= \langle \tilde{h}^2(0, 0) \rangle + \frac{2A}{L} \min(t, t') \\ &+ \frac{AL}{2\pi^2\Gamma} \sum_{m=1}^{\infty} \frac{1}{m^2} \left[e^{-\Gamma \frac{4\pi^2 m^2}{L^2} |t-t'|} - e^{-\Gamma \frac{4\pi^2 m^2}{L^2} (t+t')} \right] \\ &\times \cos\left(\frac{2\pi mu}{L}(t-t')\right). \end{aligned} \quad (4.13)$$

Utilizing this expression in $C_L(t_0 + t, t_0)$, and then taking the limit $t_0 \rightarrow \infty$, we finally get

$$\sigma^2(L, t) = \frac{2A}{L}t + \frac{AL}{\pi^2\Gamma} \sum_{m=1}^{\infty} \frac{1}{m^2} \left[1 - e^{-\Gamma \frac{4\pi^2 m^2}{L^2} t} \cos\left(\frac{2\pi mu}{L}t\right) \right]. \quad (4.14)$$

This is an exact formula for $\sigma^2(L, t)$ within the linear interface model. Next, we consider the various limits.

- $t \ll L/u$. Let $\frac{2\pi ut}{L}m = k$. With $\Delta m = 1$, we get $\Delta k = \frac{2\pi ut}{L}$. Now, $ut \ll L$ implies that Δk is small, and hence, one can replace the sum over m in Eq. 4.14 by an integral over k to get

$$\sigma^2(L, t) \approx \frac{2Aut}{\pi\Gamma} \int_0^{\infty} \frac{dk}{k^2} \left[1 - e^{-\frac{\Gamma k^2}{u^2 t}} \cos(k) \right], \quad (4.15)$$

where, in obtaining the last equation, we have dropped the first term on the right of Eq. 4.14 in comparison with the second term. The integral on the right can be done exactly, see Appendix C. Using its value, we get

$$\sigma^2(L, t) = \frac{Au}{\Gamma} \left[2 \frac{\sqrt{\Gamma}}{\sqrt{\pi u}} \sqrt{t} e^{-\frac{u^2 t}{4\Gamma}} + t \operatorname{erf}\left(\frac{u}{2\sqrt{\Gamma}} \sqrt{t}\right) \right]. \quad (4.16)$$

Now we consider two cases:

- (a) $t \ll \frac{4\Gamma}{u^2}$: In this limit, the error function is approximately zero, and we get

$$\sigma^2(L, t) \approx \frac{2A}{\sqrt{\pi\Gamma}} \sqrt{t}. \quad (4.17)$$

- (b) $\frac{4\Gamma}{u^2} \ll t \ll \frac{L}{u}$. Here,

$$\sigma^2(L, t) \approx \frac{Au}{\Gamma} t. \quad (4.18)$$

- $t \sim \frac{L}{u}$: Let $t = \frac{nL}{u}$ with $n \in I$. Also, let $\frac{2\pi m\sqrt{\Gamma}}{\sqrt{uL}} = k$. Substituting in Eq. 4.14 after replacing, for large L , the sum over m by an integral over k , we get

$$\sigma^2(L, t = \frac{nL}{u}) \approx \frac{2At}{L} + \frac{2A}{\pi} \sqrt{\frac{L}{u\Gamma}} \int_0^{\infty} \frac{dk}{k^2} (1 - e^{-k^2 n}). \quad (4.19)$$

The integral on the right can be done exactly, and its value is $\sqrt{n\pi}$. This gives

$$\sigma^2(L, t = \frac{nL}{u}) \approx \frac{2A}{L}t + \frac{2A}{\sqrt{\pi\Gamma}}\sqrt{t}. \quad (4.20)$$

For large L , keeping t fixed, when the first term on the right hand side goes to zero, we have

$$\sigma^2(L, t = \frac{nL}{u}) \approx \frac{2A}{\sqrt{\pi\Gamma}}\sqrt{t}. \quad (4.21)$$

Since the function $\Lambda^2(L, t)$, defined in Chapter 3, Eq. 3.19, coincides with $\sigma^2(L, t)$ at the local minima of the latter, observed at times, $t = \frac{nL}{u}$ with $n \in I$ (see Fig. 3.9), we conclude that

$$\Lambda^2(L, t = \frac{nL}{u}) \approx \frac{2A}{\sqrt{\pi\Gamma}}\sqrt{t}. \quad (4.22)$$

- $t \gg L^2$: In this limit, the exponential term in the sum on the right hand side of Eq. 4.14 drops out for all m to give

$$\begin{aligned} \sigma^2(L, t) &\approx \frac{2A}{L}t + \frac{AL}{\pi^2\Gamma} \sum_{m=1}^{\infty} \frac{1}{m^2} \\ &= \frac{2A}{L}t + \frac{AL}{\pi^2\Gamma} \left(\frac{\pi^2}{6} \right). \end{aligned} \quad (4.23)$$

In the limit of large t , the first term on the right hand side dominates so that

$$\sigma^2(L, t) \approx \frac{2A}{L}t. \quad (4.24)$$

As discussed following Eq. 3.19 in Chapter 3, beyond the time T_2 , there is no distinction between the temporal behavior of $\sigma^2(L, t)$ and $\Lambda^2(L, t)$. Thus, we conclude that for $t \gg T_2$,

$$\Lambda^2(L, t) \approx \frac{2A}{L}t + \frac{AL}{\pi^2\Gamma} \left(\frac{\pi^2}{6} \right), \quad (4.25)$$

so that in the limit of large times, one gets

$$\Lambda^2(L, t) \approx \frac{2A}{L}t. \quad (4.26)$$

Note that the large time behavior of $\sigma^2(L, t)$ is determined by the zero mode ($m = 0$) in the Fourier expansion of $h(x, t)$.

With the values of the exponents β and z for EW given in Chapter 2, Eq. 2.40, we summarize the behavior of $\sigma^2(L, t)$ for the linear interface in Table 4.2.

The scaling of the diffusion constant $D(L)$ as the inverse of the system size in the regime $t \gg T_2 \sim L^z$ with $z = z_{EW} = 2$ can be obtained by matching the behavior of the $\sigma^2(L, t)$ across the time T_2 .

$t \ll T_1 \sim L:$ (a) $t \ll \frac{4\Gamma}{u^2}.$ (b) $\frac{4\Gamma}{u^2} \ll t \ll T_1.$	$\sigma^2(L, t) \approx \frac{2A}{\sqrt{\pi\Gamma}}\sqrt{t}.$ $\sigma^2(L, t) \approx \frac{A}{\Gamma}t.$
$T_1 \ll t \ll T_2 \sim L^z.$ $z = z_{EW} = 2.$ $t = \frac{nL}{u}$ with $n \in I.$	$\sigma^2(L, t) \approx \frac{2A}{\sqrt{\pi\Gamma}}t^{2\beta}.$ $\beta = \beta_{EW} = 1/4.$
$t \gg T_2.$	$\sigma^2(L, t) \approx \frac{2A}{L}t.$ The diffusion constant $D(L) = \frac{2A}{L}.$

Table 4.2: Behavior of $\sigma^2(L, t)$ in different time regimes for the linear interface.

Let $\sigma^2(L, t) \sim D(L)t$ with $D(L) \sim L^\gamma$ for $t \gg T_2$.

On the lower side of T_2 , we have $\sigma^2(L, t) \sim t^{2\beta}$.

Then, to match the t and L dependence at T_2 , we must have

$$(T_2)^{2\beta} \sim D(L)T_2. \quad (4.27)$$

This gives $2\beta = \gamma/z + 1$ whence, with $z = 2$ and $\beta = 1/4$ for the linear interface model, $\gamma = -1$.

On the basis of the above results for the linear interface model, we expect the time-dependence of $\sigma^2(L, t)$ for the KPZ class as in Table 4.3. Here, $z = z_{KPZ} = 3/2$ and $\beta = \beta_{KPZ} = 1/3$ so that $\gamma = -1/2$. This value for γ leads to the inverse square root scaling of the diffusion constant $D(L)$ with system size L .

$t \ll T_1 \sim L:$ (a) $t \ll \frac{4\Gamma}{u^2}.$ (b) $\frac{4\Gamma}{u^2} \ll t \ll T_1.$	$\sigma^2(L, t) \sim \sqrt{t}.$ $\sigma^2(L, t) \sim t.$
$T_1 \ll t \ll T_2 \sim L^z.$ $z = z_{KPZ} = 3/2.$ $t = \frac{nL}{u}$ with $n \in I.$	$\sigma^2(L, t) \sim t^{2\beta}.$ $\beta = \beta_{KPZ} = 1/3.$
$t \gg T_2.$	$\sigma^2(L, t) \sim \frac{1}{\sqrt{L}}t.$ The diffusion constant $D(L) \sim 1/\sqrt{L}.$

Table 4.3: Behavior of $\sigma^2(L, t)$ in different time regimes for the KPZ interface.

Note from Table 4.2 and Table 4.3 that for both the EW and the KPZ classes, in the limit of an infinite system, $\sigma^2(L, t)$ behaves asymptotically as linear in t (i.e., in the limit $L \rightarrow \infty$ first, followed by the limit $t \rightarrow \infty$, which refers to the asymptotic behavior in time for an infinite system). In terms of the interface variables, this means that the autocorrelation function of the interface, $S(0, t)$, goes linearly in t for an infinite system: $S(0, t) \sim t$. We get this behavior precisely because of the sliding density fluctuations (SDF) that contribute

a drift term proportional to its velocity ($= -u = v_K - v_P$) to the time-evolution equation of the interface (Eq. 4.2 and Eq. 4.4). This behavior of the autocorrelation function is in accordance with the renormalization group flow diagram in Chapter 2 (see Fig 2.10).

4.2.2 $s^2(L, t)$

The quantity $s^2(L, t)$ measures the variance of the displacement of the tagged particle, starting from an arbitrary but fixed configuration, randomly drawn from the stationary ensemble of ASEP configurations, and averaging over the stochastic evolution of the fixed configuration in time, see Chapter 3, Eq. 3.4. As discussed following Eq. 3.5, this quantity may be obtained from the quantity $C_L(t_0, t_0 + t)$, in the limit in which $t_0 \rightarrow 0$. Hence, we will compute

$$\begin{aligned} s^2(L, t) &= \lim_{t_0 \rightarrow 0} C_L(t_0, t_0 + t) \\ &= \langle [h(x, t) - h(x, 0) - \langle [h(x, t) - h(x, 0)] \rangle]^2 \rangle. \end{aligned} \quad (4.28)$$

Now, from Eq. 4.9, we have

$$\begin{aligned} h(x, t) - h(x, 0) &= \sum_{m=-\infty}^{\infty} [\tilde{h}(m, 0) e^{-\Gamma \frac{4\pi^2 m^2}{L^2} t} \\ &+ e^{-\Gamma \frac{4\pi^2 m^2}{L^2} t} \int_0^t dt' \tilde{\eta}(m, t') e^{\Gamma \frac{4\pi^2 m^2}{L^2} t'}] e^{\frac{i2\pi m}{L}(x+ut)} \\ &- \sum_{m=-\infty}^{\infty} \tilde{h}(m, 0) e^{\frac{i2\pi m}{L} x}. \end{aligned} \quad (4.29)$$

Noting that every time we start from the same initial condition so that $\langle \tilde{h}(m, 0) \rangle = \tilde{h}(m, 0)$, we have

$$\begin{aligned} h(x, t) - h(x, 0) - \langle [h(x, t) - h(x, 0)] \rangle &= \sum_{m=-\infty}^{\infty} e^{-\Gamma \frac{4\pi^2 m^2}{L^2} t} e^{\frac{i2\pi m}{L}(x+ut)} \\ &\times \int_0^t dt' \tilde{\eta}(m, t') e^{\Gamma \frac{4\pi^2 m^2}{L^2} t'}. \end{aligned} \quad (4.30)$$

Utilizing Eq. 4.30 and Eq. 4.8 in Eq. 4.28, we get, after a few steps,

$$s^2(L, t) = \frac{AL}{4\pi^2 \Gamma} \sum_{m=-\infty}^{\infty} \frac{1}{m^2} (1 - e^{-\Gamma \frac{8\pi^2 m^2}{L^2} t}). \quad (4.31)$$

Separating out the $m = 0$ mode and exploiting the $m \rightarrow -m$ symmetry of the remaining terms, we get the final expression for $s^2(L, t)$ as

$$s^2(L, t) = \frac{2A}{L}t + \frac{AL}{2\pi^2\Gamma} \sum_{m=1}^{\infty} \frac{1}{m^2} (1 - e^{-\Gamma \frac{8\pi^2 m^2}{L^2} t}). \quad (4.32)$$

Next, we will consider the various limits.

- $t \ll L^2$: Let $k = \frac{2\sqrt{2\Gamma}\pi m}{L}\sqrt{t}$. Since $\Delta m = 1$, we have $\Delta k = \frac{2\sqrt{2\Gamma}\pi}{L}\sqrt{t}$ is small for $t \ll L^2$. This allows the sum over m in Eq. 4.32 to be replaced by an integral over k to give

$$s^2(L, t) = \frac{2A}{L}t + \frac{A}{\pi} \sqrt{\frac{2}{\Gamma}} \sqrt{t} \int_{\frac{2\sqrt{2\Gamma}\pi\sqrt{t}}{L}}^{\infty} \frac{dk}{k^2} (1 - e^{-k^2}). \quad (4.33)$$

Since $t \ll L^2$, the lower limit of the integral on the right can be taken to be 0. Then the integral can be done exactly, and its value is $\sqrt{\pi}$. For large L , keeping t fixed, the first term on the right of Eq. 4.33 goes to zero, and we get

$$s^2(L, t) \approx A \sqrt{\frac{2}{\pi\Gamma}} \sqrt{t}. \quad (4.34)$$

- $t \gg L^2$: In this limit, the exponential term in the sum on the right hand side of Eq. 4.32 gets damped out for all m so that we finally have

$$\begin{aligned} s^2(L, t) &\approx \frac{2A}{L}t + \frac{AL}{2\pi^2\Gamma} \sum_{m=1}^{\infty} \frac{1}{m^2} \\ &= \frac{2A}{L}t + \frac{AL}{2\pi^2\Gamma} \left(\frac{\pi^2}{6} \right). \end{aligned} \quad (4.35)$$

For large t , the first term on the right hand side dominates so that

$$s^2(L, t) \approx \frac{2A}{L}t. \quad (4.36)$$

Here, as for the function $\sigma^2(L, t)$, we see that the large time behavior of $s^2(L, t)$ is determined by the zero mode ($m = 0$) in the Fourier expansion of $h(x, t)$.

Knowing the values of the exponents β and z for EW, given in Chapter 2, Eq. 2.40, we summarize the behavior of $s^2(L, t)$ for the linear interface in Table 4.4.

The fact that $D(L)$ scales as the inverse of the system size in the regime $t \gg T^* \sim L^z$ with $z = z_{EW} = 2$, can be obtained by matching the behavior of $s^2(L, t)$ across the time T^* .

Thus, let $s^2(L, t) \sim D(L)t$ with $D(L) \sim L^\gamma$ for $t \gg T^*$.

For $t \ll T^*$, we have $s^2(L, t) \sim t^{2\beta}$.

$t \ll T^* \sim L^z.$ $z = z_{EW} = 2.$	$s^2(L, t) \approx Ct^{2\beta}.$ $\beta = \beta_{EW} = 1/4.$ $C = A\sqrt{\frac{2}{\pi\Gamma}}.$
$t \gg T^*.$ $z = z_{EW} = 2.$	$s^2(L, t) \approx \frac{2A}{L}t.$ The diffusion constant $D(L) = \frac{2A}{L}.$

Table 4.4: Behavior of $s^2(L, t)$ in different time regimes for the linear interface.

Then, to match the t and L dependence at T^* , we must have

$$(T^*)^{2\beta} \sim D(L)T^*. \quad (4.37)$$

This gives $2\beta = \gamma/z + 1$. With $\beta = 1/4$ and $z = 2$ for the linear interface model, $\gamma = -1$.

The above results lead us to expect the time-dependence of $s^2(L, t)$ for the KPZ class as in Table 4.5. Here, $\beta = \beta_{KPZ} = 1/3$ and $z = z_{KPZ} = 3/2$ so that $2\beta = \gamma/z + 1$ gives $\gamma = -1/2$. This explains the inverse square root scaling of the diffusion constant $D(L)$ with system size L .

$t \ll T^* \sim L^z.$ $z = z_{KPZ} = 3/2.$	$s^2(L, t) \sim t^{2\beta}.$ $\beta = \beta_{KPZ} = 1/3.$
$t \gg T^*.$	$s^2(L, t) \sim \frac{1}{\sqrt{L}}t.$ The diffusion constant $D(L) \sim 1/\sqrt{L}.$

Table 4.5: Behavior of $s^2(L, t)$ in different time regimes for the KPZ interface.

Note that from Table 4.5, it follows that for an infinite system when the time-scale T^* diverges, one recovers the result observed by van Beijeren that $\lim_{L \rightarrow \infty} s^2(L, t) = s^2(t) \sim t^{2/3}$ [4].

4.2.3 Center-of-mass motion

One can compute the fluctuations in the motion of the center-of-mass for the linear interface. Using the definitions in Chapter 3, Section 3.5 for the center-of-mass and the mapping of the ASEP to the interface in Table 4.1, for an interface of length L , we get

$$d_{CM}(t) = \frac{1}{L} \int_0^L dx [h(x, t) - h(x, 0) - \langle [h(x, t) - h(x, 0)] \rangle]. \quad (4.38)$$

We have $\tilde{h}(m, t) = \frac{1}{L} \int_0^L dx h(x, t) e^{-i\frac{2\pi m}{L}(x+ut)}$. It follows that $\tilde{h}(0, t) = \frac{1}{L} \int_0^L dx h(x, t)$. Substituting in Eq. 4.38, we get

$$d_{CM}(t) = \tilde{h}(0, t) - \tilde{h}(0, 0) - \langle [\tilde{h}(0, t) - \tilde{h}(0, 0)] \rangle. \quad (4.39)$$

Using Eq. 4.9, we finally get

$$d_{CM}(t) = \int_0^t dt' \tilde{\eta}(0, t') \quad (4.40)$$

so that

$$\begin{aligned} \langle d_{CM}^2(t) \rangle &= \int_0^t \int_0^t dt' dt'' \langle \tilde{\eta}(0, t') \tilde{\eta}(0, t'') \rangle \\ &= \frac{2At}{L}, \end{aligned} \quad (4.41)$$

where we have used Eq. 4.8 in arriving at the last equation. This exact result matches with the one obtained on the basis of scaling arguments in Chapter 3, Eq. 3.33.

To conclude this chapter, we reiterate that the exact solution for the linear interface qualitatively explains the occurrence of characteristic oscillations and different L -dependent regimes in the variance of the displacement on a finite lattice, as observed, for instance, in the the Monte Carlo simulations for the ASEP. We also note that in the large time limit ($t \gg L^z$ with $z = 3/2$ for the ASEP and $z = 2$ for the linear interface), both $\sigma^2(L, t)$ and $s^2(L, t)$ grow linearly in time with the same constant of proportionality or the diffusion constant $D(L)$. For the linear interface, $D(L) \sim \frac{1}{L}$, while $D(L) \sim \frac{1}{\sqrt{L}}$ for the ASEP. This difference arises from the different values of the exponents β and z for the linear interface and the ASEP. As a result, the exponent γ , characterizing the scaling of $D(L)$ with L (namely, $D(L) \sim L^\gamma$), and related to β and z by the relation $2\beta = \gamma/z + 1$ (see the discussions following Eq. 4.27 and Eq. 4.37), takes on different values for the linear interface and the ASEP.

In the next chapter, we will show the correspondence of the linear interface model to different models of interacting particle systems.

References

- [1] S. N. Majumdar and M. Barma, Phys. Rev. B **44**, 5306 (1991).
- [2] M. Kardar, G. Parisi, and Y. C. Zhang, Phys. Rev. Lett. **56**, 889 (1986).
- [3] S. F. Edwards and D. R. Wilkinson, Proc. R. Soc. London, Ser A **381**, 17 (1982).
- [4] H. van Beijeren, J. Stat. Phys. **63**, 47 (1991).

Chapter 5

Correspondence of the linear interface model to different interacting particle systems

“Then you should say what you mean,” the March Hare went on. “I do,” Alice hastily replied; “atleast—atleast I mean what I say—that’s the same thing, you know.”

Lewis Carroll

In the previous chapter, we related the tagged particle correlations in the ASEP to the height fluctuations of an interface in the Kardar-Parisi-Zhang (KPZ) universality class. The time-evolution equation for the interface is the usual KPZ equation, augmented by a drift term. Next, we considered the time-evolution equation in the absence of the nonlinear term to get the Edwards-Wilkinson (EW) equation with a drift term. This equation describes the evolution of a linear interface, and is reproduced below.

$$\frac{\partial h(x, t)}{\partial t} = v_P + \Gamma \frac{\partial^2 h}{\partial x^2} + u \frac{\partial h}{\partial x} + \eta(x, t). \quad (5.1)$$

In this chapter, we wish to show that the evolution equation, Eq. 5.1, in addition to being a linear approximation to the KPZ equation with a drift term, also arises in a number of microscopic interacting particle systems. Examples are the Katz-Lebowitz-Spohn (KLS) model at a specified value of the temperature, and the Asymmetric Random Average Process (ARAP). These correspondences are discussed below in Sections 5.1 and 5.2, respectively.

5.1 Correspondence to the KLS model

The aim of this subsection is to explain how the variance of the displacement, computed in the linearized continuum theory in Chapter 4 and defined in terms of the macroscopic

parameters (Γ , A , velocity u), compares to the same quantity evaluated by numerical simulations in the (discrete) KLS model, which uses one single microscopic parameter, namely, the temperature, for a special value of the latter. All the results of this subsection were derived by C. Godrèche.

5.1.1 The model

The one-dimensional KLS model generalizes the ASEP, in that interactions between particles are added on top of the exclusion constraint [1]. The ASEP is the infinite temperature limit of the KLS model.

The precise definition of the KLS model is as follows. Consider a chain of Ising spins s_n ($n = 1, \dots, N$), evolving under the Kawasaki dynamics with the heat-bath rule, and submitted to a drift. The energy of the chain reads

$$E = -\tilde{J} \sum_n s_n s_{n+1}. \quad (5.2)$$

In the heat-bath dynamics, for a pair of opposite spins ($s_n + s_{n+1} = 0$), the move ($s_n \rightarrow -s_n, s_{n+1} \rightarrow -s_{n+1}$) is realized with probability

$$W(\Delta E) = \frac{\mathcal{P}}{e^{\beta \Delta E} + 1}, \quad (5.3)$$

where $\Delta E = 2\tilde{J}(s_{n-1}s_n + s_{n+1}s_{n+2}) = 0, \pm 4\tilde{J}$ is the energy difference between the configurations after and before the move, and the numerator \mathcal{P} is taken equal to p if the $+$ spin is exchanged to the right (i.e., $+- \rightarrow -+$), and to q if it is exchanged to the left ($-+ \rightarrow +-$). Associating a particle to a $+$ spin, and a hole to a $-$ spin, this particle hops to the right with probability p , and to the left with probability q .

The moves corresponding to the three possible values of the difference ΔE are listed in Table 5.1, with the corresponding acceptance probabilities. Evaporation corresponds to the detachment of a $+$ spin from a positive domain, or, equivalently, to the detachment of a particle from a cluster of particles. Condensation, conversely, corresponds to the attachment of an isolated $+$ spin to a positive domain, or, equivalently, to that of a particle to a cluster of particles, and the two diffusion mechanisms, to the motion of an isolated $-$ spin in a positive domain (or, hole in a cluster of particles) or to that of an isolated $+$ spin in a negative domain (or, particle amongst empty sites).

The heat-bath rule, Eq. 5.3, has the non-trivial property that the steady state is independent of the asymmetry [1, 2]. It obeys detailed balance with respect to the energy, Eq. 5.2, at temperature $T = 1/(k_B \beta)$ (k_B : Boltzmann constant), i.e., $W(\Delta E) = W(-\Delta E)e^{-\beta \Delta E}$.

The KLS model can also be viewed as a migration process (or, urn model). Generally speaking, a migration process can be seen as a generalization of the zero-range process (ZRP) [3, 4] (also, Chapter 6), where the particles hop on a lattice, but where the hopping rate depends both on the departure and arrival sites [4, 5]. Particles (or $+$ spins) are

Type	ΔE	Acceptance Prob.	Moves
Condensation	$-4\tilde{J}$	$\mathcal{P}e^{4\beta\tilde{J}}/(e^{4\beta\tilde{J}} + 1)$	$- + - + \rightarrow - - + +$ $+ - + - \rightarrow + + - -$
Diffusion	0	$\mathcal{P}/2$	$+ + - + \leftrightarrow + - + +$ $- - + - \leftrightarrow - + - -$
Evaporation	$+4\tilde{J}$	$\mathcal{P}/(e^{4\beta\tilde{J}} + 1)$	$+ + - - \rightarrow + - + -$ $- - + + \rightarrow - + - +$

Table 5.1: Types of moves in the partially asymmetric Kawasaki dynamics, and corresponding acceptance probabilities with the heat-bath rule. The probability \mathcal{P} is equal to p when the $+$ spin exchanges to the right, to q when it exchanges to the left.

identified with the sites of a lattice, and the holes (or $-$ spins) with particles located on these sites. At infinite temperature, this maps the ASEP onto the usual ZRP. At finite temperature, the rate at which a particle hops to the neighboring site is still given by Eq. 5.3 with $\Delta E = -4\delta\tilde{J}$ where δ is the variation of the number of empty sites before and after moving the particle. This mapping is effectively used in numerical simulations.

5.1.2 The variance of the displacement

The displacement of a tagged particle in the KLS model obeys the same laws as for the ASEP, i.e., all phenomena presented in Chapter 3 for the ASEP exist likewise for the KLS model. More precisely, the temporal behavior of the variance of the displacement of the tagged particle is the same as for the ASEP, up to prefactors which depend continuously on the temperature. The question is now to make a link between the microscopic model and its continuum limit description, i.e., to compare the prediction of Chapter 4, Section 4.2 for the temporal evolution of the variance, in the linear theory, to numerical simulations of the model.

For that purpose, we will (i) express the parameters of the continuum theory (Γ , A , and u) in terms of the temperature, which is the only parameter of the KLS model, (ii) explain the relevance of the linear theory for a special value of the temperature, for which the coefficient of the nonlinear term in the KPZ equation vanishes. This identification is possible in the present case because the stationary state of the KLS model is known. The method is given in [6]. It needs to be slightly generalized here, as now explained. For the sake of simplicity, we will restrict the computations to the case of zero magnetization M , or, equivalently, of density $\rho = 1/2$ (since $M = 2\rho - 1$).

First, the following relationship between the diffusion constant Γ and the strength of the noise A is always valid, independently of the asymmetry [6],

$$A = \Gamma \chi, \tag{5.4}$$

where χ is the susceptibility, explicitly known for the Ising chain, $\chi = e^{2\beta\tilde{J}}$. In order to find

an expression of Γ and of the velocity of the tagged particle, we write the equation for the temporal evolution of the magnetization $\langle s_n \rangle$. This reads

$$\frac{d\langle s_n \rangle}{dt} = J_n^{sp} - J_{n+1}^{sp}, \quad (5.5)$$

where the spin current J_n^{sp} through the link $(n-1, n)$ has the following expression.

$$\begin{aligned} J_n^{sp} = & \frac{p-q}{4} \left(1 - \langle s_{n-1} s_n \rangle + \frac{e^{4\beta\tilde{J}} - 1}{2(e^{4\beta\tilde{J}} + 1)} \langle (s_n - s_{n-1})(s_{n-2} - s_{n+1}) \rangle \right) \\ & + \frac{1}{4} \left(\langle s_{n-1} \rangle - \langle s_n \rangle + \frac{e^{4\beta\tilde{J}} - 1}{2(e^{4\beta\tilde{J}} + 1)} (\langle s_{n+1} \rangle - \langle s_{n-2} \rangle + \langle s_{n-2} s_{n-1} s_n \rangle \right. \\ & \left. - \langle s_{n-1} s_n s_{n+1} \rangle) \right). \end{aligned} \quad (5.6)$$

The first line in Eq. 5.6 is the drift term. It is only present when the dynamics is asymmetric. It does not contribute to the computation of the diffusion constant Γ . Putting aside the drift term, the right-hand side of Eq. 5.6 appears as a second-order difference, consistently with the diffusive nature of the second term. (Note also that the first term is even in the spin variable, while the second one is odd.) In other words, the expression of Γ is the same both in the symmetric (EW) or asymmetric (KPZ) cases. It reads (see [6] for the computation)

$$\Gamma = \frac{1}{(e^{2\beta\tilde{J}} + 1)(e^{4\beta\tilde{J}} + 1)}. \quad (5.7)$$

Note that this expression differs by a factor 2 with that given in [6]. This is due to the difference in the definitions of the scale of time chosen in the present work (see Table 5.1), and in [6]. Utilizing Eq. 5.4 and the fact that the susceptibility $\chi = e^{2\beta\tilde{J}}$, we get

$$A = \frac{1}{(e^{-2\beta\tilde{J}} + 1)(e^{4\beta\tilde{J}} + 1)}. \quad (5.8)$$

It remains to evaluate the velocity u , as well as the coefficient of nonlinearity λ , appearing in the KPZ equation, Eq. 4.2. We use Eqns. B.11 and B.12 in Appendix B for this purpose. Now, without loss of generality, we consider completely asymmetric particle (i.e., + spin) motion with $p = 1$ and $q = 0$. For zero magnetization (or, equivalently, at density $\rho = 1/2$), since u is given by $u = \left[v_P - \frac{\partial J}{\partial \rho} \right] \Big|_{\rho=1/2} = \left[v_P - 2 \frac{\partial J}{\partial M} \right] \Big|_{M=0}$, while λ is given by $\lambda = 2 \frac{\partial^2 J}{\partial M^2} \Big|_{M=0}$, we need to evaluate the current of particles J as a function of the magnetization M . Note that $J = J^{sp}/2$. We use Eq. 5.6, with $\langle s_n \rangle = M$, $\langle s_n s_{n+1} \rangle = \langle s_1 s_2 \rangle$, by translation invariance, etc. Hence, the current reads

$$J = \frac{1}{8} \left(1 + \frac{e^{4\beta\tilde{J}} - 1}{e^{4\beta\tilde{J}} + 1} \langle s_1 s_3 \rangle - \frac{2e^{4\beta\tilde{J}}}{e^{4\beta\tilde{J}} + 1} \langle s_1 s_2 \rangle \right). \quad (5.9)$$

The correlators have been evaluated earlier by the transfer matrix method which gives J as

[6]

$$J = \frac{2M^2 + e^{4\beta\tilde{J}}(1 - M^2) - (1 + M^2)(M^2 + e^{4\beta\tilde{J}}(1 - M^2))^{1/2}}{2(e^{8\beta\tilde{J}} - 1)(1 - M^2)}. \quad (5.10)$$

Utilizing the last equation, we finally get

$$u = v_P = 2J|_{M=0} = \frac{e^{2\beta\tilde{J}}}{(e^{2\beta\tilde{J}} + 1)(e^{4\beta\tilde{J}} + 1)}, \quad (5.11)$$

while

$$\lambda = \frac{1 - 3e^{2\beta\tilde{J}}}{e^{2\beta\tilde{J}}(e^{2\beta\tilde{J}} + 1)(e^{4\beta\tilde{J}} + 1)}. \quad (5.12)$$

Hence, for $e^{-2\beta\tilde{J}} = 3$ (antiferromagnetic chain), λ vanishes. For such a value of the ‘temperature’ (actually, of $\beta\tilde{J}$), though the dynamics is asymmetric, the continuum theory is linear. This yields

$$\Gamma = \frac{27}{40}, \quad u = \frac{9}{40}, \quad A = \frac{9}{40}. \quad (5.13)$$

Note that the unit of time is such that at infinite temperature

$$\Gamma = \frac{1}{4}, \quad u = \frac{1}{4}, \quad A = \frac{1}{4}. \quad (5.14)$$

These quantities differ by a factor 2 from their expression for the SEP (see Appendix B). As above, the origin of this difference lies in the definitions of the scale of time for these two models (see Table 5.1).

The result of the comparison of the quantity $\sigma^2(L, t)$ as obtained from simulation of the KLS model on a ring of size L for the temperature T satisfying $e^{-2\beta\tilde{J}} = 3$, and that from the exact solution of the linear interface as given in Chapter 4, Eq. 4.14 (with the corresponding values of the constants Γ, A and u given in Eq. 5.13) is shown in Fig. 5.1 for three different system sizes ($L = 64, 128, 256$). The simulation of the KLS model, performed by C. Godrèche, was done in the equivalent migration process described above, with equal number of particles and sites, which corresponds to half filling ($\rho = 1/2$) in the original particle system (i.e., the KLS model). The variance of the displacement of a given tagged particle in the KLS model translates into the variance of the number of particles which passed through a given bond in the migration process.

5.2 Correspondence to the ARAP

The Asymmetric Random Average Process involves hard core particles hopping on a continuous line as opposed to a lattice for the ASEP [7]. We consider a system of particles of average density ρ . We denote by $x_i(t)$ the location of the i -th particle on the continuous line with periodic boundary conditions. The dynamics is stochastic and involves the following moves during an infinitesimal time dt : a randomly chosen particle jumps with probability pdt to the right, with probability qdt to the left, and with probability $1 - (p + q)dt$, it

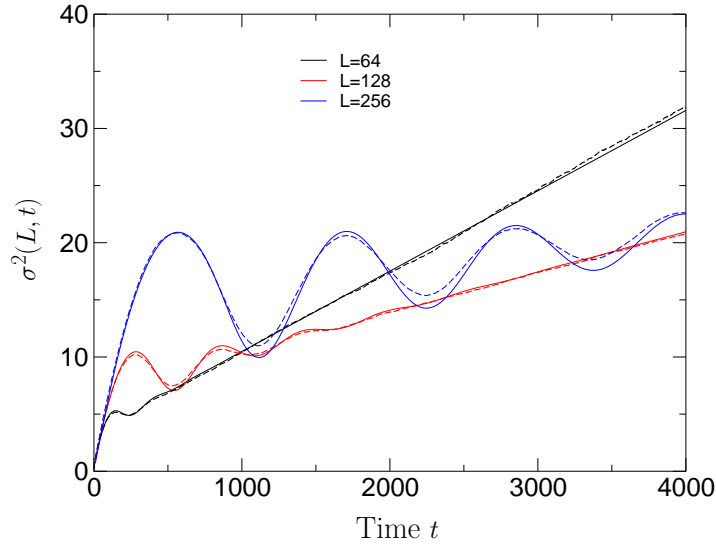


Figure 5.1: Comparison of the variance $\sigma^2(L, t)$ of the displacement of the tagged particle in the KLS model obtained from simulations (dashed lines) and exact solution (full lines) of the corresponding continuum linear theory for the temperature T satisfying $e^{-2\tilde{J}/k_B T} = 3$. Results are shown for three different system sizes ($L = 64, 128, 256$). Simulation of the KLS model, performed by C. Godrèche, was done with the equivalent migration process.

continues to occupy its original location. The amount by which the particle moves either to the right or to the left is a random fraction of the gap to the next particle to the right or to the left. Thus, for the i -th particle, the jump to the right is by the amount $r_i^+(x_{i+1} - x_i)$, while to the left is by the amount $r_i^-(x_i - x_{i-1})$. Here, the random variables r_i^\pm are independently drawn from the interval $[0, 1]$, each being distributed according to the same pdf $f(r)$, which is arbitrary. The time-evolution equation of the positions x_i 's is represented by the exact Langevin equation

$$x_i(t + dt) = x_i(t) + \gamma_i(t), \quad (5.15)$$

where the random variables $\gamma_i(t)$ are given by

$$\gamma_i(t) = \begin{cases} r_i^+[x_{i+1}(t) - x_i(t)] & \text{with prob. } p dt, \\ r_i^-[x_{i-1}(t) - x_i(t)] & \text{with prob. } q dt, \\ 0 & \text{with prob. } 1 - (p + q) dt. \end{cases} \quad (5.16)$$

The average velocity of a tagged particle v_P is given by

$$v_P = \frac{d\langle x_i(t) \rangle}{dt} = \langle \gamma_i(t) \rangle. \quad (5.17)$$

Using the expression for γ_i in Eq. 5.16, we can compute its average. This gives the average velocity of an ARAP particle as $v_P = \frac{(p-q)\mu_1}{\rho}$, where $\mu_1 = \int_0^1 dr r f(r)$. Thus the average

particle current $J = \rho v_P$ is independent of ρ . The derivation of the corresponding interface equation can be done along the lines outlined in Appendix B. Noting that all derivatives of J with respect to ρ are zero, Eq. B.11 implies $u = v_P$, while $\lambda = 0$ from Eq. B.12. Thus, we recover the equation for the linear interface, Eq. 4.4. Based on our exact solution for the linear interface, we expect the tagged-particle correlation in the ARAP in an infinite system as measured by $\sigma^2(t) \equiv \lim_{L \rightarrow \infty} \sigma^2(L, t)$ to vary as t (cf. Chapter 4, Table 4.2). This has been confirmed by an exact solution of the tagged-particle correlation for the ARAP on an infinite system [8].

References

- [1] S. Katz, J. L. Lebowitz, and H. Spohn, *Phys. Rev. B* **28**, 1655 (1983); *J. Stat. Phys.* **34**, 497 (1984).
- [2] J. M. Luck, C. Godrèche, *J. Stat. Mech.* P08009 (2006).
- [3] M. R. Evans and T. Hanney, *J. Phys. A* **38**, R195 (2005).
- [4] C. Godrèche, cond-mat/0603249; also, *Lecture Notes in Physics 716*, (Springer-Verlag, 2007).
- [5] F. Kelly, *Reversibility and Stochastic Networks* (Wiley, Chichester, 1979).
- [6] C. Godrèche and J. M. Luck, *J. Phys. A* **36**, 9973 (2003).
- [7] J. Krug and J. Garcia, *J. Stat. Phys.* **99**, 31 (2000); R. Rajesh and S. N. Majumdar, *ibid* **99**, 943 (2000).
- [8] R. Rajesh and S. N. Majumdar, *Phys. Rev. E* **64**, 036103 (2001).

Chapter 6

The Zero-Range Process (ZRP)

Alice laughed. “There is no use trying,” she said: “one can’t believe impossible things.” “I dare say you haven’t had much practice,” said the Queen. “When I was your age, I always did it for half-an-hour a day. Why, sometimes I’ve believed as many as six impossible things before breakfast.”

Lewis Carroll

Our earlier discussions on tagged particle correlations in the ASEP showed a strong interplay of the nonequilibrium dynamics with finite-size effects in determining the behavior of stationary state fluctuations. The interplay led to the occurrence of many interesting dynamical phenomena, e.g., motion of density fluctuations around a periodic system as a dissipating kinematic wave. It is interesting to ask about how does the dynamics of stationary state fluctuations get affected as a system, driven out of equilibrium, passes through a phase transition. Such transitions are often observed in certain interacting particle systems as one tunes an external parameter such as the particle density; the system may go over from a low-density disordered phase to an ordered phase at high density. In the absence of a general framework, it is evidently of interest to develop a detailed understanding of the effects of phase transitions on the behavior of fluctuations using simple models of interacting particles. In this thesis, we have pursued such a study within the ambit of a paradigmatic model, the zero-range process (ZRP).

The ZRP involves biased hopping of particles between nearest neighbor sites of a periodic lattice with a rate that depends solely on the occupancy at the departure site. Here, the microscopic configurations evolve by a random sequential dynamics, i.e., in a small time interval $dt \rightarrow 0$, to leading order in dt , at most one particle hopping over the entire lattice takes place. At long times, the system reaches a nonequilibrium current-carrying stationary state. The ZRP is one of the very few models of interacting particles whose stationary state measure can be found exactly in any dimension, for any choice of the hop rates, and even in the presence of quenched disorder; in all these cases, the stationary state measure is given by a simple factorized form, thereby offering an opportunity to analyze many stationary state properties of the ZRP exactly. For certain classes of the hop rates, as the particle density

crosses a critical value, the ZRP undergoes a continuous phase transition from a disordered phase with uniform average density to a condensed phase where a finite fraction of particles accumulates on a single site. Although first introduced in the mathematical literature by Spitzer in 1970 [1], in view of the condensation phenomena, the ZRP or modifications thereof has since appeared in many unexpected contexts, e.g., to model wealth condensation in macroeconomics [2], jamming in traffic [3, 4], coalescence in granular systems [5, 6], gelation in networks [7, 8]. Besides, it has recently been invoked to provide a criterion for phase separation in one-dimensional driven diffusive systems by mapping them to the ZRP [9], though the correctness of this mapping is not clear for all models with driven diffusive dynamics [10]. Finally, a generalization of the ZRP that retains the property of a factorized stationary state has been identified [11, 12]. The generalization comprises (i) making the site occupancy a continuous variable, in this case, called the mass (ii) allowing arbitrary amounts of mass to move from one site to another, and (iii) allowing for parallel dynamics; these considerations have led to the construction of a general mass transfer model which encompasses a wide range of specific models studied earlier as disparate cases.

The layout of the chapter is as follows. Section 6.1 gives the definition of the model of our study, namely, the homogeneous ZRP on a one-dimensional periodic lattice. The ZRP can be mapped to a generalization of the totally asymmetric simple exclusion process; the mapping is discussed in Section 6.2. In Section 6.3, we obtain the stationary state measure of the ZRP over the configuration space. This is followed in Section 6.4 by a discussion of the condensation transition, where we obtain the conditions on the hop rate to observe condensation. In this thesis, we consider the ZRP with a particular choice of the hop rate that leads to a condensation transition. In Section 6.5, for our choice of the hop rate, we obtain the critical density, the single-site occupancy distribution in the various phases, the behavior of the mean particle current in the stationary state as a function of the particle density, both within a grand canonical and a canonical ensemble, and finally, the kinematic wave velocity.

6.1 The model

The ZRP involves N indistinguishable particles of unit mass on a one-dimensional periodic lattice of L sites with arbitrary occupancy of particles allowed at any site [1, 13, 14]. The dynamics in discrete time involves moving a particle from a randomly chosen site i with occupancy n_i to its right neighbor site $i + 1$ with a specified rate $u(n_i)$, a function solely of the occupancy n_i at the departure site i , see Fig. 6.1. The hop rate out of a site with zero occupancy is defined to be zero: $u(0) = 0$. The specific dependence of the hopping rate on the departure site occupancy models the interaction between the particles at the departure site. For example, if $u(n_i) = n_i$, the dynamics of each particle at site i is independent of the others, while $u(n_i) = \text{constant}$ implies an attractive on-site interaction, since particle hop-out rates are lower than those for noninteracting particles. In general, the hop rate

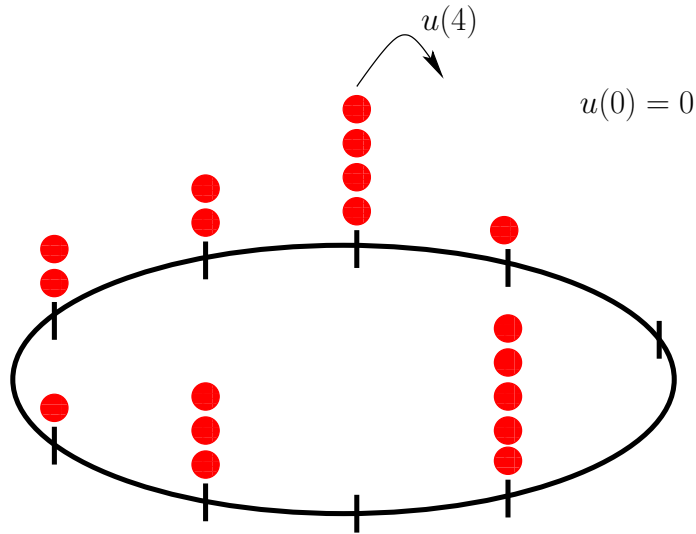


Figure 6.1: Definition of the homogeneous ZRP on a one-dimensional periodic lattice. A possible dynamical move is also shown in the figure.

function $u(n)$ may even be site dependent. In our work, we consider the homogeneous ZRP where the rates are site independent and depend only on the departure site occupancy in a way as to induce condensation transition as a function of the particle density (see Section 6.4 below).

6.2 Mapping to a generalized exclusion process

The homogeneous ZRP in the preceding section can be mapped to a particle hopping model which is a generalization of the totally asymmetric simple exclusion process (TASEP) [13, 14]. Figure 6.2 illustrates the mapping which is achieved by thinking of the ZRP particles as empty sites in the particle model, while the ZRP sites are interpreted as moving particles in the particle model. For example, in Fig. 6.2, site 1 in the ZRP becomes particle 1 in the particle model, while the particle occupying site 1 in the ZRP becomes the vacant site behind the particle 1 in the particle model. Next, site 2 in the ZRP becomes particle 2 in the particle model, while the fact that site 2 in the ZRP is vacant leaves no vacancies between particles 1 and 2 in the particle model, and so on. Following this procedure, a ZRP with N particles and L sites is mapped to the particle model with L hard core particles moving on a lattice of $L + N$ sites. The hop rates in the ZRP, which depend on the number of particles at the departure site, become hop rates in the particle model which depend on the distance to the next particle in front, thereby inducing a long-ranged particle hopping. Note that the ordinary TASEP, defined in Chapter 2, corresponds to the ZRP with hop rate $u(n) = 1$.

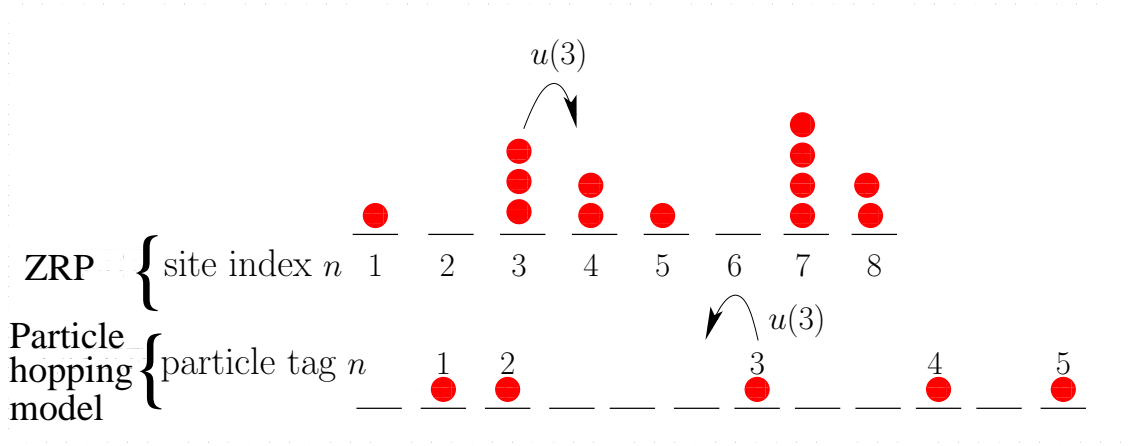


Figure 6.2: Mapping between the ZRP and the particle hopping model, which is a generalization of the TASEP.

6.3 The stationary state measure

From the definition of the model, it is clear that the ZRP dynamics conserves the total number of particles in the system. At long times, the system reaches a nonequilibrium stationary state. An important attribute of the ZRP is that for any choice of the hop rates, the stationary state measure over the configuration space can be found exactly. Thus, the stationary state probability $P(\{n_i\})$ of finding the system in configuration $\{n_1, n_2, \dots, n_L\}$ has a factorized form, being given by a product of factors, one for each site of the system [1, 13, 14]. Specifically, for the homogeneous ZRP that we study, $P(\{n_i\})$ is given by

$$P(\{n_i\}) = \frac{1}{Z_{L,N}} \prod_{i=1}^L f(n_i) \delta \left(\sum_{i=1}^L n_i - N \right), \quad (6.1)$$

where the delta function reminds us that we are working with a fixed number of particles, namely, N (i.e., within a canonical ensemble). From Eq. 6.1, it follows that in the ZRP in the stationary state, the only correlation between sites is arising out of the overall conservation of particles. In Eq. 6.1, $Z_{L,N}$ is the normalization or the canonical partition function that ensures that the probabilities for all configurations containing N particles add up to one, hence

$$Z_{L,N} = \sum_{\{n_i=0\}}^{\infty} \prod_{i=1}^L f(n_i) \delta \left(\sum_{i=1}^L n_i - N \right). \quad (6.2)$$

The factors $f(n_i)$ in Eq. 6.1 are determined by the hop rates, and are given by

$$f(n) = \begin{cases} \left(\prod_{m=1}^n u(m) \right)^{-1} & \text{if } n > 0, \\ 1 & \text{if } n = 0. \end{cases} \quad (6.3)$$

The probability $p(n)$ that any given site, say, site 1, contains n particles is obtained from $P(\{n_i\})$ by fixing n_1 at n , and summing $P(\{n_i\})$ over allowed occupancies of the remaining sites, $i = 2, \dots, L$, subject to the constraint that the remaining number of particles is $N - n$. This gives

$$p(n) = \sum_{n_2, n_3, \dots, n_L} P(n, n_2, n_3, \dots, n_L) \delta \left(\sum_{i=2}^L n_i - (N - n) \right) = \frac{Z_{L-1, N-n}}{Z_{L, N}}. \quad (6.4)$$

6.3.1 Stationary state measure within the grand canonical ensemble in the thermodynamic limit

In the grand canonical ensemble (GCE), the total particle number N , instead of being fixed, as in Eq. 6.1, is allowed to fluctuate, so that the delta function constraint in Eq. 6.1 is removed and one obtains the stationary weight of configurations in the grand canonical ensemble from the canonical weight as

$$W_{GCE}(\{n_i\}) \propto \sum_{N=0}^{\infty} v^N \prod_{i=1}^L f(n_i) \delta \left(\sum_{i=1}^L n_i - N \right) = \prod_{i=1}^L v^{n_i} f(n_i), \quad (6.5)$$

where the fugacity v fixes the overall particle number N . From Eq. 6.5, it follows that in the grand canonical ensemble, there is no correlation between sites in the stationary state.

In order to normalize $W_{GCE}(\{n_i\})$ over all possible configurations, we define the grand canonical partition function as

$$\mathcal{Z}_L(v) = \sum_{\{n_i=0\}}^{\infty} \prod_{i=1}^L v^{n_i} f(n_i) = [F(v)]^L, \quad (6.6)$$

where

$$F(v) = \sum_{n=0}^{\infty} v^n f(n). \quad (6.7)$$

Note that the grand canonical partition function $\mathcal{Z}_L(v)$ is related to the canonical partition function $Z_{L, N}$ through

$$\mathcal{Z}_L(v) = \sum_{N=0}^{\infty} v^N Z_{L, N}. \quad (6.8)$$

Now, the stationary state probability of configurations within the grand canonical ensemble is given by

$$P_{GCE}(\{n_i\}) = \frac{1}{\mathcal{Z}_L(v)} \prod_{i=1}^L v^{n_i} f(n_i) = \prod_{i=1}^L \frac{v^{n_i} f(n_i)}{F(v)}. \quad (6.9)$$

The distribution of the number of particles at a given site within the grand canonical ensemble becomes

$$p(n) = \frac{v^n f(n)}{F(v)}. \quad (6.10)$$

The fugacity v fixes the overall particle number N through the condition

$$N = \sum_{i=1}^L \langle n_i \rangle = L \frac{vF'(v)}{F(v)}, \quad (6.11)$$

where the angular brackets denote averaging with respect to the grand canonical stationary state measure, Eq. 6.9.

Next, we take the thermodynamic limit, $N \rightarrow \infty, L \rightarrow \infty$, keeping the particle density $\rho = \frac{N}{L}$ fixed and finite. Now, Eq. 6.11 reduces to the following relation between the fugacity v and the density ρ .

$$\rho = \frac{vF'(v)}{F(v)}. \quad (6.12)$$

To summarize, in the thermodynamic limit, within a grand canonical ensemble, the probability for a randomly chosen site to have n particles reads

$$p(n) = \frac{v^n f(n)}{F(v)}; F(v) = \sum_{n=0}^{\infty} v^n f(n), \quad (6.13)$$

where the fugacity v is related to the density ρ through Eq. 6.12.

6.3.2 Proof of stationarity

The proof of the stationary state measure, Eqns. 6.1, 6.3, proceeds along the following lines [13, 14]. First, we write down the stationarity condition on the probability of any configuration. This condition balances the probability current due to hops into a configuration with the probability current due to hops out of the same configuration, and hence, reads

$$0 = \sum_{i=1}^L [u(n_{i-1} + 1)P(\dots, n_{i-1} + 1, n_i - 1, \dots) - u(n_i)P(\{n_i\})]\theta(n_i), \quad (6.14)$$

where the Heaviside step function $\theta(n)$ on the right emphasizes that site i must be occupied so as to have hops out of and into the configuration $\{n_i\}$. Next, we substitute Eq. 6.1 into Eq. 6.14 and equate the quantity within the square brackets to zero for each i so that we finally have, after cancelling the common factors,

$$u(n_{i-1} + 1)f(n_{i-1} + 1)f(n_i - 1) = u(n_i)f(n_{i-1})f(n_i). \quad (6.15)$$

The above equation can be put into the form

$$u(n_{i-1} + 1) \frac{f(n_{i-1} + 1)}{f(n_{i-1})} = u(n_i) \frac{f(n_i)}{f(n_i - 1)} = \text{constant}, \quad (6.16)$$

for all values of i . Without any loss of generality, the constant can be set equal to one, so that we have

$$f(n_i) = \frac{f(n_i - 1)}{u(n_i)}, \quad (6.17)$$

which, when iterated, yields Eq. 6.3 on putting $f(0) = 1$, without any loss of generality. Thus, the stationary state measure of the homogeneous ZRP is given by the set of equations, Eqns. 6.1 - 6.3.

6.4 The condensation transition

As discussed in the introduction, for certain classes of the hop rates, the ZRP shows a condensation transition from a disordered phase at low density to a condensed phase at high density. In this section, we obtain the condition on the hop rate $u(n)$ that induces such a transition [13, 14]. To do this, we work within the grand canonical ensemble. First, note that the fugacity v has a maximum value, v_{\max} , given by the radius of convergence of the infinite series $F(v)$ in v in Eq. 6.7. From the ratio test for convergence [15], it follows that, for the series $F(v)$ to converge, the ratio of the $(n+1)$ -term to the n -th term for large n must be smaller than 1 so that

$$v_{\max} = u(\infty). \quad (6.18)$$

Next, we examine the relation between the density ρ and the fugacity v , namely,

$$\rho = \frac{vF'(v)}{F(v)}. \quad (6.19)$$

By taking the derivative with respect to v , one can show that the right hand side is an increasing function of v so that the density increases with the fugacity. If it so happens that the right hand side diverges as v approaches its maximum possible value, v_{\max} , then it is always possible to satisfy Eq. 6.19 for any density such that $v \leq v_{\max}$, and there is no condensation. On the other hand, if the right hand side approaches a constant as $v \rightarrow v_{\max}$, there is a critical density ρ_c beyond which Eq. 6.19 can no longer be satisfied; the excess particles $\sim (\rho - \rho_c)L$ condenses onto a randomly chosen site, thereby breaking the translational symmetry of the system. The fugacity v increases with the density ρ and attains its maximum value v_{\max} at the critical value ρ_c ; for densities $\rho > \rho_c$, the fugacity remains constant at v_{\max} . The two cases of no condensation and condensation are shown schematically in Fig. 6.3. The critical density ρ_c is given by

$$\rho_c = \lim_{v \rightarrow v_{\max} = u(\infty)} \frac{vF'(v)}{F(v)}. \quad (6.20)$$

In this case, for ρ larger than ρ_c , Eq. 6.19 is replaced by

$$\rho = \frac{\langle n_1 \rangle}{L} + \frac{L-1}{L} \rho_c, \quad (6.21)$$

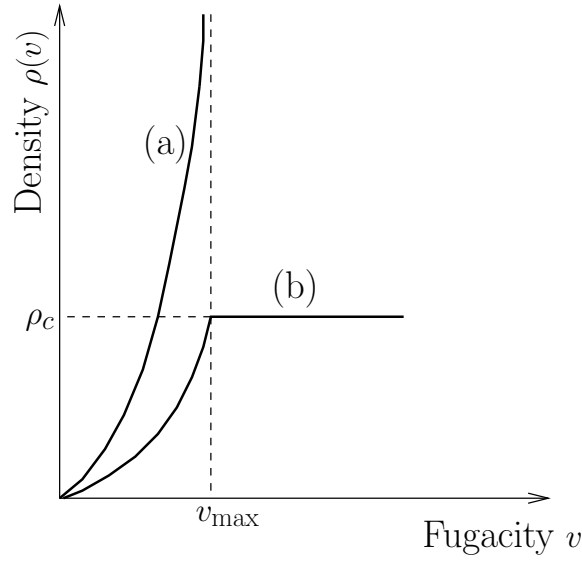


Figure 6.3: Schematic plot of the density ρ as a function of the fugacity v , for case (a) when there is no condensation, and for case (b), when there is a condensation transition.

where site 1 has been arbitrarily chosen to hold the condensate.

In view of the above discussion, the condition for the condensation transition is given by

$$\lim_{v \rightarrow v_{\max} = u(\infty)} \frac{vF'(v)}{F(v)} < \infty, \quad (6.22)$$

i.e., the infinite series $vF'(v) = \sum_{n=1}^{\infty} nv^n f(n)$ must converge as $v \rightarrow v_{\max} = u(\infty)$. For this infinite series to converge, the ratio of the $(n+1)$ -term to the n -term, namely, $(1 + \frac{1}{n}) \frac{u(\infty)}{u(n+1)}$ must fall slower than $(1 - \frac{1}{n})$ for large n , i.e., $(1 + \frac{1}{n}) \frac{u(\infty)}{u(n+1)} < (1 - \frac{1}{n})$ for large n [15]. This implies that $u(n)$ for large n must exceed $u(\infty)(1 + \frac{2}{n})$. Thus, condensation occurs when the hop rate $u(n)$ satisfies either of the two conditions.

- Condition A: For large n ,

$$u(n) \sim u(\infty) \left(1 + \frac{b}{n}\right) \text{ with } b > 2. \quad (6.23)$$

- Condition B: For large n ,

$$u(n) \sim u(\infty) \left(1 + \frac{b}{n^\sigma}\right) \text{ with arbitrary } b > 0 \text{ and } \sigma < 1. \quad (6.24)$$

6.5 The case $u(n) = 1 + \frac{b}{n}$ with $b > 2$

In this thesis, we consider the hop rate $u(n) = 1 + \frac{b}{n} \forall n > 0$ and $b > 2$, for which the single-site weights are given by

$$f(n) = \left(\prod_{m=1}^n u(m) \right)^{-1} = \left(\prod_{m=1}^n \left(1 + \frac{b}{m} \right) \right)^{-1} = \frac{n!}{(b+1)_n}, \quad (6.25)$$

where

$$(a)_n = a(a+1)\dots(a+n-1) \quad (6.26)$$

is the Pochhammer symbol.

The behavior of $f(n)$ for large n can be found by taking the logarithm of $f(n)$:

$$\ln f(n) = - \sum_{m=1}^n \ln \left(1 + \frac{b}{m} \right) \quad (6.27)$$

$$\approx -B - \sum_{n^*}^n \frac{b}{m}. \quad (6.28)$$

Here, n^* is such that $\frac{b}{n^*} \gg 1$, so that $\ln \left(1 + \frac{b}{n^*} \right) \approx \frac{b}{n^*}$. In Eq. 6.28, B stands for the sum, $\sum_{m=1}^{n^*} \ln \left(1 + \frac{b}{m} \right)$. The sum on the right hand side of Eq. 6.28 may be replaced by an integral, which, when evaluated, finally yields

$$f(n) \approx An^{-b} \text{ for large } n, \quad (6.29)$$

where A is a constant.

6.5.1 The critical density ρ_c and the phase diagram

For our choice of the hop rate, one can calculate the critical density exactly, following Eq. 6.20 [16, 17]. In our case, $v_{\max} = 1$. Using Eq. 6.25, we have

$$F(v) = \sum_{n=0}^{\infty} v^n \frac{n!}{(b+1)_n} = \sum_{n=0}^{\infty} v^n \frac{(1)_n (1)_n}{(b+1)_n n!}. \quad (6.30)$$

Thus

$$F'(v) = \sum_{n=0}^{\infty} v^n \frac{(n+1)(n+1)!}{(b+1)_{n+1}} = \frac{1}{b+1} \sum_{n=0}^{\infty} v^n \frac{(2)_n (2)_n}{(b+2)_n n!}. \quad (6.31)$$

Next, one uses the following identity involving the hypergeometric function [18].

$$\sum_{n=0}^{\infty} \frac{(a)_n (b)_n}{(c)_n n!} = \frac{\Gamma(c)\Gamma(c-a-b)}{\Gamma(c-a)\Gamma(c-b)} \text{ for } c > a+b. \quad (6.32)$$

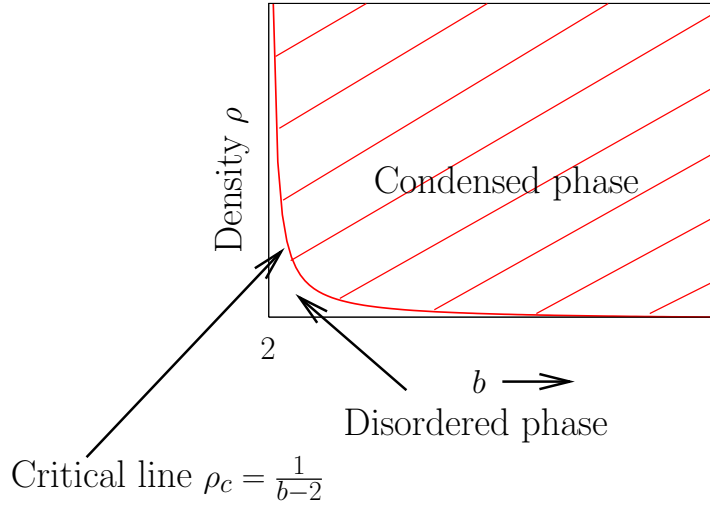


Figure 6.4: ZRP phase diagram for the hop rate $u(n) = 1 + \frac{b}{n}$, with $n > 0$ and with $b > 2$. The critical line $\rho_c = \frac{1}{b-2}$ is also marked in the figure.

This gives

$$F(v_{\max}) = b/(b-1) \quad (6.33)$$

and

$$F'(v_{\max}) = b/((b-1)(b-2)). \quad (6.34)$$

Finally, on using Eq. 6.20, we get

$$\rho_c = \frac{1}{b-2}. \quad (6.35)$$

Thus, for $u(n) = (1 + \frac{2}{n})$, the ZRP goes over from a disordered phase across the critical density $\rho_c = \frac{1}{b-2}$ to a condensed phase, as shown in Fig. 6.4.

6.5.2 Single site occupancy distribution within the canonical ensemble

Once the hop rates $u(n)$ or, equivalently, the single-site factors $f(n)$ are given, one can compute, using Eq. 6.4, the single-site occupancy distribution $p(n)$ within the canonical ensemble in the disordered phase ($\rho < \rho_c$), at the critical point ($\rho = \rho_c$), and in the condensed phase ($\rho > \rho_c$). To do this, one has to know the canonical partition function, which is obtained by first fixing the density ρ to be in one of the phases, then computing the corresponding grand canonical partition function $\mathcal{Z}_L(v)$ and finally, inverting Eq. 6.8 to extract the associated canonical partition function. The most challenging part is the inversion of Eq. 6.8, which can be performed exactly only for a few $f(n)$'s, e.g., when $f(n) = \frac{2}{\sqrt{\pi}} \frac{1}{n^{5/2}} e^{-1/n}$; in this case, $p(n)$ in different phases can be computed exactly and are shown in Fig. 6.5 [19, 20]. To compute $p(n)$ for a general $f(n)$, one relies on an asymptotic analysis, as detailed in [19, 20]. In our case, with $f(n)$ for large n given in Eq. 6.29, the forms of the single-site canonical distribution $p(n)$ in different phases, computed using the

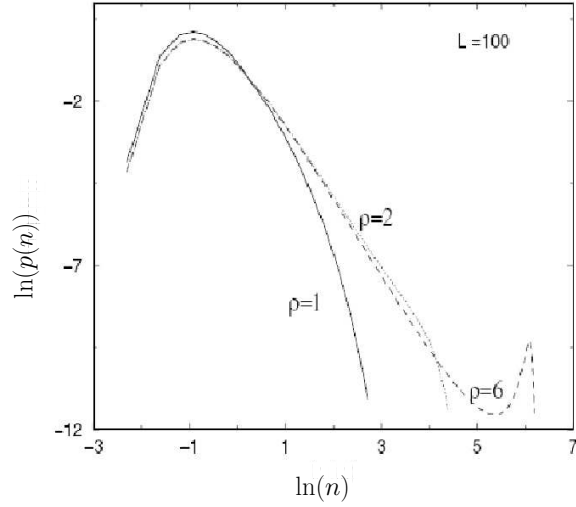


Figure 6.5: The single-site distribution $p(n)$ as a function of occupancy n for the exactly solvable case, $f(n) = \frac{2}{\sqrt{\pi}} \frac{1}{n^{5/2}} e^{-1/n}$, plotted using *Mathematica* for $L = 100$ and $\rho = 1$ (disordered phase), $\rho = \rho_c = 2$ (critical point), and $\rho = 6$ (condensed phase). The condensate shows up as an additional bump near the tail of $p(n)$ in the condensed phase. The figure is adapted from Ref. [19], with the permission of one of the authors.

asymptotic analysis, are summarized below [19, 20].

Disordered phase ($\rho < \rho_c$)

Here,

$$p(n) \sim f(n)e^{-n/n^*} \text{ for } 1 \ll n \ll N, \quad (6.36)$$

where the characteristic occupancy n^* diverges as ρ approaches ρ_c from below as $(\rho - \rho_c)^{-1}$ for $b > 3$ and as $(\rho - \rho_c)^{-1/(b-2)}$ for $2 < b < 3$.

To summarize, the single-site distribution $p(n)$ in the disordered phase is exponential in n for large n .

Critical point ($\rho = \rho_c$)

Here, one has

$$p(n) \propto f(n)V_b(n/L^{1/(b-1)}) \text{ for } 2 < b < 3, \quad (6.37)$$

$$p(n) \propto f(n)e^{-n^2/2\Delta^2L} \text{ for } b > 3, \quad (6.38)$$

where the asymptotic forms of the scaling function $V_b(z)$ are given by

$$\begin{aligned} V_b(z) &\simeq A|z|^{-b} \text{ as } z \rightarrow -\infty, \\ &= c_0 \text{ at } z = 0, \\ &\simeq c_1 z^{(3-b)/2(b-2)} e^{-c_2 z^{(b-1)/(b-2)}} \text{ as } z \rightarrow \infty. \end{aligned} \quad (6.39)$$

Here, $c_0 = \beta^{-1/(b-1)}/[(b-1)\Gamma((b-2)/(b-1))]$, $c_1 = [2\pi(b-2)(\beta(b-1))^{1/(b-2)}]^{-1/2}$, $c_2 = (b-2)/(b-1)(\beta(b-1))^{1/(b-2)}$, where $\beta = A\Gamma(1-b)$.

Thus, at the critical point, $p(n)$ decays as a power law n^{-b} for large n , which is cut-off by a finite-size scaling function; the cut-off occupancy scales as

$$n_{\text{cut-off}} \sim L^{1/(b-1)} \text{ for } 2 < b < 3, \quad (6.40)$$

$$\sim L^{1/2} \text{ for } b > 3. \quad (6.41)$$

Condensed phase ($\rho > \rho_c$)

Here, one has

$$p(n) \simeq f(n) \text{ for } 1 \ll n \ll O(L), \quad (6.42)$$

$$\begin{aligned} p(n) &\simeq f(n) \frac{1}{(1-x)^b} \\ &\text{for } n = x(\rho - \rho_c)L \text{ where } 0 < x < 1, \end{aligned} \quad (6.43)$$

$$p(n) \sim p_{\text{cond}}(n) \text{ for } n \sim (\rho - \rho_c)L. \quad (6.44)$$

Here, p_{cond} is the part of $p(n)$ that represents the condensate; it is centered on $(\rho - \rho_c)L$ and its integral equals $1/L$, implying that there is a *single* condensate site. p_{cond} takes two different forms, depending on whether $2 < b < 3$ or $b > 3$. In the former case,

$$p_{\text{cond}}(n) \simeq L^{-b/(b-1)} V_b \left[\frac{n - (\rho - \rho_c)L}{L^{1/(b-1)}} \right], \quad (6.45)$$

where the asymptotic forms of $V_b(z)$ are given in Eq. 6.39. Thus, the shape of the condensate bump is non-Gaussian for $2 < b < 3$, and this is referred to as an anomalous condensate. For $b > 3$, one has

$$p_{\text{cond}}(n) \simeq \frac{1}{\sqrt{2\pi\Delta^2 L}} e^{-(n - (\rho - \rho_c)L)^2 / 2\Delta^2 L} \text{ for } |n - (\rho - \rho_c)L| \ll O(L^{2/3}), \quad (6.46)$$

i.e., here, $p_{\text{cond}}(n)$ is Gaussian on the scale $|n - (\rho - \rho_c)L| \ll O(L^{2/3})$, but, far to the left of the peak, $p(n)$ decays as a power law:

$$p_{\text{cond}}(n) \simeq f(n) (1 - n/(\rho - \rho_c)L)^{-b} \text{ for } (\rho - \rho_c)L - n \sim O(L). \quad (6.47)$$

To summarize, in the condensed phase, for $b > 3$, the condensate near the peak is Gaussian distributed with width $\sim L^{1/2}$, while for b between 2 and 3, the fluctuations in the number of particles in the condensate are anomalously large ($\sim L^{1/(b-1)}$).

6.5.3 Particle current

In the stationary state, the mean particle current is the same across every pair of neighboring bonds.

Grand canonical ensemble

In the thermodynamic limit, within a grand canonical ensemble, the mean current J is obtained by noting that in order to have a particle hop across a bond, the site to the left has to be occupied in the first place (with probability $p(n)$ for $n > 0$), followed by a hop with rate $u(n)$ when the left site has n particles. Hence, J is given by

$$J = \sum_{n=1}^{\infty} p(n)u(n) = v, \quad (6.48)$$

using Eq. 6.13. Thus, the current increases with the density ρ , attains its maximum value $v_{max} = u(\infty) = 1$ at the critical density ρ_c , and remains constant at this maximum value for $\rho > \rho_c$.

Canonical ensemble

Within the canonical ensemble, the mean particle current $J_{L,N}$ is given by

$$J_{L,N} = \sum_{n_1=1}^{\infty} f(n_1)u(n_1) \sum_{\{n_j=0, j \neq 1\}}^{\infty} \prod_{j=2}^L f(n_j) \delta \left(\sum_{k=1}^L n_k - N \right) / Z_{L,N} \quad (6.49)$$

$$= \frac{Z_{L,N-1}}{Z_{L,N}}, \quad (6.50)$$

where we have chosen to evaluate the mean current across the bond next to site 1. In arriving at the last step, we have used the definition of the canonical partition function $Z_{L,N}$ in Eq. 6.2. $J_{L,N}$ can be obtained from Eq. 6.50 by first computing the canonical partition function $Z_{L,N}$ numerically for given values of L and N , starting from Eq. 6.4 [21]; one has

$$p(n) = \frac{f(n)Z_{L-1,N-n}}{Z_{L,N}}. \quad (6.51)$$

Now, $p(n)$ being normalized,

$$\sum_{n=0}^N p(n) = 1, \quad (6.52)$$

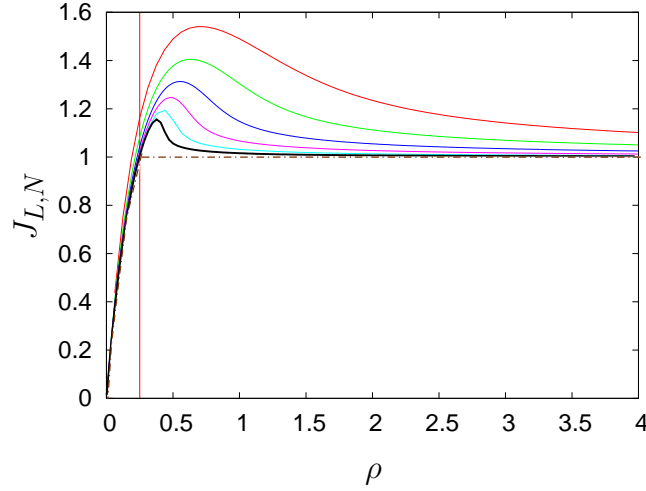


Figure 6.6: Mean current $J_{L,N}$ within the canonical ensemble. Here $b = 6, L = 16, 32, 64, 128, 256, 512$ from top downwards. The vertical line is at $\rho_c = 1/(6 - 2) = 0.25$. The dotted line shows the behavior of the current J within the grand canonical ensemble in the thermodynamic limit.

which gives

$$Z_{L,N} = \sum_{n=0}^N Z_{L-1,N-n} f(n). \quad (6.53)$$

Equation 6.53 can be solved recursively with the initial conditions

$$\begin{aligned} Z_{l,0} &= 1 \text{ for } l = 0, 1, 2, \dots, L, \\ Z_{0,n} &= 0 \text{ for } n = 1, 2, \dots, N. \end{aligned} \quad (6.54)$$

Note that $Z_{l,1} = lf(1)$ for $l = 1, 2, \dots, L$. The single-site weights $f(n)$ are given by Eq. 6.25.

The mean current $J_{L,N}$, as computed using the above procedure, is shown in Fig. 6.6. From the figure, it is clear that with increasing system size, the current $J_{L,N}$ at a fixed density approaches the behavior predicted in the thermodynamic limit.

6.5.4 Kinematic wave velocity

The kinematic wave velocity is given by (See Appendix A)

$$v_K = \frac{\partial J}{\partial \rho} = \left[\frac{\partial J}{\partial v} \right] / \left[\frac{\partial \rho}{\partial v} \right]. \quad (6.55)$$

In the thermodynamic limit, within a grand canonical ensemble, we have, from Eq. 6.48,

$$\frac{\partial J}{\partial v} = 1, \quad (6.56)$$

so that

$$\frac{1}{v_K} = \frac{\partial \rho}{\partial v} = \frac{\rho(1-\rho)}{v} + \frac{vF''(v)}{F(v)}, \quad (6.57)$$

using Eq. 6.12. Now, we have, from Eq. 6.31,

$$vF''(v) = \sum_{n=0}^{\infty} nv^n \frac{(n+1)(n+1)!}{(b+1)_{n+1}} = \frac{1}{b+1} \sum_{n=0}^{\infty} nv^n \frac{(2)_n(2)_n}{(b+2)_n n!}, \quad (6.58)$$

so that

$$\frac{1}{v_K} = \frac{\rho(1-\rho)}{v} + \frac{1}{b+1} \sum_{n=0}^{\infty} nv^n \frac{(2)_n(2)_n}{(b+2)_n n!} / \sum_{n=0}^{\infty} v^n \frac{(1)_n(1)_n}{(b+1)_n n!}, \quad (6.59)$$

on using Eq. 6.30.

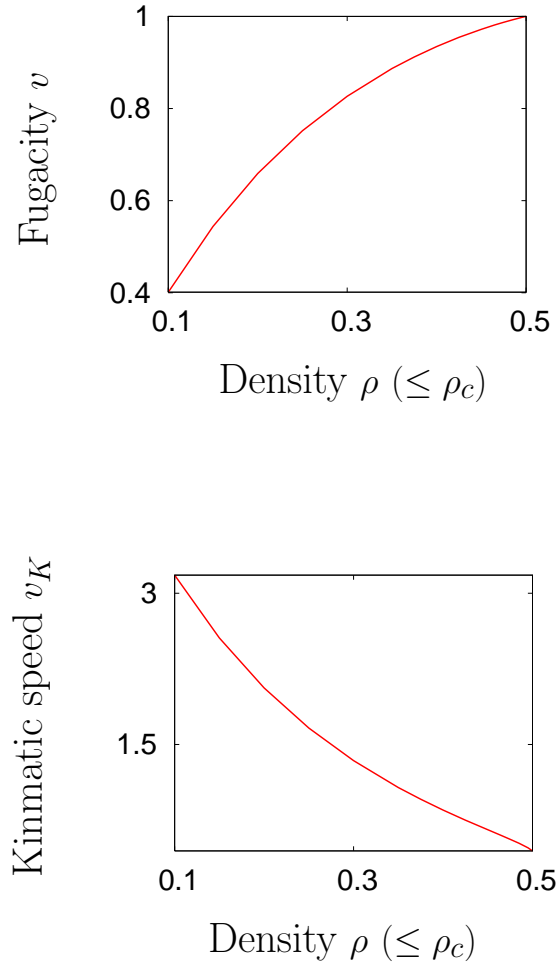


Figure 6.7: Fugacity v and the kinematic wave velocity v_K as a function of the particle density $\rho (\leq \rho_c)$, computed numerically, using Eq. 6.12 and Eq. 6.59. Here, the hop rate is $u(n) = 1 + \frac{4}{n}$ so that the critical density $\rho_c = 0.5$.

For a given density ρ , one can find the kinematic wave velocity v_K from Eq. 6.59 by first

finding the fugacity v corresponding to the density ρ from Eq. 6.12, then substituting this value of v in Eq. 6.59, and evaluating the right hand side. Figure 6.7 shows an illustration of this procedure, showing the fugacity v and the kinematic wave velocity v_K as a function of the density ρ ($\leq \rho_c$), computed numerically using Eq. 6.12 and Eq. 6.59; the value of b here is 4. In the condensed phase, the kinematic wave velocity remains pinned to its value at the critical point.

It is interesting to ask about the kinematic wave velocity at the critical density $\rho_c = 1/(b-2)$ as a function of b ; here, $v \rightarrow v_{max} = 1$, so that we have

$$v_{max}F''(v_{max}) = \frac{1}{b+1} \sum_{n=0}^{\infty} n \frac{(2)_n(2)_n}{(b+2)_n n!}. \quad (6.60)$$

For the above series, the ratio of the $(n+1)$ -th to n -th term, for large n , behaves as $\sim (1 - (b-2)/n)$. Using the ratio test for convergence [15], one concludes that the series diverges for $2 < b < 3$ and converges for $b > 3$; for the latter case, the series may be summed using *Mathematica* with the result $v_{max}F''(v_{max}) = \frac{4b}{(b-3)(b-2)(b-1)}$.

Now, from Eq. 6.33, we have

$$F(v_{max}) = \frac{b}{b-1}, \quad (6.61)$$

so that, using Eq. 6.59, we finally have [16]

$$[v_K]_{\rho_c} = \begin{cases} 0 & \text{for } 2 < b < 3, \\ \frac{(b-3)(b-2)^2}{(b-1)^2} & \text{for } b > 3. \end{cases} \quad (6.62)$$

$$(6.63)$$

In the next chapter, we will report our results on size effects on the dynamics of fluctuations in the ZRP as the system passes through the condensation transition. We make the following choice for the hop rate: $u(n) = 1 + \frac{b}{n}$ for all $n > 0$, with $b > 2$. The particular quantity that we monitor is the variance of the integrated particle current across a bond in the stationary state. We show that the variance exhibits striking differences in behavior as the system goes over from the disordered to the condensed phase. In the disordered phase, and also at the critical point, the variance behaves similarly to the tagged particle correlations in the ASEP, summarized in Chapter 3. Thus, the variance shows damped oscillations in time due to the kinematic wave of density fluctuations, and has two size-dependent time scales, set by the circulation time and the decay time of the kinematic wave, respectively. On the contrary, in the condensed phase, numerical simulations and strong scaling arguments show that the fluctuation dynamics is governed by the condensate relocation from site to site.

References

- [1] F. Spitzer, *Adv. Math.* **5**, 246 (1970).
- [2] Z. Burda, D. Johnston, J. Jurkiewicz, M. Kaminski, M. A. Novak, G. Papp, and I. Zahed, *Phys. Rev. E* **65**, 026102 (2002).
- [3] M. R. Evans, *Europhys. Lett.* **36**, 13 (1996).
- [4] D. Chowdhury, L. Santen, and A. Schadschneider, *Phys. Rep.* **329**, 199 (2000).
- [5] J. Eggers, *Phys. Rev. Lett.* **83**, 5322 (1999).
- [6] D. van der Meer, K. van der Weele, and D. Lohse, *J. Stat. Mech.* P04004 (2004).
- [7] P. L. Krapivsky, S. Redner, and F. Leyvraz, *Phys. Rev. Lett.* **85**, 4629 (2000).
- [8] G. Bianconi and A-L Barabási, *Phys. Rev. Lett.* **86**, 5632 (2001).
- [9] Y. Kafri, E. Levine, D. Mukmael, G. M. Schütz, and J. Török, *Phys. Rev. Lett.* **89**, 035702 (2002).
- [10] S. Chatterjee and M. Barma, *Phys. Rev. E* **77**, 061124 (2008).
- [11] M. R. Evans, S. N. Majumdar, and R. K. P. Zia, *J. Phys. A* **37**, L275 (2004).
- [12] R. K. P. Zia, M. R. Evans, and S. N. Majumdar, *J. Stat. Mech.* L10001 (2004).
- [13] M. R. Evans, *Braz. J. Phys.* **30**, 42 (2000).
- [14] M. R. Evans and T. Hanney, *J. Phys. A* **38**, R195 (2005).
- [15] See, e.g., J. Mathews and R. L. Walker, *Mathematical Methods of Physics* 2nd edn (Addison-Wesley, 1971).
- [16] S. Großkinsky, G. M. Schütz, and H. Spohn, *J. Stat. Phys.* **113**, 389 (2003).
- [17] C. Godrèche, *J. Phys. A* **36**, 6313 (2003).
- [18] G. E. Andrews, R. Askey, and R. Roy, *Special Functions* (Cambridge University Press, Cambridge, 1999).

- [19] S. N. Majumdar, M. R. Evans, and R. K. P. Zia, *Phys. Rev. Lett.* **94**, 180601 (2005).
- [20] M. R. Evans, S. N. Majumdar, and R. K. P. Zia, *J. Stat. Phys.* **123**, 357 (2006).
- [21] O. J. O'Loan, M. R. Evans, and M. E. Cates, *Phys. Rev. E* **58**, 1404 (1998).

Chapter 7

Current fluctuations in the ZRP

“I can’t explain *myself*, I’m afraid, Sir,” said Alice, “because, I’m not myself, you see.”

Lewis Carroll

In this chapter, we study size effects on the dynamics of fluctuations in the zero-range process (ZRP) [1] as the system passes through the condensation transition, discussed in Chapter 6. We report our results for the choice of the hop rate $u(n) = 1 + \frac{b}{n}$ for all $n > 0$, with $b > 2$. The particular quantity that we monitor is the variance of the integrated particle current across a bond in the stationary state. As we explain below, the variance shows striking differences in behavior as the system goes over from the disordered to the condensed phase (see Fig. 7.1). In the disordered phase, and also at the critical point, the variance behaves similarly to the tagged particle correlations in the ASEP, summarized in Chapter 3. Thus, the variance shows damped oscillations in time due to the kinematic wave of density fluctuations, and has two size-dependent time scales, set by the circulation time and the decay time of the kinematic wave, respectively. On the contrary, in the condensed phase, numerical simulations and strong scaling arguments show that the fluctuation dynamics is governed by the condensate relocation from site to site, and the variance has four distinct size-dependent time regimes, the two relevant time scales being the survival time and the relocation time of the condensate, respectively.

The chapter is organized in the following way. We start in Section 7.1 with the definition of the variance measuring the integrated current fluctuations, besides giving the exact details of the ZRP studied in this thesis. Next, in Section 7.2, we discuss a coarse-grained description of the ZRP, valid in the disordered phase and at the critical point; through a mapping, the coarse-grained density profile in the ZRP is related to the height of a nonequilibrium interface in the Kardar-Parisi-Zhang (KPZ) universality class [2]. Next, we come to stating and explaining the behavior of the current fluctuations in the disordered phase (Section 7.3.1), at the critical point (Section 7.3.2), and finally, in the condensed phase (Section 7.3.3). In each of the phases, we point out all the relevant size-dependent time scales in the behavior of the variance, and also provide simple explanations for the underly-

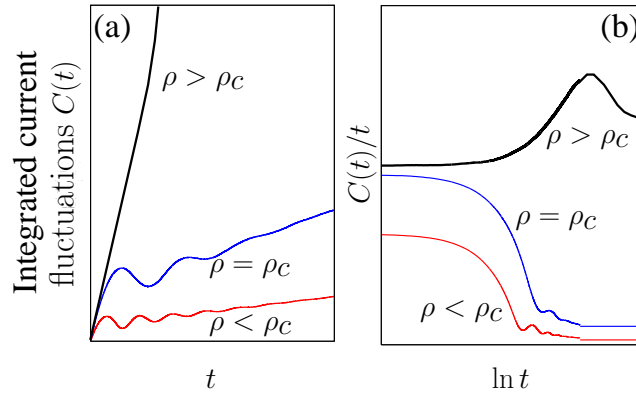


Figure 7.1: Integrated current fluctuations in the disordered phase ($\rho < \rho_c$), at the critical point ($\rho = \rho_c$), and in the condensed phase ($\rho > \rho_c$).

ing dynamical processes. In the condensed phase, an essential ingredient in explaining the behavior of the variance is the dynamics through which the condensate relocates from site to site. We discuss this in detail in Section 7.3.3; based on this discussion, we introduce a simple model in Section 7.3.3 in order to compute the long-time behavior of the variance in the condensed phase.

7.1 Integrated current fluctuations: Definitions

We consider the homogeneous ZRP with N indistinguishable particles of unit mass on a one-dimensional periodic lattice of L sites [1]; see also Chapter 6. The rate with which a particle out of a randomly chosen site hops to its right neighbor site is taken to be $u(n) = 1 + \frac{b}{n}$ with $b > 2$, where $n \geq 0$ is the occupancy at the departure site. In the limit of long times, the system settles into a current-carrying nonequilibrium stationary state, where the probability of occurrence of configurations has a factorized form (Section 6.3). For our choice of the hop rate, the system, in the stationary state, undergoes a nonequilibrium phase transition, as discussed in Section 6.4. As ρ crosses the critical value $\rho_c = 1/(b-2)$ [3] (Section 6.5), a low-density disordered phase with occupancy of $O(1)$ at each site evolves to a high-density condensed phase where a macroscopic collection of particles of average mass $(\rho - \rho_c)L$ condenses onto a randomly selected site, while the remaining sites have the average occupancy ρ_c .

Recent work on the ZRP has dealt with the relaxation of an initial homogeneous density distribution toward the condensed phase [3]. By contrast, here we are interested in the dynamics of density fluctuations in the stationary state in both the disordered and the condensed phases.

In the stationary state, the mean current of particles between every pair of neighboring sites is the same. In the thermodynamic limit, within a grand canonical ensemble, the mean

current is $J = v$, as discussed in Section 6.5.3; moreover, the mean current J increases with the density ρ , attaining its maximum value $v_{\max} = u(\infty) = 1$ at ρ_c , and remaining pinned to this value in the condensed phase. To address the dynamics of density fluctuations, we examine the fluctuations in the integrated particle current across any bond in the stationary state.

The large deviation function of the integrated current has been studied for the ZRP with open boundaries in [4]. Let the function $H(i, t)$ count the total number of particles crossing the bond $(i, i + 1)$ in time t . Thus, we have

$$H(i, t) = \sum_{t'=0}^t J(i, t'), \quad (7.1)$$

where $J(i, t')$ is the instantaneous current across the bond $(i, i + 1)$ at time t' . For our studies, we monitor the variance $C(i, t)$ of the integrated current $H(i, t)$. Thus, we have

$$C(i, t) \equiv \overline{\left\langle \left[H(i, t) - \overline{H(i, t)} \right]^2 \right\rangle}, \quad (7.2)$$

where, as for the ASEP, the overbar stands for the averaging with respect to the initial stationary ensemble of configurations, while the angular brackets denote averaging with respect to stochastic evolution of configurations. Through the mapping to a particle hopping model which is a generalization of the TASEP, discussed in Section 6.2, it follows that $C(i, t)$ is a measure of the tagged particle correlations in the equivalent particle model, being given by the variance of the i -th tagged particle around its average displacement in time t ; hence, $C(i, t)$ is identical to the quantity $\sigma^2(L, t)$, defined in Chapter 3, the only difference being that the particle model now involves a long-ranged particle hopping (see Section 6.2).

7.2 Coarse-grained description of the density profile for $\rho \leq \rho_c$

Before we come to a presentation of our results for the integrated current fluctuations, we show below that in the disordered phase and at the critical point, the coarse-grained density profile of the ZRP maps onto a nonequilibrium growing interface in the KPZ universality class [2], governed by the usual KPZ equation with an additional drift term. The derivation follows the same lines of reasoning as for the ASEP in Chapter 2, Section 2.6 and Section 2.7. The time-evolution equation for the coarse-grained density profile, defined as a function of the spatial variable $x \in [0, 1]$, is (see Eq. 2.21)

$$\frac{\partial \delta \rho(x, t)}{\partial t} = \Gamma \frac{\partial^2 \delta \rho(x, t)}{\partial x^2} - v_K \frac{\partial \delta \rho(x, t)}{\partial x} + \frac{\lambda}{2} \frac{\partial (\delta \rho)^2}{\partial x} - \frac{\partial \eta(x, t)}{\partial x}, \quad (7.3)$$

where the noise $\eta(x, t)$ satisfies: $\overline{\eta(x, t)} = 0$, $\overline{\eta(x, t)\eta(x', t')} = 2A\delta(x - x')\delta(t - t')$. Also, $v_K = \frac{\partial J}{\partial \rho}$, while $\lambda = 2\frac{\partial^2 J}{\partial \rho^2}$. Here, both the kinematic wave velocity v_K and the coefficient λ can be computed for the ZRP, knowing the expression for the particle current J (see Section 6.5 for the computations of J and v_K). To construct the equivalent interface, one introduces the height function $h(x, t)$ through the time-integrated particle current, as for the ASEP (Section 2.7). We have

$$h(x, t) = \int_0^t ds J(x, s), \quad (7.4)$$

where $J(x, t)dxdt$ gives the net number of particles flowing out of the length between x and $x + dx$ of the system, between times t and $t + dt$. Thus, on the level of a lattice, comparing Eq. 7.4 with the definition of the integrated current $H(i, t)$ in Eq. 7.1, we find the height of the interface at site i at time t is precisely given by the integrated particle current $H(i, t)$ across the bond $(i, i + 1)$ in time t . On the basis of the mapping in Eq. 7.4, we find that the time evolution of the interface is governed by (Section 2.7)

$$\frac{\partial h(x, t)}{\partial t} = \Gamma \frac{\partial^2 h}{\partial x^2} - v_K \frac{\partial h}{\partial x} + \frac{\lambda}{2} \left(\frac{\partial h}{\partial x} \right)^2 + \eta(x, t). \quad (7.5)$$

After applying Galilean transformation, $x \rightarrow x' = x - v_K t$, to get rid of the drift term $-v_K \frac{\partial h}{\partial x}$, Eq. 7.5 reduces to the usual KPZ equation [2]. Note that the above coarse-grained description of the ASEP is applicable only to the disordered phase and the critical point and not to the condensed phase. This is because the starting point in the derivation of the coarse-grained description is the continuity equation which embodies the conservation of particles in the system. In the condensed phase, the continuity equation holds only far away from the condensate, but not in the spatial region including the condensate site. To understand this, let us examine the continuity equation in some detail. In terms of the fluctuations $\delta\rho(x, t)$ about the mean density ρ (so that $\delta\rho(x, t) = \rho(x, t) - \rho$), the continuity equation reads

$$\frac{\partial \delta\rho(x, t)}{\partial t} = -\frac{\partial J(x, t)}{\partial x}, \quad (7.6)$$

according to which the increase in density/unit time over a small spatial region of extent δx is due to the net current flowing into the region. In the condensed phase, let us consider a small spatial region of length δx including the condensate site. The difference in the current of particles flowing into this region would definitely tend to increase the density over this region. However, since the condensate mass fluctuates on a much larger scale (as $L^{1/2}$ for $b > 3$, and as $L^{1/(b-1)}$ for $2 < b < 3$ [5]; also, Chapter 6, Section 6.5.2), the fluctuations induced by the net current (which is of $O(1)$) would not manifest itself in appreciable increase in the density over this region in time. This is to say that fluctuations are subsumed at the condensate, and cannot pass through, leading to non-validity of the equation of continuity in a small spatial region including the condensate site. As a result,

a coarse-grained description, akin to that in the disordered phase, is not possible in the condensed phase.

7.3 Behavior in different phases

In order to study the dynamics of fluctuations in the various phases, we monitor $C(t) = \sum_{i=1}^L C(i, t)/L$ in Monte Carlo simulations of the ZRP for our choice of the hop rate. We find that it shows strong differences in behavior in the disordered and the condensed phases, reflecting very different underlying physical processes in the two phases. The relevant time scales in the behavior of fluctuations in the two phases and the physical effects underlying them are summarized below. In Fig. 7.1, we show schematically the behavior of the variance of the integrated current as a function of time in different phases. In all the phases, at short times, the integrated current is Poisson distributed, implying that the variance grows linearly in time, a behavior which holds for all times in an infinite system. In a finite system, in the disordered phase and at criticality, the variance shows oscillations at times proportional to the system size L . This results from kinematic waves transporting density fluctuations around the system with a well-defined velocity. At longer times ($\sim L^{3/2}$), the wave decays, and then the variance increases linearly with time with a small slope that decreases with increasing system size. In the condensed phase, however, the kinematic wave cannot pass through the condensate; thus, fluctuations do not circulate around. The initial linear behavior continues until, after a characteristic time which grows as a power of the system size, the condensate relocates itself. This results in the variance showing a linear rise in time with a much larger slope than at early times. Subsequently, after the condensate has relocated to another site, the slope of the linear rise slowly approaches a size-dependent constant.

We explain each of our above findings below.

7.3.1 Disordered phase

In this phase, the variance $C(t)$ of the integrated current behaves similarly to the tagged particle correlation in the ASEP, discussed in Chapter 3. Thus, there are two size-dependent time scales $T_1 \sim L$, set by the circulation time of a kinematic wave of density fluctuations, and $T_2 \sim L^{3/2}$, given by the time taken by this wave to decay (Fig. 7.2). We elaborate below on the behavior of $C(t)$ in various time regimes.

- Initial linear regime ($t \ll T_1$):

Here, $C(t)$ grows linearly in time: $C(t) = vt$. This follows from the result that, in this time regime, $H(i, t)$ is Poisson distributed with intensity v over all bonds $(i, i + 1)$. Specifically, the probability $P_{out}(n, t) \equiv \text{Prob}(H(i, t) = n)$ that n particles have crossed any bond $(i, i + 1)$ in time t is given by $P_{out}(n, t) = \frac{e^{-vt}(vt)^n}{n!}$. The proof is relegated to Appendix D. Briefly, the proof goes along the following lines. The

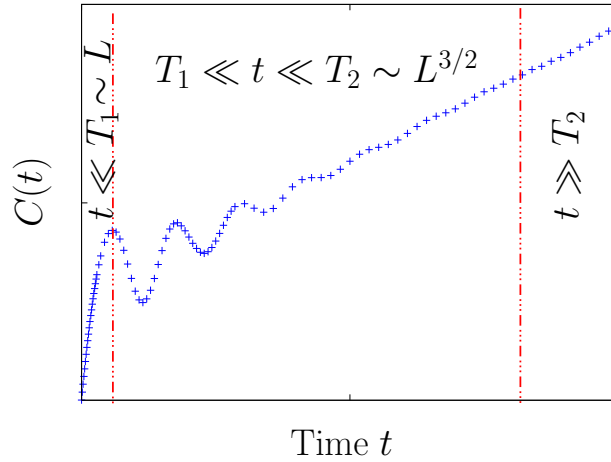


Figure 7.2: Behavior of the variance $C(t)$ of the integrated current in the disordered phase of the ZRP.

population at a ZRP site undergoes a time-reversible birth-death process where a birth (particle input) occurs with rate v , while a population of n particles undergoes a death with rate $u(n)$. For a reversible birth-death process with Poisson inputs, Burke's theorem implies an identical Poisson distribution of outputs [6]. Since in the ZRP, the output from one site forms the input to the next site, it then follows that the distribution $P_{out}(n, t)$ is Poissonian [7].

- Oscillatory regime ($T_1 \ll t \ll T_2$):

In this regime, $C(t)$ oscillates as a function of time. In a driven system with homogeneous density ρ and a density-dependent current $J(\rho)$, density fluctuations are transported as a kinematic wave with velocity $v_K = \partial J / \partial \rho$ [8]; the physical arguments are briefly summarized in Appendix A. For the ZRP, this wave is dissipated over a time scale $\sim L^z$, where $z = z_{\text{KPZ}} = 3/2$ is the dynamic exponent, characteristic of the KPZ universality class to which the ZRP belongs; this follows from the mapping of the coarse-grained density profile of the ZRP to the KPZ interface (Section 7.2) and from the scaling properties of the KPZ equation (Chapter 2, Section 2.8). Since $z > 1$, fluctuations circulate many times around a periodic system before getting dissipated, and revisit every site after a time L/v_K , which makes the variance oscillate in time with this period. The kinematic wave velocity v_K can be evaluated in the disordered phase in accordance with the discussion in Chapter 6, Section 6.5.4. As in the ASEP, a measure of the growth of dissipation in time is given by the lower envelope of the oscillations, which behaves as $t^{2\beta}$ where $\beta = \beta_{\text{KPZ}} = 1/3$ (see the discussions on the scaling properties of the KPZ equation in Section 2.8).

- Late-time regime ($t \gg T_2$):

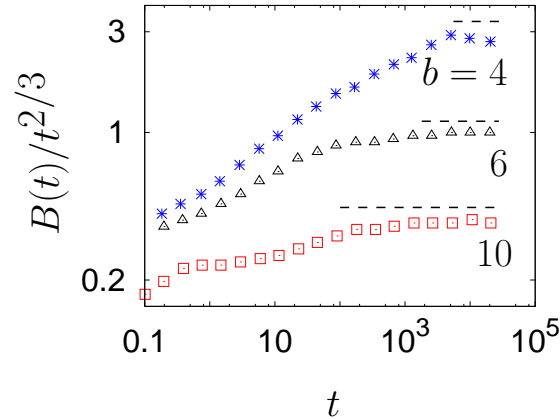


Figure 7.3: Monte Carlo simulation results for $B(t)/t^{2/3}$ as a function of time t with the hop rate $u(n) = 1 + \frac{b}{n}$ for different b 's at $\rho_c = 1/(b-2)$. The system size is $L = 16\,384$. The dashed lines show the asymptotic $t^{2/3}$ approach.

The time scale T_2 marks the dissipation time of an initial density profile. For times $t \gg T_2$, the variance grows diffusively: $C(t) \sim D(L)t$. Matching this behavior at T_2 with that of the lower envelope of $C(t)$ in (ii) above gives $D(L) \sim L^{-1/2}$, as for the ASEP [9]. The late-time linear behavior is attributed to the diffusive motion of the center-of-mass of the system, as for the ASEP (see discussions for the ASEP in Chapter 3, Section 3.4.2).

7.3.2 Critical point

At the critical density $\rho_c = \frac{1}{b-2}$, the variance behaves differently for values of $b \leq 3$ and $b > 3$.

$b \leq 3$

For $b \leq 3$, there is no moving kinematic wave [3]; see the discussion in Section 6.5.4. Hence, the integrated current is Poisson distributed with intensity $v_{\max} = 1$, implying that the variance continues to grow linearly with slope 1. The fact that $v_{\max} = 1$ follows from noting that $v_{\max} = u(\infty)$, so that, with $u(n) = 1 + \frac{b}{n}$, we get $v_{\max} = 1$ (Chapter 6, Eq. 6.18).

$b > 3$

For $b > 3$, however, the kinematic wave velocity is nonzero and the Poisson distribution for the integrated current is expected to hold for times smaller than the return time of the kinematic wave. At criticality, the largest mass in the system, scaling as $\sim L^{1/2}$ for $b > 3$ and as $L^{1/(b-1)}$ for $2 < b < 3$ (see Section 6.5.2), proves insufficient to block the circulation of the kinematic wave around the system. As for $\rho < \rho_c$, the function $C(t)$ oscillates in

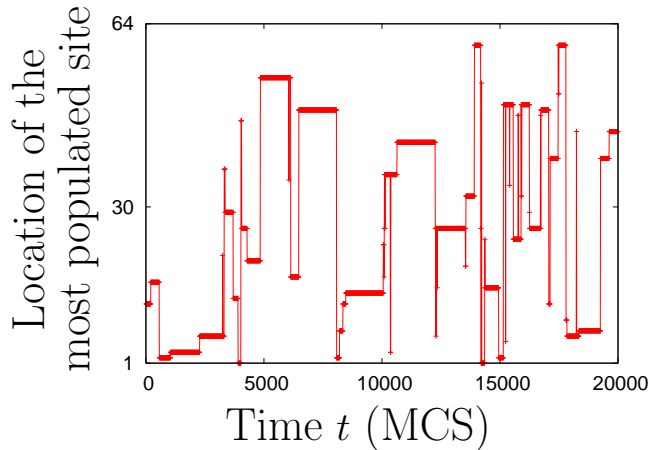


Figure 7.4: Monte Carlo simulation of the ZRP in the condensed phase in the stationary state, showing the motion of the most populated site (the condensate) over the system in time. Here, time is measured in Monte Carlo Step (MCS). The system size $b = 3$, $L = 64$, $\rho (> \rho_c = 1/(b - 2) = 1) = 4$. One can see that the condensate stays on one site for a certain length of time before disappearing and then reappearing on another site.

time, with return time T_1 and decay time T_2 of the kinematic wave. To find the exponent β at criticality, we monitor the variance $B(t)$ of the integrated current by starting from an arbitrary but fixed initial configuration, drawn from the stationary ensemble [10]. Thus, one has

$$B(t) \equiv \langle [H(i, t) - \langle H(i, t) \rangle]^2 \rangle, \quad (7.7)$$

where an average over i is implicit. The function $B(t)$ is similar to the function $s^2(L, t)$ for the ASEP, defined in Chapter 2. As discussed for the ASEP in Chapter 3, this function captures the dissipation of the density profile of the initial configuration, and is expected to grow asymptotically with time as $t^{2\beta}$ for $t \ll L^{3/2}$ (Section 3.4.1). We find that β at criticality has the KPZ value of $1/3$, independent of b (Fig. 7.3).

7.3.3 Condensed phase

For $\rho > \rho_c$, a finite fraction of the total mass (the condensate) resides on one site. On performing Monte Carlo simulation of the ZRP in the condensed phase, one finds that, for a finite system, the condensate executes an ergodic motion over the system: it stays on one site for a certain interval of time before disappearing and then reappearing on another site (see Fig. 7.4). The typical value of the time intervals for which the condensate remains on one site defines the survival time T_s of the condensate, while the typical value of the time intervals between disappearance of the condensate on one site and its reappearance on another site defines the relocation time scale T_r . The characteristic survival time T_s scales as $T_s \sim (\rho - \rho_c)^{b+1} L^b$, as shown in [11]; we briefly summarize the arguments in Appendix

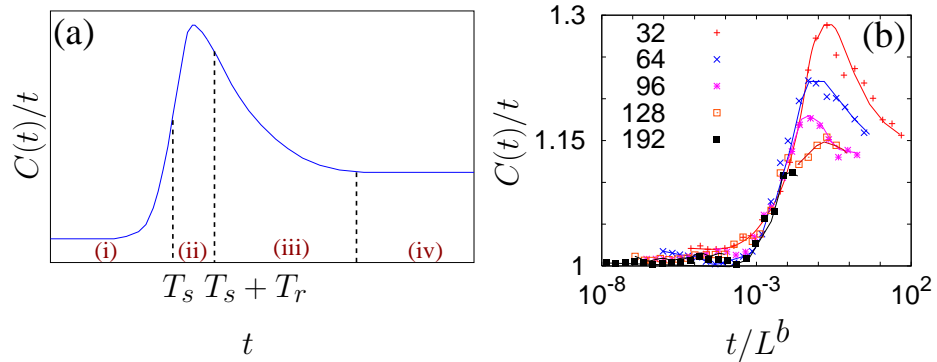


Figure 7.5: (a) Schematic plot of $C(t)/t$ as a function of time t in the condensed phase. The various regimes (see text) are also marked. (b) Scaling of the rise time T_s in $C(t)/t$ with t/L^b for $b = 3$ in the condensed phase ($\rho = 4$). Various system sizes L considered are marked in the figure. The data points, obtained from Monte Carlo simulations, are connected by smooth curves.

E. On the other hand, one has $T_r \sim (\rho - \rho_c)^2 L^2$, as discussed below.

One may recall the occurrence of similar time scales in more familiar models like the ferromagnetic Ising model. At equilibrium in the low temperature phase, there are two possible equilibrium states with the same energy, one of which has positive magnetization, while the other has negative magnetization; the two states are connected to one another by spin symmetry (which is tantamount to reversing all the spins simultaneously). For an infinite system, the symmetry gets spontaneously broken and the preferred state has either positive or negative magnetization. For a large but finite system, however, the magnetization keeps flipping between the two equilibrium states in time, consequently restoring the ergodicity in the dynamics. The typical time for which the magnetization remains of a particular sign is equivalent to the survival time T_s in the ZRP, the difference being that while in the ZRP, it scales as a power of the system size (L^b , with $b > 2$), for the Ising model, it is exponential in L^{d-1} , where d is the spatial dimension in which the Ising model is being considered. The relocation time T_r in the Ising model is the typical interval of time between which the magnetization ceases to become of one sign and then, becomes of the opposite sign; in this case, T_r scales as L^2 , as in the ZRP.

The behavior of $C(t)$ in the condensed phase is best depicted by plotting $C(t)/t$ as a function of time, as shown schematically in Fig. 7.5(a), where the various regimes are also marked.

The behaviors of $C(t)$ in different time regimes are summarized below.

- $t \ll T_s$: Here, $C(t)/t$ equals 1, with a mild upward deviation for longer times.
- $t \sim T_s$: In this regime, $C(t)/t$ rises rapidly in time.
- $t \gtrsim T_s + T_r$: Here, $C(t)/t$ falls slowly in time.

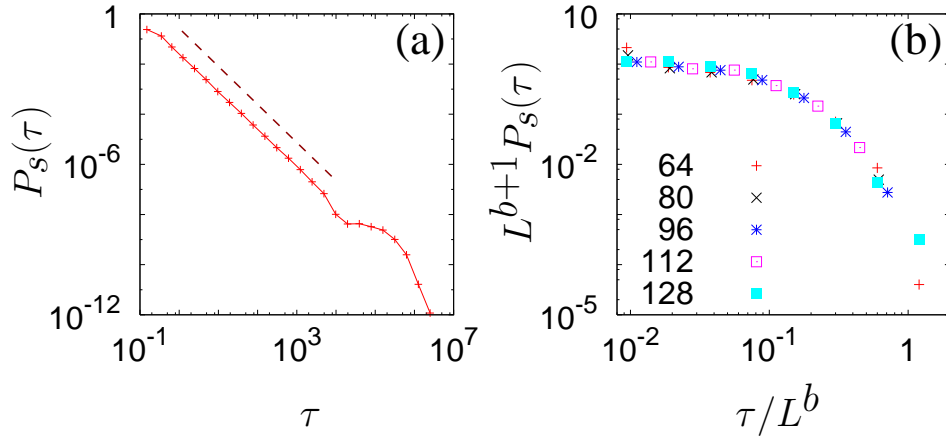


Figure 7.6: (a) Survival probability distribution $P_s(\tau)$ of the largest mass in the condensed phase. The system size $L = 128$, the parameter $b = 3$, while $\rho = 4$. The dashed line is a guide to the eye for the part of $P_s(\tau)$ behaving as $\tau^{-3/2}$. (b) Scaling of the bump in $P_s(\tau)$. Various system sizes L are marked in the figure. The data are obtained from Monte Carlo simulations.

- $t \gg T_s + T_r$: Here, $C(t)/t$ begins to approach a size-dependent constant, as predicted by a simple model described later in this chapter.

The last three of the features, listed above, result from enhanced fluctuations due to the condensate relocation. To understand this, we need to first discuss the dynamics of condensate relocation.

The relocation dynamics

The condensate relocation occurs through exchange of particles between two sites. On monitoring the time evolution of the largest and the second largest mass in simulation, the following picture emerges. Let $M(t)$ denote the largest mass in the stationary state at time t . $M(t)$ has the average value $M_0 \equiv \langle M(t) \rangle = (\rho - \rho_c)L$, with fluctuations ΔM_0 which scale as $L^{1/2}$ for $b > 3$, and as $L^{1/(b-1)}$ for $2 < b < 3$ [5] (see Section 6.5.2). These fluctuations may build up in time, and over the time scale T_s , the largest mass fluctuates to $\sim M_0/2$, while a mass $\sim M_0/2$ also builds up at another site. Subsequent to this, two sites with mass $\sim M_0/2$ exchange particles between themselves resulting in relatively rapid (of the order of 1 Monte Carlo step in simulations) alternating relocations of the largest mass from one site to the other. The difference of masses on these two sites performs an unbiased random walk in time until fluctuations populate one of the sites to $\sim M_0$ at the expense of the other, which happens over the time scale $T_r \sim (\rho - \rho_c)^2 L^2$ (this follows from the scaling properties of an unbiased random walk).

Figure 7.6(a) shows the Monte Carlo results for the survival probability distribution $P_s(\tau)$ of the largest mass, obtained by computing the distribution of the time interval τ

between successive relocations. $P_s(\tau)$ has two parts,

(i) a power law part $\sim \tau^{-3/2}$, and

(ii) another part, which corresponds to the bump in Fig. 7.6(a), and has the scaling form $(\rho - \rho_c)^{-(b+2)} L^{-(b+1)} f(\tau/T_s)$, as shown in Fig. 7.6(b). The prefactor comes from the normalization of $P_s(\tau)$ to unity with the cutoff for the $\tau^{-3/2}$ part taken to scale as T_r ; this is explained below.

First, we assume that $P_s(\tau)$ can be written approximately as a sum of the two parts, (i) and (ii), as

$$P_s(\tau) \approx \tau^{-3/2} + N f(\tau/T_s), \quad (7.8)$$

where N is such that $\int_1^{T_s} d\tau P_s(\tau) = 1$. In writing Eq. 7.8, we have neglected the correlation between the two parts in $P_s(\tau)$ (which is justified in view of the different physical processes resulting in the two parts, see the paragraph following Eq. 7.12). Now, since N normalizes $P_s(\tau)$, we have

$$\int_1^{T_s} d\tau P_s(\tau) \approx \int_1^{T_r} d\tau \tau^{-3/2} + N \int_{T_r}^{T_s} d\tau f(\tau/T_s) = 1, \quad (7.9)$$

where we have assumed that the lower limit for the integral involving the scaling part is T_r , which is the cutoff for the power law part. Next, the last equation can be rewritten as

$$\int_1^{T_r} d\tau \tau^{-3/2} + NT_s \int_{T_r/T_s}^1 d(\tau/T_s) f(\tau/T_s) = 1. \quad (7.10)$$

Noting that in the scaling limit, $T_r/T_s \rightarrow 0$, we have

$$\int_1^{T_r} d\tau \tau^{-3/2} + NT_s C = 1, \quad (7.11)$$

where C is a constant standing for $\int_0^1 dy f(y)$. On evaluating the integral in Eq. 7.11, we get the desired scaling form for N .

$$N \sim (\rho - \rho_c)^{-(b+2)} L^{-(b+1)}. \quad (7.12)$$

The power law part in $P_s(\tau)$ holds for times when the two sites with mass $\sim M_0/2$ compete to hold the largest mass. The random walk argument, discussed above, predicts a $\tau^{-3/2}$ decay, since $P_s(\tau)$ then stands for the probability for the random walker to cross the origin for the first time [12]. The second part in $P_s(\tau)$ arises from the relatively long time for which the condensate is stationary on one site.

We now explain the behavior of $C(t)/t$ in the different regimes seen in Fig. 7.5(a). The condensate is stationary on one site for a long time τ_1 , which is a random interval distributed as $p(\tau_1) \sim (\rho - \rho_c)^{-(b+2)} L^{-(b+1)} f(\tau_1/T_s)$, with the characteristic survival time T_s . In regime (i), when $t \ll T_s$, the condensate is stationary and acts as a reservoir for fluctuations, preventing their transport around the system as a kinematic wave. As a result,

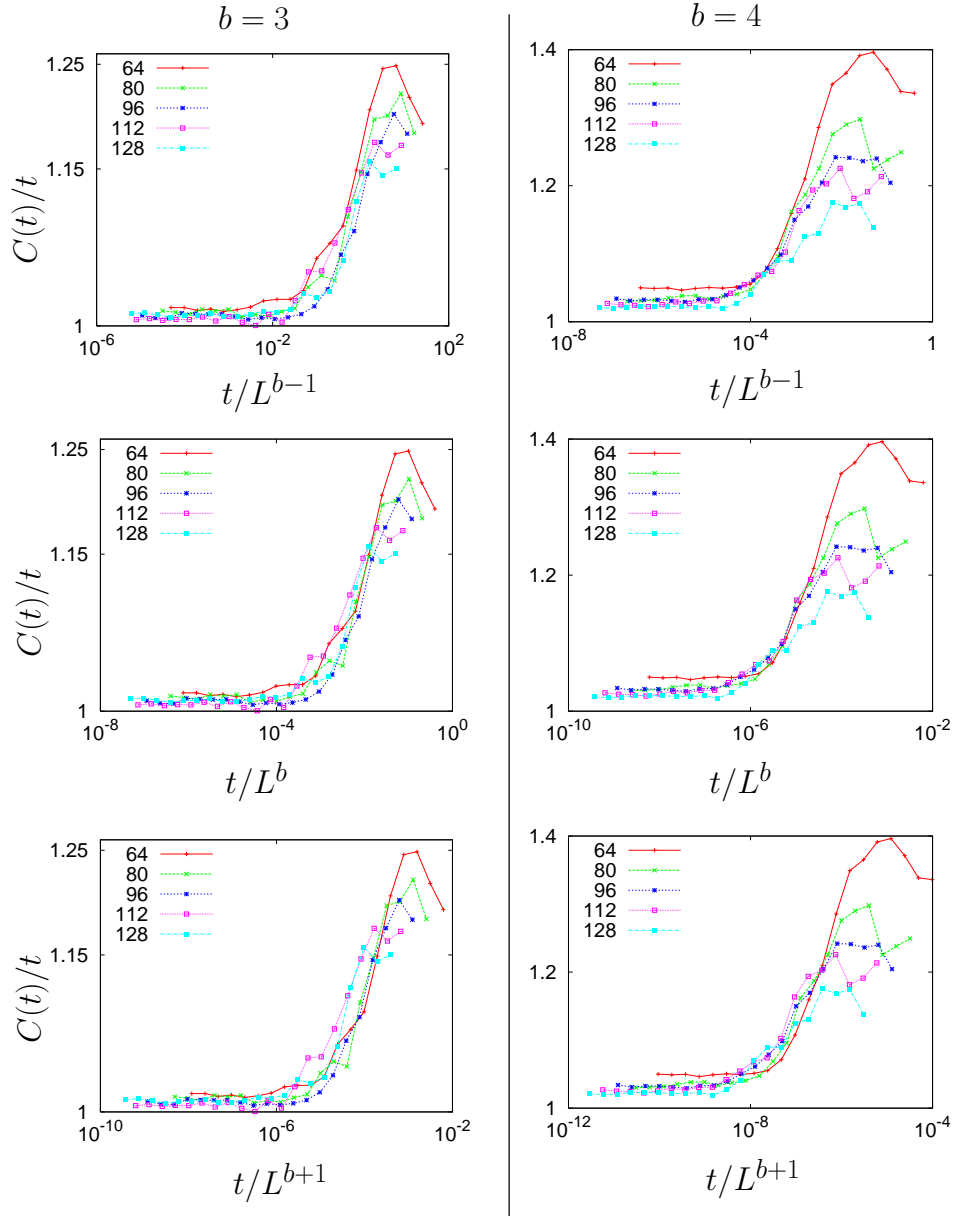


Figure 7.7: Scaling of the rise time T_s in $C(t)/t$ with t/T_s in the condensed phase, where, successively, we have taken $T_s \sim L^{b-1}$, $T_s \sim L^b$ and $T_s \sim L^{b+1}$, one finds the best scaling collapse with $T_s \sim L^b$. We have considered two different values of b , namely, 2, 3. For $b = 3$, the density ρ ($> \rho_c = 1/(b-2) = 1$) = 4, while for $b = 4$, the density ρ ($> \rho_c = 1/(b-2) = 0.5$) = 2. The system sizes are marked on each of the plots.

Burke's theorem is valid over this time scale and the integrated current is Poisson distributed with intensity $v_{\max} = 1$, implying $C(t)/t = 1$ (Appendix D). When $t \sim T_s$, the condensate starts to move from one site to another by transferring its mass across the intervening bonds. As a result, these bonds pick up enhanced fluctuations [$\propto (\Delta M_0)^2$] in the integrated current over the relocation time interval τ_2 , which is a random variable with the characteristic time T_r . These enhanced fluctuations lead to the rise in $C(t)/t$ as a function of t in regime (ii). The collapse of the rise times seen in the scaling plot of Fig. 7.5(b) confirms this picture. The fact that the time scale T_s indeed scales as L^b is further consolidated by Fig. 7.7, where the rise times in $C(t)/t$ as a function of t can be seen to be showing better scaling collapse with $T_s \sim L^b$ compared to any other scaling of T_s with L , e.g., $T_s \sim L^{b-1}$ or $T_s \sim L^{b+1}$. In regime (iii), after $t \sim T_s + T_r$, the condensate has completed relocating, so current fluctuations revert to Burke-like behavior, resulting in the fall of $C(t)/t$ in time. The slow fall in regime (iii) arises from the wide distribution of the time τ_2 , and further relocations. To predict the behavior in regime (iv), where $t \gg T_s + T_r$, we construct below a simple relocation model that describes the effect of condensate relocation on the long-time behavior of current fluctuations.

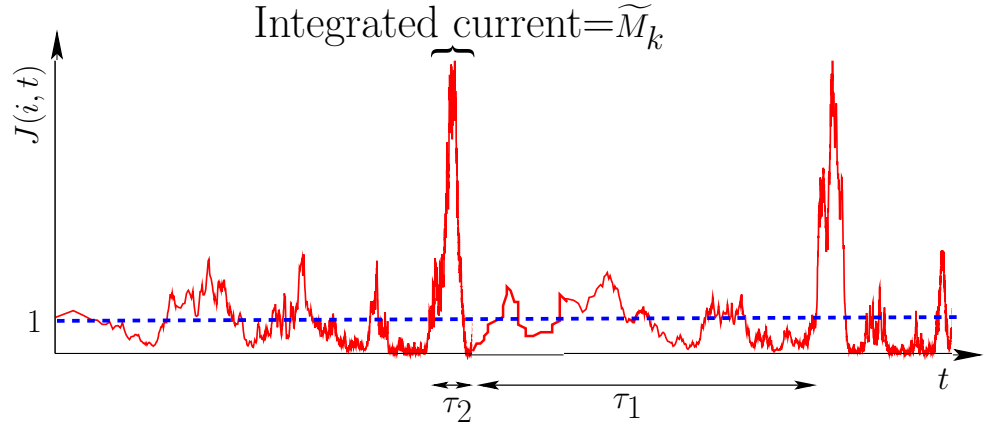


Figure 7.8: Schematic plot of the instantaneous current $J(i, t)$ across the bond $(i, i + 1)$ at time t as a function of time. The random variable τ_1 is the time for which the condensate is stationary on a site, while the random variable τ_2 stands for the relocation time of the condensate. \widetilde{M}_k is the integrated current over time τ_2 , arising from the k th relocation of the condensate across the bond $(i, i + 1)$.

The relocation model

Figure 7.8 shows schematically the instantaneous current $J(i, t)$ across the bond $(i, i + 1)$ as a function of time. When the condensate is stationary on one site, the mean current equals $v_{\max} = 1$ (see Chapter 6, Section 6.5.3). In a given history, let

$$K = \text{Number of condensate relocations in a fixed time } t. \quad (7.13)$$

Here, K is a random variable with mean given approximately by

$$\langle K \rangle \approx \frac{t}{(DT_s + BT_r)}, \quad (7.14)$$

where B and D are constants, independent of the density and the system size. At the k -th relocation of the condensate ($k = 1, 2, \dots, K$), let

$$\widetilde{M}_k = \text{Amount of mass transferred across the bond } (i, i + 1) \text{ over the interval } \tau_2. \quad (7.15)$$

The random variable \widetilde{M}_k in Eq. 7.15 has an average M_0 and variance ΔM_0 . As discussed in Section 7.3.3, one has $M_0 \equiv \langle M(t) \rangle = (\rho - \rho_c)L$, while the fluctuations ΔM_0 scale as $L^{1/2}$ for $b > 3$, and as $L^{1/(b-1)}$ for $2 < b < 3$.

The integrated current $H(i, t)$ is given approximately as

$$H(i, t) \approx \sum_{k=1}^K \widetilde{M}_k + \sum_0^{t-KBT_r} J(i, t'), \quad (7.16)$$

where we neglect the correlations between the events contributing to the current for times during which the condensate is stationary on one site and during which it is relocating from one site to another.

For $b > 3$, on computing the variance of the integrated current, given by $C(i, t) \equiv \left\langle \left[H(i, t) - \overline{H(i, t)} \right]^2 \right\rangle$, we get

$$C(i, t) \approx GL\langle K \rangle + (t - \langle K \rangle BT_r), \quad (7.17)$$

where G is a constant. In arriving at the above equation, we have used the fact that during times the condensate is stationary on one site, the integrated current is Poisson distributed with intensity $v_{\max} = 1$, so that the fluctuations in the integrated current during such times equal $v_{\max} = 1$ (see Section 7.3.3).

Since the expression for the variance of the integrated current in Eq. 7.17 is the same for all bonds $(i, i + 1)$, on averaging over i , one gets

$$C(t) \approx GL\langle K \rangle + (t - \langle K \rangle BT_r). \quad (7.18)$$

On substituting for $\langle K \rangle$ from Eq. 7.14 in Eq. 7.18, and neglecting the time scale $T_r \sim (\rho - \rho_c)^2 L^2$ in comparison to $T_s \sim (\rho - \rho_c)^{b+1} L^b$, we obtain the asymptotic behavior

$$C(t) \sim [L^{-\theta}(\rho - \rho_c)^{-(b+1)} + 1]t. \quad (7.19)$$

In Eq. 7.19, the exponent θ is given by

$$\theta = \begin{cases} b - 1 & \text{for } b > 3, \\ (b^2 - b - 2)/(b - 1) & \text{for } 2 < b < 3. \end{cases} \quad (7.20)$$

Thus, the relocation model predicts that, for all values of b , at long times $t \gg T_s + T_r$ [regime (iv) in Fig. 7.5(a)], $C(t)/t$ approaches a size-dependent constant which scales down with the system size. This long-time regime (iv) could not be accessed in simulations for the system sizes shown in Fig. 7.5(b), but we confirmed its existence for smaller systems.

In summary, we addressed the dynamics of stationary state fluctuations in a zero-range process which undergoes a nonequilibrium phase transition from a disordered to a condensed phase. Different dynamical properties emerge in the two phases. In the disordered phase, fluctuations move around the system as a kinematic wave. Such a wave, though present far away from the condensate, cannot circulate around in the condensed phase because the condensate subsumes fluctuations. The dynamics is governed by the condensate relocation through a slower process of transfer of particles from site to site, contributing enhanced fluctuations to the particle current across the intervening bonds.

References

- [1] M. R. Evans and T. Hanney, *J. Phys. A* **38**, R195 (2005).
- [2] M. Kardar, G. Parisi, and Y. C. Zhang, *Phys. Rev. Lett.* **56**, 889 (1986).
- [3] S. Großkinsky, G. M. Schütz, and H. Spohn, *J. Stat. Phys.* **113**, 389 (2003); C. Godrèche, *J. Phys. A* **36**, 6313 (2003).
- [4] R. J. Harris, A. Rákos, and G. M. Schütz, *J. Stat. Mech.* P08003 (2005).
- [5] S. N. Majumdar, M. R. Evans, and R. K. P. Zia, *Phys. Rev. Lett.* **94**, 180601 (2005).
- [6] P. J. Burke, *Oper. Res.* **4**, 699 (1956); E. Reich, *Ann. Math. Stat.* **28**, 768 (1957).
- [7] We are grateful to J. Lebowitz and E. Speer for pointing out the applicability of the Burke's theorem to the ZRP.
- [8] M. J. Lighthill and G. B. Whitham, *Proc. R. Soc. London, Ser. A* **229**, 281 (1955).
- [9] B. Derrida, M. R. Evans, and D. Mukamel, *J. Phys. A* **26**, 4911 (1993); B. Derrida and K. Mallick, *ibid.* **30**, 1031 (1997).
- [10] H. van Beijeren, *J. Stat. Phys.* **63**, 47 (1991).
- [11] C. Godrèche and J. M. Luck, *J. Phys. A* **38**, 7215 (2005).
- [12] W. Feller, in *An Introduction to Probability Theory and Its Applications*, (John Wiley, New York, 1968), Vol. I.

Chapter 8

The Exclusion Process with Extended Objects

“Contrariwise, if it was so, it might be; and if it were so, it would be; but as it isn’t, it ain’t. That’s logic.”

Lewis Carroll

The exclusion process with extended objects generalizes the asymmetric simple exclusion process (ASEP) to the case where particles in the ASEP are replaced by objects of finite extent, moving along a lattice in accordance with a stochastic hopping dynamics. While in the ASEP, the moving object, namely, a particle, covers a single lattice site, with extended objects, the coverage is more than one site, i.e., for a k -mer, k adjacent sites are covered. With $k = 1$, we recover the usual ASEP involving particles. The dynamical rules are the same for both the ASEP and the exclusion process with extended objects, namely, if the moving entity finds a vacant site in front, it advances by one lattice site, while, if there is a vacancy behind the moving entity, it steps backward by one lattice site with a probability different from the one with which it advances forward.

The concept of the exclusion process with extended objects is accredited to MacDonald *et al.* [1, 2], who, in their attempts to understand protein synthesis inside living cells, introduced this model as a simple setting in which the process of synthesis may be addressed. The synthesis proceeds with the following steps. The ribosomes move from codon to codon along the messenger RNA (m-RNA), read off genetic information, and thereby, generate the protein stepwise. In the exclusion process with extended objects, the moving ribosomes are modelled by the extended objects, while the lattice sites represent the codons. The finite extent of the objects takes care of the blocking of several codons by a single ribosome. Steric hindrance, excluding overlap of ribosomes, is incorporated in the model through the exclusion constraint, which implies that a single lattice site can be occupied by at most one extended object at a time. Ribosomes, attaching to the m-RNA to initiate the protein synthesis, and detaching at the point of termination are modelled with open boundaries,

whereby the extended objects enter and exit the lattice at the boundaries, much like the ASEP with open boundaries, discussed in Chapter 2.

The exclusion process with extended objects has been much studied in the past. MacDonald *et al.* treated the model at the mean-field level in deriving the stationary state density profile [1, 2]. More recently, several authors have studied the process, analyzing the time-dependent conditional probabilities of finding the k -mers at specific sites at a given time, starting with a given initial distribution of k -mers on lattice sites [3], the dynamical exponent [4], the phase diagram of the open system [5, 6, 7, 8], the hydrodynamic limit governing the evolution of density [9], and the effects of defect locations [10].

Because of the similarity in the dynamics of the ASEP to that in the exclusion process with extended objects, every configuration involving the extended objects can be mapped to an equivalent and unique configuration in the ASEP, defined on a smaller lattice, as we discuss below [11]. As a result, the stationary state of the exclusion process with extended objects on a one-dimensional ring is the one in which all allowed configurations with the same number of k -mers occur with the same weight. However, there are significant differences in the stationary state properties between the two that warrants a detailed study of the system with extended objects in its own rights. For example, there is no site-site correlation in the ASEP in the thermodynamic limit. Thus, a site can be occupied or empty, independently of any other site; this follows from the fact that all configurations in the stationary state are equally likely (see Chapter 2). This property is however no longer valid in the exclusion process with extended objects, where, if a site is occupied by one end, say, the right end of a k -mer, the next $k - 1$ sites to the left are occupied for sure, since the k -mers are non-reconstituting or hard objects; this is true despite the fact that all allowed configurations are equally likely.

In this chapter, we will basically explore the equivalence of the exclusion process with extended objects to the ASEP in deriving a number of stationary state properties, both statics and dynamics. We will consider a one-dimensional lattice with periodic boundary conditions. We will show that the two-point density-density correlation function exhibits distinct oscillations due to the finite-size of the moving entities.

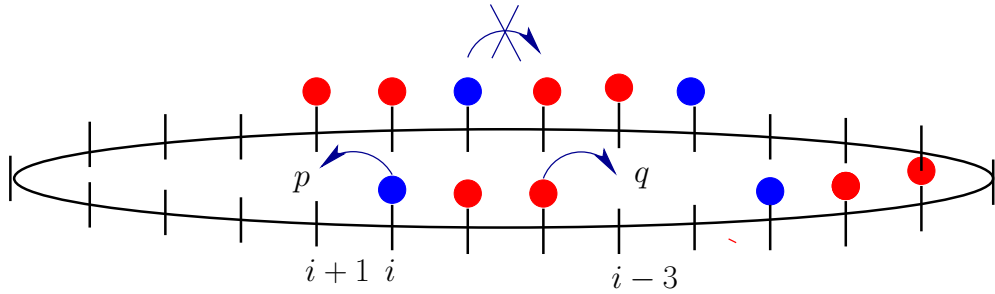
The layout of the chapter is as follows. We start in Section 8.1 with a precise definition of the exclusion process with extended objects on a one-dimensional ring. In Section 8.2, we discuss the mapping of the model to the ASEP, and its immediate consequence for the stationary state weight of k -mer configurations, and a number of stationary state properties like the average k -mer current and the kinematic wave velocity of density fluctuations. In Section 8.3, we discuss an important effect that shows up in the process of mapping between sites in the k -mer system and in the ASEP. This effect corresponds to wheeling motion around a periodic system of an ASEP site that corresponds to a fixed site in the k -mer problem.

Next, we come to discussing correlation functions in the stationary state of the k -mer problem. In Section 8.4, we compute the equal-time density-density correlation function

in a closed form. We point out and explain how, in the approach to a proper continuum limit of the k -mer problem, this correlation function assumes a scaling form. We provide numerical evidence in support of the scaling form. In Section 8.5, we consider the unequal-time density-density correlation function, and discuss the scaling form that it assumes in the limit of large distances and long times. We conclude the chapter in Section 8.6.

8.1 The model with periodic boundary conditions

(a) A configuration of $N = 4$ trimers ($k = 3$) on a lattice of $L = 26$ sites.



(b) Equivalent ASEP configuration of $N = 4$ particles on a lattice of $L - N(k - 1) = 26 - 4(3 - 1) = 18$ sites.

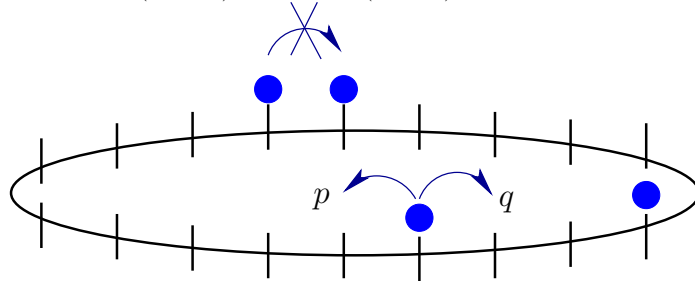


Figure 8.1: Definition of the exclusion process with extended objects (k -mers) on a ring. In (a), we show a typical k -mer configuration with $k = 3$, while (b) shows the corresponding equivalent ASEP configuration, in which each k -mer in (a) has been replaced by a particle in the ASEP, such that each particle represents the ‘engine’ or the right end of the corresponding k -mer, coloured blue. The disallowed transitions of the k -mers, equivalently, the particles are marked by crosses.

We consider N k -mers on a one-dimensional periodic lattice of L sites. The lattice sites are labelled by the index $i = 1, 2, \dots, L$. Each k -mer occupies k adjacent sites on the lattice, and is a rigid object. The system evolves according to a stochastic Markovian dynamics: at each time step, a site i is chosen at random. If the site i contains the right end (called the ‘engine’) of a k -mer, then, with probability p , the k -mer advances forward by one lattice site, provided the site $i + 1$ in front is unoccupied. On the other hand, with probability q , it

moves backward by one lattice site, provided the site $i - k$ behind the k -mer is unoccupied. The k -mer continues to occupy its original position with probability $1 - (p + q)$. Figure 8.1(a) shows a schematic view of the process. Note that for $k = 1$, the dynamics becomes exactly identical to that of the ASEP, discussed in Chapter 2, Section 2.1. The system of k -mers with the above mentioned dynamics, in the limit of long times, settles into a nonequilibrium stationary state with a steady current of k -mers through the system.

Earlier studies of the model dealt with dimers ($k = 2$) that do not retain their identities and are allowed to reconstitute [11, 12]. Specifically, on a lattice of L sites, one considers single particles or monomers (denoted by 1) and paired particles or dimers (denoted by 11) to be distributed with at most one particle per site (i.e., the site occupancy can be either 0 or 1). A configuration is thus denoted by an L -bit binary string. The dynamics of the model follows closely that described in the preceding paragraph for the k -mers. Thus, a dimer moves by one lattice site either forward or backward without violating the hard core constraint on site occupancies. The pairing of the dimers is impermanent, thereby allowing for reconstitution, e.g., 11010 \rightarrow 01110 \rightarrow 01011, in which the middle particle is paired with the particle to the left in the first transition, and with the particle to the right in the second transition. Both asymmetric ($p \neq q$) [11] as well as symmetric ($p = q$) [12] motion of the dimers were considered, and in both the cases, the phase space was shown to break up into an infinite number of dynamically disjoint sectors. A non-local construct, called the irreducible string (IS), was shown to uniquely label the different sectors. The IS corresponding to a given configuration is constructed from the corresponding L -bit binary string by deleting recursively any pair of adjacent 1's until no further deletion is possible. The model exhibits dynamical diversity with quantities like the density autocorrelation function showing strong sector-dependent behaviors, ranging from power laws to stretched exponentials. This diversity is explained in terms of the difference in the IS from sector to sector. Interestingly, the sector whose IS is given by the null string corresponds to hard non-reconstituting dimers. This is because, for a configuration involving non-reconstituting dimers only, the deletion algorithm for the construction of the corresponding IS will result in an IS which is a null string of 0's. As a result, the sector whose IS is given by the null string corresponds to the k -mer system considered in this chapter for the special case of dimers (i.e., $k = 2$) [11].

8.2 The stationary state measure

In order to obtain the stationary state measure of the k -mer configurations, we note that every k -mer configuration is uniquely mapped to an ASEP configuration on a smaller lattice [11]. The ASEP configuration is obtained from the k -mer configuration by replacing each of the k -mers by a particle which may be taken to represent the engine of the corresponding k -mer, as shown in Fig. 8.1(b). This procedure generates a one-to-one mapping between a configuration of N k -mers on a lattice of L sites and an ASEP configuration of N particles

on a lattice of $L' = L - N(k - 1)$ sites. The k -mer density is given by $\rho_{k\text{-mer}} = Nk/L$, while the corresponding ASEP particle density ρ is given by $\rho = N/L' = N/(L - N(k - 1))$. Thus, the two densities are related to one another through

$$\rho_{k\text{-mer}} = \frac{\rho k}{1 + \rho(k - 1)}. \quad (8.1)$$

Also, we have

$$\frac{L'}{L} = \frac{1}{1 + \rho(k - 1)}. \quad (8.2)$$

Now, the stationary state of the ASEP on a periodic lattice allows all configurations with the same number of particles to be equally likely (Chapter 2, Section 2.2). Because of the one-to-one correspondence of the configurations in the ASEP to the k -mer system, it follows that on a periodic lattice, in the stationary state, all configurations with the same number of k -mers are also equally likely. The probability of occurrence of an allowed k -mer configuration is given by the reciprocal of the total number of allowed k -mer configurations, equivalently, the total number of allowed ASEP configurations; this number is computed by counting the number of ways in which N particles may be placed over a lattice of $L' = L - N(k - 1)$ sites, and is, thus, given by $\binom{L - N(k - 1)}{N} = \frac{(L - N(k - 1))!}{N!(L - Nk)!}$. In the following, we consider the k -mer system in the thermodynamic limit, $N \rightarrow \infty, L \rightarrow \infty$, with finite k -mer density $\rho_{k\text{-mer}}$. This implies thermodynamic limit for the equivalent ASEP system as well: the number of particles, namely, N is infinite, while the number of lattice sites, $L' = L - N(k - 1) = L(1 - \rho_{k\text{-mer}}(k - 1)/k)$, is also infinite. The density of particles ρ in the ASEP is, however, finite.

In the ASEP, the probability that a randomly chosen site is occupied by a particle is given by the ASEP particle density ρ . This probability is properly normalized in the sense that in the ASEP lattice of L' sites, there are L' sites to choose, and each is occupied with probability ρ , so that $\rho L' = N$, the total number of particles, as desired. In the k -mer system, the probability that a randomly chosen site is occupied by an engine is the same as the probability that the corresponding site in the ASEP is occupied by a particle, and hence equals ρ . However, this probability is not properly normalized in the sense that for our k -mer system of L sites, ρL should equal the total number of engines in the system, namely, N , which it does not; for proper normalization, one has to have this probability to be given by $\rho L'/L$. The normalized probabilities are different in the k -mer system and the ASEP because of the number of lattice sites being different in the two cases. To compute the probability of any event in the k -mer system, one needs to first compute the corresponding probability in the ASEP, and then, for normalization, multiply it by L'/L . Using Eq. 8.2, we conclude that

$$\text{Prob(a site is occupied by the engine of a } k\text{-mer)} = \frac{\rho}{1 + \rho(k - 1)}. \quad (8.3)$$

Next, we compute the current due to the motion of the k -mers. Across a bond $(i, i + 1)$,

a k -mer current will be registered in the following two cases. (i) The i -th site is occupied by the engine of a k -mer, while the $(i + 1)$ -th site is empty, so that, in one time step, the k -mer advances forward by one lattice site with probability p ; corresponding to this k -mer motion, in the equivalent ASEP configuration, a particle, occupying site i , will have hopped into the empty site $i + 1$ with probability p . (ii) The $(i + k)$ -th site is occupied by the engine of a k -mer, while the i -th site is empty, so that, in one time step, the k -mer advances backward by one lattice site with probability q ; corresponding to this k -mer motion, in the equivalent ASEP configuration, a particle, occupying site $i + 1$, will have hopped into the empty site i with probability q . Thus, in the stationary state, the average k -mer current will be the same as the average particle current in the equivalent ASEP system, excepting for the normalization factor, L'/L , coming from the difference in the number of sites in the two cases. In the thermodynamic limit, the ASEP particle current at density ρ has the average value J , given by $J = (p - q)\rho(1 - \rho)$ (see Chapter 2, Section 2.4). We conclude that the average k -mer current will equal JL'/L , and will, thus, be given by

$$J_{k\text{-mer}} = \frac{(p - q)\rho(1 - \rho)}{1 + \rho(k - 1)}, \quad (8.4)$$

where we have used Eq. 8.2.

The kinematic wave velocity $v_K^{k\text{-mer}}$ in the k -mer problem, given by $\frac{\partial J}{\partial \rho}$ (see Appendix A), reads

$$v_K^{k\text{-mer}} = (p - q) \left[\frac{1 - 2\rho}{1 + \rho(k - 1)} - \frac{\rho(1 - \rho)(k - 1)}{(1 + \rho(k - 1))^2} \right]. \quad (8.5)$$

8.3 The wheeling effect

The wheeling effect is an important effect that shows up in the process of mapping between sites in the k -mer system and in the ASEP [11]. As a consequence of this effect, a fixed site in the k -mer problem corresponds to a site in the ASEP, which wheels or moves around the ring with a finite velocity. This is because, as shown in Fig. 8.2, following a k -mer motion, one finds that the images of the central sites of the k -mer advances by one unit, while the images of the two boundary sites remain unchanged. This wheeling of ASEP-images of the central sites of the k -mer by one lattice unit in unit time occurs when one of the following situations arises.

(i) There is a vacancy in front of the engine of the k -mer so that with probability p , the k -mer advances forward by one lattice site in unit time, and the images move forward by one lattice site; the weight for this event to take place is given by $p\rho(1 - \rho)$, and thus, the corresponding probability will be $\frac{p\rho(1 - \rho)}{1 + \rho(k - 1)}$.

(ii) There is a vacancy behind the k -mer so that with probability q , the k -mer moves backward by one lattice site in unit time, and the images move backward by one lattice site; the weight for this event to take place is given by $q\rho(1 - \rho)$, and thus, the corresponding

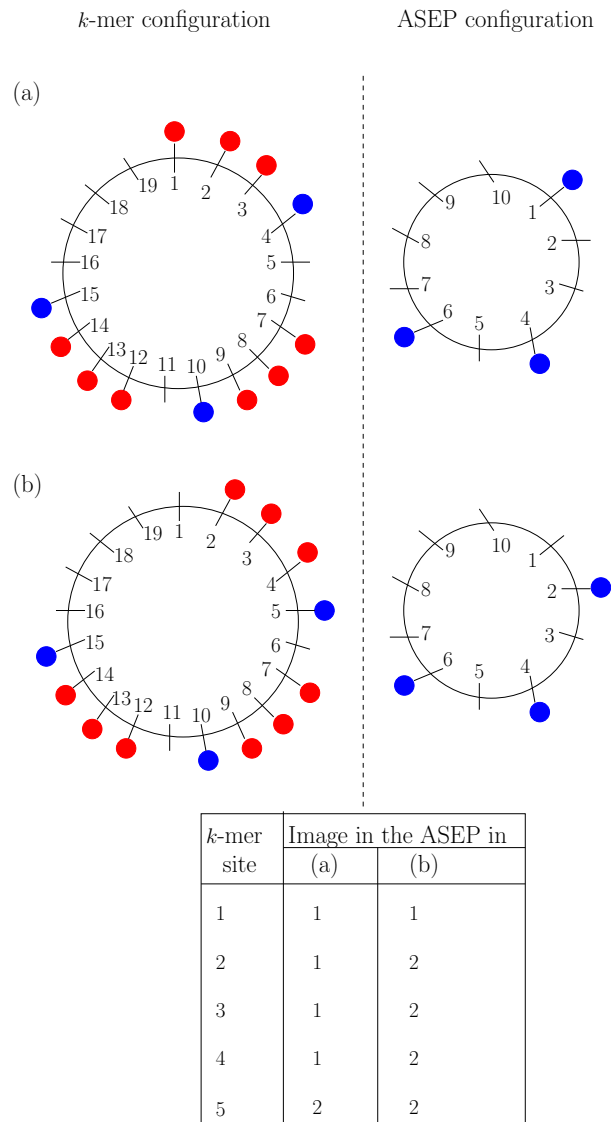


Figure 8.2: The wheeling effect, showing how, corresponding to a k -mer motion, the image of a fixed site in the k -mer problem corresponds to a site in the ASEP, which wheels or moves around the ring. Here, $k = 4$, the engine of each of the k -mers is colored blue. We have listed the images of only those sites which have been affected by the motion of the k -mer occupying sites 1, 2, 3, 4 in (a).

probability will be $\frac{q\rho(1-\rho)}{1+\rho(k-1)}$.

Thus, the average wheeling velocity W is given by

$$W = \frac{(p-q)\rho(1-\rho)}{1+\rho(k-1)}. \quad (8.6)$$

8.4 The equal-time density-density correlation

Let n_i denote the occupation variable of site i , taking values 0 or 1 according as the site is empty or occupied by a k -mer, respectively. We have $\overline{n_i} = \rho_{k\text{-mer}}$, where the overbar denotes averaging with respect to the stationary ensemble of k -mer configurations. We are interested in computing the (unsubtracted) equal-time density-density correlation function, given by

$$C(r) = \overline{n_i n_{i+r}}. \quad (8.7)$$

The above correlation function can be evaluated in terms of the engine-engine correlation $\mathcal{E}(r)$, defined as the joint probability of finding an engine at site i and another one at site $i+r$. The function $C(r)$ can be expressed in terms of $\mathcal{E}(r)$ in the following way. Keeping site i occupied by the engine of the k -mer, in order to have a non-zero contribution to $C(r)$, the $(i+r)$ -th site has to be occupied by either the engine or any of the successive $k-1$ parts of a k -mer with probabilities $\mathcal{E}(r), \mathcal{E}(r+1), \mathcal{E}(r+2), \dots, \mathcal{E}(r+(k-1))$, respectively. In this way, one considers all possible ways in which site i remains occupied by a k -mer, and for each such way, one lists down all the different ways in which $i+r$ may be occupied by a k -mer. One finally gets

$$C(r) = k\mathcal{E}(r) + \sum_{m=1}^{k-1} m[\mathcal{E}(r+(k-m)) + \mathcal{E}(r-(k-m))]. \quad (8.8)$$

The engine-engine correlation function $\mathcal{E}(r)$ can be computed in the following way [11]. $\mathcal{E}(r)$ is obtained from all configurations in which there is an engine at each of the sites i and $i+r$, with the gap between the two k -mers containing $r-k$ sites. The weights of all such configurations are obtained by mapping each one of them to an equivalent ASEP configuration, allowing for the weights to have an ASEP particle at both the sites i and $i+r$, and also for m k -mers and $r-k-km$ vacancies in between, and then considering all possible ways in which m k -mers may be distributed over $r-k-km+m$ sites. Lastly, one sums over m from 0 to the maximum number of k -mers that may be put into the gap of $r-k$ sites between the two engines at sites i and $i+r$; this maximum number is given by the integer part of $(r-k)/k$. Finally, in order to normalize the resultant weight, one has to multiply it by $L'/L = 1/(1 + \rho(k-1))$, as discussed above; one gets

$$\mathcal{E}(r) = \frac{\rho^2}{1 + \rho(k-1)} \sum_{m=0}^{\text{Integer}[(r-k)/k]} \binom{r-k-km+m}{m} \rho^m (1-\rho)^{r-k-km}. \quad (8.9)$$

In getting the above result, we have used the fact that in the ASEP, in the thermodynamic limit, the joint probability of several sites being occupied at the same time is given by the product of the probability ρ that each site is occupied, independently of the others (see Chapter 2, Section 2.3).

For $k = 2$, the sum in Eq. 8.9 can be evaluated exactly with the result [11]

$$\mathcal{E}(r) = \frac{\rho^2}{(1+\rho)^2} [1 - (-\rho)^{r-1}]. \quad (8.10)$$

For general $k > 3$, the sum in Eq. 8.9 could not be evaluated analytically. Instead, we performed a numerical evaluation of the sum; the result for a particular k is shown in Fig. 8.3.

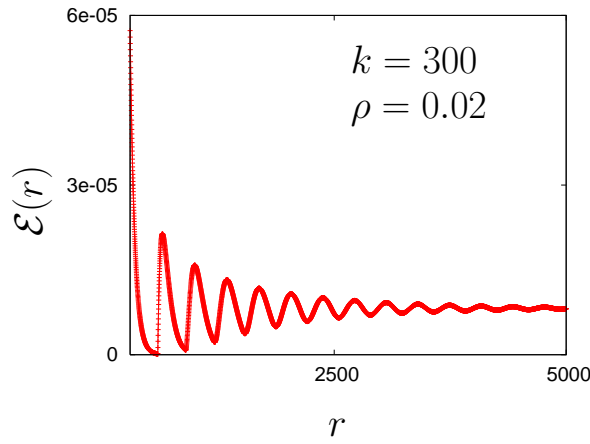


Figure 8.3: Engine-engine correlation function $\mathcal{E}(r)$, evaluated numerically, using Eq. 8.9. Here, $k = 300$, the ASEP density $\rho = 0.02$.

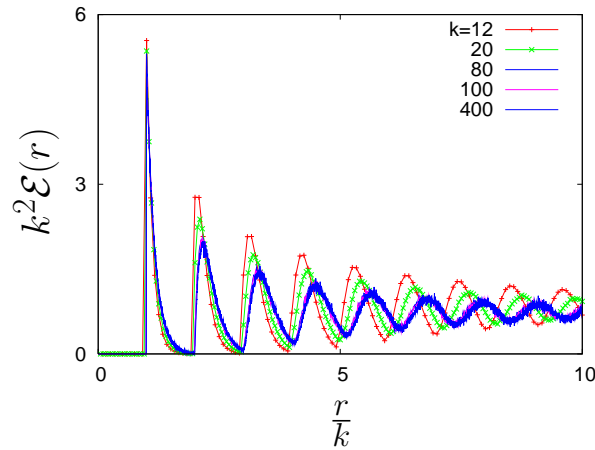


Figure 8.4: Scaling plot of $k^2 \mathcal{E}(r)$ as a function of r/k . For different k 's, and at ASEP densities ρ such that $\rho k = \text{constant} = 6$, the function $\mathcal{E}(r)$ is evaluated numerically, using Eq. 8.9. For large k , the function $\mathcal{E}(r)$ assumes the scaling form in Eq. 8.11.

One observes that for large k , and at ASEP densities ρ such that $\rho k = \text{fixed}$, the function $\mathcal{E}(r)$ assumes a scaling form, as confirmed by the scaling plot of Fig. 8.4. One concludes

that

$$\mathcal{E}(r) \sim \frac{1}{k^2} f\left(\frac{r}{k}\right), \quad (8.11)$$

where $f(u)$ is the scaling function.

In order to explain the scaling behavior in Eq. 8.11, we consider the k -mer system in the ‘continuum’ limit, explained below, which is obtained by letting $k \rightarrow \infty$. First, note that a k -mer configuration with a desired density $\rho_{k\text{-mer}}$ can be generated by first generating the equivalent ASEP configuration with density ρ , given from Eq. 8.1, and then, dilating each particle in the ASEP so as to occupy k adjacent sites. If a is the lattice spacing in the ASEP, each k -mer has a length $l = ka$. To achieve the continuum limit of the k -mer system, we first generate the continuum limit of the ASEP system by letting the lattice spacing a in the ASEP to go to 0, and simultaneously, the ASEP particle density ρ to go to 0. This gives, corresponding to the ASEP system of particles on a lattice, a system of particles of infinitesimal size, $a \rightarrow 0$, with finite density $\rho_0 = \rho/a$ on a continuous line. Next, we let k go to infinity, keeping $l = ka$ finite. In this limit, the equivalent k -mer system now has rods of finite length l distributed over a continuous line. Thus, the continuum limit of the k -mer system involves taking the following limits: (i) ASEP lattice spacing $a \rightarrow 0$, (ii) ASEP particle density $\rho \rightarrow 0$, keeping $\rho_0 = \rho/a$ finite, and (iii) $k \rightarrow \infty$, keeping $l = ka$ finite. One thus has $\rho k = \rho_0 l = a$ finite constant. In this continuum limit, the right hand side of Eq. 8.9 evaluates to

$$\frac{\rho_0^2 a^2}{1 + \rho_0 l} \sum_{m=0}^{\text{Integer}[(R-l)/l]} \frac{[R - (m+1)l]^m}{m!} e^{-\rho_0 [R - (m+1)l]} \rho_0^m. \quad (8.12)$$

where $R = ra$ is finite in the limit $r \rightarrow \infty, a \rightarrow 0$. We can rewrite the above equation as

$$\left(\frac{a^2}{l^2}\right) \frac{\rho_0^2 l^2}{1 + \rho_0 l} \sum_{m=0}^{\text{Integer}[R/l-1]} \frac{[R/l - (m+1)]^m}{m!} e^{-(\rho_0 l)[R/l - (m+1)]} (\rho_0 l)^m. \quad (8.13)$$

Noting that in the continuum limit, $\rho_0 l = \text{constant}$, and that $a/l = 1/k$, we conclude that the above equation has the scaling form $\sim \frac{1}{k^2} f\left(\frac{R}{l}\right)$. Since $R/l = r/k$, we get the following scaling form for the engine-engine correlation function,

$$\mathcal{E}(r) \sim \frac{1}{k^2} f\left(\frac{r}{k}\right), \quad (8.14)$$

which is consistent with the form proposed in Eq. 8.11.

8.5 The unequal-time density-density correlation

The unequal time density-density correlation function in the k -mer problem is defined as

$$C(r = |i - j|, t) \equiv \overline{\langle n_i(0) n_j(t) \rangle} - \rho_{k\text{-mer}}^2, \quad (8.15)$$

where $n_i(0)$ is the occupancy of site i at time 0, $n_j(t)$ is the occupancy of site j at time t , the overbar denotes averaging over the initial stationary ensemble of k -mer configurations (i.e., the ensemble in which all configurations with the same number of k -mers are equally likely), while the angular brackets denote averaging with respect to their subsequent stochastic evolutions in time. The scaling form of $C(r, t)$ has been investigated earlier for the case of dimers in Ref. [11]. To obtain the scaling form of the function $C(r, t)$ for general k , we will explore the mapping of the k -mer problem to the ASEP problem.

As discussed in Chapter 2, Section 2.5, in the ASEP, the unequal-time density-density correlation function $C_X(r = |i - j|, t) \equiv \overline{\langle n_i(0)n_j(t) \rangle} - \rho^2$, in the limit of long times and large distances, assumes the scaling form [13]

$$C_X(r, t) \propto t^{-2/3} f(u); \quad u = \frac{1}{2}(J_X t^2)^{-1/3}(r - v_K t). \quad (8.16)$$

In the above equation, J_X is the average value of the ASEP particle current, where ρ is the ASEP particle density. Also, v_K is the kinematic velocity of density fluctuations, discussed in Chapter 2, and also in Appendix A. In the limit of large u , the function $f(u)$ is known to behave exponentially as $f(u) \sim \exp(-\mu|u|^3)$ with the constant $\mu \approx -0.295$ [13]. Thus, at long times, the function $C_X(r, t)$ decays as an exponential in time.

The function $C(r, t)$ will be as in the ASEP once the wheeling of sites, discussed in Section 8.3 above, is taken care of [11]. Thus, in the limit of long times and at large distances, the unequal-time density-density correlation function $C(r, t)$ will have the scaling form

$$C(r, t) \propto t^{-2/3} f(r + (W - v_K)t). \quad (8.17)$$

The autocorrelation function $C(r = 0, t) \equiv C(t)$ will behave as $t^{-2/3}e^{-\kappa t}$ at long times, where κ is a constant proportional to the difference of the wheeling velocity and the kinematic wave velocity, $W - v_K$. On the other hand, if the k -mer density $\rho_{k\text{-mer}}$ (equivalently, the ASEP density ρ) is such that $W - v_K$ vanishes, then the autocorrelation, at late times, is expected to fall in time as a power law: $C(t) \sim t^{-2/3}$. The corresponding ASEP density is called the compensating density ρ_c . In the thermodynamic limit, since $W = \frac{(p-q)\rho(1-\rho)}{1+\rho(k-1)}$ and $v_K = (p-q)(1-2\rho)$ (see Chapter 2, Eq. 2.11), for $W - v_K$ to vanish, the density ρ_c satisfies the following equation.

$$\rho_c^2(k-1) + 2\rho_c - 1 = 0. \quad (8.18)$$

Solving for ρ_c , one gets $\rho_c = \frac{-1 \pm \sqrt{k}}{k-1}$. Since ρ_c has to be a positive quantity, one gets

$$\begin{aligned} \rho_c &= \frac{\sqrt{k} - 1}{k-1} \\ &= \frac{1}{\sqrt{k} + 1}. \end{aligned} \quad (8.19)$$

The above result for the compensating density matches with that derived earlier for dimers

with $k = 2$ [11]. Note that at ρ_c , the kinematic wave velocity $v_K^{k\text{-mer}}$ in the k -mer problem also becomes zero.

8.6 Concluding remarks

In this chapter, we considered the exclusion process with extended objects. The process involves k -mers that occupy k adjacent sites on a lattice, with $k > 1$. These k -mers undergo a driven motion along the lattice in accordance with a stochastic hopping dynamics. We considered the model in one dimension with periodic boundary conditions. We showed that many stationary state properties of the k -mer system, e.g., the correlation functions for site occupancies can be derived rather simply by mapping every configuration in the k -mer problem to an equivalent and unique configuration in an ASEP on a smaller lattice [11]. We showed that these correlation functions show distinctive size effects like characteristic oscillations, etc., arising from the finite size of the extended objects, and have scaling forms in the proper continuum limit of the model.

References

- [1] C. T. MacDonald, J. H. Gibbs, and A. C. Pipkin, *Biopolymers* **6**, 1 (1968).
- [2] C. T. MacDonald and J. H. Gibbs, *Biopolymers* **7**, 707 (1969).
- [3] T. Sasamoto and M. Wadati, *J. Phys. A* **31**, 6057 (1998).
- [4] F. Alacaraz and R. Z. Bariev, *Phys. Rev. E* **60**, 79 (1999).
- [5] G. Lakatos and T. Chou, *J. Phys. A* **36**, 2027 (2003).
- [6] L. B. Shaw, R. K. P. Zia, and K. H. Lee, *Phys. Rev. E* **68**, 021910 (2003).
- [7] L. B. Shaw, A. B. Kolomeisky, and K. H. Lee, *J. Phys. A* **37**, 2105 (2004).
- [8] L. B. Shaw, J. P. Sethna, and K. H. Lee, *Phys. Rev. E* **70**, 021901 (2004).
- [9] G. Schönherr and G. M. Schütz, *J. Phys. A* **37**, 8215 (2004).
- [10] J. J. Dong, B. Schmittmann, and R. K. P. Zia, *Phys. Rev. E* **76**, 051113 (2007).
- [11] M. Barma, M. D. Grynberg, and R. B. Stinchcombe, *J. Phys.: Condens. Matter* **19**, 065112 (2007).
- [12] G. I. Menon, M. Barma, and D. Dhar, *J. Stat. Phys.* **86**, 1237 (1997).
- [13] M. Prähofer and H. Spohn in *In and Out of Equilibrium (Progress in Probability Vol. 51)*, edited by V. Sidoravicius (Boston, MA: Birkhauser), pp 185-204: also, eprint:arXiv:cond-mat/010200.

Chapter 9

Summary and discussion

“Be what you would seem to be—or, if you’d like it put more simply—never imagine yourself not to be otherwise than what it might appear to others that what you were or might have been was not otherwise than what you had been would have appeared to them to be otherwise.”

Lewis Carroll

In this thesis, we addressed the issue of how the dynamics of fluctuations in the stationary state of driven diffusive systems gets affected by the finiteness of the system size. Finite-size effects in equilibrium systems, particularly those that occur close to the critical point of a second order phase transition, have been studied extensively in the past. These effects lead to slowing down of the dynamics of the system close to the critical point, a phenomenon referred to as critical slowing down. Size effects show up in quantities, for example, the equal-time two-point correlation function for the fluctuations in the order parameter characterizing the phase transition. This correlation function exhibits power-law behavior with a size-dependent cut-off. Finite-size effects, by virtue of the scaling hypothesis, have been proved to be extremely useful in extracting, from finite-size simulations, the universal critical exponents characterizing the power-law behavior of thermodynamic quantities close to a critical point [1]. Size effects are also observed in a first-order transition, for which a comprehensive scaling theory has been developed in the past [2].

However, the theoretical development for study of nonequilibrium stationary states is much in its infancy. This could be attributed partly to the lack of a general framework akin to that of Gibbs-Boltzmann for equilibrium systems. Although, in principle, the very general Master equation approach exists to find the stationary distribution for stochastic Markovian systems driven out of equilibrium, in practice, solving the equation often proves to be formidable in view of the many-body character of most nonequilibrium systems. In this respect, driven diffusive systems [3], and in particular, the two paradigmatic examples studied in this thesis, namely, the asymmetric simple exclusion process (ASEP) and the zero-range process (ZRP) serve as base camps for starting an expedition into the uncharted areas of nonequilibrium stationary states. These are systems of interacting par-

ticles in which each particle has a diffusive motion in addition to an overall drift due to the application of an external field; in the limit of long times, these systems relax to a current-carrying nonequilibrium stationary state [3]. Although, in recent past, several authors have considered the problem of studying fluctuations for the ASEP and the ZRP, a complete and coherent picture of size effects on the dynamics has been lacking. This thesis has made some efforts in this regard in providing an exhaustive study of size effects on nonequilibrium stationary states within the ambit of the ASEP and the ZRP in one dimension.

The ASEP involves stochastic biased hopping of hard core particles between nearest neighbor sites of a lattice [4, 5]. In this thesis, we have revisited the problem of tagged particle correlation in the ASEP on a one-dimensional lattice with periodic boundary conditions, with particular emphasis on finite-size effects. The particular quantity that we monitored is the stationary state variance of the displacement of a tagged particle about the average, where the average is with respect to the initial stationary ensemble of ASEP configurations and subsequent stochastic evolution of the configurations in time. Scaling analysis, supported by cogent physical arguments, suggests that the behavior of the variance in time captures the motion of stationary state density fluctuations around the system as a dissipating kinematic wave [6], and can be characterized by two distinct size-dependent time scales, $T_1 \sim L$, and $T_2 \sim L^{3/2}$ for a periodic lattice of L sites. Here, the time scale T_1 marks the circulation time of the kinematic wave, while T_2 sets the scale over which the wave dissipates in time. The behavior of the variance is linear for both the time regimes $t \ll T_1$ and $t \gg T_2$; for times $t \ll T_1$, the variance grows linearly with a size-independent slope [7], while that for $t \gg T_2$ has a specific size-dependence, scaling as the inverse square root of the system size [8]; this late-time behavior is attributed to the diffusive motion of the center-of-mass of the system. For intermediate times, $T_1 \ll t \ll T_2$, the variance shows pronounced oscillations with a well-defined size-dependent time period, given by $L/(v_P - v_K)$. We understood the oscillations as arising from the sliding density fluctuations (SDF), relating to the phenomenon of density fluctuations moving with the kinematic speed v_K relative to the particles which drift with a different speed v_P .

Following van Beijeren [9], we also studied the variance of the displacement of the tagged particle by averaging with respect to only stochastic evolution of a fixed initial configuration, drawn from the ensemble of stationary states. We saw that the variance effectively captures the dissipation of the kinematic wave in time, and its behavior in time is characterized by only one time scale $T^* \sim L^{3/2}$. The variance grows linearly in time for times $t \gg T^*$ with a constant scaling as the inverse square root of the system size, while for times $t \ll T^*$, it grows as $t^{2/3}$ [9]. The late-time behavior was understood in terms of the diffusive motion of the center-of-mass.

The tagged particle correlations in the ASEP was related to the height fluctuations of a nonequilibrium interface in the Kardar-Parisi-Zhang (KPZ) universality class [10]. This is achieved by interpreting the particle label as horizontal coordinate for the interface, while the particle location maps onto the local height of the interface [11]. The corresponding

time-evolution equation for the interface is the usual KPZ equation, with an additional drift term that accounts for the SDF. This equation is nonlinear and cannot be solved exactly. By dropping the nonlinear term, we obtained a linear interface whose time evolution is governed by the Edwards-Wilkinson (EW) evolution equation [12], augmented by the drift term due to the SDF; we solved the resultant equation exactly for the height fluctuations, equivalently, the tagged particle correlations. This exact solution was helpful in understanding the occurrence of size-dependent time-scales T_1 , T_2 and T^* in the tagged particle correlations in the ASEP. The linear interface also provides an effective coarse-grained description of two other interacting particle systems, namely, the asymmetric random average process (ARAP) [13] and the Katz-Lebowitz-Spohn (KLS) model at a particular value of the temperature [14]. The ARAP is the generalization of the ASEP to a continuum, where, hard-core particles, instead of hopping on a lattice, move along a continuous line. The KLS model, on the other hand, adds Ising interaction to the hard core exclusion between particles in the ASEP.

A general observation made in our study is that both the EW and the KPZ fixed points are unstable with respect to the SDF fixed point, a flow towards which is generated on adding a drift term to the EW and the KPZ time-evolution equations. This means that the least amount of drift in either the EW or the KPZ equation would make the large distance long time behavior of fluctuations for these equations be determined by the SDF fixed point.

In this thesis, we also considered the homogeneous zero-range process (ZRP) on a one-dimensional periodic lattice of L sites. The ZRP involves biased hopping of unit-mass particles between nearest neighbor sites of the lattice with a rate that depends solely on the occupancy at the departure site [4, 15]. Here, the hop rate function is the same for all sites. The stationary state measure of the process is known exactly to have a factorized form, being given by a product of factors, one for each site of the system. For certain classes of the hop rates, the ZRP, as a function of the particle density, undergoes a continuous phase transition on increasing the particle density ρ beyond a critical value ρ_c ; the system goes over from a low-density disordered phase with uniform average density to a condensed phase at high density, where a finite fraction of particles of average mass $(\rho - \rho_c)L$ accumulates on a single site. In this thesis, we studied how different are the effects of size on the dynamics of fluctuations as the system passes through the condensation transition. We reported our results for a particular choice of the rate, namely, $u(n) = 1 + \frac{b}{n}$ with $b > 2$, where n is the occupancy at the departure site. The particular quantity that we monitored is the variance of the integrated particle current across a bond in the stationary state. We found that the variance shows striking differences in behavior as the system goes over from the disordered to the condensed phase.

A general result that applies to all the phases is that at short times, when the fluctuations did not have time to circulate around, the integrated current is Poisson distributed, implying that the variance grows linearly in time, a behavior which holds for all times in an infinite system.

In a finite system, in the disordered phase, and also at the critical point, the variance behaves similarly to the tagged particle correlations in the ASEP, described above. Thus, the variance shows damped oscillations in time due to the kinematic wave of density fluctuations, and has two size-dependent time scales, $T_1 \sim L$ and $T_2 \sim L^{3/2}$, set by the circulation time and the decay time of the kinematic wave, respectively.

In the condensed phase, numerical simulations and strong scaling arguments show that the fluctuation dynamics is governed by the condensate relocation from one site to another, which occurs through a slower process of transfer of particles across the intervening bonds resulting in these bonds picking up enhanced fluctuations in the integrated current. In order to characterize the relocation dynamics, we studied the survival probability distribution in Monte Carlo simulations, obtained by computing the distribution of the time interval τ between successive relocations, and found that the distribution has two parts, (i) a power law part $\sim \tau^{-3/2}$ and (ii) another part, which has the scaling form $(\rho - \rho_c)^{-(b+2)} L^{-(b+1)} f(\tau/T_s)$; the scaling part arises from the long time T_s (growing as a power of the system size as $(\rho - \rho_c)^{b+1} L^b$ [16]) for which the condensate is stationary on one site, while the power law part holds for relatively small time T_r ($\sim (\rho - \rho_c)^2 L^2$) for which two sites, containing, on the average, approximately half of the condensate mass, compete to hold the largest mass.

Our results for the condensed phase showed that in this phase, the kinematic wave cannot pass through the condensate; thus, fluctuations do not circulate around. The behavior of the variance of the integrated current has four distinct size-dependent regimes, the two relevant size-dependent time scales being the survival time T_s and the relocation time T_r of the condensate. In this phase, the initial linear behavior of the variance continues until, after the survival time, the condensate relocates itself. This results in the variance showing a linear rise in time with a much larger slope than at early times. Subsequently, after the condensate has relocated to another site, the slope of the linear rise slowly approaches a size-dependent constant; we computed this constant and in particular, its scaling with the system size on the basis of a simple relocation model. We found that the constant scales with the system size as $[L^{-\theta}(\rho - \rho_c)^{-(b+1)} + 1]$, with $\theta = b - 1$ for $b > 3$. For b between 2 and 3, one gets $\theta = (b^2 - b - 2)/(b - 1)$. Thus, the relocation model predicts that, for all values of b , at long times $t \gg T_s + T_r$, the variance grows linearly with time with a size-dependent constant which scales down with the system size.

Another problem studied in this thesis involved the exclusion process with extended objects that generalizes the ASEP to the case where the particles in the ASEP are replaced by objects of finite extent that cover several lattice sites, i.e., k -mers covering k adjacent lattice sites, with $k > 1$. The motivation to study this model was mainly biological, since this model provides a setting to address the process of synthesis of proteins through the motion of ribosomes on messenger RNA [17, 18]. For the exclusion process with extended objects on a one-dimensional ring, we derived a number of stationary state properties by mapping each k -mer configuration to an equivalent and unique ASEP configuration on a smaller lattice [19]. The equal-time engine-engine correlation function (where engine refers

to the right end of the k -mer; one may equivalently choose to correlate the left ends of k -mers as well) was found to have a particular scaling form, which was shown to be a consequence of a proper continuum limit of the model. The unequal-time density-density correlation was shown to be related to that in the usual ASEP, if only one takes care of the wheeling effect, according to which, a fixed site in the k -mer problem corresponds to a moving site in the ASEP which wheels around the ring with a finite velocity [19].

9.1 Generalization and future direction

If the particle motion in either the ASEP or the ZRP is made symmetric, we get an equilibrium model of particles diffusing on a lattice. The coarse-grained density profile will map onto an equilibrium interface in the EW class (for the symmetric ZRP, this will be true only in the disordered phase and at the critical point). For the symmetric exclusion process, the average displacement of a tagged particle will be zero. Moreover, the variance of the tagged particle displacement will have a single time scale $T \sim L^z$, where $z = z_{\text{EW}} = 2$ such that for $t \ll T$, the variance grows with time as a power law, behaving as $t^{2\beta}$; $\beta = \beta_{\text{EW}} = 1/4$, while, for $t \gg T$, the variance would behave linearly with time, with the diffusion constant scaling with the system size as $1/L$ (see Chapter 4). Unlike the asymmetric case, the variance behaves in the same manner, irrespective of averaging over both the initial stationary ensemble and stochastic evolution, or, just the latter. Similar results would hold for the variance of the integrated current for the symmetric ZRP in the disordered phase, and at the critical point.

We studied the homogeneous ZRP for a very specific choice of the hop rate, namely, $u(n) = 1 + \frac{b}{n}$ with $b > 2$. In this case, the survival time T_s of the condensate grows as a power in the system size as L^b [16]. However, one can also study the process for other choices of the hop rate that induces condensation, namely, $u(n) = 1 + \frac{b}{n^\sigma}$ for $\sigma < 1$ (see Chapter 6, Section 6.4). In this case, also, similar results as we reported in this thesis are expected to hold, the only difference being that now the survival time T_s will be a stretched exponential in the system size [16]. Thus, our results on the ZRP hold for a wide class of hop rates; for those that do not induce condensation, the variance of the integrated current will have two time scales, $T_1 \sim L$ and $T_2 \sim L^{3/2}$, while, for those that allow for a condensation transition, the behavior of the variance will remain essentially unaltered in the disordered phase and at the critical point. In the condensed phase, however, the variance behaves very differently from the disordered phase, exhibiting four size-dependent time regimes, with two time scales $T_r \sim L^2$ and T_s , which goes either as a power or as a stretched exponential in the system size, depending on the form of the hop rate.

On the basis of our findings for the ASEP and the ZRP, a common picture emerges. For any one-dimensional system with driven diffusive dynamics, in a phase characterized by a homogeneous density ρ and a density-dependent current $J(\rho)$, density fluctuations would be transported around the system as a dissipating kinematic wave with velocity $v_K = \frac{\partial J}{\partial \rho}$. For

the ASEP and the ZRP (in the absence of the condensation transition), we found that the dynamic universality class is the KPZ class. Studies on disordered versions of these models have shown that so long as the kinematic wave speed is nonzero, disorder has little effect in changing the dynamic universality class from the pure model, a fact which has been borne out by extensive numerical simulations [20, 21]. The reasoning which has been put forward behind such an observation is that if the kinematic wave speed is nonzero, each density fluctuation encounters a particular patch of disorder only once in an infinite system, since the probability of returning is exponentially small. As a result, it was conjectured that the time-dependent correlation function, averaged over both the initial stationary ensemble and stochastic evolution, that monitors the dynamics of fluctuations in the system, behaves as in the pure system. Thus, this correlation function grows linearly with time at small and very long times, while, for intermediate times, it would oscillate with a period $\sim L$, where L is the size of the system. Knowing the kinematic speed, the correlation function has to be appropriately modified to keep track of the temporal growth of dissipation at a point on the density profile; such a correlation function (the sliding tag correlation function, in the case of the ASEP) does not oscillate in time; instead, for times $t \ll L^z$; $z = z_{\text{KPZ}} = 3/2$, it grows with time as $t^{2\beta}$, where $\beta = \beta_{\text{KPZ}} = 1/3$. However, when the kinematic wave speed is zero, the above argument of the negligible effects of disorder fails and the disorder is expected to change the dynamic universality class. Most studies have looked at the sliding tag correlation function to get an estimate of the growth exponent β , and hence, an idea of the dynamic universality class. However, when the kinematic wave speed is zero, sliding of tag yields no new results, different from the usual correlation function, making an estimate of β impossible this way. A way out could be to monitor the correlation function by starting from an arbitrary but fixed initial configuration, drawn from the stationary ensemble, and averaging over stochastic evolution. This quantity was introduced by van Beijeren [9], and on the basis of our findings, we find that this quantity directly measures the dissipation in time without doing any sliding of tag; thus, this quantity might prove useful in elucidating the effects of quenched disorder in changing the dynamic universality class of a model from the pure case. The quantity due to van Beijeren proves useful in tracking the dissipation of the density profile in cases where there are two or more kinematic waves moving at different velocities; in such cases, sliding of tag, equivalent to a Galilean transformation for the corresponding time-evolution equation, can not get rid of the effects of kinematic waves, all at the same time [22], thereby making determination of β a difficult task. Such an exercise was recently performed in Ref. [23]. Another remarkable fact about the correlation function due to van Beijeren is that its definition does not involve the velocity of the kinematic wave, as does the sliding tag correlation function; thus, in cases, where one does not know the kinematic wave speed *a priori*, dissipation of the density profile in time may still be effectively captured by the correlation function due to van Beijeren.

We briefly mention a possible extension of our study, namely, to those systems with open boundaries, to see how size effects interplay with nonequilibrium dynamics in gov-

erning the behavior of fluctuations in the stationary state. Systems with open boundaries resemble physical situations more closely, for example, the ASEP with open boundaries models motion of molecular motors on one-dimensional microtubules inside living cells. A recent study of the totally asymmetric simple exclusion process in one dimension with open boundaries considers the total number of particles present in the system at any time in the stationary state. Its time average, which is the same as its ensemble average, is easily calculated from the known stationary distribution of the ASEP with open boundaries. However, as a fluctuating quantity, the power spectrum of the total number of particles at any time was shown to contain time-correlation information, exhibiting finite-size effects in the form of oscillations, deep within the high and the low density phases [24].

To conclude, the results reported in this thesis provide an exhaustive study of size effects on the dynamics of fluctuations in two prototypical driven diffusive systems in one dimension with periodic boundary conditions. Our findings lend strong evidence to an intricate interplay of size effects with nonequilibrium dynamics in determining the behavior of fluctuations in driven diffusive systems. A particular highlight of our studies is that we have been able to identify all the relevant time scales in the behavior of fluctuations, and also provide simple explanations of the physical processes underlying these time scales. It remains to be investigated how the behavior of fluctuations, predicted in this thesis, gets modified in driven diffusive systems in higher dimensions.

References

- [1] M. E. Fisher, in *Critical Phenomena, Proceedings of the 51st 'Enrico Fermi' Summer School, Varenna, Italy*, edited by M. S. Green (Academic, New York, 1971).
- [2] V. Privman and M. E. Fisher, *J. Stat. Phys.* **33**, 385 (1983).
- [3] B. Schmittmann and R. K. P. Zia, in *Phase Transitions and Critical Phenomena*, edited by C. Domb and J. L. Lebowitz (Academic, London, 1995), Vol. 17.
- [4] F. Spitzer, *Adv. Math.* **5**, 246 (1970).
- [5] T. M. Liggett, *Interacting Particle Systems* (Springer-Verlag, New York, 1985).
- [6] M. J. Lighthill and G. B. Whitham, *Proc. R. Soc. London A* **229**, 281 (1955).
- [7] A. De Masi and P. A. Ferrari, *J. Stat. Phys.* **38**, 603 (1985); R. Kutner and H. van Beijeren, *ibid.* **39**, 317 (1985).
- [8] B. Derrida, M. R. Evans, and D. Mukamel, *J. Phys. A* **26**, 4911 (1993); B. Derrida and K. Mallick, *ibid.* **30**, 1031 (1997).
- [9] H. van Beijeren, *J. Stat. Phys.* **63**, 47 (1991).
- [10] M. Kardar, G. Parisi, and Y. C. Zhang, *Phys. Rev. Lett.* **56**, 889 (1986).
- [11] S. N. Majumdar and M. Barma, *Phys. Rev. B* **44**, 5306 (1991).
- [12] J. M. Hammersley, in *Proceedings of the fifth Berkeley Symposium on Mathematical Statistics and Probability*, edited by L. M. Le Cam and J. Neyman (University of California Press, Berkeley, 1967); S. F. Edwards and D. R. Wilkinson, *Proc. R. Soc. London, Ser A* **381**, 17 (1982).
- [13] J. Krug and J. Garcia, *J. Stat. Phys.* **99**, 31 (2000); R. Rajesh and S. N. Majumdar, *ibid.* **99**, 943 (2000).
- [14] S. Katz, J. L. Lebowitz, and H. Spohn, *Phys. Rev. B* **28**, 1655 (1983); *J. Stat. Phys.* **34**, 497 (1984).
- [15] M. R. Evans and T. Hanney, *J. Phys. A* **38**, R195 (2005).

-
- [16] C. Godrèche and J. M. Luck, *J. Phys. A* **38**, 7215 (2005).
- [17] C. T. MacDonald, J. H. Gibbs, and A. C. Pipkin, *Biopolymers* **6**, 1 (1968).
- [18] C. T. MacDonald and J. H. Gibbs, *Biopolymers* **7**, 707 (1969).
- [19] M. Barma, M. D. Grynberg, and R. B. Stinchcombe, *J. Phys.: Condens. Matter* **19**, 065112 (2007).
- [20] G. Tripathy and M. Barma, *Phys. Rev. Lett.* **78**, 3039 (1997).
- [21] K. Jain and M. Barma, *Phys. Rev. Lett.* **91**, 135701 (2003).
- [22] S. Ramaswamy, M. Barma, D. Das, and A. Basu, *Phase Transitions* **75**, 363 (2002).
- [23] S. Chatterjee and M. Barma, *J. Stat. Mech.* L01004 (2007).
- [24] D. A. Adams, R. K. P. Zia, and B. Schmittmann, *Phys. Rev. Lett.* **99**, 020601 (2007).

Appendix A

A Primer on Kinematic Waves

The notion of kinematic waves goes back to the work of Lighthill and Whitham, who showed how their occurrence follows from the continuity equation. We briefly recapitulate their arguments [1, 2] here, as applied to a stochastic driven diffusive system in one dimension, of the type considered in this thesis.

For definiteness, let us consider a closed driven diffusive system in its nonequilibrium stationary state, characterized by a homogeneous density $\bar{\rho}$. Here, the overbar represents an average over the stationary state probability distribution of configurations for the system at hand. A particular configuration will have fluctuations $\delta\rho(x, t)$ in the local density about the average $\bar{\rho}$; since these fluctuations are of statistical origin, we expect that $\delta\rho(x, t) \ll \bar{\rho}$. Note that here, we are considering the system on a coarse-grained scale. Since the system is closed, particle number is conserved so that density fluctuations $\delta\rho(x, t)$ at an arbitrary location x evolves in time following the equation of continuity, i.e.,

$$\frac{\partial(\delta\rho(x, t))}{\partial t} = -\frac{\partial J(x, t)}{\partial x}, \quad (\text{A.1})$$

where $J(x, t)$ is the particle current at location x at time t . We have, by definition,

$$\delta\rho(x, t) = \rho(x, t) - \bar{\rho}, \quad (\text{A.2})$$

where $\rho(x, t)$ is the local density of particles. Since the stationary state mean density $\bar{\rho}$ is constant in space and time, using Eq. A.2 in Eq. A.1 gives

$$\frac{\partial\rho(x, t)}{\partial t} = -\frac{\partial J(x, t)}{\partial x}. \quad (\text{A.3})$$

One cannot get two unknowns, namely, $\rho(x, t)$ and $J(x, t)$, by solving only one equation, Eq. A.3, unless further assumptions are made relating the two quantities to one another; Lighthill and Whitham made the assumption that

$$J(x, t) = J(\rho(x, t)). \quad (\text{A.4})$$

In other words, the current $J(x, t)$ derives its space and time dependence only through its dependence on the local density $\rho(x, t)$. Alternatively, with $v(x, t)$ representing the local density of particles constituting the system, since $J(x, t) = \rho(x, t)v(x, t)$, according to the assumption in Eq. A.4, it follows that $v(x, t)$ is a function solely of the local density $\rho(x, t)$. Under the assumption in Eq. A.4, Eq. A.3 reads

$$\frac{\partial \rho(x, t)}{\partial t} = - \left[v(\rho(x, t)) + \rho(x, t) \frac{dv}{d\rho} \right] \frac{\partial \rho(x, t)}{\partial x} = -v_K(\rho) \frac{\partial \rho(x, t)}{\partial x}, \quad (\text{A.5})$$

where $v_K(\rho) = \frac{dJ}{d\rho}$, and, in anticipation of its interpretation below as the “kinematic” wave velocity, we have added the subscript “ K ”. Equation A.5 is nonlinear because of the dependence of $v(\rho(x, t))$ on the local density $\rho(x, t)$. Since $\rho(x, t) = \bar{\rho} + \delta\rho(x, t)$, we get, on expanding $v_K(\rho(x, t))$ about $v_K(\bar{\rho})$,

$$v_K(\rho(x, t)) = v_K(\bar{\rho}) + \left[\frac{dv_K}{d\rho} \right]_{\bar{\rho}} \delta\rho(x, t) + \text{higher order terms in } \delta\rho(x, t). \quad (\text{A.6})$$

It is reasonable to drop higher order terms in $\delta\rho$ in the above equation, since, as noted earlier, $\delta\rho \ll \bar{\rho}$. To a first approximation, we take

$$v_K(\rho(x, t)) \approx v_K(\bar{\rho}). \quad (\text{A.7})$$

In this approximation, Eq. A.5 reduces to the following linear equation.

$$\frac{\partial \rho(x, t)}{\partial t} = -v_K(\bar{\rho}) \frac{\partial \rho(x, t)}{\partial x}. \quad (\text{A.8})$$

Equation A.8 has the general solution of the form

$$\rho(x, t) = f(x - v_K(\bar{\rho})t), \quad (\text{A.9})$$

where f is an arbitrary function of its argument; the solution of any particular problem would be found by matching the value of the function f to the corresponding given initial condition. Such a solution may be interpreted as an initial density profile getting translated in time by a distance $v_K(\bar{\rho})t$ in an interval of time t without any change in its shape. The solution, thus, represents a signal being transferred from one spatial point to another with a recognizable velocity of propagation, given by $v_K(\bar{\rho})$; it is in this sense that the solution, represented by Eq. A.9 represents a wave, which Lighthill and Whitham chose to refer to as “kinematic” wave. $v_K(\bar{\rho})$ is the kinematic wave velocity. The attribute “kinematic” is to emphasize the purely kinematic origin of these waves, arising, as they do, out of equation of continuity. This is in contrast to more commonly encountered acoustic and elastic waves which are consequences of Newton’s second law of motion, together with some assumptions relating the stress produced in the propagating medium to the resulting strain. In the context of interacting particle systems, $v_K(\bar{\rho})$ is identical to the collective velocity discussed

in [3].

Kinematic waves are known to arise in a variety of circumstances involving flow, e.g., in flood movement in long rivers [1], traffic [4, 5], flow of granular particles through vertical tubes and hoppers [6], motion of transverse fluctuations in interfaces [7, 8], field-induced transport in random media as in drop-push dynamics [9].

It is to be noted that in the above description, the kinematic wave velocity $v_K(\rho(x, t))$ is constant only in the first approximation in the Taylor series expansion in Eq. A.6. Including higher order terms in Eq. A.6 makes the kinematic wave velocity an explicit function of the local density $\rho(x, t)$. As a result, different points on the initial density profile will move with different velocities $v_K(\rho(x, t))$, so that the initial density profile would not move as a whole with a constant velocity $v(\bar{\rho})$ without any change in shape; rather, the fact that different points on the profile move with different velocities would lead to a distortion of the initial density profile in time. This is referred to as the dissipation of the kinematic wave in time.

Improvement over the Lighthill-Whitham theory: As discussed above, the crucial assumption in deriving the Lighthill-Whitham theory of kinematic waves is the fact that the current $J(x, t)$ is a function solely of the local density $\rho(x, t)$ (see Eq. A.4). To improve, we now assume that in addition, the current also depends on the gradient of the density. In other words, Eq. A.4 is to be replaced by

$$J(x, t) = J(\rho(x, t)) - D \frac{\partial \rho}{\partial x}, \quad (\text{A.10})$$

where D is a positive constant. The second term accounts for the fact that the current flows in space in the direction of decreasing density. This assumption is reasonable in the case of traffic flow (to which Lighthill and Whitham first applied their theory), since, it follows from Eq. A.10 that, for fixed $\rho(x, t)$ (and, hence, fixed $J(\rho(x, t))$), a positive (negative) density gradient leads to a lower (higher) flux of traffic as one expects the drivers to reduce (increase) the speed of their vehicles depending on whether they are approaching a more (less) congested region. Using Eq. A.10 in Eq. A.3 leads to

$$\frac{\partial \rho(x, t)}{\partial t} + v_K(\rho(x, t)) \frac{\partial \rho(x, t)}{\partial x} = D \frac{\partial^2 \rho(x, t)}{\partial x^2}. \quad (\text{A.11})$$

Now we see that the fact that the velocity $v_K(\rho(x, t))$ depends on the density $\rho(x, t)$ and that there is diffusion (represented by the right hand side of the above equation) lead to two competing effects: while the term $v_K(\rho(x, t)) \frac{\partial \rho(x, t)}{\partial x}$ tends to distort the wave, the term $D \frac{\partial^2 \rho(x, t)}{\partial x^2}$ smoothens out the density profile. Similarly, corrections to Lighthill-Whitham theory may be constructed by including higher order derivatives of density in Eq. A.10.

References

- [1] M. J. Lighthill and G. B. Whitham, Proc. R. Soc. London A **229**, 281 (1955).
- [2] G. B. Whitham, *Linear and Nonlinear Waves* (John Wiley & Sons, New York, 1974).
- [3] G. M. Schütz in *Phase Transitions and Critical Phenomena 19*, edited by C. Domb and J. L. Lebowitz (Academic, London, 2001) Section 4.2.2.
- [4] M. J. Lighthill and G. B. Whitham, Proc. R. Soc. London A **229**, 317 (1955).
- [5] D. Chowdhury, L. Santen, and A. Schadschneider, Phys. Rep. **329**, 199 (2000) Section 4.1.
- [6] J. Lee, Phys. Rev. E **49**, 281 (1994).
- [7] M. Barma, J. Phys. A: Math. Gen. **25**, L693 (1992).
- [8] M. Barma, in *Non Linear Phenomena in Materials Science III - Instabilities and Patterning*, edited by G. Ananthakrishna, L. P. Kubin, and G. Martin (Scitec Publications, Untermüli, 1995).
- [9] M. Barma and R. Ramaswamy, in *Non-Linearity and Breakdown in Soft Condensed Matter*, edited by K. K. Bardhan, B. K. Chakrabarti, and A. Hansen (Springer-Verlag, Berlin, 1994).

Appendix B

Derivation of the equation of the interface corresponding to the tagged particle displacement

Here, we derive the interface equation, Eq. 4.2, following [1].

The local interparticle distance in the ASEP is given by

$$\frac{1}{\rho(x, t)} = \frac{\partial y}{\partial x}, \quad (\text{B.1})$$

where $y(x, t)$ is the position of the x -th particle at time t . Now,

$$y(x, t) = \frac{x}{\rho} + h(x, t), \quad (\text{B.2})$$

where ρ is the mean density of particles and $h(x, t)$ is the displacement of the x -th particle from the position it would have had, had the particles been uniformly placed. Then, we have $\rho(x, t)^{-1} = \rho^{-1} + \frac{\partial h}{\partial x}$, implying

$$\rho(x, t) = \frac{\rho}{1 + \rho \frac{\partial h}{\partial x}}. \quad (\text{B.3})$$

Expanding in a power series in $\frac{\partial h}{\partial x}$,

$$\rho(x, t) = \rho - \rho^2 \frac{\partial h}{\partial x} + \rho^3 \left(\frac{\partial h}{\partial x} \right)^2 + \dots \quad (\text{B.4})$$

The above equation can be rewritten as

$$\rho(x, t) = \rho + \psi(x, t) \quad \text{where} \quad \psi(x, t) = -\rho^2 \frac{\partial h}{\partial x} + \rho^3 \left(\frac{\partial h}{\partial x} \right)^2 + \dots \quad (\text{B.5})$$

In the absence of any drift velocity, the equation of motion of $h(x, t)$ is diffusive.

$$\frac{\partial h}{\partial t} = \Gamma' \frac{\partial^2 h}{\partial x^2} + \eta(x, t). \quad (\text{B.6})$$

The noise term $\eta(x, t)$ is Gaussian: $\langle \eta(x, t) \rangle = 0$, $\langle \eta(x, t) \eta(x', t') \rangle = 2A \delta(x - x') \delta(t - t')$.

In the presence of a drift velocity $v(x, t)$, an additional term $v(x, t)$ appears on the right hand side of the above equation. The drift velocity depends on x and t only through the local density $\rho(x, t)$ which is the only possibility in the coarse-grained lattice gas. Thus $v(x, t) = v(\rho(x, t))$. We now substitute $\rho(x, t) = \rho + \psi(x, t)$ and expand in a power series in $\psi(x, t)$.

$$v(x, t) = v(\rho) + \left[\frac{\partial v}{\partial \rho} \right]_{\rho} \psi(x, t) + \frac{1}{2} \left[\frac{\partial^2 v}{\partial \rho^2} \right]_{\rho} \psi^2(x, t) + \dots \quad (\text{B.7})$$

Thus, we get

$$\begin{aligned} \frac{\partial h}{\partial t} &= v(\rho) + \Gamma' \frac{\partial^2 h}{\partial x^2} - \rho^2 \left[\frac{\partial v}{\partial \rho} \right]_{\rho} \frac{\partial h}{\partial x} + \frac{1}{2} \left[\frac{\partial^2 v}{\partial \rho^2} \right]_{\rho} \rho^4 \left(\frac{\partial h}{\partial x} \right)^2 \\ &+ \left[\frac{\partial v}{\partial \rho} \right]_{\rho} \rho^3 \left(\frac{\partial h}{\partial x} \right)^2 + \dots + \eta(x, t) \end{aligned} \quad (\text{B.8})$$

$$= v(\rho) + \Gamma' \frac{\partial^2 h}{\partial x^2} + u' \frac{\partial h}{\partial x} + \frac{\lambda'}{2} \left(\frac{\partial h}{\partial x} \right)^2 + \dots + \eta(x, t). \quad (\text{B.9})$$

Here, $v(\rho)$ is the mean drift velocity of the particle and hence, equals v_P in our notation. Also, $u' = \rho \left[v(\rho) - \frac{\partial J}{\partial \rho} \right]_{\rho}$ where $J(\rho) = \rho v(\rho)$ is the mean current. In terms of the kinematic wave velocity v_K , we have $u' = \rho(v_P - v_K)$. The nonlinearity coefficient $\lambda' = \rho^3 \left[\frac{\partial^2 J}{\partial \rho^2} \right]_{\rho}$. Note that x in the above equation stands for the tag variable in the continuum. Now, dividing x by the particle density ρ to make it into a spatial variable, we finally get from Eq. B.9, to lowest order of nonlinearity,

$$\frac{\partial h}{\partial t} = v_P + \Gamma' \frac{\partial^2 h}{\partial x^2} + u \frac{\partial h}{\partial x} + \frac{\lambda}{2} \left(\frac{\partial h}{\partial x} \right)^2 + \eta(x, t), \quad (\text{B.10})$$

where

$$u = v_P - v_K, \quad (\text{B.11})$$

while

$$\lambda = \rho \left[\frac{\partial^2 J}{\partial \rho^2} \right]_{\rho}. \quad (\text{B.12})$$

Using $J(\rho) = (p - q)\rho(1 - \rho)$ and $v_P = (p - q)(1 - \rho)$ for the ASEP, we get

$$u = \rho(p - q), \quad (\text{B.13})$$

$$\lambda = -2\rho(p - q). \quad (\text{B.14})$$

Utilizing the above expressions for u and λ in Eq. B.10, we get the time evolution equation for the interface equivalent to the ASEP, Eq. 4.2.

Expressions for the coefficients Γ and A in terms of microscopic parameters can be found by setting $p = q = 1/2$, in which case the ASEP reduces to the SEP. The coefficient Γ can then be calculated explicitly [2, 3], with the result

$$\Gamma = \frac{1}{2}. \quad (\text{B.15})$$

Further, Eq. B.10 reduces to the EW equation, Eq. 4.3, and $\sigma^2(t)$ can be found from Chapter 4, Section 4.2 by considering the limit $u \rightarrow 0$. The result is $\sigma^2(t) \approx \frac{2A}{\sqrt{\pi\Gamma}}\sqrt{t}$. Comparing with the exact result $\sigma^2(t) \approx \sqrt{\frac{2}{\pi}}\left(\frac{1-\rho}{\rho}\right)\sqrt{t}$ for the SEP [4], one gets $\frac{A}{\sqrt{\Gamma}} = \frac{1}{\sqrt{2}}\left(\frac{1-\rho}{\rho}\right)$. Using Eq. B.15, we finally get

$$A = \frac{1}{2}\left(\frac{1-\rho}{\rho}\right). \quad (\text{B.16})$$

References

- [1] S. N. Majumdar, Ph. D. Thesis (Bombay University) (1992) (unpublished).
- [2] R. Kutner, Phys. Lett. **81A**, 239 (1981).
- [3] R. B. Stinchcombe, M. D. Grynberg, and M. Barma, Phys. Rev. E **47**, 4018 (1993).
- [4] T. M. Liggett, *Interacting Particle Systems* (Springer-Verlag, New York, 1985).

Appendix C

Evaluation of the integral

$$\int_{k=0}^{\infty} \frac{dk}{k^2} [1 - e^{-ck^2} \cos(k)]$$

Let

$$I(c) = \int_{k=0}^{\infty} \frac{dk}{k^2} [1 - e^{-ck^2} \cos(k)]. \quad (\text{C.1})$$

Thus,

$$\frac{dI}{dc} = \int_{k=0}^{\infty} dk e^{-ck^2} \cos(k) = \frac{1}{2} \sqrt{\frac{\pi}{c}} e^{-1/4c}. \quad (\text{C.2})$$

Also, $I(0) = \frac{\pi}{2}$. Hence,

$$I(c) = \frac{\pi}{2} + \frac{1}{2} \int_0^c dx \sqrt{\frac{\pi}{x}} e^{-1/4x}. \quad (\text{C.3})$$

Doing the integral on the rhs by parts, we finally get

$$I(c) = \frac{\pi}{2} + \sqrt{\pi c} e^{-1/4c} - \frac{\sqrt{\pi}}{2} \int_{1/4c}^{\infty} dy e^{-y} y^{-1/2}. \quad (\text{C.4})$$

Using the usual definition of the complementary error function, $\text{erfc}(z) = \frac{2}{\sqrt{\pi}} \int_z^{\infty} dt e^{-t^2} = 1 - \text{erf}(z)$, (where $\text{erf}(z)$ is the usual error function), we can rewrite the above expression as

$$\begin{aligned} I(c) &= \frac{\pi}{2} + \sqrt{\pi c} e^{-1/4c} - \frac{\pi}{2} \text{erfc}\left(\frac{1}{2\sqrt{c}}\right) \\ &= \sqrt{\pi c} e^{-1/4c} + \frac{\pi}{2} \text{erf}\left(\frac{1}{2\sqrt{c}}\right). \end{aligned} \quad (\text{C.5})$$

Appendix D

Proof of the Poisson distribution for the integrated current in the ZRP

We prove below that for the Zero-Range Process (ZRP) in the grand canonical ensemble in the thermodynamic limit, the stationary state integrated particle current $H(i, t)$ across any bond $(i, i + 1)$ in time t follows a Poisson distribution: $P_{out}(n, t) \equiv \text{Prob}(H(i, t) = n) = \frac{e^{-vt}(vt)^n}{n!}$. Here, v is the mean current in the stationary state. The result applies to all forms of the hop rate function $u(n)$.

The proof of the above result relies on an adaptation of the Burke's theorem in queueing theory [1, 2] to the ZRP. The theorem states that for a reversible birth-death process with Poisson input, the output is also a Poisson process with the same intensity as the input.

Proof: The proof goes along the following lines.

(i) Focussing on the ZRP dynamics at a single site, we show, utilizing the stationary state weights of the ZRP, that the population of the site undergoes a time-reversible birth-death process. Here, the birth, corresponding to the input of a particle, is a Poisson process with intensity equal to the mean current $J = v$. On invoking time reversibility of the dynamics, we conclude that the output of particles from the site also follows an identical Poisson distribution.

(ii) Noting that the output from one site forms the input to the next site then implies the result.

Without loss of generality, we consider below fully asymmetric particle motion to the right. Also, we take time to be discrete, though the proof can easily be generalized to continuous time.

(i) We begin by recalling from Chapter 6, Section 6.3.1 that in the thermodynamic limit, within a grand canonical ensemble, the probability of a site to have n particles in the

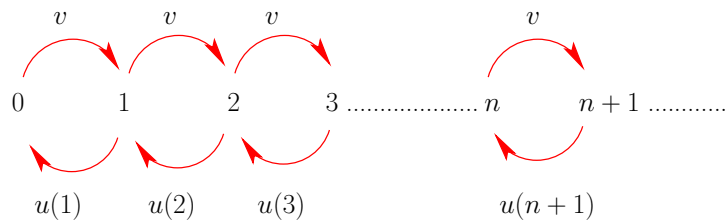


Figure D.1: Birth-death dynamics at a ZRP site. The birth rate is v , while the death from state n to $n - 1$ occurs with rate $u(n)$.

stationary state is given by

$$p(n) = \frac{v^n f(n)}{F(v)};$$

$$f(n) = \begin{cases} (\prod_{m=1}^n u(m))^{-1} & \text{if } n > 0 \\ 1 & \text{if } n = 0. \end{cases} \quad (\text{D.1})$$

Here v is the fugacity, $F(v) = 1 + \sum_{n=1}^{\infty} v^n f(n)$ is the single site grand canonical partition function. One can check from Eq. D.1 that the stationary state weights $p(n)$ satisfy the identity

$$vp(n) = u(n+1)p(n+1). \quad (\text{D.2})$$

Since the stationary state is unique, the distribution of the integrated current across any bond is also unique. The mean current of particles is the same across any bond and is given by $J = \sum_{n=1}^{\infty} u(n)p(n) = v$.

Next, we note that the population at a site can be interpreted to be undergoing a birth-death process in the stationary state. Here a birth corresponds to the input of a particle into the site with rate $\sum_{n=1}^{\infty} u(n)p(n) = v$, utilizing Eq. D.1. This is because for a particle to hop into the site, the site to the left has to be occupied in the first place with probability $p(n)$ (with $n \geq 1$), followed by the hopping out of a particle with rate $u(n)$. In unit time, the probability that there is a hop into the site is v . The population undergoes a death of its individual when, at the instant the site has $n \geq 1$ particles, a particle hops out with rate $u(n)$. The state space for the population takes on integer values $n = 0, 1, 2, \dots$. The birth-death dynamics is represented schematically in Fig. D.1.

Let us assume that the input of particles into the site follows a Poisson distribution with intensity v . In other words, the probability that n particles hop into the site in time t is given by

$$P_{in}(n, t) \equiv \text{Prob}(n \text{ particles hop into the site in time } t) = e^{-vt} \frac{(vt)^n}{n!}. \quad (\text{D.3})$$

The intensity of the Poisson distribution is chosen to be v to be consistent with the fact that in unit time, the probability that there is a hop into the site equals v , as discussed

earlier.

A realization of the birth-death dynamics at a site for a fixed time T is given by the set of occupancies $\{n(t); 0 \leq t \leq T\}$, where $n(t)$ is the occupancy of the site at time instant t . Demonstrating that the dynamics is reversible in the stationary state is tantamount to showing that for every given realization of the dynamics is associated the time-reversed realization of the same dynamics occurring with equal probability. Time-reversibility is demonstrated here for a given realization but can easily be checked to be true for any arbitrary realization of the dynamics.

Consider the realization (a) in Fig. D.2, observed for a total time $T = 9$ for illustration. In Fig. D.2(b), we show the corresponding time-reversed realization of the dynamics.

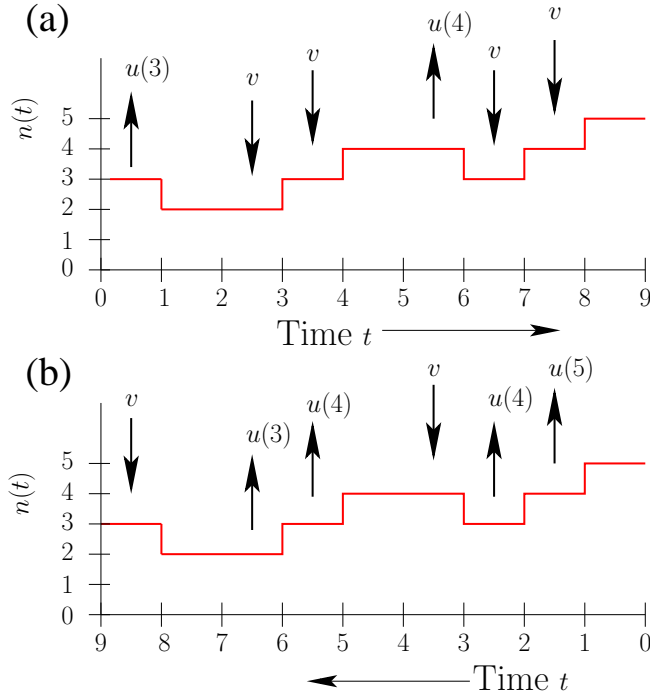


Figure D.2: (a) shows a typical realization of the ZRP dynamics at a site for a total time $T = 9$. The downward arrows correspond to the input of particles into the site with probability v , while the upward arrows represent hopping out of particles. (b) shows the corresponding time-reversed realization which, as shown in the text, occurs with the same probability as the realization (a).

The probability to observe the realization (a) is given by

$$P_{Forward} = p(3)u(3)[1 - v - u(2)]vv[1 - v - u(4)]u(4)vv[1 - v - u(5)], \quad (D.4)$$

while the probability to observe the time-reversed realization (b) equals

$$P_{Reverse} = p(5)[1 - v - u(5)]u(5)u(4)v[1 - v - u(4)]u(4)u(3)[1 - v - u(2)]v. \quad (D.5)$$

Here we have used the fact that the input distribution of particles into the site is Poissonian so that particle-hop into the site occurs as uncorrelated events at different time instants with a constant probability v .

Using Eq. D.2, it is easily shown that

$$P_{Forward} = P_{Reverse}. \quad (\text{D.6})$$

We have thus demonstrated that the birth-death dynamics at a ZRP site is time reversible in the stationary state.

We are interested in the statistics of the number of occurrences of upward arrows in a fixed time in (a), since this number equals the integrated particle current out of the site in the same time. Define

$$P_{out}(n, t) \equiv \text{Prob}(n \text{ particles hop out of any site } i \text{ in time } t, \text{ i.e., } H(i, t) = n). \quad (\text{D.7})$$

Now, for every upward arrow in (a), there is a corresponding downward arrow in the time-reversed realization (b). The latter follows the Poisson distribution $P_{in}(n, t)$ in Eq. D.3. Since both the realizations (a) and (b) occur with equal probability, we conclude that the integrated particle current out of the site follows the distribution $P_{in}(n, t)$. Thus, with the assumption that the input distribution of particles into a site is Poissonian, given by Eq. D.3, the integrated current out the site follows the same distribution: $P_{out}(n, t) = P_{in}(n, t)$.

Since the output distribution is unique, we conclude that

$$P_{out}(n, t) = e^{-vt} \frac{(vt)^n}{n!}. \quad (\text{D.8})$$

(ii) Now, we consider the full assembly of sites in the ZRP. Since the output from a site forms the input to the next site, it follows that the integrated current across any site follows a Poisson distribution with intensity v .

Validity of the result in the canonical ensemble: The proof given above for the Poisson distribution of the integrated current is strictly valid in the grand canonical ensemble in the thermodynamic limit, where there is no correlation between sites in the ZRP in the stationary state, and the mean current equals the fugacity v (see Chapter 6, Section 6.3.1 and Section 6.5.3). In the canonical ensemble, because of correlation between sites (see Section 6.3), the proof for the Poissonian character of the integrated current is not valid unless one considers the ZRP in the thermodynamic limit, when the two ensembles become equivalent, at least in the disordered phase. At the critical point, although the equivalence of ensembles in the thermodynamic limit breaks down, Eq. D.1 for the single-site distribution is still valid, with the fugacity v replaced by its maximum possible value v_{\max} (see Chapter 6, Eq. 6.38). In the condensed phase, the integrated current is Poisson distributed for times smaller than the survival time of the condensate (see Chapter 7, Section 7.3.3).

References

- [1] P. J. Burke, *Oper. Res.* **4**, 699 (1956); E. Reich, *Ann. Math. Stat.* **28**, 768 (1957). See also F. P. Kelly, *Reversibility and Stochastic Networks*, (Wiley, Chichester, 1979).
- [2] We are grateful to J. Lebowitz and E. Speer for pointing out the applicability of the Burke's theorem to the ZRP.

Appendix E

Survival time of the condensate in the ZRP

In this appendix, we briefly summarize the arguments in [1] leading to the result that in the ZRP, with the hop rate $u(n) = 1 + b/n$ (with $b > 2$), the characteristic survival time scale T_s of the condensate scales with the system size L in the following way: $T_s \sim L^b$.

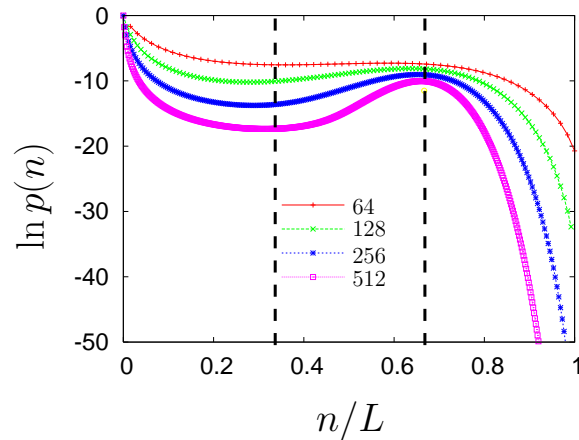


Figure E.1: The single-site probability distribution $p(n)$, plotted on a logarithmic scale, as a function of n/L in the stationary state of the ZRP within the canonical ensemble. We have taken $b = 5$ so that the critical density $\rho_c = 1/(b - 2) = 1/3$, the particle density $\rho = N/L = 1$; the various system sizes L considered are marked in the figure. Here, $p(n)$'s are obtained by first evaluating the canonical partition function $Z_{L,N}$ numerically for given values of b , N , and L , and then, making use of the formula in Eq. E.1. The two dotted lines represent the asymptotic locations of the maximum at $\Delta/L = (\rho - \rho_c) = 2/3$, and the minimum at $\Delta/2L = (\rho - \rho_c)/2 = 1/3$, respectively (for definitions, see text).

We start with the following result that in the ZRP within the canonical ensemble, the probability for a single site to hold n particles in the stationary state reads (see Chapter 6,

Eq. 6.4)

$$p(n) = \frac{Z_{L-1, N-n}}{Z_{L, N}}, \quad (\text{E.1})$$

where $Z_{L, N}$ is the canonical partition function for a system of N particles executing the ZRP dynamics on a lattice of L sites with periodic boundary conditions. For given values of L and N , the partition function $Z_{L, N}$ may be evaluated recursively, as detailed in Chapter 6, Section 6.5.3. This allows one to compute the single-site probability distribution $p(n)$; the result is shown in Fig. E.1 for the choice of the hop rate $u(n) = 1 + b/n$, with $b = 5$ (so that the critical density $\rho_c = 1/(b-2) = 1/3$), the particle density $\rho = 1$. The system sizes considered are marked in the figure.

To understand the essential features in the plot of Fig. E.1, we recall the discussion in Chapter 6, Section 6.5.2, from which we know that, with $f(n) \approx An^{-b}$ (A being a constant) for large n , and $\Delta = (\rho - \rho_c)L$ denoting the mean number of excess particles in the condensed phase, the distribution $p(n)$ is given by the following set of equations [2, 3].

$$p(n) \simeq f(n) \text{ for } 1 \ll n \ll O(L), \quad (\text{E.2})$$

$$p(n) \simeq f(n) \frac{1}{(1-x)^b} \quad \text{for } n = x(\rho - \rho_c)L \text{ where } 0 < x < 1, \quad (\text{E.3})$$

$$p(n) \sim p_{\text{cond}}(n) \text{ for } n \sim (\rho - \rho_c)L. \quad (\text{E.4})$$

Here, $p_{\text{cond}}(n)$ takes two different forms, depending on whether $2 < b < 3$ or $b > 3$. In the former case,

$$p_{\text{cond}}(n) \simeq L^{-b/(b-1)} V_b \left[\frac{n - (\rho - \rho_c)L}{L^{1/(b-1)}} \right], \quad (\text{E.5})$$

where the asymptotic forms of the scaling function $V_b(z)$ are given by

$$\begin{aligned} V_b(z) &\simeq A|z|^{-b} \text{ as } z \rightarrow -\infty, \\ &= c_0 \text{ at } z = 0, \\ &\simeq c_1 z^{(3-b)/2(b-2)} e^{-c_2 z^{(b-1)/(b-2)}} \text{ as } z \rightarrow \infty. \end{aligned} \quad (\text{E.6})$$

Here, $c_0 = \beta^{-1/(b-1)}/[(b-1)\Gamma((b-2)/(b-1))]$, $c_1 = [2\pi(b-2)(\beta(b-1))^{1/(b-2)}]^{-1/2}$, $c_2 = (b-2)/(b-1)(\beta(b-1))^{1/(b-2)}$, where $\beta = A\Gamma(1-b)$.

For $b > 3$, the distribution $p_{\text{cond}}(n)$ reads

$$p_{\text{cond}}(n) \simeq \frac{1}{\sqrt{2\pi\Delta^2 L}} e^{-(n - (\rho - \rho_c)L)^2/2\Delta^2 L} \text{ for } |n - (\rho - \rho_c)L| \ll O(L^{2/3}), \quad (\text{E.7})$$

i.e., here, $p_{\text{cond}}(n)$ is Gaussian on the scale $|n - (\rho - \rho_c)L| \ll O(L^{2/3})$, but, far to the left of the peak, $p(n)$ decays as a power law:

$$p_{\text{cond}}(n) \simeq f(n) (1 - n/(\rho - \rho_c)L)^{-b} \text{ for } (\rho - \rho_c)L - n \sim O(L). \quad (\text{E.8})$$

From Eq. E.2, it is clear that for $n \ll L$, the single-site distribution $p(n)$ is a power law that accounts for the critical background; this part in $p(n)$ does not change with the system size. The condensate appears as a hump in the probability distribution around $n = \Delta$, the mean number of excess particles forming the condensate; this part is represented by Eq. E.4. In between the critical background and the condensate hump develops a broad and shallow dip in the probability distribution, as represented by Eq. E.3. On substituting the explicit form of the factor $f(n)$ in Eq. E.3, we have, for the single-site probability distribution in the dip region,

$$p_{\text{dip}}(n) \approx \frac{A}{n^b} \frac{\Delta^b}{(\Delta - n)^b} \text{ for } n \gg 1, \Delta - n \gg 1. \quad (\text{E.9})$$

From the above equation, one concludes that the dip region is dominated by configurations where the excess particles are shared by two sites. This is because, with the single-site factor $f(n) \approx An^{-b}$ for large n , the probability that the excess particles Δ are shared by two sites, one of which has n particles while the other one has the remaining $\Delta - n$ particles, will be proportional to $n^{-b}(\Delta - n)^{-b}$. The minimum in the distribution $p_{\text{dip}}(n)$ occurs at $n \approx \Delta/2$, while the maximum occurs at $n \approx \Delta$. Note that the point at which the maximum in $p_{\text{dip}}(n)$ occurs is approximately the point about which the condensate hump, represented by $p_{\text{cond}}(n)$ in Eq. E.4 is centered. The plot of $p(n)$ against n/L in Fig. E.1 shows the asymptotic locations of the minimum and the maximum at $\Delta/2L = (\rho - \rho_c)/2$ and $\Delta/L = (\rho - \rho_c)$, respectively.

Now, let us define a potential landscape $V(n)$ through

$$V(n) \equiv -\ln p(n), \quad (\text{E.10})$$

where the zero level of the potential is given by $V(0) = -\ln p(1) = 0$. According to the definition in Eq. E.10, with respect to the zero level of the potential $V(n)$, the minimum at $n/L \approx (\rho - \rho_c)/2$ in the distribution $p_{\text{dip}}(n)$ is at a higher potential than the maximum occurring at $n/L \approx (\rho - \rho_c)$.

The survival time T_s of the condensate is the typical interval of time for which the condensate stays on one site, before dissolving to the background. As discussed in Chapter 7, Section 7.3.3, after the dissolution of the condensate to the background, reorganization in the background over the relocation time scale $T_r \sim L^2$ leads to the condensate reforming at another site. During the relocation time T_r , typical configurations are those in which the condensate mass is shared between two sites, and is thus represented by the distribution $p_{\text{dip}}(n)$. Thus, for a given system of L sites, an order of estimate of the time scale T_s is given by the time that the system takes to go from the maximum point in the distribution $p(n)$ occurring at $n/L \approx (\rho - \rho_c)$ (corresponding to the occurrence of the condensate) to the minimum point with $n/L \approx (\rho - \rho_c)/2$ (corresponding to the condensate mass being shared by two sites). Since, as noted earlier, the latter point is at a higher potential than the former point, the problem is that of barrier crossing. According to Kramers' theory [4],

the time to cross the barrier is exponentially large in the barrier height ΔV , which, in the present case is given by

$$\Delta V = -\ln p_{\text{dip}}(\Delta/2) - (-\ln p_{\text{cond}}(\Delta)) \sim \ln L^b. \quad (\text{E.11})$$

Here, we have used the form of $p_{\text{cond}}(\Delta)$ from either Eq. E.5 or Eq. E.7, depending on whether $2 < b < 3$ or $b > 3$, respectively. It thus follows that the survival time T_s , given by the Kramers' theory as $\exp(\Delta V)$, will have the following dependence on the system size L .

$$T_s \sim L^b. \quad (\text{E.12})$$

A more precise treatment, detailed in [1], produces the prefactors in the survival time T_s , which then reads

$$T_s \approx \frac{b\Gamma(b+1)}{(b-1)\Gamma(2b+2)} (\rho - \rho_c)^{b+1} L^b. \quad (\text{E.13})$$

References

- [1] C. Godrèche and J. M. Luck, *J. Phys. A* **38**, 7215 (2005).
- [2] S. N. Majumdar, M. R. Evans, and R. K. P. Zia, *Phys. Rev. Lett.* **94**, 180601 (2005).
- [3] M. R. Evans, S. N. Majumdar, and R. K. P. Zia, *J. Stat. Phys.* **123**, 357 (2006).
- [4] H. A. Kramers, *Physica (Utrecht)*, **7**, 284 (1940).